AFWL-TR-
72-53

POLARIZATION OF INFRARED WAVES CAUSED BY PROPAGATION THROUGH THE ATMOSPHERE

J. Philip Castillo

TECHNICAL REPORT NO. AFWL-TR-72-53

April 1972

AIR FORCE WEAPONS LABORATORY
Air Force Systems Command
Kirtland Air Force Base
New Mexico

Approved for public release; distribution unlimited.

AIR FORCE WEAPONS LABORATORY
Air Force Systems Command
Kirtland Air Force Base
New Mexico 87117

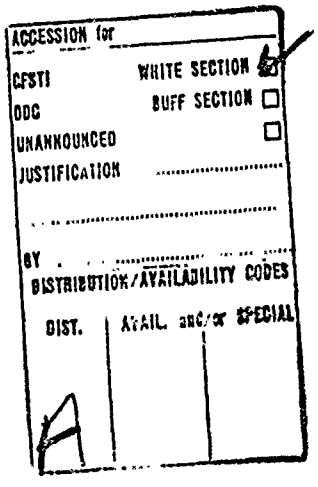

UNCLASSIFIED

Security Classification

DOCUMENT CONTROL DATA - R & D

(Security classification of title, body of abstract and indexing annotation must be entered when the overall report is classified)

1. ORIGINATING ACTIVITY (Corporate author)	2a. REPORT SECURITY CLASSIFICATION
Air Force Weapons Laboratory (SRA) Kirtland Air Force Base, New Mexico 87117	UNCLASSIFIED
	2b. GROUP

3. REPORT TITLE

POLARIZATION OF INFRARED WAVES CAUSED BY PROPAGATION THROUGH THE ATMOSPHERE

4. DESCRIPTIVE NOTES (Type of report and inclusive dates)

August 1971 through March 1972

5. AUTHOR(S) (First name, middle initial, last name)

J. Philip Castillo

6. REPORT DATE	7a. TOTAL NO. OF PAGES	7b. NO. OF REFS
April 1972	230	29

8a. CONTRACT OR GRANT NO.	9a. ORIGINATOR'S REPORT NUMBER(S)
b. PROJECT NO. 5791	AFWL-TR-72-53
c. Task 36	9b. OTHER REPORT NO(S) (Any other numbers that may be assigned this report)
d.	

10. DISTRIBUTION STATEMENT

Approved for public release; distribution unlimited.

11. SUPPLEMENTARY NOTES	12. SPONSORING MILITARY ACTIVITY
	AFWL (SRA) Kirtland AFB, NM 87117

13. ABSTRACT

(Distribution Limitation Statement A)

This study presents an investigation of the polarization of infra-red waves due to propagation through the atmosphere. Cumulus cloud and Haze M particle size distributions are considered for various optical depths at wavelengths of 4.0 and 10.0μ. Results at these wavelengths are compared to results at a wavelength of 0.5μ for the same physical atmosphere.

Initially the radiative transfer integral equations are derived which include the Stokes polarization vector. From these integral equations a Monte Carlo simulation technique is used to photon histories through the atmosphere. The effects of multiple scattering on the polarization state of the scattered intensity is included. A diffuse scattering ground which causes complete depolarization of the incident intensity is included in the simulation model.

Numerical results are obtained for cloudy and hazy atmospheres. It is shown that the degree of depolarization is a function of atmospheric particle density and wavelength, thereby leading to the conclusion that in a linear, homogeneous, isotropic scattering medium, depolarization is a result of multiple scattering. Significant depolarization at wavelengths of 0.5 and 4.0μ is shown to occur for cumulus clouds and optical depths of 3.0 when the cloud is 1 km in height. Polarization factors are obtained with and without ground reflections, with ground albedos playing a significant part in the polarization of the backscatter intensity. Detectors are judiciously placed below and above the cloud layer so that forward and backscatter are measured.

DD FORM 1 NOV 65 1473

UNCLASSIFIED

Security Classification

14. KEY WORDS	LINK A		LINK B		LINK C	
	ROLE	WT	ROLE	WT	ROLE	WT
Polarization						
Propagation						
Infrared						
Atmosphere						
Scattering						

AFWL-TR-72-53

POLARIZATION OF INFRARED WAVES CAUSED BY PROPAGATION THROUGH THE ATMOSPHERE

J. Philip Castillo

TECHNICAL REPORT NO. AFWL-TR-72-53

FOREWORD

This research was performed under Program Element 62601F, Project 5791, Task 36.

Inclusive dates of research were August 1971 through March 1972. The report was submitted 12 April 1972 by the Air Force Weapons Laboratory Project Officer, Mr. J. Philip Castillo (SRA).

The author wishes to express his sincere appreciation and gratitude to Dr. Ahmed Erteza for suggesting the dissertation topic and for providing the encouragement and basic approach to the dissertation problem. Dr. Erteza also provided the guidance as chairman of the Committee on Studies and the Dissertation Committee. Dr. Erteza spent much of his valuable time with the author in solving the many theoretical problems encountered during this research.

Many thanks are also due to Dr. Arnold Koschmann and Dr. Martin Bradshaw who served on the Committee on Studies and the Dissertation Committee. Their comments and recommendations added to the clarity of this study.

The author also thanks Dr. Henry Horak of the Los Alamos Scientific Laboratory who enthusiastically provided his time and energies during two meetings before the selection of the dissertation topic. Dr. Horak's patience in pointing out several problem areas to the author contributed immeasureably to the completion of this study.

This technical report has been reviewed and is approved.

J. PHILIP CASTILLO
Project Officer

WILLIAM J. MOULDS
Acting Chief, Applications Branch

DURWARD D. YOUNG, JR.
Lt Colonel, USAF
Chief, Radiation Division

ABSTRACT

(Distribution Limitation Statement A)

This study presents a study of the polarization of infrared waves due to propagation through the atmosphere. Cumulus cloud and Haze M particle size distributions are considered for various optical depths at wavelengths of 4.0 and 10.0μ. Results at these wavelengths are compared to results at a wavelength of 0.5μ for the same physical atmosphere. Initially the radiative transfer integral equations are derived which include the Stokes polarization vector. From these integral equations a Monte Carlo simulation technique is used to simulate photon histories through the atmosphere. The effects of multiple scattering on the polarization state of the scattered intensity is included. A diffuse scattering ground which causes complete depolarization of the incident intensity is included in the simulation model. Numerical results are obtained for cloudy and hazy atmospheres. It is shown that the degree of depolarization is a function of atmospheric particle density and wavelength, thereby leading to the conclusion that in a linear, homogeneous, isotropic scattering medium, depolarization is a result of multiple scattering. Significant depolarization at wavelengths of 0.5 and 4.0μ is shown to occur for cumulus clouds and optical depths of 3.0 when the cloud is 1 km in height. Polarization factors are obtained with and without ground reflections, with ground albedos playing a significant part in the polarization of the backscatter intentity. Detectors are judiciously placed below and above the cloud layer so that forward and backscatter are measured.

CONTENTS

ILLUSTRATIONS

TABLES

ABBREVIATIONS AND SYMBOLS

A_i	Element of the transformation matrix
a_ℓ	Amplitude for parallel electric field component
a_r	Amplitude for perpendicular electric field component
a_n, b_n	Mie coefficients
D	Polarization factor
D_C	Polarization factor for circular polarization
D_L	Polarization factor for linear polarization
dA	Element of area
dE	Element of energy
dm	Element of mass
ds	Element of thickness
$d\omega$	Element of solid angle
E_c	Cross polarized electric field component
E_p	Colinear polarized electric field component
$E_{\ell LHC}$	Parallel electric field component for left hand circular polarization
$E_{\ell RHC}$	Parallel electric field component for right hand circular polarization
E_{rLHC}	Perpendicular electric field component for left hand circular polarization
E_{rRHC}	Perpendicular electric field component for right hand circular polarization
E[r]	Expected value of r
F	Scattering matrix for Stokes parameters
$\tilde{F}$	Scattering matrix for modified Stokes parameters
G	Source intensity pattern

H	Scale height
h	Planck's constant
$h_n^{(2)}(x)$	Spherical Bessel function of the second kind
I	Intensity (first Stokes parameter)
I_ℓ	Parallel intensity component
I_r	Perpendicular intensity component
I_0	Initial intensity
I_D	Stokes vector for direct intensity
I_s	Stokes vector for scattered intensity
j	Emission coefficient
J	Source function
$j_n(x)$	Spherical Bessel function of the first kind
k	Propagation constant
L	Rotation matrix
$\vec{\ell}$	Unit vector in the parallel direction
m	Index of refraction
N	Number of particles per cm^3
$\vec{n}$	Normal unit vector
$n(r)$	Particle size distribution
P	Degree of polarization
$P_i(\mu)$	Legendre polynomial
p	Dipole moment
Q	Second Stokes parameter
Q_c	Cross-polarization ratio
Q_{ext}	Extinction efficiency factor
R	Rayleigh scattering matrix
R	Fresnel reflection coefficient

$\vec{r}$	Unit vector in the perpendicular direction
r_m	Modal radius
S_i	Amplitude scattering function
t	Time parameter
$\tan \beta$	Ellipticity
U	Third Stokes parameter
V	Fourth Stokes parameter
Var	Variance
v	Velocity
x	Size parameter
α	Polarizability
ϵ_1	Phase angle for parallel component
ϵ_2	Phase angle for perpendicular component
η, ξ	Random variables
κ	Mass absorption or scattering coefficient
λ	Wavelength
λ_0	Wavelength in free space
μ	Cosine of the scattering angle
π_n, τ_n	Functions for representing Mie series
ν	Photon frequency
ρ	Density
$\sum_{ext}$	Volume extinction cross section
$\sum_s$	Scattering function
$\sum_{vs}$	Volume scattering function
σ_a	Absorption cross section
σ_c	Standard deviation for Cumulus Cloud distribution
σ_{ext}	Extinction cross section

σ_H	Standard deviation for Haze M distribution
σ_s	Scattering cross section
τ	Optical distance or depth
χ	Polarization ellipse rotation angle
ω	Angular frequency
$\bar{\omega}_0$	Albedo for single scattering

SECTION I

INTRODUCTION

Polarization is a fundamental characteristic of electromagnetic waves. The polarization of a wave propagating in a media is defined as the orientation and direction of the electric field vector. The polarization properties of electromagnetic waves have been used sparingly in describing the properties of a scatterer. In radar circular polarization has been used to discriminate between desired targets and rain. Orthogonal polarization has been used in communication systems to prevent interference between two overlapping channels.

One of the obstacles in the greater use of polarization has been the difficulty of controlling and measuring the polarization state of a system. Interference between targets which causes depolarization beyond that which was expected has been another problem. The polarization of television signals used in the United States is different from that used in Great Britain. In Great Britain the polarization is vertical. Vertical polarization is used to reduce ground reflections and interference from overhead wires. Horizontal polarization is used in the United States. Ignition and industrial noise contains vertical components which are usually greater than the horizontal components and therefore interfere with vertically polarized signals.

Optimum discrimination can be achieved if the unwanted reflected wave is completely depolarized with respect to the wave reflected from the desired target. In practice this situation is never achieved. In real life both the desired and unwanted signals will be partially

polarized with the extent of depolarization of one greater than the other. If the difference in depolarization between the two signals is sufficient some degree of discrimination can be achieved.

Recently, Manz [1][1] has proposed a discrimination technique using polarization which will separate simultaneous returns from clouds and terrain when using a laser. In his model of the cloud and the terrain, Manz has assumed that the cloud is composed of Mie particles, i.e., spherical particles, and that the terrain is rough for all wavelengths of interest. The backscattered return from the cloud consisting of Mie particles will be depolarized less than the backscattered return from the terrain. Mie's work [2] shows that for incident linear polarization, as Manz has proposed, perpendicular or parallel to the plane of scatter, no depolarization will occur. On the other hand, for very rough terrain one would expect, on the average, to receive equal parallel and perpendicular components for an incident linearly polarized wave. Recent workers [3, 4, 5] have calculated the cross-polarization ratio for rough terrain defined by

$$Q_c = \frac{\langle E_c \, E_c^* \rangle}{\langle E_p \, E_p^* \rangle} \tag{1}$$

where E_c is the cross polarized electric field component of the scattered electromagnetic field and E_p is the component of the scattered electromagnetic field which is colinear with the incident field. The asterisk denotes the complex conjugate. Using random sampling from a normal distribution to simulate the surface function, Beckmann [6] shows

[1]The numbers in brackets refer to the corresponding numbers in the references.

that the cross-polarization ratio Q depends on the angle of incidence, the rms slope of the terrain, and the dielectric constant. Minimum depolarization, according to Beckmann and others [3, 4, 5], occurs at a zero angle of incidence. The ratio Q increases with angle of incidence. It is therefore reasonable to assume that at optical frequencies, where the terrain is relatively rougher than at microwave frequencies, the ratio Q is equal to at least one-half. While it is true that, at optical frequencies, the distance between particles in a cloud is large compared to a wavelength so that near field effects may be neglected, far-field multiple scattering will probably cause some depolarization of the backscattered wave. Therefore Manz's discrimination technique does not give a sure way of separating returns from clouds and rough targets for all situations as borne out by his experimental results. Fung has also shown that, for smooth reflecting plane surfaces, the cross-polarized component will be zero for

(a) locally grazing incidence,

(b) incident polarization parallel with or perpendicular to the local plane of incidence, and

(c) $R^+ + R^- = 0$. Where R^+ is the Fresnel reflection coefficient for incident polarization in the plane of incidence and R^- is the Fresnel reflection coefficient for incident polarization perpendicular to the plane of incidence.

Depolarization of electromagnetic waves can be caused by different phenomena. As implied above, a wave can be depolarized by multiple scattering. One has to take care when discussing multiple scattering since it may be understood to occur when two objects are within mutual near-fields or it may be understood to occur as a result of multiple

reflections, i.e., the reflecting objects may not be in mutual near-fields. One example of depolarization due to near-field scattering is that of two or more spheres in close proximity, where the individual scattering functions can no longer be considered separately but must be derived only by including the interdependence of the individual sphere's field. In this case the conglomerate scattering function will give rise, in general, to polarization in a particular direction which is different than if one had considered the individual scattering functions separately. When considering depolarization due to multiple reflection or multiple bounce one assumes that the scatterers are in each other's radiation or far-field zone. In this case one can consider the individual scattering functions separately; and these will, in general, lead to a different polarization state than had the scatterers been in close proximity. The difference in polarization state between the two types of multiple scattering may be greater than or less than that given by the other method, depending on the scattering angle being considered. There is one possible solution to this dilemma. If we approach the problem of scattering from a photon-particle collision standpoint and if we further select the particle-scattering function which was determined for a single particle in the radiation zone to represent the probability density for scattering in a certain direction, we can then bring particles as close together as we wish without touching. This approach will give some approximation to the multiple scattering problem since if we run many photon-particle collision histories for the conglomerate, we may now measure the probability scattering function for the conglomerate. The new probability scattering function will not in general be equal to the sum of individual particle scattering functions because of the multiple collisions which were allowed to take

place. For example, consider the scattering of an electromagnetic wave by a sphere. A single sphere may have a scattering function which is highly peaked in the forward scattering direction (figure 1).

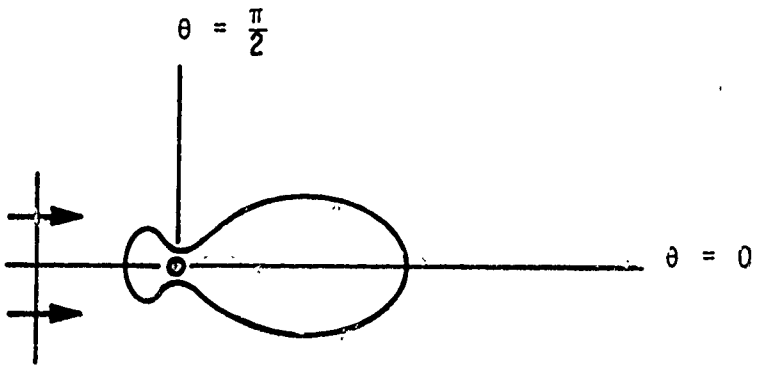

Figure 1. Scattering Function for a Single Sphere

For this particular case, other spheres placed at $\theta = \pm \pi/2$ will interfere negligibly with the original sphere since the probability of scattering in the direction $\theta = \pm \pi/2$ is almost zero. If we place a sphere along $\theta = 0$ we will certainly be faced with multiple scattering since the probability of forward scattering is large. Thus by using this simple model one can account for multiple scattering at least to the first order. One thing we have not discussed is the phase dependence on the position of the scatterers relative to each other. This mutual dependence leads to the phenomenon of interference. If two beams of light originate from the same source, the fluctuations in the two beams are generally correlated and the beams are said to be either partially or completely coherent [7]. If two beams originate from two independent

sources, they are said to be mutually incoherent or uncorrelated. We can therefore conclude that for scattering by two spheres placed at $\theta = 0$ in figure 1, the waves scattered by the two spheres will be at least partially coherent since the incident plane wave originated from a single source. We can also consider that the two spheres are two different sources which are partially correlated. If we consider a large number of spheres placed at random relative to each other, the scattered waves due to each sphere in the random collection will be uncorrelated and the scattering will thus be incoherent. This situation is similar to the problem of scattering by two spheres that are vibrating randomly, i.e., the waves scattered from them will be uncorrelated. Thus, if we assume that the atmosphere, for example, is made up of many randomly placed spheres, we can determine the scattered intensity at any point incoherently, i.e., without regard to phase. This is the manner in which we will approach the problem of scattering in the atmosphere.

Depolarization of electromagnetic waves is also caused by anisotropic media where one or more of the characteristics of the medium depends on direction. In anisotropic media, depolarization takes place because of the reradiation of secondary waves with characteristic polarizations depending on direction. Crystals are a good example of anisotropic medium in which the preferred direction is determined by the direction of the magnetic field. Due to the anisotropy of the medium charges can move only in a specific direction and are not free to move in the direction of an incident field with general polarization. Only if the incident field is parallel to these characteristic directions will the polarization of the reradiated field be the same as the incident field.

Faraday rotation is another phenomenon which causes the depolarization of an electromagnetic wave. Michael Faraday in 1845 and Fresnel in 1837 found that when light propagates through a medium in the direction of magnetic field the plane of polarization rotates with the angle of rotation proportional to the path length between two points. The exact derivation of this phenomenon can be accomplished only through the use of quantum mechanics. This form of depolarization occurs in the earth's ionosphere [8] and can cause problems for radar tracking systems.

In this study we wish to investigate the depolarization of electromagnetic waves in the atmosphere. We will consider wavelengths small compared to interparticle distances. We will begin in section II by discussing the radiative transfer of energy in the atmosphere and derive the appropriate integral equations. Section II follows the work of Chandrasekhar [9] and Kourganoff [10] closely. The class of integral equations which describe the problem of radiative transfer are the nonhomogeneous Fredholm equations

$$\psi(\xi) = F(\xi) + \lambda \int_a^b K(\xi;x)\, \psi(x)\, dx \qquad (2)$$

which has been solved by Chandrasekhar [9] for the isotropic scattering function. Evans et al. [11] have produced solutions for this equation for anisotropic scattering functions. Both Chandrasekhar and Chu have used Gauss quadrature in solving the resulting integral equations. The scattering function is expanded in the form

$$K(\Omega,\Omega') = f(\mu) = \frac{1}{4\pi} \sum_{i=0}^{N} a_i\, P_i(\mu) \qquad (3)$$

where

$\mu = \cos \theta$

θ = angle of scatter

= angle between Ω and Ω'

$P_i(\mu)$ are the Legendre polynomials

and a_i are the coefficients of the expansion. Equation (3) has the same form as the exact expression for spheres.

Solutions of equation (2) by Gauss quadrature are very complicated and difficult to obtain. In this study we obtain numerical results to the problem of depolarization of electromagnetic waves by the atmosphere through the use of Monte Carlo techniques [12, 13]. We assume that the atmosphere is composed of spherical scattering particles such as water droplets in clouds or fogs. An excellent summary of various forms of atmospheric conditions is contained in [1].

In section III we discuss the polarization and depolarization of electromagnetic waves by scattering. We also present the Stokes parameters in describing the polarization of an electromagnetic wave. Section III follows Van De Hulst [14] closely in obtaining an analytical description of the polarization parameters. Two basic forms of scattering by particles will be used in this study. One is Rayleigh scattering where the scatterer is small compared to a wavelength and the other is Mie scattering where we consider scattering by arbitrary spheres.

Also in section III we present a general method, as was obtained by Deirmendjian [15], for describing the size distribution of particles in the atmosphere. The exact solution of scattering by spheres originally derived by Gustav Mie [2] as a function of the size parameter

$$x = \frac{2\pi r}{\lambda} \tag{4}$$

will be used. In equation (4) r is the sphere's radius and λ is the wavelength of the incident wave. The Mie scattering function is averaged over the size distribution, which results in a volume scattering function. If $f(\theta, r/\lambda)$ is the scattering function as a function of θ, the scattering angle and the ratio r/λ is as defined above; and $n(r)$ is the size distribution, then

$$F(\theta) = \int_{r_1}^{r_2} f(\theta, r/\lambda)\, n(r)\, dr \tag{5}$$

is the volume scattering function for particles of radius between r_1 and r_2.

In section IV we describe the computer program used for simulating the depolarization of polarized electromagnetic waves in the atmosphere. The computer program is based on previous work by Kattawar and Plass [16] and by Collins and Wells [17]. The program was used on the Air Force Weapons Laboratory CDC-6600 computers.

In section V we present the results of some sample problems. We will present the microscopic scattering functions for Mie Scattering by "Cumulus Clouds" and "Haze M" size distributions. By microscopic we mean that several representative size particles from each type distribution are obtained. We will also obtain and present the volume scattering functions for each size distribution. The microscopic and volume scattering functions will be presented for several different wavelengths varying from 0.5 micron to 10.0 microns. The volume scattering functions are then used to analyse different atmospheric problems containing either

the "Cumulus Cloud" or the "Haze M" size distribution or combinations of both. The computer program has been written to accomodate linear or circular polarization. In general, the distances being considered here are small, i.e., in the order of 10 km to 20 km maximum. Scattering from the ground is included and we will therefore include the ground albedo in each problem. The albedo is defined as the ratio of scattered to incident energy.

The result of all these problems is the determination of the degree of depolarization of the initial source electromagnetic wave. Depolarization for the various geometries being considered is presented for different wavelengths. The polarization factor defined by

$$D = \frac{I_r - I_\ell}{I_r + I_\ell} \tag{6}$$

is given as a function of polar angle; where I_r is the perpendicular intensity component and I_ℓ is the parallel intensity component. In equation (6) both I_r and I_ℓ are referred to a vertical plane which contains the propagation vector (figure 2).

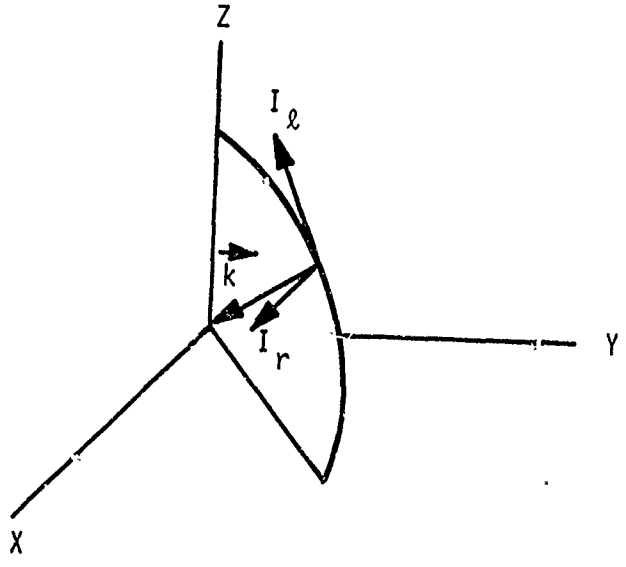

Figure 2. Vertical Polarization Reference Plane

SECTION II

ELECTROMAGNETIC SCATTERING IN THE ATMOSPHERE

1. INTRODUCTION

For the past seventy years, astrophysicists have been concerned with the transfer of radiation in the atmospheres of planets and stars. Physicists have been concerned with similar problems in the diffusion of neutrons in various materials. We should also mention that radar has been used extensively in the study of certain atmospheric properties.

Recently, with the invention of the laser, problems of light transfer in the atmosphere have become of interest to a greater number of scientists and engineers. In this section we are concerned with the formulation of the problem of the transfer of polarized light in the atmosphere. We are particularly interested in the depolarization effects of scattering on the propagating light beam. The notation used in this study is, for the most part, that used by astrophysicists and follows along the same lines as in the books by Chandrasekhar and Kourganoff [9, 10].

Basically, the problem of radiative transfer must deal with a spherical geometry (if we can assume a spherical earth); but the problem is simplified somewhat if the atmosphere is plane parallel. In this study we are concerned with problems with short range transmission of highly directive, monochromatic light, i.e., the distances involved are short compared to the curvature of the earth. It is also assumed that, at the frequencies considered, absorption is negligible.

2. DERIVATION OF BASIC QUANTITIES

In this subsection we are concerned with the derivation of the essential quantities necessary for the solution of the problem as defined. Since all quantities defined in this study are for monochromatic light no special notation is used to denote frequency dependence, although the reader should keep in mind that all quantities are highly dependent functions of frequency.

Let dE be the energy transported across an element of area dA, in time dt, and in a direction confined to an element of solid angle dω and making an angle θ with the normal $\vec{n}$ to dA (figure 3).

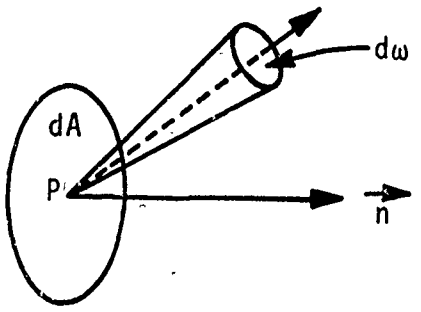

Figure 3. Energy Across dA in the Direction dω.

Then, dE can be expressed in terms of the specific intensity or more briefly the intensity by

$$dE = I \cos\theta \, dA \, d\omega \, dt \tag{7}$$

If the intensity I is independent of the direction at a point the radiation field is said to be isotropic. The radiation field is said to be homogeneous if the intensity is the same at all points and in all directions.

Radiation which is propagating through a medium may be partially scattered or absorbed by the material in the medium which in essence weakens or attenuates the incident intensity I. The incident intensity I becomes I + dI after traversing a thickness ds (figure 4) in the direction of propagation. Therefore,

$$dI = -\kappa\rho\ I\ ds \tag{8}$$

where κ is the mass absorption or scattering coefficient and ρ is the density of the material. In what follows κ will be assumed to be a scattering coefficient exclusively.

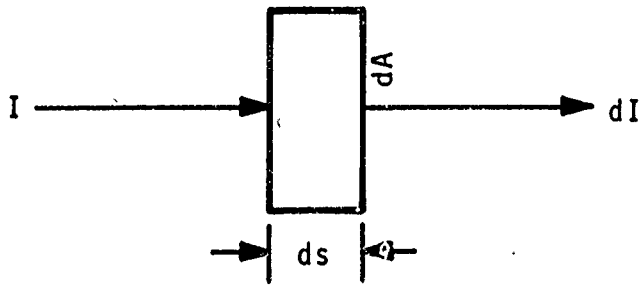

Figure 4. Intensity Through Element ds.

Consider a pencil beam of radiation incident on an element of mass with cross-section dA and thickness ds. The scattered intensity in a direction $d\omega$ is given by

$$dE_s = (\kappa\rho\ Ids)\ dA\ d\omega\ dt\ \frac{1}{4\pi} \tag{9}$$

The mass of the element is

$$dm = \rho\ dA\ ds \tag{10}$$

Now we can write

$$dE_s = \kappa\ I\ dm\ d\omega\ dt\ \frac{1}{4\pi} \tag{11}$$

Obviously, in the most general case the scattered energy will be dependent on direction; therefore, a scattering function $P(\cos \Theta)$ is introduced to account for this dependence. The energy scattered into an element of solid angle $d\omega'$ making an angle Θ with the direction of incidence is then

$$dE_s = \kappa I P(\cos \Theta) \frac{d\omega'}{4\pi} dm \, d\omega \, dt \tag{12}$$

and the total scattered energy is

$$E_s = \kappa I \, dm \, dt \, d\omega \frac{1}{4\pi} \int P(\cos \Theta) \, d\omega' \tag{13}$$

where the integration is carried out over all solid angles. In general, for perfect scattering (no absorption)

$$\frac{1}{4\pi} \int P(\cos \Theta) \, d\omega' = 1 \tag{14}$$

in general, where both scattering and absorption occur

$$\bar{\omega}_0 = \frac{1}{4\pi} \int P(\cos \Theta) \, d\omega' \leq 1 \tag{15}$$

where $\bar{\omega}_0$ is the fraction of intensity lost due to scattering and $1 - \bar{\omega}_0$ is the fraction absorbed; $\bar{\omega}_0$ is referred to as the albedo for single scattering. If

$$\text{constant} = P(\cos \Theta) \tag{16}$$

the scattered intensity is isotropic.

An important quantity is the emission coefficient j. The emission coefficient indicates the amount of energy emitted by an element of mass dm in a direction of solid angle $d\omega$. The emitted energy includes scattered energy both from the element being considered and any other scattered energy originating at some other source contained in the

solid angle $d\omega$ being considered. Thus the energy emitted by mass dm in the direction $d\omega$ is given by

$$E_e = j \, dm \, d\omega \, dt \tag{17}$$

The scattering of energy incident from a direction (θ',ϕ') into a direction (θ,ϕ) results in

$$E_s = \frac{1}{4\pi} \kappa \, dm \, d\omega \, P(\theta,\phi;\theta',\phi') \, I(\theta',\phi') \sin\theta' \, d\theta' \, d\phi' \, dt \tag{18}$$

Thus, comparing (17) and (18)

$$j = \frac{\kappa}{4\pi} \int_0^{2\pi} \int_0^{\pi} P(\theta,\phi;\theta',\phi') \, I(\theta',\phi') \sin\theta' \, d\theta' \, d\phi' \tag{19}$$

for a scattering medium. In this study we consider scattering only.

The ratio of the emission to the absorption coefficient is called the source function and is written as

$$J = \frac{j}{\kappa} \tag{20}$$

or from equation (19)

$$J(\theta,\phi) = \frac{1}{4\pi} \int_0^{2\pi} \int_0^{\pi} P(\theta,\phi:\theta',\phi') \, I(\theta',\phi') \sin\theta' d\,\theta' d\,\phi' \tag{21}$$

3. THE EQUATION OF TRANSFER

Consider a cylinderical element (figure 5) of cross-section dA and length ds. The amount of energy absorbed by the element is

$$E_a = (\kappa\rho I \, d\, s) \, d\, A \, d\omega \, dt \tag{22}$$

the amount emitted is

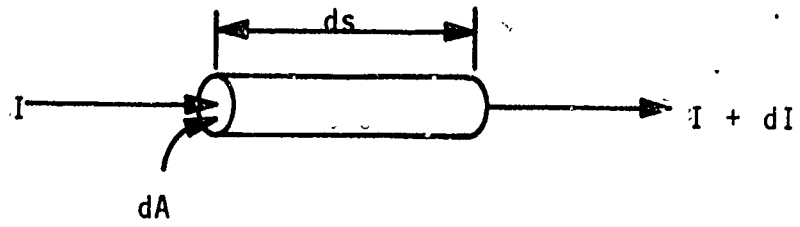

Figure 5. Cylindrical Element for Derivation of the Equation of Transfer

$$E_e = j\,\rho\,d\,s\,d\,A\,d\omega dt \tag{23}$$

The difference between the absorbed and the emitted energy results in the net energy crossing the two faces of the element in the normal direction, and

$$dI\ dA\ d\omega dt = E_e - E_a$$

or using (22) and (23)

$$\frac{dI}{ds} = -\kappa\rho\ I + j\rho \tag{24}$$

Using equation (20) and rearranging we obtain the equation of transfer

$$-\frac{dI}{\kappa\rho ds} = I - J \tag{25}$$

The equation of transfer (25) can be solved easily through the use of the method of variation of parameters. We can rewrite equation (25) as

$$\frac{dI}{ds} + \kappa\rho I = \kappa\rho\ J \tag{26}$$

Then

$$I_h(s) = \exp\left[-\int_0^s \kappa\rho d\,s''\right] \tag{27}$$

is a solution of the corresponding homogeneous linear equation. We must find a function f(s) such that

$$I_g(s) = f(s)\ I_h(s) \tag{28}$$

is the general solution of (26). Substituting (28) into (26) we obtain

$$f'\ I_h + \left(I_h' + \kappa\rho\ I_h\right) f = \kappa\rho\ J \tag{29}$$

where

$$f' = \frac{df}{ds}$$

and

$$I_h' = \frac{dI_h}{ds}$$

Since I_h is the solution to the homogeneous equation

$$I_h' + \kappa\rho\ I_h = 0 \tag{30}$$

and we are left with

$$f'\ I_h = \kappa\rho\ J \tag{31}$$

or

$$\frac{df}{ds} = \kappa\rho\ \frac{J(s)}{I_h(s)}$$

$$= \kappa\rho\ J(s)\ \exp\left[\int_0^s \kappa\rho\ ds''\right] \tag{32}$$

Integrating equation (32) yields

$$f(s) = \kappa\rho \int_0^s J(s')\ \exp\left[\int_0^{s'} \kappa\rho\ d\,s''\right] ds' + C \tag{33}$$

where C is a constant of integration. Combining (27) and (33) according to (28), we have

$$I_g = I(s) = C\, e^{-\tau(s,0)} + \int_0^s \kappa\rho\, J(s')\, e^{-\tau(s,s')}\, ds' \qquad (34)$$

where

$$\tau(s,s') = \int_{s'}^{s} \kappa\rho\, ds \qquad (35)$$

is the optical thickness of the material between s and s'. At s = 0 we find that

$$I(0) = C$$

therefore

$$I(s) = I(0)\, e^{-\tau(s,0)} + \int_0^s \kappa\rho\, J(s')\, e^{-\tau(s,s')}\, ds' \qquad (36)$$

is the solution to the equation of transfer (25).

For the case of scattering in a plane-parallel atmosphere we measure linear distances normal to the plane of stratification, then the equation of transfer becomes (figure 6)

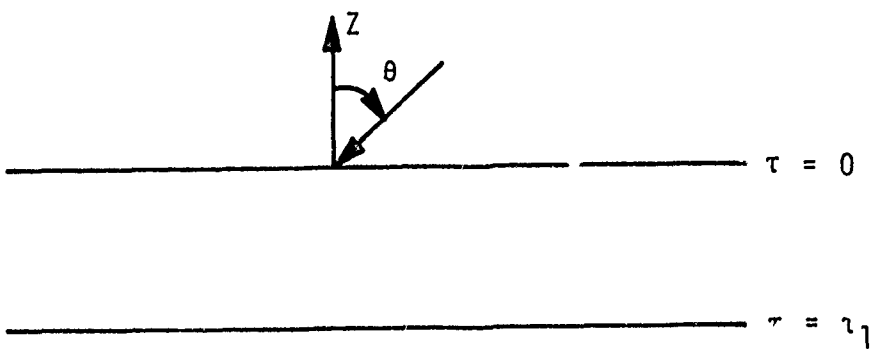

Figure 6. Plane-Parallel Atmosphere

$$-\cos\theta \frac{dI(z,\theta,\phi)}{\kappa\rho dz} = I(z,\theta\ \phi) - J(z,\theta,\phi) \tag{37}$$

were the angle θ is measured from the z axis and ϕ is the azimuthal angle. We can set

$$\frac{d\tau}{dz} = -\kappa\rho \tag{38}$$

and substitute into (37) to obtain

$$\mu \frac{dI(\tau,\mu,\phi)}{d\tau} = I(\tau,\mu,\phi) - J(\tau,\mu,\phi) \tag{39}$$

where $\mu = \cos\theta$. For an atmosphere with finite optical thickness the solution (36) reduces to (figure 5)

$$I(\tau,+\mu,\phi) = I(\tau,\mu,\phi)\ e^{-(\tau_1-\tau)/\mu}$$

$$+ \int_{\tau}^{\tau_1} J(t,\mu,\phi)\ e^{-(t-\tau)/\mu} \frac{dt}{\mu} \tag{40}$$

and

$$I(\tau,-\mu,\phi) = I(0,-\mu,\phi)\ e^{-\tau/\mu}$$

$$+ \int_{0}^{\tau} J(t,-\mu,\phi)\ e^{-(\tau-t)/\mu} \frac{dt}{\mu} \tag{41}$$

where $1 \geq \mu > 0$ for both equations (40) and (41). Equation (40) represents the intensity in the positive z or outward direction, while equation (41) represents the intensity in the negative z or downward direction. The intensities emerging from the atmosphere at $\tau = 0$ and $\tau = \tau_1$ are given by

$$I(0,+\mu,\phi) = I(\tau,\mu,\phi)\, e^{-\tau_1/\mu} + \int_0^{\tau_1} J(t,\mu,\phi)\, e^{-t/\mu}\, \frac{dt}{\mu} \qquad (42)$$

and

$$I\left(\tau_1,-\mu,\phi\right) = I(0,-\mu,\phi)\, e^{-\tau_1/\mu} + \int_0^{\tau_1} J(t,-\mu,\phi)\, e^{-\left(\tau_1-t\right)/\mu}\, \frac{dt}{\mu} \qquad (43)$$

The first term on the right hand side of equations (40) through (43) may be interpreted as the direct intensity attenuated exponentially; the second term is the sum of the intensities due to all orders of scattering within the atmosphere.

The source function (equation (21)) may now be written as

$$J(\tau,\mu,\phi) = \frac{1}{4\pi}\int_0^{2\pi}\int_{-1}^{+1} P(\mu,\phi;\mu',\phi')\, I(\tau,\mu',\phi')\, d\mu'\, d\phi' \qquad (44)$$

Writing

$$I_s(\tau,+\mu,\phi) = \int_{\tau}^{\tau_1} J(t,\mu,\phi)\, e^{-(t-\tau)/\mu}\, \frac{dt}{\mu} \qquad (45)$$

and

$$I_s(\tau,-\mu,\phi) = \int_0^{\tau} J(t,-\mu,\phi)\, e^{-(\tau-t)/\mu}\, \frac{dt}{\mu} \qquad (46)$$

for the scatter contributions in equations (40) and (41) and substituting equation (44) into (45) and (46), we obtain

$$I_S(\tau,+\mu,\phi) = \frac{1}{4\pi}\int_{\tau}^{\tau_1}\int_{0}^{2\pi}\int_{-1}^{+1} P(\mu,\phi;\mu',\phi')$$

$$I(t,\mu',\phi')\, d\mu'\, d\phi'\, e^{-(t-\tau)/\mu}\,\frac{dt}{\mu} \qquad (47)$$

and

$$I_S(\tau,-\mu,\phi) = \frac{1}{4\pi}\int_{0}^{\tau}\int_{0}^{2\pi}\int_{-1}^{+1} P(-\mu,\phi;\mu',\phi')$$

$$I(t,\mu',\phi')\, d\mu'\, d\phi'\, e^{-(\tau-t)/\mu}\,\frac{dt}{\mu} \qquad (48)$$

If we now compare equations (47) and (48) with equations (40) and (41) we can see that we now have a set of integral equations to solve in order to acquire the intensity at any point. We can also write

$$I_D(\tau,+\mu,\phi) = I\left(\tau_1,\mu,\phi\right) e^{-\left(\tau_1-\tau\right)/\mu} \qquad (49)$$

and

$$I_D(\tau,-\mu,\phi) = I(0,-\mu,\phi)\, e^{-\tau/\mu} \qquad (50)$$

as the direct contributions of the incident intensity. Therefore, using equations (47) through (50), we can now write equations (40) and (41) as

$$I(\tau,+\mu,\phi) = I_D\left(\tau_1,+\mu,\phi\right) + I_S(\tau,+\mu,\phi) \qquad (51)$$

and

$$I(\tau,-\mu,\phi) = I_D(\tau,-\mu,\phi) + I_S(\tau,-\mu,\phi) \qquad (52)$$

i.e., the intensities propagating in positive and negative directions can be considered as being made up of a direct contribution attenuated

exponentially and a contribution consisting of the intensity from all orders of scattering.

4. RADIATIVE TRANSFER FOR POLARIZED LIGHT

Polarized light can be described in terms of the Stokes parameters (section III). There are four Stokes parameters which describe the total intensity, the polarization ellipse, and the orientation of the polarization ellipse. The four Stokes parameters are written as

$$\mathbf{I} = (I,Q,U,V) \tag{53}$$

where the boldface letters will indicate a matrix representation.

Proceding with matrix notation, we can now represent the scattering function by a scattering transformation matrix. The transformation matrix will be a 4 X 4 matrix and is of the form (see Section III) [18]

$$\mathbf{F} = \begin{pmatrix} a_1 & b_1 & b_3 & b_5 \\ c_1 & a_2 & b_4 & b_6 \\ c_3 & c_4 & a_3 & b_2 \\ c_5 & c_6 & c_2 & a_4 \end{pmatrix} \tag{54}$$

Furthermore, if we write the polarization parameters as

$$\mathbf{I} = \left(I_\ell, I_r, U, V\right) \tag{55}$$

then the matrix transformation will be denoted by $\mathbf{F}'$. We will find, in section III, that, for a spherical scattering particle, the scattering matrix will be of the form

$$F' = \begin{pmatrix} a_1' & 0 & 0 & 0 \\ 0 & a_2' & 0 & 0 \\ 0 & 0 & a_3' & b_2' \\ 0 & 0 & c_2' & a_4' \end{pmatrix} \tag{56}$$

where $b_2' = -c_2'$ and $a_3' = a_4'$.

Using matrix notation we can now write equations (51) and (52) as

$$I(\tau,+\mu,\phi) = I_D(\tau,+\mu,\phi) + I_s(\tau,+\mu,\phi) \tag{57}$$

and

$$I(\tau,-\mu,\phi) = I_D(\tau,-\mu,\phi) + I_s(\tau,-\mu,\phi) \tag{58}$$

where

$$I_D(\tau,+\mu,\phi) = I(\tau_1,\mu,\phi)\, e^{-(\tau_1-\tau)/\mu} \tag{59}$$

$$I_D(\tau,-\mu,\phi) = I(0,-\mu,\phi)\, e^{-\tau/\mu} \tag{60}$$

$$I_s(\tau,+\mu,\phi) = \frac{1}{4\pi} \int_{\tau}^{\tau_1} \int_{0}^{2\pi} \int_{-1}^{+1} F(\mu,\phi;\mu',\phi') \, I(t,\mu',\phi') \, d\mu' \, d\phi' \, e^{-(t-\tau)/\mu} \frac{dt}{\mu} \tag{61}$$

$$I_s(\tau,-\mu,\phi) = \frac{1}{4\pi} \int_{0}^{\tau} \int_{0}^{2\pi} \int_{-1}^{+1} F(-\mu,\phi,\mu',\phi') \, I(t,\mu',\phi') \, d\mu' \, d\phi' \, e^{-(\tau-t)/\mu} \frac{dt}{\mu} \tag{62}$$

Equations (57) through (62) describe the intensity of radiation at any point in a semi-infinite, plane parallel scattering atmosphere.

The solutions (57) and (58) are nonhomogeneous Fredholm integral equations. The difficulty in solving this type of integral equation

is that the function being solved for also appears under the integral equation. Generalized physically realizable kernals may be solved numerically through the judicious use of series expansions.

5. MODELING THE TRANSFER PROBLEM

A study of equations (57) and (58) will help in envisioning the physical events which take place during the propagation of energy through a scattering atmosphere. First, as already indicated, the intensity at any point can be thought of consisting of the direct intensity attenuated exponentially and of the scattered intensity from all scatterers surrounding the observation point. The polarization properties of the direct beam do not change, while the scattered intensity will in general have its polarization properties modified by the scattering function matrix of each individual scatterer.

The intensity of electromagnetic radiation is defined [19] as the energy per unit time, passing through a unit area at right angles to the direction of propagation. In terms of a beam of monochromatic photons the intensity is given by

$$I = E_p \text{ (Photon Flux)} \tag{63}$$

where $E_p = h\nu$. h is Planck's constant and ν is the photon frequency. Equation (63) suggests that a beam of monochromatic photons is the proper representation for directed electromagnetic radiation. Suppose we approximate equations (61) and (62) by the triple summation of a large number of terms

$$\sum_{i=1}^{n}\sum_{j=1}^{m}\sum_{k=1}^{\ell} \frac{1}{4\pi\mu} F\left(\mu,\phi;\mu_i',\phi_j'\right) I\left(t_k,\mu_i',\phi_j'\right) e^{-(\tau-t_k)/\mu} \Delta\mu'\Delta\phi'\Delta t \tag{64}$$

this triple summation is equal to (61) in the limit as $\Delta\mu'$,$\Delta\phi'$, and Δt go to zero and n, m, ℓ go to infinity. Furthermore, the beam may be thought of as being composed of many photons according to equation (63). We may therefore simulate a beam of radiation by individual photons or individual photons individually propagating and scattered randomly about throughout the medium. Since we are only considering noncoherent scattering, the results may be added arithmetically at some point of observation. It will further be assumed that near field effects are negligible.

The essence of the model is this: Consider a photon or group of photons with a defined set of Stokes polarization parameters, launched from an isotropic source; these photons will be attenuated exponentially as they propagate through the medium, and upon colliding with a particle the photons' polarization parameters will be modified according to the scattering matrix and scattered in a new direction. The history of this group of photons may be followed to all orders of scattering. In this way many histories may be followed and estimates of the intensities at a detector (observation point) may be made. This technique has been used by other investigators [16, 17, 20] with excellent agreement with experimental results for natural, i.e., unpolarized electromagretic radiation. In this study we use this approach for the case of a polarized light source and determine the effect of scattering on the initial polarization state of the beam of light.

In the next section we discuss the Stokes parameters and determine the effect of scattering on these parameters.

SECTION III

POLARIZATION AND DEPOLARIZATION OF EM WAVES

1. INTRODUCTION

Electromagnetic waves have several properties which can be used to convey information from one point to another. The most commonly used properties are the frequency, phase, and amplitude. The electromagnetic wave propagating in a medium whether it be a wire, a waveguide, or the atmosphere can be used to carry information by modulating the frequency, the phase, or the amplitude according to some prescribed code. The information can be recovered at the receiving end through demodulation.

Another property of electromagnetic waves which has not been used to a great extent is the polarization of the wave propagating through a medium. It is known that the electric and magnetic field vectors are transverse to the direction of propagation in an isotropic, homogeneous medium. The orientation of the electric field vector defines the polarization of the electromagnetic wave. By convention, if the direction of the electric vector is constant in time the wave is said to be linearly polarized, if electric vector rotates then the wave is said to be elliptically polarized.

The polarization of an electromagnetic wave propagating through a continuum remains unchanged if the medium is homogeneous and isotropic. On the other hand, if scattering occurs the polarization characteristics will, in general, change. Therefore, if the polarization characteristics of a wave prior to and after scattering are

known, it is possible, at least in principle, to categorize the particular type of scatterer causing the depolarization. In this study, we are primarily interested in the depolarization of a completely polarized wave by a scattering atmosphere. By depolarization we mean the degree to which an arbitrarily polarized transmitted wave is transformed to some other polarization state.

2. POLARIZATION AND THE STOKES PARAMETERS

The most general type of polarized wave can be written as

$$\vec{E} = \vec{\ell} E_\ell + \vec{r} E_r \tag{65}$$

where

$\vec{E}$ is the total electric field vector

E_ℓ is the parallel component

E_r is the perpendicular component

$\vec{\ell}$ and $\vec{r}$ are unit vectors

In writing equation (65) we used the same notation used by Chandrasekhar [9] and Van De Hulst [14], where the subscripts ℓ and r refer to the last letters in the words parallel and perpendicular, respectively. The parallel and perpendicular components are referenced to some arbitrary plane, usually the plane of scattering. In general, we can write each component as

$$E_\ell = a_\ell \, e^{-\varepsilon_1} \, e^{-ikz + i\omega t} \tag{66}$$

and

$$E_r = a_r \, e^{-i\varepsilon_2} \, e^{-ikz + i\omega t} \tag{67}$$

where

a_ℓ and a_r are the positive real amplitudes

ε_1 and ε_2 are the phase angles

$k = 2\pi/\lambda$ is the propagation constant

$\omega = 2\pi f$ is the monochromatic angular frequency

Equations (66) and (67) represent a plane wave propagating in the positive z direction. These equations also represent a general elliptically polarized wave. In this study we are using the Stokes parameters to characterize the polarization. The Stokes parameters (I, Q, U, V) are defined as

$$I = E_\ell E_\ell^* + E_r E_r^* \tag{68}$$

$$Q = E_\ell E_\ell^* - E_r E_r^* \tag{69}$$

$$U = E_\ell E_r^* + E_\ell^* E_r \tag{70}$$

$$V = i\left(E_\ell E_r^* - E_\ell^* E_r\right) \tag{71}$$

from (66) and (67) we have

$$E_\ell E_\ell^* = a_\ell^2 \tag{72}$$

$$E_r E_r^* = a_r^2 \tag{73}$$

$$E_\ell E_r^* = a_\ell a_r e^{-i\left(\varepsilon_1 - \varepsilon_2\right)} \tag{74}$$

$$E_\ell^* E_r = a_\ell a_r e^{i\left(\varepsilon_1 - \varepsilon_2\right)} \tag{75}$$

applying equations (72) through (75) to equations (68) through (71) we obtain

$$I = a_\ell^2 + a_r^2 \tag{76}$$

$$Q = a_\ell^2 - a_r^2 \tag{77}$$

$$U = 2a_\ell\, a_r \cos\delta \tag{78}$$

$$V = 2a_\ell\, a_r \sin\delta \tag{79}$$

where

$$\delta = \varepsilon_1 - \varepsilon_2$$

From equations (76) through (79) we see that for parallel polarization ($a_r = 0$)

$$I = a_\ell^2 \tag{80}$$

$$Q = a_\ell^2 \tag{81}$$

$$U = 0 \tag{82}$$

$$V = 0 \tag{83}$$

for perpendicular polarization ($a_\ell = 0$)

$$I = a_r^2 \tag{84}$$

$$Q = -a_r^2 \tag{85}$$

$$U = 0 \tag{86}$$

$$V = 0 \tag{87}$$

For circular polarization, we must define a convention for describing the sense of rotation. For this we use the standard convention which defines right handed polarization with a wave that is viewed traveling away from the observer and whose electric vector rotates in the same direction as a right handed screw. Similarly, left handed polarization is defined with a wave viewed traveling away from the observer and whose electric vector rotates in the opposite direction to that of a right handed screw. Figures 7a and 7b show typical right hand and left hand polarization, respectively.

Now, let us write

$$E_\ell = a_\ell \cos(\omega t - \delta) \tag{88}$$

$$E_r = a_r \cos \omega t \tag{89}$$

If we let $\delta = + \pi/2$, we obtain

$$E_\ell = a_\ell \cos (\omega t - \pi/2) = a_\ell \sin \omega t \tag{90}$$

But, since

$$\vec{E} = \vec{\ell}\, E_\ell + \vec{r}\, E_r = \vec{\ell}\, a_\ell \sin \omega t + \vec{r}\, a_r \cos \omega t \tag{91}$$

this is a general right hand elliptically polarized wave (figure 8). From figure 8 we can also see that if $a_r = a_\ell$ right hand circular (RHC) polarization is obtained. If $\delta = - \pi/2$, equation (88) becomes

$$E_\ell = a_\ell \cos (\omega t + \pi/2) = - a_\ell \sin \omega t \tag{92}$$

and

$$\vec{E} = - \vec{\ell}\, a_\ell \sin \omega t + \vec{r}\, a_r \cos \omega t \tag{93}$$

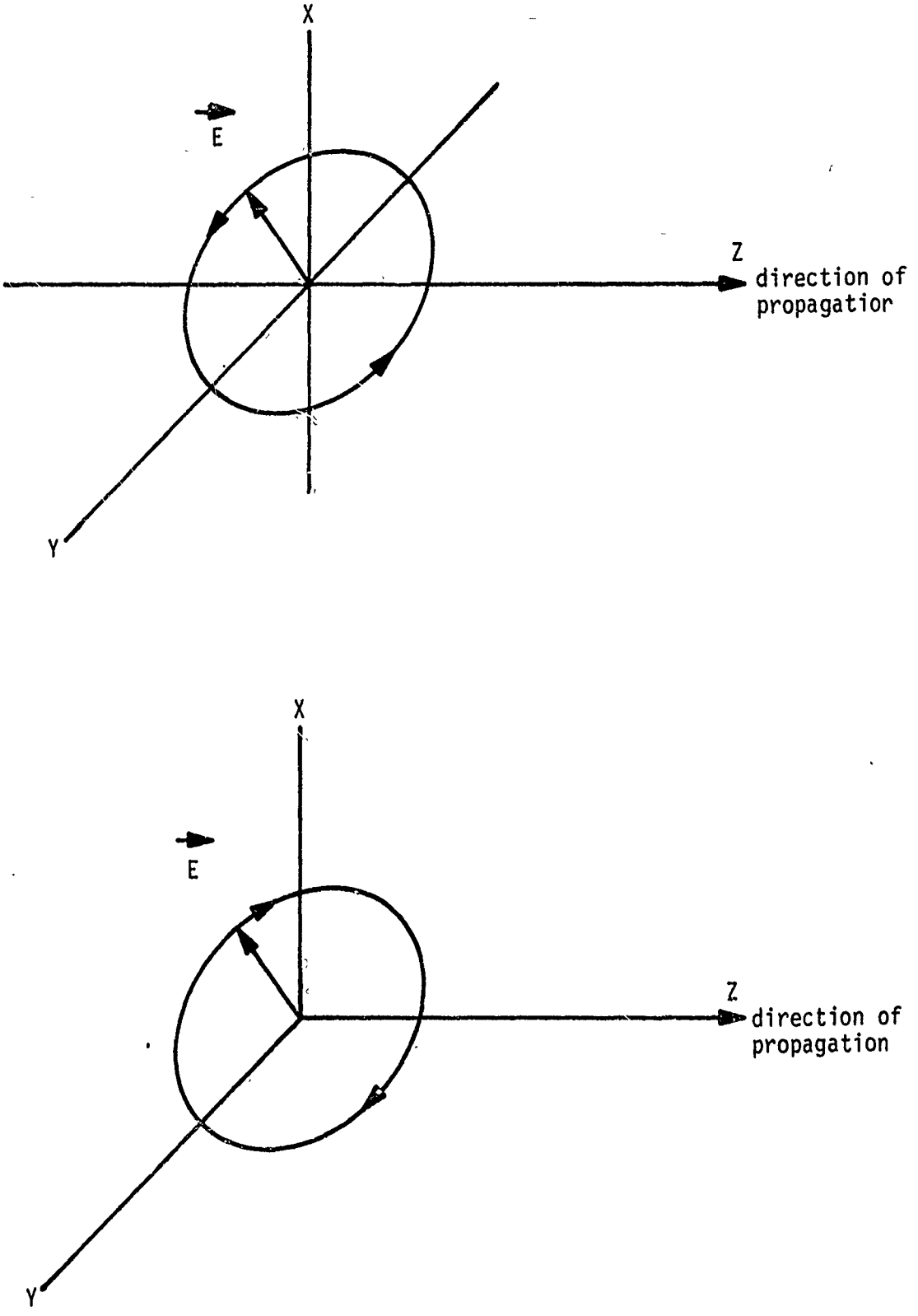

Figure 7. Typical Right and Left Hand Polarization

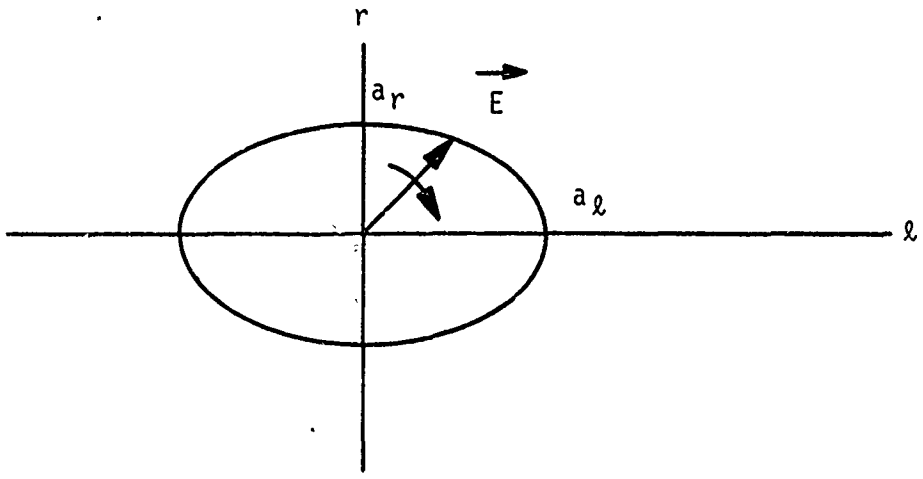

Figure 8. Right Hand Elliptical Polarization

Equation (93) is the general representation of a left hand elliptically polarized wave. Figure 9 shows equation (93) for $a_r = a_\ell = a_0$.

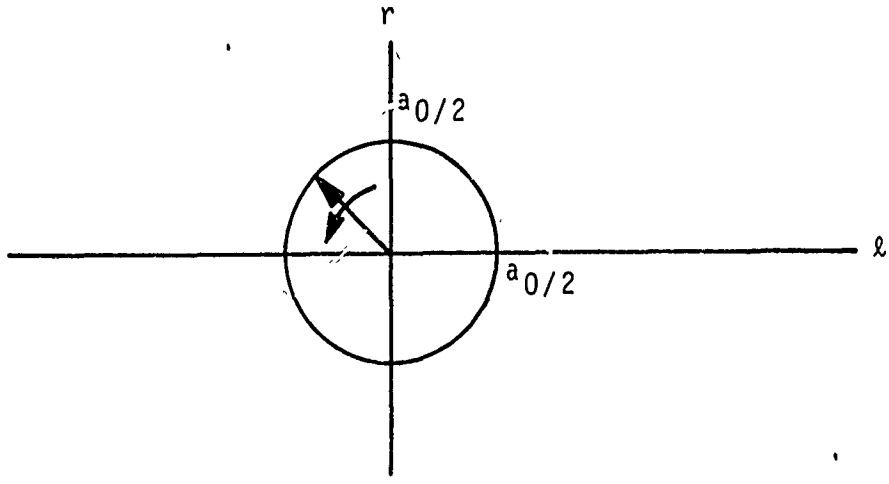

Figure 9. Circular Polarization for $a_r = a_\ell = a_0$

Therefore, letting $\delta = +\pi/2$ and $a_\ell = a_r = a_0$, the Stokes parameters for right hand circular polarization are

$$I = 2a_0^2 \tag{94}$$

$$Q = 0 \tag{95}$$

$$U = 0 \tag{96}$$

$$V = 2a_0^2 \tag{97}$$

Similarly, if $\delta = -\pi/2$ and $a_r = a_\ell = a_0$, the Stokes parameters for left hand circular polarization (LHC) are

$$I = 2a_0^2 \tag{98}$$

$$Q = 0 \tag{99}$$

$$U = 0 \tag{100}$$

$$V = -2a_0^2 \tag{101}$$

If we let

$$I_\ell = a_\ell^2$$

and

$$I_r = a_r^2$$

where I_ℓ and I_r are the intensities for the parallel and perpendicular intensities, respectively, we can rewrite equations (76) through (79) as

$$I = I_\ell + I_r \tag{102}$$

$$Q = I_\ell - I_r \tag{103}$$

$$U = 2\sqrt{I_\ell I_r}\cos\delta \tag{104}$$

$$V = 2\sqrt{I_\ell I_r}\sin\delta \tag{105}$$

A more intuitive representation of the polarization would be to use the set (I_ℓ, I_r, U, V) rather than (I, Q, U, V). This new set of parameters is more pleasing in that the relative size of parallel and perpendicular components can be quickly determined.

Up to this point we have discussed the Stokes polarization parameters for the case where the major and minor axis of the polarization ellipse are along the ℓ and r axes. In general, this may not be true although a simple rotation of axis would realign the axes in the proper orientation. Suppose the axis of the polarization ellipse were rotated by an angle χ (figure 10)

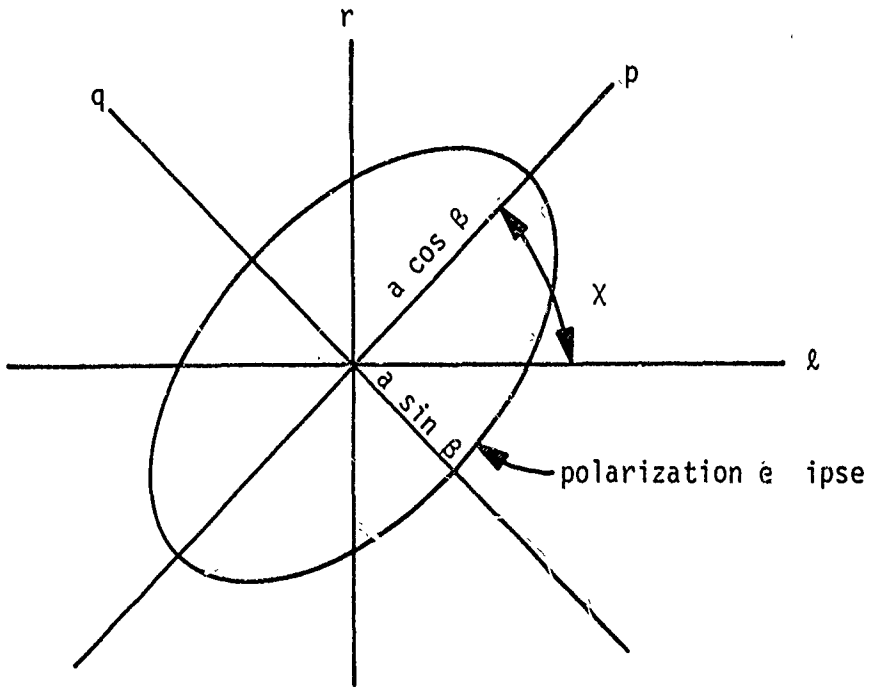

Figure 10. Rotation of Polarization Axis

along the new axes p and q. The electric vector can be written as

$$\vec{E} = a\,\vec{p}\,\cos\beta\,\sin(\omega t - kz) + a\,\vec{q}\,\sin\beta\,\cos(\omega t - kz) \qquad (106)$$

where

$a \cos\beta$ is the amplitude along the p axis

$a \sin\beta$ is the amplitude along the q axis

$\vec{p}$ and $\vec{q}$ are unit vectors

If we let $\beta = 0$ in (106), then

$$\vec{E} = a \vec{p} \sin(\omega t - kz) \tag{107}$$

which is a linearly polarized plane wave. Similarly if $\beta = \pi/4$ we have RHC polarization and if $\beta = -\pi/4$ we have LHC polarization. In general, the ellipticity is given by $\tan\beta$, if it is 0 we have linear polarization, if it is -1 we have LHC polarization and if it is +1 we have RHC polarization. The orientation of the ellipse is given by the angle χ. From figure 10 we have

$$r = p \sin\chi + q \cos\chi \tag{108}$$

$$\ell = p \cos\chi - q \sin\chi \tag{109}$$

Rewriting equations (66) and (67)

$$E_\ell = a_\ell e^{-i\varepsilon_1} e^{-ikz + i\omega t} \tag{66}$$

$$E_r = a_r e^{-i\varepsilon_2} e^{-ikz + i\omega t} \tag{67}$$

we have that

$$\vec{E} = \mathrm{Re}\left(E_\ell \vec{\ell} + E_r \vec{r}\right) \tag{110}$$

Substituting (66) and (67) into (110) results in

$$\vec{E} = \vec{\ell} a_\ell \cos(\omega t - kz - \varepsilon_1) + \vec{r}\, a_r \cos(\omega t - kz - \varepsilon_2) \tag{111}$$

Upon equating equations (106) and (111), introducing equations (108) and (109), and equating like terms we have

$$a_\ell \cos(\omega t - kz - \varepsilon_1) = a \cos\beta \cos\chi \sin(\omega t - kz) - a \sin\beta \sin\chi \cos(\omega t - kz) \tag{112}$$

$$a_r \cos(\omega t - kz - \varepsilon_2) = a \cos\beta \sin\chi \sin(\omega t - kz) + a \sin\beta \cos\chi \cos(\omega t - kz) \tag{113}$$

We can now apply the relations

$$A \cos\theta + B \sin\theta = \sqrt{A^2+B^2} \cos\left(\theta - \tan^{-1}\frac{B}{A}\right) \tag{114}$$

and

$$A \sin\theta - B \cos\theta = \sqrt{A^2+B^2} \cos\left(\theta + \tan^{-1}\frac{A}{B}\right) \tag{115}$$

to the right hand side of equations (112) and (113) as follows

$$a_\ell \cos(\omega t - kz - \varepsilon_1) = a \sqrt{\cos^2\beta \cos^2\chi + \sin^2\beta \sin^2\chi} \cos\left(\omega t - kz + \tan^{-1}\frac{\cos\beta \cos\chi}{\sin\beta \sin\chi}\right) \tag{116}$$

$$a_r \cos(\omega t - kz - \varepsilon_2) = a \sqrt{\cos^2\beta \sin^2\chi + \sin^2\beta \cos^2\chi} \cos\left(\omega t - kz - \tan^{-1}\frac{\cos\beta \sin\chi}{\sin\beta \cos\chi}\right) \tag{117}$$

so that

$$a_\ell^2 = a^2 (\cos^2\beta \cos^2\chi + \sin^2\beta \sin^2\chi) \tag{118}$$

$$a_r^2 = a^2 (\cos^2\beta \sin^2\chi + \sin^2\beta \cos^2\chi) \tag{119}$$

and

$$\tan \varepsilon_1 = - \cot \beta \cot \chi \tag{120}$$

$$\tan \varepsilon_2 = \cot \beta \tan \chi \tag{121}$$

or since

$$\varepsilon_1 - \varepsilon_2 = \delta = -\tan^{-1}(\cot \beta \cot \chi) - \tan^{-1}(\cot \beta \tan \chi) \tag{122}$$

we have that

$$\tan \delta = - \frac{\tan\left[\tan^{-1}(\cot \beta \cot \chi)\right] + \tan\left[\tan^{-1}(\cot \beta \tan \chi)\right]}{1 - \tan\left[\tan^{-1}(\cot \beta \cot \chi)\right] \tan\left[\tan^{-1}(\cot \beta \tan \chi)\right]}$$

$$= \frac{\cot \beta \cot \chi + \cot \beta \tan \chi}{\cot^2 \beta - 1}$$

$$= \frac{1}{\cot 2 \beta} \cdot \frac{\tan^2 \chi + 1}{2 \tan \chi}$$

$$= \frac{\tan 2 \beta}{\sin 2 \chi} \tag{123}$$

Using equations (118), (119), and (123), the Stokes parameters become

$$I = a_\ell^2 + a_r^2 = a^2 \tag{124}$$

$$Q = a_\ell^2 - a_r^2 = a^2 \cos 2 \beta \cos 2 \chi \tag{125}$$

$$U = 2a_\ell a_r \cos \delta = 2a^2(\cos^2 \beta \cos^2 \chi + \sin^2 \beta \sin^2 \chi)^{1/2}$$
$$(\cos^2 \beta \sin^2 \chi + \sin^2 \beta \cos^2 \chi)\cos \delta$$

To obtain cos δ we use equation (123) and figure 11.

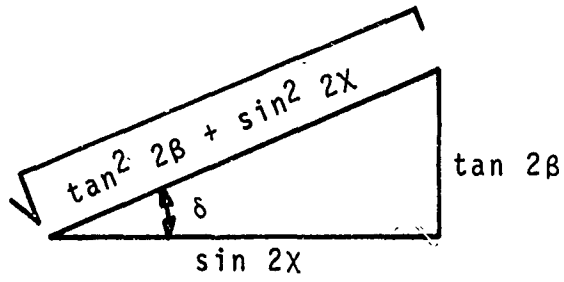

Figure 11. Triangle for Deriving Cos δ

Therefore, we have

$$\cos \delta = \frac{\sin 2\chi}{\sqrt{\tan^2 2\beta + \sin^2 2\chi}}$$

and using straightforward algebra

$$U = a^2 \sin 2\chi \cos 2\beta \tag{126}$$

Again from figure 11 we obtain

$$\sin \delta = \frac{\tan 2\beta}{\sqrt{\tan^2 2\beta + \sin^2 2\chi}}$$

and

$$V = a^2 \sin 2\beta \tag{127}$$

Equations (124) through (127) lead us to another way of describing the polarization state of an electromagnetic wave, namely through the use of the Poincaré Sphere.

For convenience we now rewrite equations (124) through (127)

$$I = a^2 \tag{128}$$

$$Q = a^2 \cos 2\beta \cos 2\chi \tag{129}$$

$$U = a^2 \cos 2\beta \sin 2\chi \tag{130}$$

$$V = a^2 \sin 2\beta \tag{131}$$

If P is any point on a sphere (see figure 12) it can be described by the parameters (I, Q, U, V).

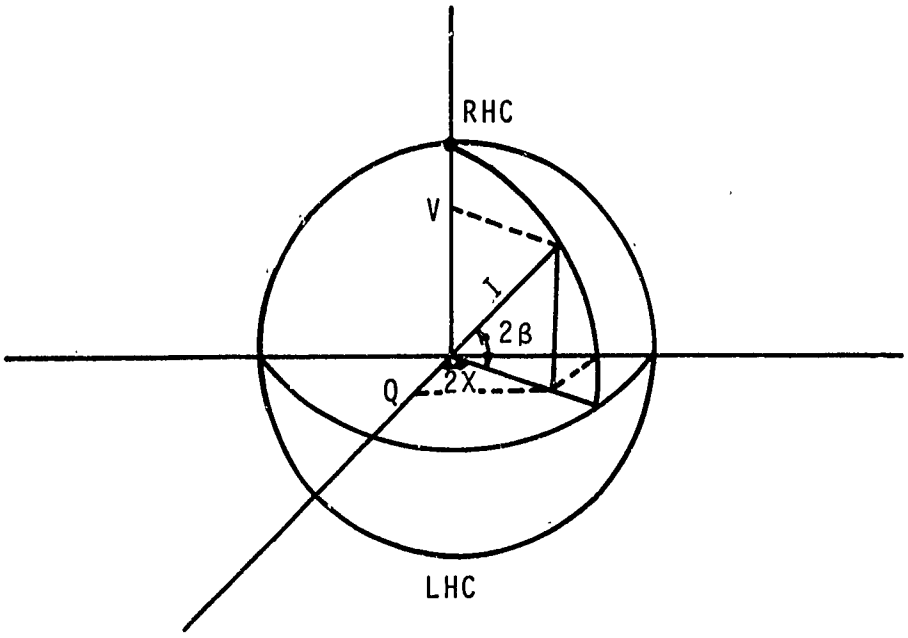

Figure 12. Representation of the Polarization Parameters with the Poincaré Sphere

Comparing equations (124) through (127) with equations (94) through (97) we can see that if $2\beta = \pi/2$ we obtain right hand circular polarization; this is the north pole of the sphere. Comparing equations (128) through (131) with equations (98) through (101) and letting $2\beta = -\pi/2$ we obtain left hand circular polarization; this is the south pole of the sphere. If $2\beta = 2\chi = 0$, we get parallel polarization; for $2\beta = 0$ and $2\chi = \pi$, we get perpendicular polarization. In general, the upper hemisphere yields right handed elliptical polarization, the lower hemisphere yields left handed elliptical polarization, and the equator yields linear polarization. The total intensity is given by the magnitude of the radius vector. Shurcliff [21] discusses the graphical mapping of one polarization state to another through the use of the Poincaré Sphere.

3. RESOLUTION OF A GENERAL ELLIPTICALLY POLARIZED WAVE INTO RHC AND LHC COMPONENTS

According to the previous subsection, an elliptically polarized wave may always be resolved into a perpendicular polarization component and a parallel polarization component with a phase difference between them. In like manner, an elliptically polarized wave can be resolved into an RHC component and an LHC component. This latter representation yields more information than the former because the phase difference is automatically included. In this subsection, a general elliptically polarized wave will be resolved into its RHC and LHC components.

Consider a polarized wave of the form

$$\vec{E} = \vec{\ell}\, E_\ell + \vec{r}\, E_r \tag{65}$$

as before, with

$$E_\ell = a_\ell \cos \omega t \tag{132}$$

$$E_r = a_r \cos (\omega t - \delta) \tag{133}$$

Each component, E_ℓ and E_r, may be individually resolved into RHC and LHC components, i.e.,

$$\vec{\ell}\, E_\ell = \vec{E}_{\ell RHC} + \vec{E}_{\ell LHC} \tag{134}$$

with

$$\vec{E}_{\ell RHC} = \frac{a_\ell}{2} (\vec{\ell} \cos \omega t - \vec{r} \sin \omega t) \tag{135}$$

$$\vec{E}_{\ell LHC} = \frac{a_\ell}{2} (\vec{\ell} \cos \omega t + \vec{r} \sin \omega t) \tag{136}$$

While for the perpendicular component

$$\vec{r}E_r = \vec{E}_{rRHC} + \vec{E}_{rLHC} \tag{137}$$

where

$$\vec{E}_{rRHC} = \frac{a_r}{2}\left[\vec{\ell} \sin(\omega t-\delta) + \vec{r} \cos(\omega t-\delta)\right] \tag{138}$$

$$\vec{E}_{rLHC} = \frac{a_r}{2}\left[-\vec{\ell} \sin(\omega t-\delta) + \vec{r} \cos(\omega t-\delta)\right] \tag{139}$$

Therefore, from equations (65), (134), and (137)

$$\vec{E} = \left(\vec{E}_{\ell RHC} + \vec{E}_{\ell LHC}\right) + \left(\vec{E}_{rRHC} + \vec{E}_{rLHC}\right) \tag{140}$$

or

$$\vec{E} = \left(\vec{E}_{\ell RHC} + \vec{E}_{rRHC}\right) + \left(\vec{E}_{\ell LHC} + \vec{E}_{rLHC}\right) \tag{141}$$

letting

$$\vec{E}_{RHC} = \vec{E}_{\ell RHC} + \vec{E}_{rLHC} \tag{142}$$

and

$$\vec{E}_{LHC} = \vec{E}_{\ell LHC} + \vec{E}_{rLHC} \tag{143}$$

we arrive at

$$\vec{E} = \vec{E}_{RHC} + \vec{E}_{LHC} \tag{144}$$

Substituting equations (135), (136), (138), and (139) into (144) and writing the RHC and LHC components separately we have

$$\vec{E}_{RHC} = \frac{a_\ell}{2}\left[\vec{\ell}\cos\omega t - \vec{r}\sin\omega t\right]$$

$$+ \frac{a_r}{2}\left[\vec{\ell}\sin(\omega t - \delta) + \vec{r}\cos(\omega t - \delta)\right]$$

$$= 1/2\,\vec{\ell}\left[a_\ell\cos\omega t + a_r\sin(\omega t - \delta)\right]$$

$$+ 1/2\,\vec{r}\left[-a_\ell\sin\omega t + a_r\cos(\omega t - \delta)\right] \qquad (145)$$

and

$$\vec{E}_{LHC} = \frac{a_\ell}{2}\left[\vec{\ell}\cos\omega t + \vec{r}\sin\omega t\right]$$

$$+ \frac{a_r}{2}\left[-\vec{\ell}\sin(\omega t - \delta) + \vec{r}\cos(\omega t - \delta)\right]$$

$$= 1/2\,\vec{\ell}\left[a_\ell\cos\omega t - a_r\sin(\omega t - \delta)\right]$$

$$+ 1/2\,\vec{r}\left[a_\ell\sin\omega t + a_r\cos(\omega t - \delta)\right] \qquad (146)$$

For (145) and (146) we can write

$$\sin(\omega t - \delta) = \sin\omega t\cos\delta - \cos\omega t\sin\delta \qquad (147)$$

and

$$\cos(\omega t - \delta) = \cos\omega t\cos\delta + \sin\omega t\sin\delta \qquad (148)$$

Substituting (147) and (148) into (145) and (146) we obtain

$$\vec{E}_{RHC} = 1/2\,\vec{\ell}\left[(a_\ell - a_r\sin\delta)\cos\omega t + a_r\cos\delta\sin\omega t\right]$$

$$+ 1/2\,\vec{r}\left[-(a_\ell - a_r\sin\delta)\sin\omega t + a_r\cos\delta\cos\omega t\right] \qquad (149)$$

and

$$\vec{E}_{LHC} = 1/2\ \vec{\ell}\left[(a_\ell + a_r \sin\delta)\cos\omega t - a_r \cos\delta \sin\omega t\right]$$

$$+ 1/2\ \vec{r}\left[(a_\ell + a_r \sin\delta)\sin\omega t + a_r \cos\delta \cos\omega t\right] \quad (150)$$

Now, equations (149) and (150) are of the form

$$A\cos\omega t + B\sin\omega t = \sqrt{A^2 + B^2}\cos\left(\omega t - \tan^{-1}\frac{B}{A}\right) \quad (151)$$

and may be written in this form as follows:

$$\vec{E}_{RHC} = 1/2\ \vec{\ell}\sqrt{(a_\ell - a_r \sin\delta)^2 + (a_r \cos\delta)^2}$$

$$\cos\left(\omega t - \tan^{-1}\frac{a_r \cos\delta}{a_\ell - a_r \sin\delta}\right)$$

$$+ 1/2\ \vec{r}\sqrt{(a_\ell - a_r \sin\delta)^2 + (a_r \cos\delta)^2}$$

$$\cos\left(\omega t + \tan^{-1}\frac{a_\ell - a_r \sin\delta}{a_r \cos\delta}\right) \quad (152)$$

$$\vec{E}_{LHC} = 1/2\ \vec{\ell}\sqrt{(a_\ell + a_r \sin\delta)^2 + (a_r \cos\delta)^2}$$

$$\cos\left(\omega t + \tan^{-1}\frac{a_r \cos\delta}{a_\ell\ a_r \sin\delta}\right)$$

$$+ 1/2\ \vec{r}\sqrt{(a_\ell + a_r \sin\delta) + (a_r \cos\delta)^2}$$

$$\cos\left(\omega t - \tan^{-1}\frac{a_\ell + a_r \sin\delta}{a_r \cos\delta}\right) \quad (153)$$

Furthermore we may write from equation (152)

$$\phi_{\ell RHC} = \tan^{-1} \frac{a_r \cos \delta}{a_\ell - a_r \sin \delta} \tag{154}$$

$$\phi_{rRHC} = \tan^{-1} \frac{a_\ell - a_r \sin \delta}{a_r \cos \delta} \tag{155}$$

with

$$\phi_{\ell RHC} = \pi/2 - \phi_{rRHC} \tag{156}$$

(see figure 13).

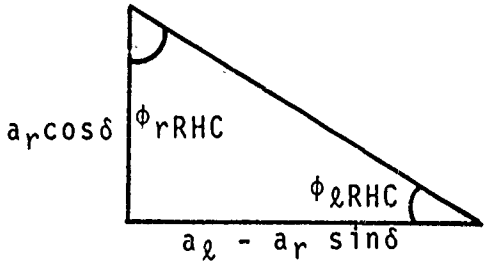

Figure 13. Triangle for Deriving ϕ_{rRHC} and $\phi_{\ell RHC}$

Similarly, from equation (153)

$$\phi_{\ell LHC} = \tan^{-1} \frac{a_r \cos \delta}{a_\ell + a_r \sin \delta} \tag{157}$$

$$\phi_{rLHC} = \tan^{-1} \frac{a_\ell + a_r \sin \delta}{a_r \cos \delta} \tag{158}$$

with

$$\phi_{\ell LHC} = \pi/2 - \phi_{rLHC} \tag{159}$$

(see figure 14).

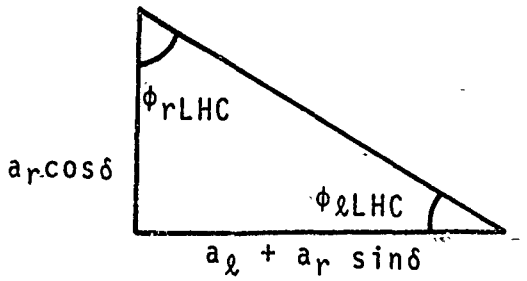

Figure 14. Triangle for Deriving ϕ_{rLHC} and $\phi_{\ell LHC}$

Using equations (154) through (159) and carrying out the squaring of the terms under the radicals equations (152) and (153) become

$$\vec{E}_{RHC} = 1/2 \sqrt{a_\ell^2 - 2a_\ell\, a_r \sin\delta + a_r^2}$$

$$\left[\vec{\ell} \cos\left(\omega t - \phi_{\ell RHC}\right) + \vec{r} \cos\left(\omega t - \phi_{\ell RHC} + \pi/2\right)\right]$$

$$\vec{E}_{LHC} = 1/2 \sqrt{a_\ell^2 + 2a_\ell\, a_r \sin\delta + a_r^2}$$

$$\left[\vec{\ell} \cos\left(\omega t + \phi_{\ell LHC}\right) + \vec{r} \cos\left(\omega t + \phi_{\ell LHC} - \pi/2\right)\right]$$

but

$$\cos\left(\omega t - \phi_{\ell RHC} + \pi/2\right) = -\sin\left(\omega t - \phi_{\ell RHC}\right)$$

and

$$\cos\left(\omega t + \phi_{\ell LHC} - \pi/2\right) = +\sin\left(\omega t + \phi_{\ell LHC}\right)$$

therefore,

$$\vec{E}_{RHC} = 1/2 \sqrt{a_\ell^2 + 2a_\ell\, a_r \sin\delta + a_r^2}$$

$$\left[\vec{\ell} \cos\left(\omega t - \phi_{\ell RHC}\right) - \vec{r} \sin\left(\omega t - \phi_{\ell RHC}\right)\right] \qquad (160)$$

$$\vec{E}_{LHC} = 1/2 \sqrt{a_\ell^2 + 2a_\ell a_r \sin \delta + a_r^2}$$

$$\left[\vec{\ell} \cos \left(\omega t + \phi_{\ell LHC}\right) + \vec{r} \sin \left(\omega t + \phi_{\ell LHC}\right)\right] \qquad (161)$$

The phase difference is

$$\Phi = \phi_{\ell RHC} + \phi_{\ell LHC} = \tan^{-1} \frac{a_r \cos \delta}{a_\ell - a_r \sin \delta} + \tan^{-1} \frac{a_r \cos \delta}{a_\ell + a_r \sin \delta}$$

which, when using the identity

$$\tan^{-1} x + \tan^{-1} y = \tan^{-1}\left(\frac{x + y}{1 - xy}\right)$$

becomes

$$\Phi = \tan^{-1}\left(\frac{2a_\ell a_r \cos \delta}{a_\ell^2 - a_r^2}\right) \qquad (162)$$

Equations (160) through (162) constitute the RHC and LHC components of a general elliptically polarized wave. Note that Φ is defined only when the wave is not circularly polarized. When the wave is circularly polarized, either the RHC or LHC component will be zero and Φ will not be defined. That this is true can be seen by letting $a_\ell = a_r$ and $\delta = \pm \pi/2$ simultaneously as is required for circular polarization.

4. DEPOLARIZATION AND POLARIZATION FACTORS

In this study, depolarization will be defined as the change in polarization state which includes the completely depolarized state as natural light. The definition of natural or unpolarized light is taken from Chandrasekhar [9]:

> Natural light is equivalent to any two independent oppositely polarized streams of half the intensity; and no two independent polarized streams can together be equivalent to natural light unless they be oppositely polarized and of equal intensity.

Experimentally, if natural light is resolved in any direction in the transverse plane, the measured intensity is the same. The necessary and sufficient condition for light to be natural is that

$$Q = U = V = 0 \tag{163}$$

A theorm due to Stokes [22] states that the most general mixture of light can be regarded as a mixture of an elliptically polarized wave and an independent wave of natural light.

From equations (68) through (71) we can show that

$$I^2 = Q^2 + U^2 + V^2 \tag{164}$$

But, for the most general representation we can write

$$I^2 \geq Q^2 + U^2 + V^2 \tag{165}$$

since Stokes theorem says we can write the Stokes parameters as

$$I = I_\ell + I_r + I_n \tag{166}$$

$$Q = I_\ell - I_r \tag{167}$$

$$U = 2\sqrt{I_\ell I_r}\cos\delta \tag{168}$$

$$V = 2\sqrt{I_\ell I_r}\sin\delta \tag{169}$$

Where I_n is the intensity for natural light. The degree of polarization of a wave is defined as [9]

$$P = \frac{\sqrt{Q^2 + U^2 + V^2}}{I} \tag{170}$$

and from equation (165) it follows that

$$0 \leq P \leq 1 \tag{171}$$

When $P = 1$ the wave is said to be completely polarized; when $P = 0$ the wave is said to be completely unpolarized (natural light). In general

$$0 < P < 1 \tag{172}$$

and the wave is partially polarized.

In this study, we will be dealing with the transmission of completely polarized ($P = 1$) or completely unpolarized light through model atmospheres. We will be interested in the affect of scattering on the polarization properties of the transmitted wave. Comparisons with natural or unpolarized light will be made. It will further be assumed that due t the randomness of the particle distribution in the atmosphere, the intensities of the individual scattering events can be summed at the detector, the transmitted energy will be monochromatic, and the individual scattering particles are located far enough from each other such that the far zone approxi .tion may be used.

Since we are interested in the degree of depolarization, i.e., the amount of cross-polarized component produced by scattering of a polarized wave in the atmosphere, therefore, in an effort to provide qualitative results and for comparison of various cases, we will introduce the polarization factors. For linearly polarized and unpolarized transmitted waves, we will use

$$D_L = \frac{I_r - I_\ell}{I_r + I_\ell} \tag{173}$$

while for circularly polarized transmitted waves we will use

$$D_C = \frac{I_{RHC} - I_{LHC}}{I_{RHC} + I_{LHC}} \tag{174}$$

The sign of either D_L or D_C will indicate the amount of each component contained in the detected wave. The only problem which may arise will be for $D_L = 0$; this will mean that $I_r = I_\ell$ which may happen for unpolarized or for circularly polarized waves. For the type of problem being studied here, the U and V parameters are always small and circular polarization will not result for a transmitted unpolarized wave.

5. MIE AND RAYLEIGH SCATTERING

In general, the scattered components of the electric field are given by [14]

$$\begin{pmatrix} E_\ell^s \\ E_r^s \end{pmatrix} = \begin{pmatrix} S_2 & S_3 \\ S_4 & S_1 \end{pmatrix} \frac{e^{-ikr + ikz}}{ikr} \begin{pmatrix} E_\ell^i \\ E_r^i \end{pmatrix} \tag{175}$$

where the incident field is a monochromatic plane wave propagating in the positive z direction with components

$$\begin{pmatrix} E_\ell^i \\ E_r^i \end{pmatrix} = \begin{pmatrix} E_{\ell 0} \\ E_{r0} \end{pmatrix} e^{-ikz + i\omega t} \tag{176}$$

and the S_i elements are scattering functions which depend on the material properties and orientation of the scatterer.

A transformation matrix can also be defined [9] for the Stokes parameters,

$$\begin{pmatrix} I \\ Q \\ U \\ V \end{pmatrix} = \mathbf{F} \begin{pmatrix} I_0 \\ Q_0 \\ U_0 \\ V_0 \end{pmatrix} \tag{177}$$

or

$$\begin{pmatrix} I_\ell \\ I_r \\ U \\ V \end{pmatrix} = \tilde{\mathbf{F}} \begin{pmatrix} I_{\ell 0} \\ I_{r0} \\ U_0 \\ V_0 \end{pmatrix} \tag{178}$$

where $\mathbf{F}$ and $\tilde{\mathbf{F}}$ are 4 x 4 matrixes and are given by (see appendix)

$$\mathbf{F} = \begin{pmatrix} 1/2(M_1 + M_2), & 1/2(-M_1 + M_2), & 0, & 0 \\ 1/2(-M_1 + M_2), & 1/2(M_1 + M_2), & 0, & 0 \\ 0, & 0, & S_{21}, & -D_{21} \\ 0, & 0, & D_{21}, & S_{21} \end{pmatrix} \tag{179}$$

and

$$\tilde{\mathbf{F}} = \begin{pmatrix} M_2, & 0, & 0, & 0 \\ 0, & M_1, & 0, & 0 \\ 0, & 0, & S_{21}, & -D_{21} \\ 0, & 0, & D_{21}, & S_{21} \end{pmatrix} \tag{180}$$

The derivation of (178) and (179) in the appendix used the fact that for a spherical scatterer $A_3 = A_4 = 0$. This is equivalent to

setting $S_3 = S_4 = 0$ in equation (175). Therefore, we can write

$$\begin{pmatrix} E_\ell^s \\ E_r^s \end{pmatrix} = \begin{pmatrix} S_2 & 0 \\ 0 & S_1 \end{pmatrix} \frac{e^{-ikr + ikz}}{ikr} \begin{pmatrix} E_\ell^i \\ E_r^i \end{pmatrix} \tag{181}$$

Furthermore, from (180), we know that

$$M_1 = A_1 A_1^* = |A_1|^2 \tag{182}$$

$$M_2 = A_2 A_2^* = |A_2|^2 \tag{183}$$

$$S_{21} = 1/2(A_1 A_2^* + A_1^* A_2) \tag{184}$$

$$D_{21} = -\frac{i}{2}(A_1 A_2^* - A_1^* A_2) \tag{185}$$

Also, comparing (175) with (2) from the appendix, we obtain

$$A_1 = S_1 \frac{e^{-ikr + ikz}}{ikr} \tag{186}$$

$$A_2 = S_2 \frac{e^{ikr + ikz}}{ikr} \tag{187}$$

so that

$$|A_1|^2 = \frac{1}{k^2 r^2} |S_1|^2 \tag{188}$$

$$|A_2|^2 = \frac{1}{k^2 r^2} |S_2|^2 \tag{189}$$

$$S_{21} = \frac{1}{2k^2 r^2}(S_1 S_2^* + S_1^* S_2) \tag{190}$$

$$D_{21} = -\frac{i}{2k^2 r^2}(S_1 S_2^* - S_1^* S_2) \tag{191}$$

In general S_1 and S_2 will be complex:

$$S_1 = s_1 e^{i\sigma_1} \tag{192}$$

$$S_2 = s_2 e^{i\sigma_2} \tag{193}$$

where s_1 and s_2 are real amplitudes and σ_1 and σ_2 are real phases, therefore

$$|A_1|^2 = \frac{s_1^2}{k^2 r^2} \tag{194}$$

$$|A_2|^2 = \frac{s_2^2}{k^2 r^2} \tag{195}$$

$$S_{21} = \frac{s_1 s_2}{k^2 r^2} \cos(\sigma_1 - \sigma_2) \tag{196}$$

$$D_{21} = \frac{s_1 s_2}{k^2 r^2} \sin(\sigma_1 - \sigma_2) \tag{197}$$

Substituting equations (188) through (191) into equation (180) results in the phase matrix

$$\tilde{F} = \frac{1}{k^2 r^2} \begin{pmatrix} |S_2|^2 & 0 & 0 & 0 \\ 0 & |S_1|^2 & 0 & 0 \\ 0 & 0 & \mathrm{Re}(S_1 S_2^*) & -\mathrm{Im}(S_1 S_2^*) \\ 0 & 0 & \mathrm{Im}(S_1 S_2^*) & \mathrm{Re}(S_1 S_2^*) \end{pmatrix} \tag{198}$$

with $S_1 = S_1(\theta)$ and $S_2 = S_2(\theta)$ functions of the polar angle. Note that, according to (198), if the incident wave is linearly polarized in the plane of scatter the scattered wave will also be linearly polarized; this agrees with the Mie theory [7].

All scatterers treated in this study are spherical and (198) will play an important role in the results. From the theory of Mie, we have that

$$S_1(\theta) = \sum_{n=1}^{\infty} \frac{2n+1}{n(n+1)} \cdot \left[a_n \pi_n(\cos\theta) + b_n \tau_n(\cos\theta) \right] \tag{199}$$

and

$$S_2(\theta) = \sum_{n=1}^{\infty} \frac{2n+1}{n(n+1)} \cdot \left[b_n \pi_n(\cos\theta) + a_n \tau_n(\cos\theta) \right] \tag{200}$$

The detailed definition of τ_n, π_n, a_n, and b_n is postponed until the next section.

The phase matrix for Rayleigh scattering is

$$R = 3/2 \begin{pmatrix} \cos^2\theta & 0 & 0 & 0 \\ 0 & 1 & 0 & 0 \\ 0 & 0 & \cos\theta & 0 \\ 0 & 0 & 0 & \cos\theta \end{pmatrix} \tag{201}$$

Equations (198) and (201) apply only when the Stokes parameters are referred to the plane of scatter. In general, the incident wave's Stokes parameters will not be referred to the plane of scatter, therefore it will be necessary to rotate the incident Stokes parameters into the plane of scatter [9]. Referring to equations (128) through (131), it is clear that the I and V parameters are invarient to a rotation of axes. If we rotate the axes by an angle ϕ in the

clockwise direction (figure 10) then

$$Q' = a^2 \cos 2\beta \cos 2(\chi - \phi) \tag{202}$$

and

$$U' = a^2 \cos 2\beta \sin 2(\chi - \phi) \tag{203}$$

Expanding (202) and (203) we obtain

$$Q' = Q \cos 2\phi + U \sin 2\phi \tag{204}$$

and

$$U' = -Q \sin 2\phi + U \cos 2\phi \tag{205}$$

But, we also have that

$$I' = I'_\ell + I'_r = I_\ell + I_r \tag{206}$$

$$V' = V \tag{207}$$

$$Q' = I'_\ell - I'_r = (I_\ell - I_r) \cos 2\phi + U \sin 2\phi \tag{208}$$

$$U' = -(I_\ell - I_r) \sin 2\phi + U \cos 2\phi \tag{209}$$

and solving for I'_ℓ and I'_r we have

$$I'_\ell = 1/2\, I_\ell (1+\cos 2\phi) + 1/2\, I_r (1-\cos 2\phi) + 1/2\, U \sin 2\phi$$

$$= I_\ell \cos^2 \phi + I_r \sin^2 \phi + 1/2\, U \sin 2\phi \tag{210}$$

$$I'_r = 1/2\, I_\ell (1-\cos 2\phi) + 1/2\, I_r (1+\cos 2\phi) - 1/2 \sin 2\phi$$

$$= I_\ell \sin^2 \phi + I_r \cos^2 \phi - 1/2 \sin 2\phi \tag{211}$$

The transformation law for a rotation of axes is therefore

$$\begin{pmatrix} I_\ell' \\ I_r' \\ U' \\ V' \end{pmatrix} = \begin{pmatrix} \cos^2\phi & \sin^2\phi & 1/2 \sin 2\phi & 0 \\ \sin^2\phi & \cos^2\phi & -1/2 \sin 2\phi & 0 \\ -\sin 2\phi & \sin 2\phi & \cos 2\phi & 0 \\ 0 & 0 & 0 & 1 \end{pmatrix} \begin{pmatrix} I_\ell \\ I_r \\ U \\ V \end{pmatrix} \tag{212}$$

Prior to applying the scattering matrix, (198) or (201), the incident Stokes parameters must be rotated into the plane of scatter according to (212) and rotated back into a reference plane if desired after application of (198) or (201). Let us write

$$L(\phi) = \begin{pmatrix} \cos^2\phi & \sin^2\phi & 1/2 \sin 2\phi & 0 \\ \sin^2\phi & \cos^2\phi & -1/2 \sin 2\phi & 0 \\ -\sin 2\phi & \sin 2\phi & \cos 2\phi & 0 \\ 0 & 0 & 0 & 1 \end{pmatrix} \tag{213}$$

as the transformation matrix for rotation in the clockwise direction then $L(-\phi)$ is the transformation matrix for rotation in the counter-clockwise direction.

The contribution to the source function due to scattering of a pencil beam of radiation of solid angle $d\omega'$ in the direction (θ', ϕ') is

$$RI \frac{d\omega'}{4\pi} \tag{214}$$

for Rayleigh scattering and

$$FI \frac{d\omega'}{4\pi} \tag{215}$$

for Mie scattering if $\mathbf{I}(\theta', \phi')$ is referred to the directions parallel and perpendicular to the plane of scattering. In general, $\mathbf{I}(\theta', \phi')$ is not referred to the scattering plane and we must therefore rotate the incident polarization components into the plane of scatter. Suppose that $\mathbf{I}(\theta', \phi')$ is referred to directions along the meridian plane OBA in figure 15 and at right angles to it. We use equation (213) to transform $\mathbf{I}(\theta', \phi')$ into the plane of scatter, and therefore, the contribution to the source function is

$$R(\cos\Theta)\, L(-\beta_1)\, \mathbf{I}(\theta', \phi')\, \frac{d\omega'}{4\pi} \qquad (216)$$

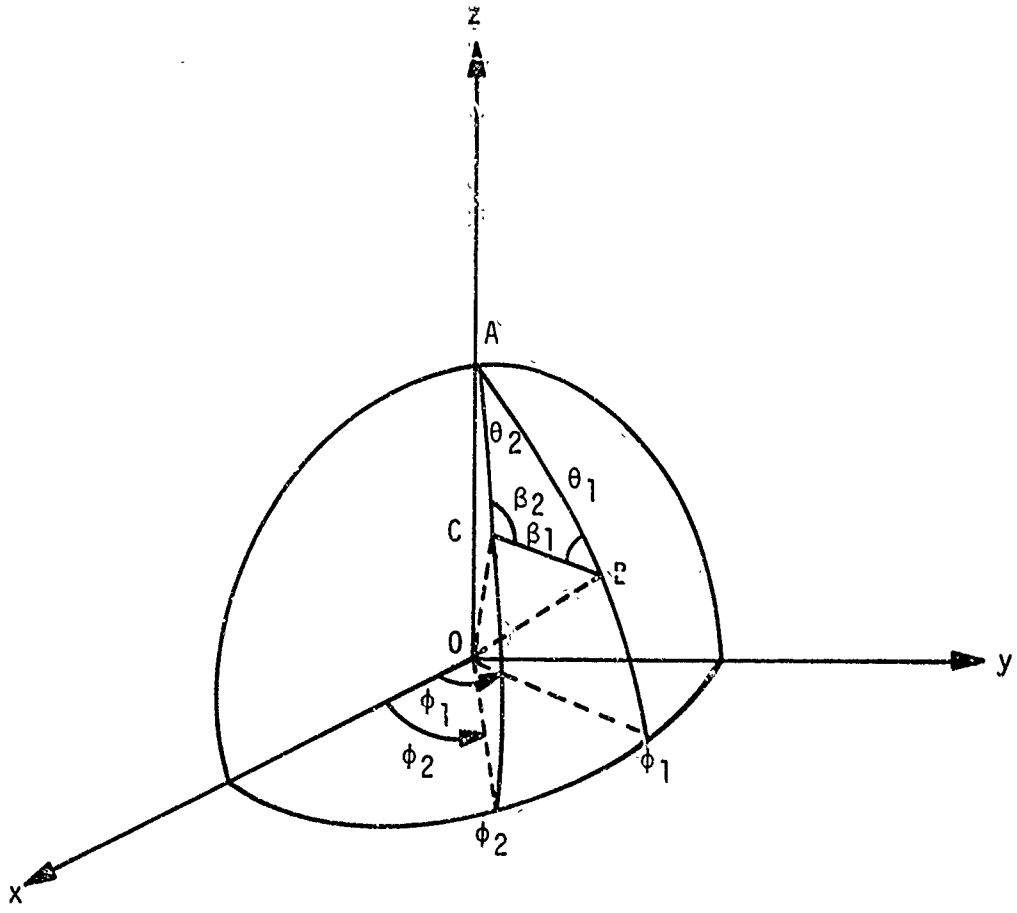

Figure 15 Polarization Reference Planes

We can then transform the Stokes parameters back into the reference plane by once again applying the transformation matrix such that

$$L(\pi - \beta_2)\ R(\cos\Theta)\ L(-\beta_1)\ I(\theta', \phi')\ \frac{d\omega'}{4\pi} \tag{217}$$

is the scattered contribution except that now the Stokes parameters are referred to the plane OCA.

If we now assume the several scattering events occur successively, that contribution due to scattering would be

$$L_n(\pi - \beta_{2n}) \cdots L_1(\pi - \beta_2)\ R(\cos\Theta)\ L_1(-\beta_1) \cdots$$
$$L_n(-\beta_n)\ I(\theta', \phi')\ \frac{d\omega'}{4\pi} \tag{218}$$

where n such scattering events occur. If Mie scattering were taking place rather than Rayleigh scattering one would simply use the scattering function F rather than R .

In this section we have shown how scattering affects the polarization properties of the incident intensity and have derived the scattering matrixes for Mie and Rayleigh scattering. These ideas will be used in the modeling of scattering of electromagnetic radiation in the atmosphere.

SECTION IV

COMPUTER SIMULATION

1. INTRODUCTION

A Monte Carlo computer simulation of electromagnetic scattering in the atmosphere, similar to those proposed by Kattawar and Plass [16] and Collins and Wells [20], is used to predict the degree of depolarization of an incident polarized electromagnetic wave. Basically, the computer program is a simulation of the equation of radiative propagation in the atmosphere as derived in section II. The atmosphere is composed of a random distribution of particles of different sizes; those which are much smaller than one wavelength are called Rayleigh particles since they follow the λ^{-4} scattering law originally derived by Lord Rayleigh in 1871; while those particles whose size is comparable to one wavelength or larger are called Mie particles after Gustav Mie who first derived a rigorous solution for the diffraction of a linearly polarized plane wave by a sphere. Since we are principally concerned about polarization effects, absorption is neglected.

The atmospheric densities considered here are selected such that near-field effects may be neglected. Also, since the particles which make up the atmosphere are randomly distributed, all scattering will be assumed to be incoherent, and therefore, the Stokes parameters can be summed without regard to phase.

2. THE SIMULATION MODEL

Consider the integral equation which governs the radiative transfer of electromagnetic energy in the atmosphere

$$I(\tau,\mu,\phi) = I_D(\tau,\mu,\phi) + I_S(\tau,\mu,\phi) \qquad (219)$$

where

$$I_D(\tau,\mu,\phi) = I(0,\mu,\phi)\ e^{-\tau/\mu}$$

and

$$I_s(\tau,\mu,\phi) = \frac{1}{u}\int_0^{2\pi}\int_{-1}^{+1}\int_0^{\tau} F(\mu,\phi;\mu',\phi')$$

$$I(t,\mu';\phi')\ e^{-(\tau - t)/\mu}\ dt\ d\mu'\ d\phi'$$

The direct intensity, $I_D(\tau,\mu,\phi)$, can be calculated easily. The scattered intensity is much more difficult to calculate since the unknown intensity also occurs under the integral. Equations of the type (219) are known as nonhomogeneous Fredholm integral equations. In an isotropic and homogenous medium the polarization parameters of the direct intensity are only attenuated and the polarization state remains the same. The polarization parameters of the scattered wave are, in general, modified during the scattering process by the scattering matrix $F(\mu,\phi;\mu',\phi')$ (see equation (179)), where μ and ϕ give the direction of the incident wave while μ' and ϕ' give the direction of the scattered wave.

a. Source Distribution

Assume a source which emits photons either isotropically or anisotropically. The probability that a photon is emitted in the direction (θ,ϕ) is proportional to the magnitude of the source intensity pattern in the direction (θ,ϕ). Let the intensity pattern be denoted by the function

$$G(\theta,\phi) \qquad (220)$$

If we normalize the intensity function

$$K \int_0^{2\pi} \int_0^{\pi} G(\theta,\phi) \sin\theta \, d\theta \, d\phi = 1 \tag{221}$$

where K is the normalizing constant, then the probability that a photon is emitted in the interval $(\theta + d\theta, \phi + d\phi)$ is

$$P(\theta,\phi) \sin\theta \, d\theta \, d\phi = \frac{G(\theta,\phi) \sin \theta \, d\theta \, d\phi}{\int_0^{2\pi} \int_0^{\pi} G(\theta,\phi) \sin\theta \, d\theta \, d\phi} \tag{222}$$

or upon integrating between fixed limits

$$P(\theta_1 \leq \theta \leq \theta_2, \phi_1 \leq \phi \leq \phi_2) = \frac{\int_{\phi_1}^{\phi_2} \int_{\theta_1}^{\theta_2} G(\theta,\phi) \sin\theta \, d\theta \, d\phi}{\int_0^{2\pi} \int_0^{\pi} G(\theta,\phi) \sin\theta \, d\theta \, d\phi} \tag{223}$$

Equation (223) gives the probability of emitting a photon between the angles (θ_1,θ_2) and (ϕ_1,ϕ_2).

Suppose the distribution is isotropic, then

$$G(\theta,\phi) = 1 \tag{224}$$

and

$$P(\theta_1 \leq \theta \leq \theta_2, \phi_1 \leq \phi \leq \phi_2) = \frac{(\phi_2 - \phi_1)(\cos\theta_1 - \cos\theta_2)}{4\pi} \tag{225}$$

Using equation (223) any intensity pattern may be used.

b. The Extinction Coefficient

All scatterers can be characterized by their scattering function, which describes the scattered intensity as a function of aspect angle. If I_0 is the intensity incident on the scatterer, then the scattered intensity

is given by

$$I = \frac{I_0 F(\theta,\phi)}{k^2 r^2} \tag{226}$$

where $F(\theta,\phi)$ is a dimensionless function which describes the intensity distribution for all directions (θ,ϕ) and $k = 2\pi/\lambda$.

We now define the scattering cross section, σ_s, by

$$\sigma_s = \frac{1}{k^2} \int_\omega F(\theta,\phi)\, d\omega \tag{227}$$

where $d\omega = \sin\theta\, d\theta\, d\phi$ is an element of solid angle, σ_s is an equivalent area such that the energy falling on σ_s is equal to the energy removed from the incident wave. Normally there is also an absorption cross section, σ_a, which describes the amount of energy removed from the incident wave through absorption. The total extinction of the incident wave is defined by the sum of the scattering cross section and absorption cross section.

$$\sigma_{ext} = \sigma_s + \sigma_a \tag{228}$$

In this paper we ignore σ_a and let

$$\sigma = \sigma_{ext} = \sigma_s$$

c. Path Lengths

Radiation intensity is attenuated exponentially through a medium according to

$$I(s) = I_0\, e^{-s/\sigma_{ext}(s)} \tag{229}$$

where I_0 is the incident intensity, s is the distance traveled, and σ is the extinction coefficient of the medium. The optical path length is

defined as

$$\tau(h) = \int_0^h \sigma_{ext}\,(h')\,dh' \qquad (230)$$

where $\tau(h)$ is also the number of mean-free-paths between 0 and h. In equation (229) the ratio $s/\sigma(s)$ is the fractional number of mean-free-paths traveled with $s = \sigma_{ext}(s)$ being equal to one mean-free-path. If we know the optical depth of the atmosphere as a function of distance in mean-free-paths, then the number of mean-free-paths traveled between collisions is distributed exponentially, i.e., the probability of a collision between ρ and $d\rho$, where $\rho = s/\sigma_{ext}(s)$, is

$$p(\rho)\,d\rho = e^{-\rho}\,d\rho \qquad (231)$$

or

$$P(\rho_1 \leq \rho \leq \rho_2) = \int_{\rho_2}^{\rho_2} e^{-\rho}\,d\rho \qquad (232)$$

Equations (231) and (232) hold for $0 \leq \rho \leq \infty$ For $0 \leq \rho \leq \rho_{max}$ we use

$$P(\rho_1 \leq \rho \leq \rho_2) = \frac{\int_{\rho_1}^{\rho_2} e^{-\rho}\,d\rho}{\int_0^{\rho_{max}} e^{-\rho}\,d\rho} \qquad (233)$$

Equations (231) and (232) hold for an atmosphere infinite in extent while equation (233) holds for a finite atmosphere

a. Rayleigh Scattering

The term Rayleigh scattering is used for scattering of electromagnetic waves from particles which are small compared to a wavelength or more precisely, particles which are small compared to the wavelength in

the particle, i.e., if λ_0 is the wavelength of the electromagnetic wave outside the particle then the wavelength inside the particle is

$$\lambda = \frac{\lambda_0}{m} \tag{234}$$

where m is the index of refraction (m = c/v) of the particle. If the particle is small compared to λ_0, the wavelength outside the particle but is comparable to the wavelength, λ, in the particle then we will be in the resonance scattering region. Resonance is associated with the modes of vibration of the particle.

For a particle fulfilling the above requirements the electric field induced in the particle can be assumed constant throughout the particle and the induced dipole moment is

$$\vec{p} = \alpha \vec{E}_0 \tag{235}$$

where α is the polarizability of the particle and $\vec{E}_0$ is the incident electric field. If

$$\vec{E} = \vec{E}_0 e^{i\omega t} \tag{236}$$

then

$$\vec{p} = \vec{p}_0 e^{i\omega t} \tag{237}$$

The electric field components of an oscillating dipole are given by [23]. (See Figure 16.)

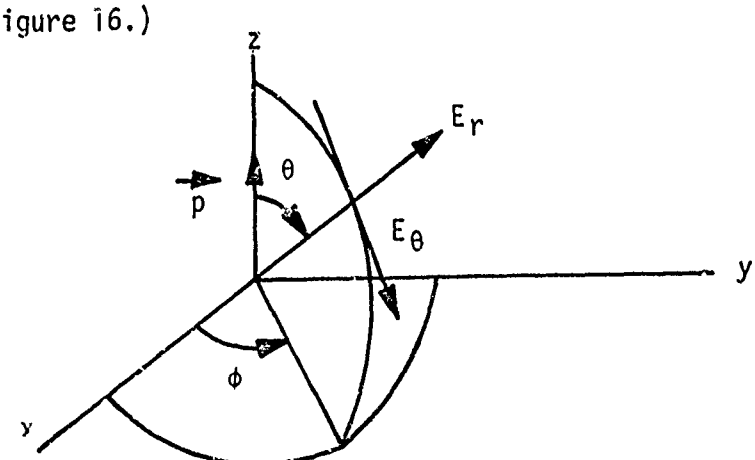

Figure 16. Oscillating Dipole Field Components

$$E_r = \left(\frac{1}{R^3} - \frac{ik}{R^2}\right) 2 \cos\theta\, |p|\, e^{i\omega(t-R/v)} \tag{238}$$

$$E_\theta = \left(\frac{1}{R^3} - \frac{ik}{R^2} - \frac{k^2}{R}\right) \sin\theta\, |p|\, e^{i\omega(t-R/v)} \tag{239}$$

For distances large compared to a wavelength ($R \gg \lambda$) the radial component, E_r, may be neglected and E_θ becomes

$$E_\theta = \frac{k^2 p \sin\theta}{R} e^{-ikR} \tag{240}$$

where

$$p = |p|\, e^{i\omega t}$$

Using (235), (240) becomes

$$E_\theta = \frac{k^2 \alpha E_0 \sin\theta}{R} e^{-ikR} \tag{241}$$

We now compare equation (241) with (175) and noting that for the perpendicular component $\theta = 90°$ and for the parallel component $\theta = 90° - \Theta$, where Θ is the scattering angle, we obtain

$$\begin{pmatrix} S_2 & S_3 \\ S_4 & S_1 \end{pmatrix} = ik^3 \alpha \begin{pmatrix} \cos\Theta & 0 \\ 0 & 1 \end{pmatrix} \tag{242}$$

or

$$\begin{pmatrix} E_\ell^s \\ E_r^s \end{pmatrix} = k^2 \alpha \begin{pmatrix} \cos\Theta & 0 \\ 0 & 1 \end{pmatrix} \frac{e^{-ikr + ikz}}{r} \begin{pmatrix} E_\ell^i \\ E_r^i \end{pmatrix} \tag{243}$$

from which we note that

$$I_\ell^s \propto |E_\ell|^2 = \frac{k^4 \alpha^2}{r^2} \cos^2\Theta\, |E_\ell^i|^2 \tag{244}$$

$$I_r^s \propto |E_r|^2 = \frac{k^4\alpha^2}{r^2} |E_r^i|^2 \tag{245}$$

$$2\sqrt{I_\ell^s I_r^s} \cos\delta \cos\Theta = \frac{k^4\alpha^2}{r^2} U^s \cos\Theta \tag{246}$$

$$2\sqrt{I_\ell^s I_r^s} \sin\delta \cos\Theta = \frac{k^4\alpha^2}{r^2} V^s \cos\Theta \tag{247}$$

Therefore, with $I^i = \left(I_\ell^i, I_r^i, U^i, V^i\right)$, the scattering matrix, for Rayleigh scattering, becomes

$$\mathbf{R} = \begin{pmatrix} \cos\Theta & 0 & 0 & 0 \\ 0 & 1 & 0 & 0 \\ 0 & 0 & \cos\Theta & 0 \\ 0 & 0 & 0 & \cos\Theta \end{pmatrix} \tag{248}$$

We can now write the matrix relation between the incident and scattered intensity

$$I^s = \frac{k^4\alpha^2}{r^2} \mathbf{R}\, I^i \tag{249}$$

which clearly shows the λ^{-4} dependence enccuntered with Rayleigh scattering ($k = 2\pi/\lambda$).

e. Mie Scattering

The exact solution to the diffraction of a linearly polarized plane wave by a sphere was first given by Gustav Mie in 1908 [2]. The scattering of electromagnetic waves by a sphere has occupied a large portion of the literature in the past. Several forms of the solution have been given by various authors [7, 23]. The term Mie scattering has been used for this problem in honor of Mie. In this paper we will be using the solution given by Van De Hulst [14]. The electric field

components as a result of scattering from a sphere are

$$E_\theta = -\frac{i}{kr} S_2(\theta) \cos\phi \, e^{-ikr+i\omega t} \tag{250}$$

and

$$E_\phi = \frac{i}{kr} S_1(\theta) \sin\phi \, e^{-ikr+i\omega t} \tag{251}$$

where $S_1(\theta)$ and $S_2(\theta)$ are the scattering functions defined by equation (175) and are given by

$$S_1(\theta) = \sum_{n=1}^{\infty} \frac{2n+1}{n(n+1)} \left[a_n \pi_n (\cos\theta) + b_n \tau_n (\cos\theta)\right] \tag{252}$$

and

$$S_2(\theta) = \sum_{n=1}^{\infty} \frac{2n+1}{n(n+1)} \left[b_n \pi_n (\cos\theta) + a_n \tau_n (\cos\theta)\right] \tag{253}$$

with

$$\pi_n (\cos\theta) = \frac{1}{\sin\theta} P_n^{(1)} (\cos\theta) \tag{254}$$

$$\pi_n (\cos\theta) = \frac{d}{d\theta} P_n^{(1)} (\cos\theta) \tag{255}$$

$$a_n = \frac{\psi_n'(y)\,\psi_n(x) - m\psi_n(y)\,\psi_n'(x)}{\psi_n'(y)\,\zeta_n(x) - m\psi_n(y)\,\zeta_n'(x)} \tag{256}$$

$$b_n = \frac{m\psi_n'(y)\,\psi_n(x) - \psi_n(y)\,\psi_n'(x)}{m\psi_n'(y)\,\zeta_n(x) - \psi_n(y)\,\zeta_n'(x)} \tag{257}$$

In equations (254) and (255) $P_n^{(1)}(\cos\theta)$ is the associated Legendre polynomial. In equations (256) and (257) $\psi_n(x)$ and $\zeta_n(x)$ are the Riccati-Bessel functions given by

$$\psi_n(x) = x\, j_n(x) \tag{258}$$

$$\zeta_n(x) = x\, h_n^{(2)}(x) \tag{259}$$

where $j_n(x)$ and $h_n^{(2)}(x)$ are spherical Bessel functions. Also in equations (256) and (257) m is the complex index of refraction of the sphere.

Equations (250) through (257) constitute a solution to the problem of the diffraction of a linearly polarized plane wave by a sphere and are valid for an arbitrary homogeneous sphere.

The scattering matrix for Mie scattering can be obtained by substituting equations (252) and (253) into equation (198). Recall that $S_1(\theta)$ is the scattering function for perpendicular incident polarization while $S_2(\theta)$ is the scattering function for parallel incident polarization.

f. Description of the Atmosphere

In this study we assume that the atmosphere consists of scattering particles only. The particles are, as is customary, assumed to be spherical. We use the Mie scattering theory to determine the particle scattering matrix. Absorption is assumed to be negligible since this phenomenon does not contribute to the depolarization of the incident wave. The atmosphere is made up of many mie particles each randomly oriented with respect to other Mie particles in the atmosphere. Therefore, all scattering is assumed to be incoherent. The assumption of incoherent scattering allows us to add the Stokes polarization parameters resulting from the various scattering events. Since the atmosphere is made up of many randomly oriented Mie particles, we can describe the size distribution

of the Mie particles and determine the average scattering matrix for a given size distribution and thus characterize the atmosphere with this average value. Deirmendjian [24] has generalized the size distribution function first proposed by Khrgian and Mazin [25] in the form

$$n(r) = a\, r^{\alpha}\, e^{-br^{\gamma}} \tag{260}$$

where $n(r)$ is the volume concentration at the radius r and a, α, b, and γ are positive constants. If N is the total number of particles per unit volume, then

$$N = \int_0^{\infty} n(r)\, dr = \frac{\alpha}{\gamma}\, b^{-\frac{\alpha+1}{\gamma}}\, \Gamma\left(\frac{\alpha+1}{\gamma}\right) \tag{261}$$

where Γ is the gamma function.

Taking the derivative of (260) with respect to r, we obtain

$$\frac{d}{dr}\, n(r) = a\, r^{\alpha-1}\, e^{-br^{\gamma}}\, (\alpha - \gamma b r^{\gamma}) \tag{262}$$

Setting (262) equal to zero we can solve for the critical or mode radius which is

$$r_m = \left(\frac{\alpha}{b\gamma}\right)^{1/\gamma} \tag{263}$$

Figure 17 is a general plot of equation (260).

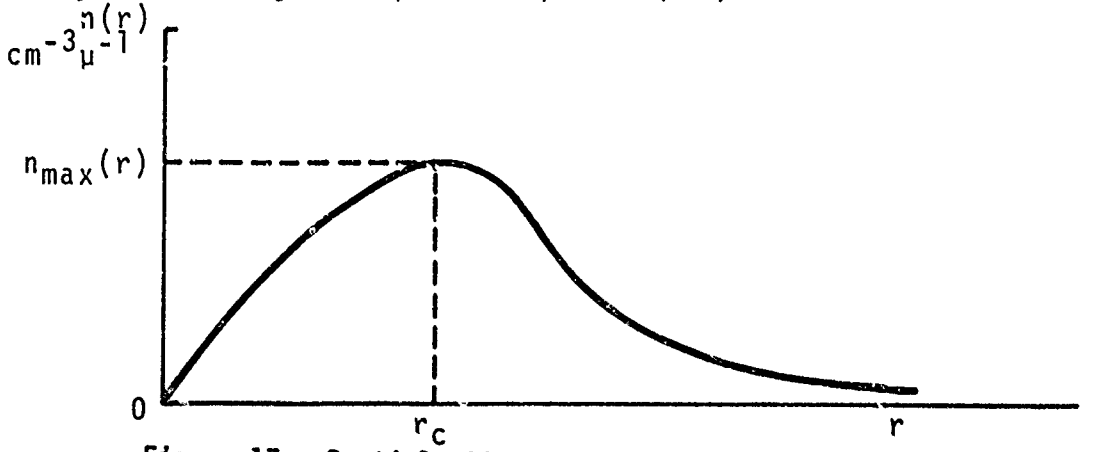

Figure 17. Particle Size Distribution

The generalized size distribution function given by Deirmendjian (equation (260)) reproduces practical particle distributions as measured by experimentors. For example, if $a = 2.373$, $\alpha = 6$, $b = 1.5$, and $\gamma = 1$ we obtain

$$n(r) = 2.373\ r^6\ e^{-1.5r}\ cm^{-3}\ \mu^{-1} \tag{264}$$

which follows the size distribution measured by Durbin [26] for cumulus clouds; for this reason the distribution (264) is called "cumulus type I" by Singleton and Smith [27]. Another example of equation (260) is obtained by setting $a = 5.33 \times 10^4$, $\alpha = 1$, $b = 8.944$, and $\gamma = 1/2$ and we have

$$n(r) = 5.33 \times 10^4\ r\ e^{-8.944r^{1/2}} \tag{265}$$

The distribution given by equation (265) may be taken to represent coastal conditions and is called the "haze M" model by Deirmendjian. Equation (264) yields

$$N = 100 \text{ particles } cm^{-3} \tag{266}$$

while equation (265) also gives

$$N = 100 \text{ particles } cm^{-3} \tag{267}$$

Equations (266) and (267) yield, on the average an interparticle distance of approximately

$$\left(\frac{1}{100}\right)^{1/3} = 0.215 \text{ cm}$$

or 2150 microns. Therefore, for the Cumulus Cloud and "Haze M" models the far field scattering approximation is certainly valid for wavelengths up to, say, 200μ.

A size distribution which may be used to represent a continental haze is

$$\begin{aligned} n(r) &= 0 && r < r_{min} \\ n(r) &= \text{constant} && r_{min} \leq r \leq r_2 \\ n(r) &= Ar^{-\nu} && r_2 \leq r \leq r_{max} \end{aligned} \tag{268}$$

where $r_{min} = 0.3\mu$, $r_2 = 0.1\mu$, $\nu = 4$, and constant $= 10^3$ has been shown by Deirmendjian to be representative of typical continental hazes and is called the "Haze C" model, i.e.,

$$\begin{aligned} n(r) &= 0 && r < 0.03\mu \\ n(r) &= 10^3 && 0.03\mu \leq r \leq 0.1\mu \\ n(r) &= 0.1r^{-4} && 0.1\mu \leq r \leq \infty \end{aligned} \tag{269}$$

for this distribution we also have

$$N \approx 100 \text{ particles cm}^{-3}$$

and near field scattering will start to become important for

$$\lambda > 200\mu$$

Therefore, it appears that for wavelengths into the infrared and shorter near field scattering may be ignored for the three postulated models.

Now that we have obtained the three particle size distributions we can now integrate the Mie functions over the applicable size distribution in order to obtain the Mie volume functions. Here we will follow the same technique used by Deirmendjian [24].

In equation (227) we defined the scattering cross section as

$$\sigma_s \frac{1}{k^2} \int_{\omega} F(\theta,\phi)\, d\omega \tag{227}$$

where the integration is carried out over all solid angles ω. If we integrate the particle cross section over ths size distribution we will obtain the volume scattering function. Before carrying out the integration let us define the Mie size parameter

$$x = \frac{2\pi r}{\lambda} = kr \tag{270}$$

where r is the Mie particle radius, $k = 2\pi/\lambda$, and λ is the wavelength. Making this substitution into (260) we obtain

$$n(x,k) = a\left(\frac{x}{k}\right)^{\alpha} e^{-b\left(\frac{x}{k}\right)^{\alpha}} \tag{271}$$

The functior $F(\theta,\phi)$ is also dependent on x and we can write

$$F(\theta,\phi) = F(\theta,\phi,x) \tag{272}$$

Now we can write, for azimuthally symmetric $F(\theta)$,

$$\sum_s(\theta,\lambda) = \frac{2\pi}{k^2}\int_{x_1}^{x_2} F(\theta,x)\, n(x,k)\, dx \tag{273}$$

The volume scattering cross section is obtained by integrating (273) over all angles, i.e.,

$$\sum_{vs}(m,\lambda) = 2\pi\int_0^{\pi} \sum_s(\theta,\lambda) \sin\theta\, d\theta \tag{274}$$

where m is the index of refraction.

We can now normalize $\sum_s$, i.e.,

$$N_s(\theta,\lambda) = \frac{\sum_s}{\sum_{vs}} \tag{275}$$

which is proportional to the probability per steradian of a photon of wavelength λ being scattered into an angle θ.

For Mie scattering we have that

$$F(\theta) = |S_1|^2 \tag{276}$$

for incident perpendicularly polarized waves, and

$$F(\theta) = |S_2|^2 \tag{277}$$

for incident parallel polarized waves where the polarization is referred to the scattering plane, i.e., either perpendicular or parallel to it.

For exponential stratification of the atmosphere [15] we can write the extinction coefficient as

$$\sigma_{ext}(h) = \sigma_0 \, e^{-h/H} \tag{278}$$

where σ_0 is the extinction coefficient at h = 0 and H is the scale altitude, e.g., H = 0.98 km for haze [15]. Using equation (230) we obtain for the optical thickness

$$\tau(h) = \int_0^h \sigma_0 \, e^{-h'/H} \, d\,h' \tag{279}$$

Or upon solving equation (279) we have

$$\tau(h) = \sigma_0 \, H\left(1 - e^{-h/H}\right) \tag{280}$$

which gives the optical thickness as a function of altitude h.

g. A Monte Carlo Simulation

Monte Carlo techniques may be used in the simulation of a random process [12, 13]. Monte Carlo techniques have been used for several years to simulate problems in neutron diffusion. The Monte Carlo technique

serves in modeling a random process when the various probability distributions are known or can at least be approximated using physical reasoning. Our problem of determining the depolarization effects due to scattering in the atmosphere is certainly a random process since the distribution of scatterers in the atmosphere is random. Here we assume that a plane, polarized wave propagates through the atmosphere, the wave being made up of a large number of photons whose average properties can be characterized in terms of wave theory. We, as originally stated, will also assume that all scattering is incoherent so that the effects of all the scattered photons may be added directly. The polarization properties of the wave are associated with each photon history. The difficulty of assigning the Stokes polarization parameters to a single photon can be overcome by assuming that we are dealing with groups of photons rather than with a single photon.

We now know that the probability of a photon being emitted into an angle (θ,ϕ) is given by equation (223), that the number of mean-free-paths traveled between collisions is given by the distribution (233). Furthermore, if Rayleigh scattering occurs the Rayleigh scattering matrix given by (250) can be used to operate on the Stokes vector as given by equation (249). Similarly, if Mie scattering occurs the Mie scattering matrix given by equations (198), (252), and (253) can be used to operate on the Stokes vector as in the case for Rayleigh scattering. Since the Rayleigh and Mie scattering matrixes are given in terms of the scattering angle, the polarization components of the incident photon must be rotated as dictated by equation (250) parallel and perpendicular to the scattering plane. Similarly, after the scattering matrix is applied to the Stokes vector, the Stokes components will be rotated back to a reference plane. The reference plane to be used here is the same as that used by Collins

and Wells [17] and is the vertical plane which also contains the propagation vector. Therefore, the parallel component at a detector is that component in the reference plane and is orthogonal to the propagation vector, while the perpendicular component will be perpendicular to both the reference plane and the propagation vector.

Again following the same method as that used by Collins and Wells, we determine the effect of multiple collisions by estimating the intensity at the detector after each collision and comparing the intensity at the detector due to single or multiple collisions. The estimate of the intensity at the detector as a function of collision number will be obtained by calculating the scattering angle toward the detector and weighting the Stokes vector with the applicable scattering matrix for that particular scattering angle. The particular photon history is continued by selecting a scattering angle from a probability density given by the normalized Rayleigh or Mie scattering functions. After selection of the scattering angle the Stokes vector is then weighted by the applicable scattering matrix for that scattering angle.

Random numbers are obtained by generating a pseudorandom sequence. Several methods for generating pseudorandom numbers are available [12]. In this simulation we will use a pseudorandom sequence which is generated by the recurrence relation

$$y_i \equiv ay_i - 1 \text{ (modulo n)} \tag{281}$$

The notation used in (281) means that y_i is the reminder when $ay_i - 1$ is divided by n. In our case we use $n = 2^{48}$ and the period is n/4, hence we are able to generate in the order of 10^{13} numbers before repeating the sequence. We will never require more than, say, 10^4 photon histories each requiring approximately 10^2 random numbers, therefore we will never

need more than 10^6 random numbers per problem. The pseudorandom sequence given by (281) has been found to be uniformly distributed and therefore a transformation from the uniform distribution to the desired distribution is needed.

A theorem by Barkovskii and Smirnov [13] states that if the random variable ξ has a probability density function $f(x)$, then the distribution of the random variable

$$\eta = \int_0^{\xi} f(x)\, dx \tag{282}$$

is uniform in the interval (0,1). Consider the arbitrary cumulative distribution function $F(\xi)$ as given in figure 18.

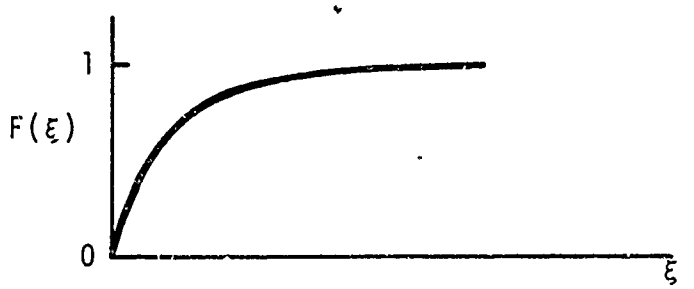

Figure 18. Arbitrary Cumulative Distribution Function

Let $\eta = F(\xi)$; we now want to find out how η is distributed. Since we know that the random variables ξ and η are functionally related through the function F we can write

$$p(\eta) = \frac{p(\xi)}{F'(\xi)} \tag{283}$$

But we know that

$$p(\xi) = F'(\xi) \tag{284}$$

therefore

$$p(\eta) = 1 \quad 0 \leq \eta \leq 1$$

$p(\eta) = 0$ otherwise, which proves that η is uniformly distributed. On the

basis of equation (282) we may therefore use the following rule. In order to obtain a random number belonging to the set of numbers $\{S_i\}$ with the density function f(x) solve the following equation for S_i

$$\int_{-\infty}^{S_i} f(x)\, dx = R_i \tag{285}$$

For example consider the distribution function given by equation (232)

$$p(\rho)\, d\rho = e^{-\rho} d\rho,\ 0 \leq \rho \leq \infty \tag{232}$$

which gives the probability of a photon traversing dρ mean-free-paths between collisions. Assume we generate a random number R_i from a rectangular distribution in the interval (0,1), then

$$R_i = \int_0^{\rho_i} e^{-\rho}\, d\rho$$

$$= -e^{-\rho} \Big|_0^{\rho_i}$$

$$= 1 - e^{-\rho_i} \tag{286}$$

Solving for ρ_i, we obtain

$$\rho_i = -\ln\left(1 - R_i\right) \tag{287}$$

In this manner we can very easily generate the random numbers ρ_i for the desired distribution from the random numbers R_i which are uniformly distributed.

Let us now summarize the methods being used to model our problem. Consider a plane-parallel atmosphere with exponential particle stratification A source of electromagnetic energy is located at an arbitrary altitude above the ground. The electromagnetic energy being radiated from

need more than 10^6 random numbers per problem. The pseudorandom sequence given by (281) has been found to be uniformly distributed and therefore a transformation from the uniform distribution to the desired distribution is needed.

A theorem by Barkovskii and Smirnov [13] states that if the random variable ξ has a probability density function $f(x)$, then the distribution of the random variable

$$\eta = \int_0^{\xi} f(x)\, dx \tag{282}$$

is uniform in the interval (0,1). Consider the arbitrary cumulative distribution function $F(\xi)$ as given in figure 18.

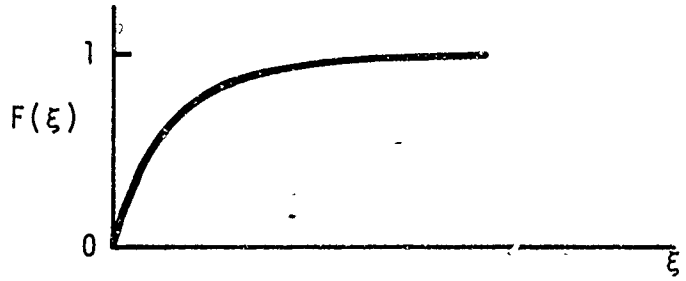

Figure 18. Arbitrary Cumulative Distribution Function

Let $\eta = F(\xi)$; we now want to find out how η is distributed. Since we know that the random variables ξ and η are functionally related through the function F we can write

$$p(\eta) = \frac{p(\xi)}{F'(\xi)} \tag{283}$$

But we know that

$$p(\xi) = F'(\xi) \tag{284}$$

therefore

$$p(\eta) = 1 \quad 0 \leq \eta \leq 1$$

$p(\eta) = 0$ otherwise, which proves that η is uniformly distributed. On the

the source will be modeled by considering that the intensity is due to the conglomerate effects of wave packets made up of photons. Each wave packet is assumed to be characterized by the Stokes polarization vector. The wave packets can be thought of as bullets which when shot into the atmosphere collide and are reflected by the scattering particles according to prescribed probabilities.

The probability that a photon (wave packet) is emitted by the source in the interval of solid angle $(\theta_1 \leq \theta \leq \theta_2, \phi_1 \leq \phi \leq \phi_2)$ is

$$P(\theta_1 \leq \theta \leq \theta_2,\ \phi_1 \leq \phi \leq \phi_2) = \frac{\int_{\phi_1}^{\phi_2} \int_{\theta_1}^{\theta_2} G(\theta,\phi) \sin\theta \, d\theta \, d\phi}{\int_{0}^{2\pi} \int_{0}^{\pi} G(\theta,\phi) \sin\theta \, d\theta \, d\phi} \tag{288}$$

where $G(\theta,\phi)$ is the source intensity distribution. Therefore once a specific function $G(\theta,\phi)$ is selected we can generate random numbers representing a random angle over the prescribed distribution through the use of equation (285).

The probability that the photon traverses the distance between ρ_1 and ρ_2 between collisions or from the source to the first collision is given by

$$P(\rho_1 \leq \rho \leq \rho_2) = \int_{\rho_1}^{\rho_2} e^{-\rho} \, d\rho \tag{289}$$

where ρ is the number of mean-free-paths traveled. We will use (287) to generate the ρ_i random numbers.

We can see from figure 19 that the exponential distribution for optical pathslengths holds for the interval $0 \leq \rho \leq \infty$.

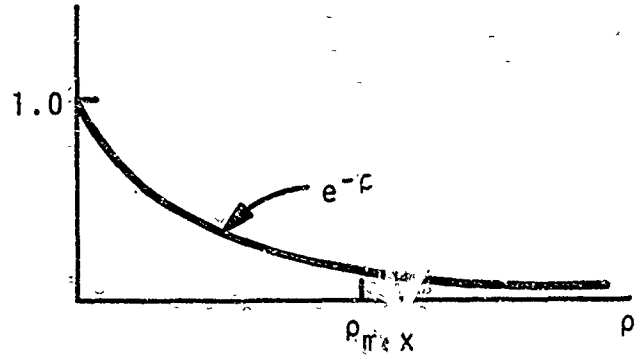

Figure 19. Exponential Distribution

If we desire to limit the optical path to the interval $0 \leq \rho \leq \rho_{max}$ as in the case of a very dense cloud with negligible scattering outside the cloud or for a finite atmosphere, a truncated exponential distribution, as depicted in figure 19 would be used. The truncated exponential random numbers may be found from

$$R_i = \int_0^{\rho_i} \frac{e^{-\rho}}{1 - e^{-\rho_{max}}} d\rho \tag{290}$$

or, upon solving for ρ_i

$$\rho_i = -\ell n \left[1 - R_i\left(1 - e^{-\rho_{max}}\right)\right] \tag{291}$$

As we have mentioned previously, we will estimate the intensity at a detector after each collision. We do this by calculating the scattering angle toward the detector, rotating the Stokes vector into the scattering plane, multiplying the scattering matrix with the rotated Stokes vector, rotating the Stokes vector back to the reference plane, and attenuating the resultant Stokes vector by the attenuation function

$$\frac{e^{-\rho_D}}{D^2}$$

where ρ_D is the optical distance from the collision point to the detector and D is the geomtric distance from the collision point to the detector.

Figure 20 shows the geometry used for calculating the intensity at a detector resulting from a collision. In figure 20, r is the horizontal radial distance from the origin to the collision point, r_D is the horizontal radial distance from the origin to the detector, Θ is the scattering angle toward the detector, ϕ_r is the Stokes rotation angle, h_D is the height of the detector, and h_c is the height of the collision point. Using the spherical triangle $\alpha\beta\Theta$ we can compute the rotation angle ϕ_r from

$$\cos \phi_r = \frac{\cos \alpha - \cos \Theta \cos \beta}{\sin \Theta \sin \beta} \tag{292}$$

$$\sin \phi_r = \frac{\sin \alpha \sin \gamma}{\sin \Theta} \tag{293}$$

where γ is the angle between the radial lines to the collision point and to the detector as shown in figure 20. The cosine of the scattering angle may be computed by taking the inner product between the unit vector in the direction of the photon prior to the collision with the unit vector in the direction from the collision point to the detector. The unit vector in the direction of the photon prior to the scattering event is

$$\vec{a}_p = \sin \beta \cos \delta \, \vec{a}_x + \sin \beta \sin \delta \, \vec{a}_y + \cos \beta \, \vec{a}_z \tag{294}$$

where the angle δ is shown in figure 20. The unit vector from the collision point to the detector is

$$\vec{a}_D = \frac{1}{D} \left(r_D \cos \gamma - r \right) \vec{a}_x + r_D \sin \gamma \, \vec{a}_y + \left(h_D - h \right) \vec{a}_z \tag{295}$$

Taking the inner product of equations (294) and (295) we obtain

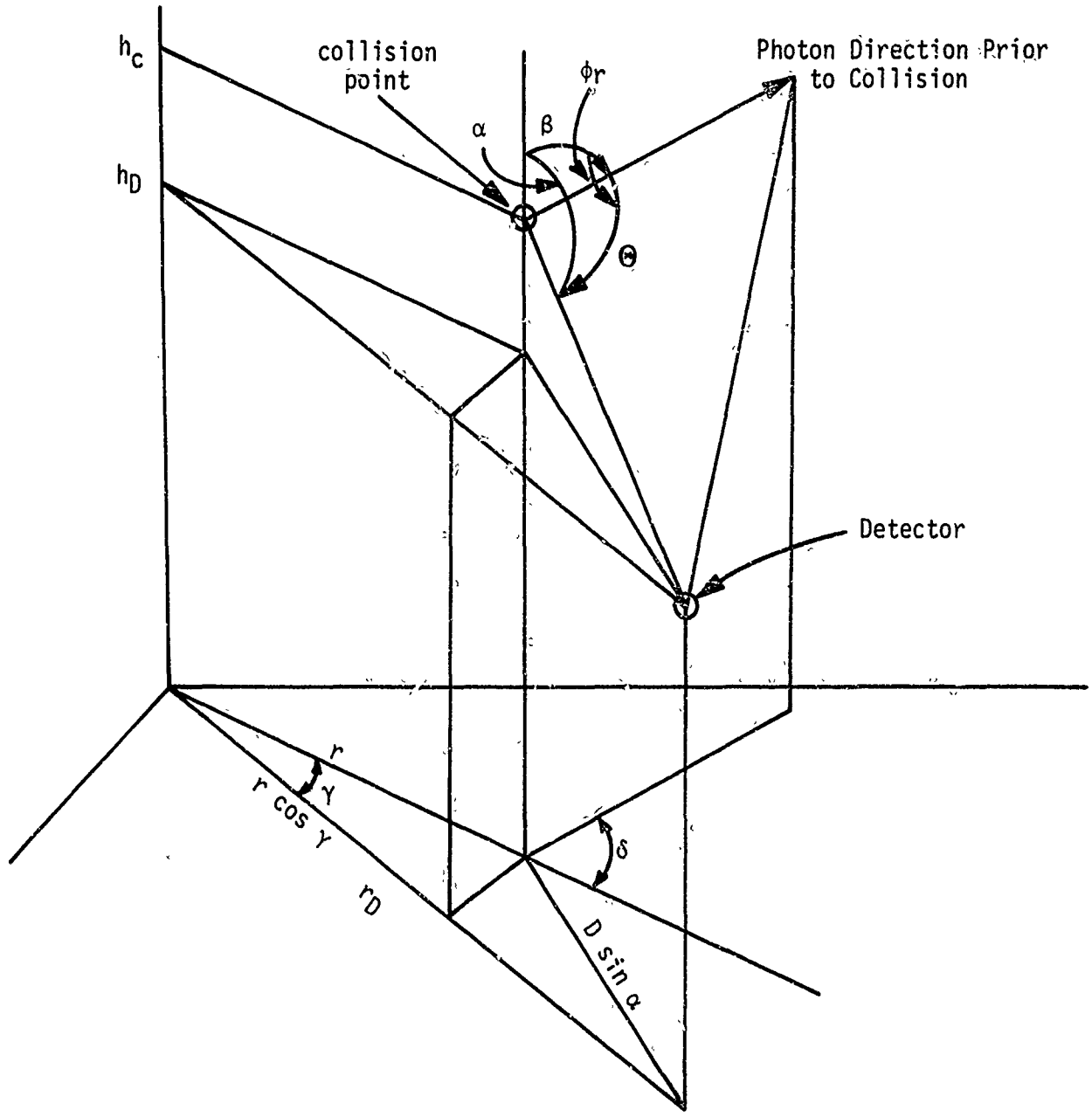

Figure 20. Geometry for Calculation of Intensity at a Detector

$$\cos\Theta = \frac{\sin\beta\cos\delta\left(r_D\cos\gamma - r\right)}{D} + \frac{r_D\sin\gamma\sin\beta\sin\delta}{D}$$

$$+ \frac{\left(h_D - h\right)\cos\beta}{D} \qquad (296)$$

After having made an estimate of the intensity at the detector after a collision, a random scattering angle is selected. The scattering event may be either Rayleigh scattering or Mie scattering. The specific type of scattering which occurs for a particular collision is determined by comparing a random number selected from a uniform distribution with the ratio of Rayleigh to Rayleigh plus Mie scattering coefficients for that altitude [28]. If the random number is less than or equal to the ratio Rayleigh scattering is selected. Otherwise we select Mie scattering.

For Rayleigh scattering the scattering angle is selected from the probability density function [9, 20]

$$P(\cos\Theta) = \frac{3}{8}\left(1 + \cos^2\Theta\right) \qquad (297)$$

Collins and Wells have shown that (297) can be written as the sum of two probability density functions

$$P(\cos\Theta) = P_1(\cos\Theta) + P_2(\cos\Theta) \qquad (298)$$

with

$$P_1(\cos\Theta) = \frac{3}{4}\frac{\sin\theta\, d\,\theta}{2} \qquad (299)$$

and

$$P_2(\cos\Theta) = \frac{3}{4}\cos^2\Theta\frac{\sin\theta\, d\,\theta}{2} \qquad (300)$$

The density function $P_1(\cos\Theta)$ is chosen to represent $P(\cos\Theta)$ half of the time and $P_2(\cos\Theta)$ the remainder of the time. If $P_1(\cos\Theta)$ is chosen,

then cos Θ may be determined by solving

$$R_i = \int_0^{\Theta_i} \frac{\sin \theta \, d\theta}{2} \tag{301}$$

for cos Θ_i, or

$$\cos \Theta_i = 1 - 2 R_i \tag{302}$$

If $P_2(\cos \Theta)$ is chosen, cos Θ_i is selected in the same manner as (302) but $\cos^2 \Theta_i$ is compared to a second random number and is accepted if it is greater than the second random number. Collins and Wells have shown that the determination of cos Θ compares very favorably with the actual distribution for Rayleigh scattering.

If Mie scattering is selected, the cumulative probability of scattering into an angle less than or equal to Θ_i is given by the normalized differential scattering cross section of equation (273):

$$P\left(0 \leq \Theta \leq \Theta_i\right) = \frac{\int_0^{\Theta_i} \Sigma_s (\Theta,\lambda) \sin \Theta \, d \Theta}{\int_0^{\pi} \Sigma_s (\Theta,\lambda) \sin \Theta \, d \Theta} \tag{303}$$

The azimuthal scattering angle which determines the orientation of the scattering plane is selected from the uniform distribution

$$p(\phi) = \frac{1}{2\pi} \quad (0 \leq \phi \leq 2\pi) \tag{304}$$

for both Rayleigh and Mie scattering.

Now that the scattering polar and azimuthal angles are known we may compute the direction of the photon after being scattered. The cosine

of the angle between the photon's direction after scatter and the vertical axis is

$$\cos \alpha' = \cos \beta' \cos \Theta + \sin \beta' \sin \Theta \cos \phi_r' \tag{305}$$

where the angles are defined as shown in figure 21.

The intensity received at each detector simulated will be recorded as a function of polar and azimuthal angles. The polar axis for each detector is defined to be the axis joining the source and detector. The x and y axes lie in a plane normal to the polar axis. The x axis is contained in the vertical plane containing the source and receiver points. The positive x axis points toward the positive vertical direction but is in general, inclined to the true vertical.

If reflections from the ground occur, we assume that the reflected light is diffuse and therefore completely depolarized. The reflected polarization parameters are given by

$$I_\ell' = a\left(\frac{I_r + I_\ell}{2}\right) \tag{306}$$

$$I_r' = a\left(\frac{I_r + I_\ell}{2}\right) \tag{307}$$

$$U' = 0 \tag{308}$$

$$V' = 0 \tag{309}$$

where the prime denotes the reflected quantities and a is the ground albedo.

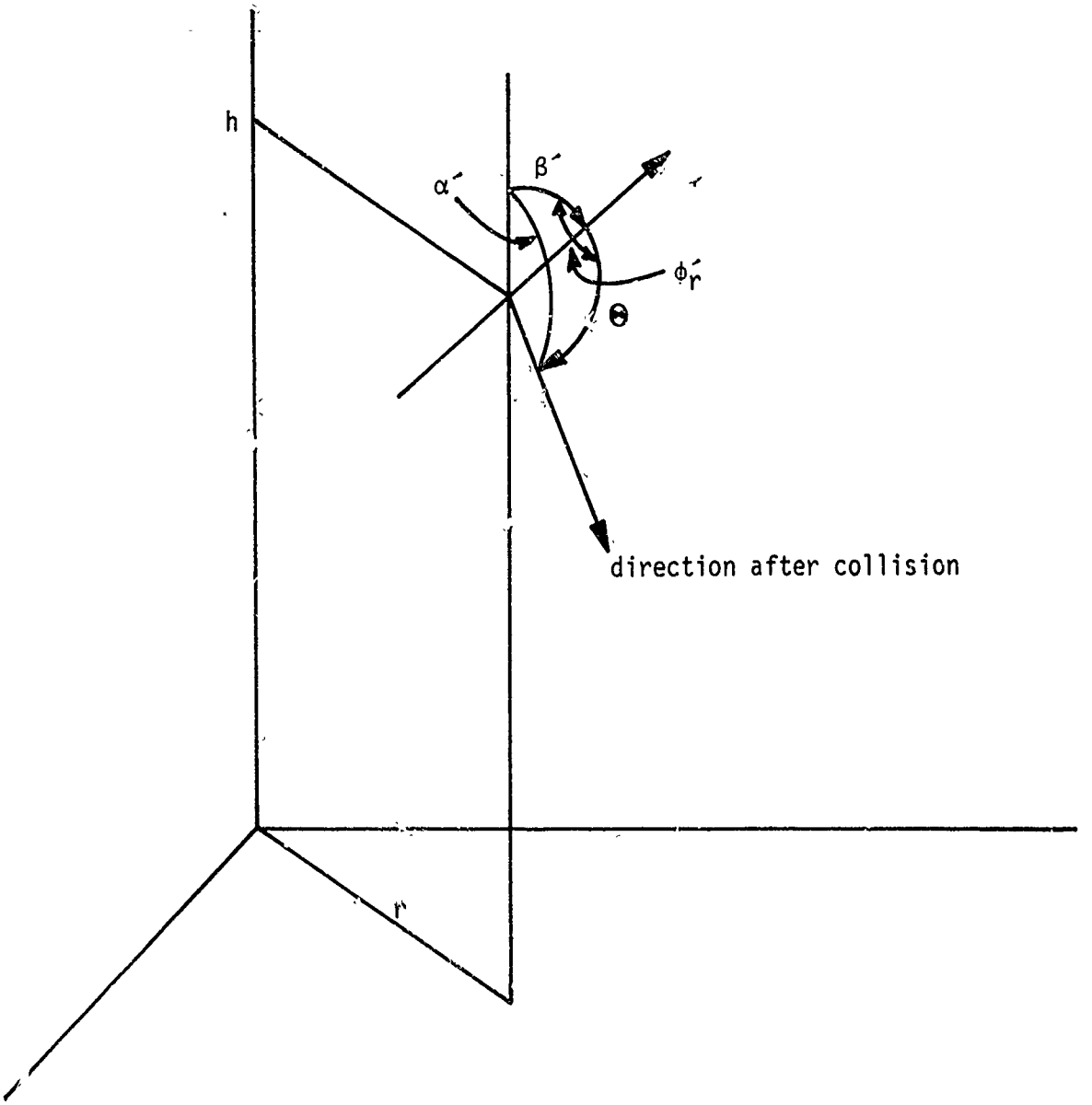

Figure 21. Geometry for Determination of Scattering Angle

SECTION V

DEPOLARIZATION BY CLOUDS: SOME EXAMPLES

1. INTRODUCTION

In the previous sections we have discussed the various facets of the problem of determining the effect of atmospheric scattering on the polarization properties of an electromagnetic wave. In section II we derived the equation of radiative transfer for a plane-parallel atmosphere. There it was found that the intensity at any point may be found by solving a complex set of integral equations. The equation of radiative transfer has been solved only for the cases of isotropic scattering and Rayleigh scattering [9]. The more general problem of anisotropic scattering has also been discussed by Evans, Chu, and Churchill [11]. The scattering function for single scattering may be expanded in a series of Legendre polynomials of the form

$$f(\cos\Theta) = \frac{1}{4\pi} \sum_{i=0}^{N} a_i P_i (\cos\Theta) \qquad (310)$$

where the a_i are the series coefficients. This expansion is of the same form as the exact solution for a sphere (see equations (252) and (253)). The scattering functions selected by Evans et al. are highly peaked in the forward direction which indicates that for that particular case near field effects would be more pronounced in the forward scattering direction. The shape of the scattering function will depend on the size parameter $x = \frac{2\pi r}{\lambda}$, where r is the radius of the spherical particle and λ is the wavelength; it will also depend on the sphere's complex index of refraction.

2. PARTICLE SCATTERING FUNCTIONS FOR THE CUMULUS CLOUD DISTRIBUTION

In section V we derived the normalized scattering function for a given particle size distribution; in this subsection we will show some results for the "Cumulus Cloud" distribution. This distribution is

$$n(r) = 2.373\, r^6\, e^{-1.5r}\ cm^{-3}\ \mu^{-1} \qquad (311)$$

as given by Deirmendjian. In equation (311) the particle density is

$$N = 100\ \frac{particles}{cm^3}$$

and the mode radius is $r_m = 4\mu$. Equation (311) is plotted in figure 22. In figures 23 through 27 are shown the scattering function for individual particles taken from the Cumulus Cloud distribution and perpendicular incident polarization, with $\lambda = 0.5\mu$ and $i_1(\theta) = |S_1(\theta)|^2$. The size parameters 13.86, 35.87, 72.31, 123.19, and 188.50 correspond to spheres of radius 1.1, 2.9, 5.8, 9.8, and 15.0μ, respectively. Notice the increase in the forward peak with size parameters.

We can normalize equation (311) as follows:

$$p(r) = \frac{n(r)}{\int_0^\infty n(r)\, dr} = \frac{n(r)}{N} \qquad (312)$$

or upon substituting for n(r) from equation (311) and using the value of N we have

$$p(r) = 0.02373\, r^6\, e^{-1.5r} \qquad (313)$$

which is the probability of finding a particle in the radius interval (r, r + dr). The expected value of r can be found from

$$E[r] = \int_0^\infty r\, p(r)\, dr \tag{314}$$

or

$$E[r] = \int_0^\infty 0.02373\, r^7\, e^{-1.5r}\, dr$$

$$= 0.02373\, (1.5)^{-8}\, \Gamma(8)$$

$$= 4.66\mu \tag{315}$$

The variance is

$$\mathrm{Var}[r] = \left[E\,(r - E[r])^2\right]$$

or

$$\mathrm{Var}[r] = E[r^2] - (E[r])^2 \tag{316}$$

We can obtain the second term on the RHS from (315) and the first term from

$$E[r^2] = \int_0^\infty r^2\, p(r)\, dr \tag{317}$$

or

$$E[r^2] = \int_0^\infty 0.02373\, r^8\, e^{-1.5r}\, dr$$

$$= 0.02373\, (1.5)^{-9}\, \Gamma(9)$$

$$= 24.9\mu^2 \tag{318}$$

so that upon using the result (315), we obtain

$$\text{Var}[r] = 24.9 - (4.66)^2$$

$$= 3.2\mu^2 \tag{319}$$

We can now obtain the standard deviation

$$\sigma_c = \sqrt{\text{Var}[r]} = 1.78\mu \tag{320}$$

Comparing the expected value of r, E[r], with the mode radius, r_m, we find that since these values do not coincide and the distribution is not symmetrical the particles of radius greater than E[r] will affect the averaging of the scattering function over the size distribution to a greater extent than those below E[r]. Comparing figures 23 through 27 we can see that the scattering functions given by figures 24 through 26 will affect the averaging of the scattering function over the size distribution to a greater extent than the scattering functions given by figure 23 or figure 27. The scattering function given by figure 25 will enter into the averaging quite heavily since it is within $1\sigma_c$ of E[r]. The fact that particles of radius greater than r_m will greatly affect the normalized scattering function can be seen by comparing figures 25 and 26 with figure 28. Figure 28 is the normalized scattering function for perpendicular incident polarization obtained from equation (275). The amplitudes of the normalized function and individual scattering function cannot be compared since the individual particle scattering functions have not been normalized. The normalized scattering function for parallel incident polarization is shown in figure 29. There is not much difference between the normalized scattering functions for perpendicular and parallel polarization except in the scattering interval from 90° to 170°. The end points at scattering

angles of 0° and 180° of the normalized scattering functions for parallel and perpendicular incident polarization are equal as required, i.e., the energy scattered in the forward or back directions are not sensitive to polarization.

If we average the normalized scattering functions for perpendicular and parallel incident polarization as follows:

$$\frac{|S_1(\theta)|^2 + |S_2(\theta)|^2}{2} = \frac{I_1(\theta) + I_2(\theta)}{2} \qquad (321)$$

we will have a relation which is proportional to the probability of scattering in any direction and we can derive the cumulative scattering distribution. This vividly shows (figure 30) the preference to forward scattering for the cumulus cloud distribution at a wavelength of 0.5μ.

If we now reduce the frequency (increase the wavelength) and continue to use the same size distribution given for cumulus clouds and consider particles of the same radius as before we can get a "feel" for the effect of wavelength on the scattering function. Figures 31 through 35 give the scattering functions for particle radii of 1.1, 2.9, 5.8, 9.8, and 15.0μ as before. These are given for perpendicular incident polarization and a wavelength of 4.0μ. Figures 36 and 37 give the normalized scattering functions for perpendicular and parallel incident polarizations, respectively. Figure 38 is the cumulative scattering function. Again we see, upon comparing figures 33 and 34 with figure 36, that radii greater than r_m affect the normalized scattering function to a great extent. We can also compare figures 30 and 38 and see that the probability of scattering in the forward direction when compared to side and back scattering has been reduced somewhat.

We continue to increase the wavelength to 6.0μ and then to 10.0μ. Figures 39 through 43 and figures 47 through 51 are the scattering functions for perpendicular incident polarization for wavelengths of 6.0 and 10.0μ, respectively and given at the same radii as in figures 23 through 27 and figures 31 through 35. The widening of the scattering functions with increasing wavelength can be seen by comparing figure 30, the cumulative probability function for $\lambda = 0.5\mu$ with figure 46, the cumulative probability function for $\lambda = 6.0\mu$ and figure 54, the cumulative probability function for $\lambda = 10.0\mu$. For example, in figure 30, the probability of scattering through an angle between 0° and 21° is 0.5, the same probability as obtained for the scattering interval from 4° to 21° in figure 54. This dependence of scattering angle on wavelength implies that for a given particle size distribution that multiple scattering will increase with wavelength, i.e., the probability of scattering over a greater range of angles is greater for large wavelength. Figures 44 and 45 are the normalized scattering functions at $\lambda = 6.0\mu$ while figures 52 and 53 are the normalized scattering functions for $\lambda = 10.0\mu$.

The extinction coefficient for Mie scattering for the cumulus cloud distribution is given in table 1 for each wavelength under consideration. The extinction coefficient for Mie scattering is given by [14]

$$\sigma_{ext}(\lambda,r,m) = \frac{\lambda^2}{2\pi} \sum_{n=1}^{\infty} (2n + 1) \, \mathrm{Re}\left(a_n + b_n\right) \tag{322}$$

where the coefficients a_n and b_n are given by equations (256) and (257).

We can define the extinction efficiency factor by

$$Q_{ext}(x,m) = \frac{\sigma_{ext}(\lambda,r,m)}{\pi r^2} \tag{323}$$

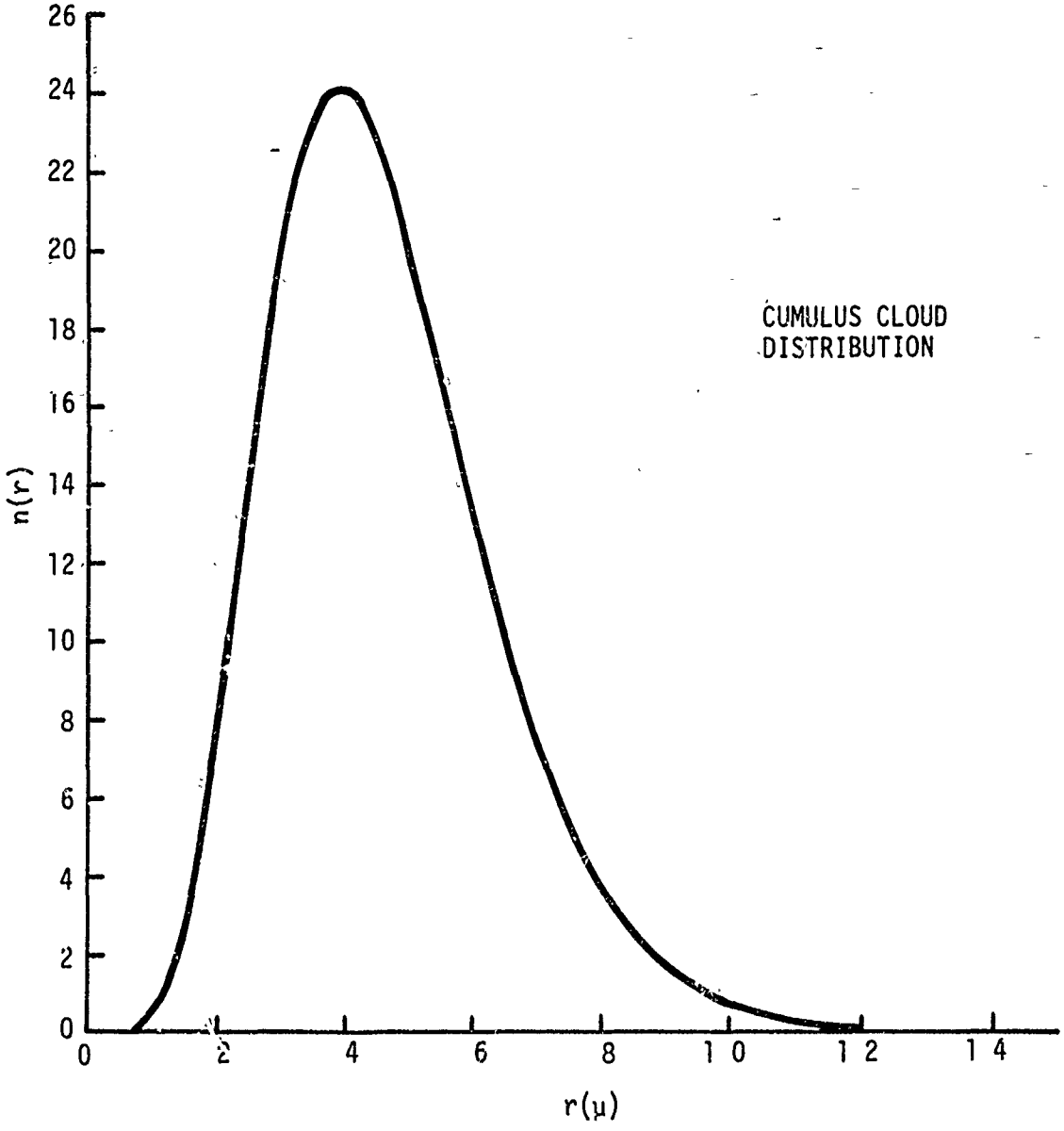

Figure 22. Cumulus Cloud Distribution

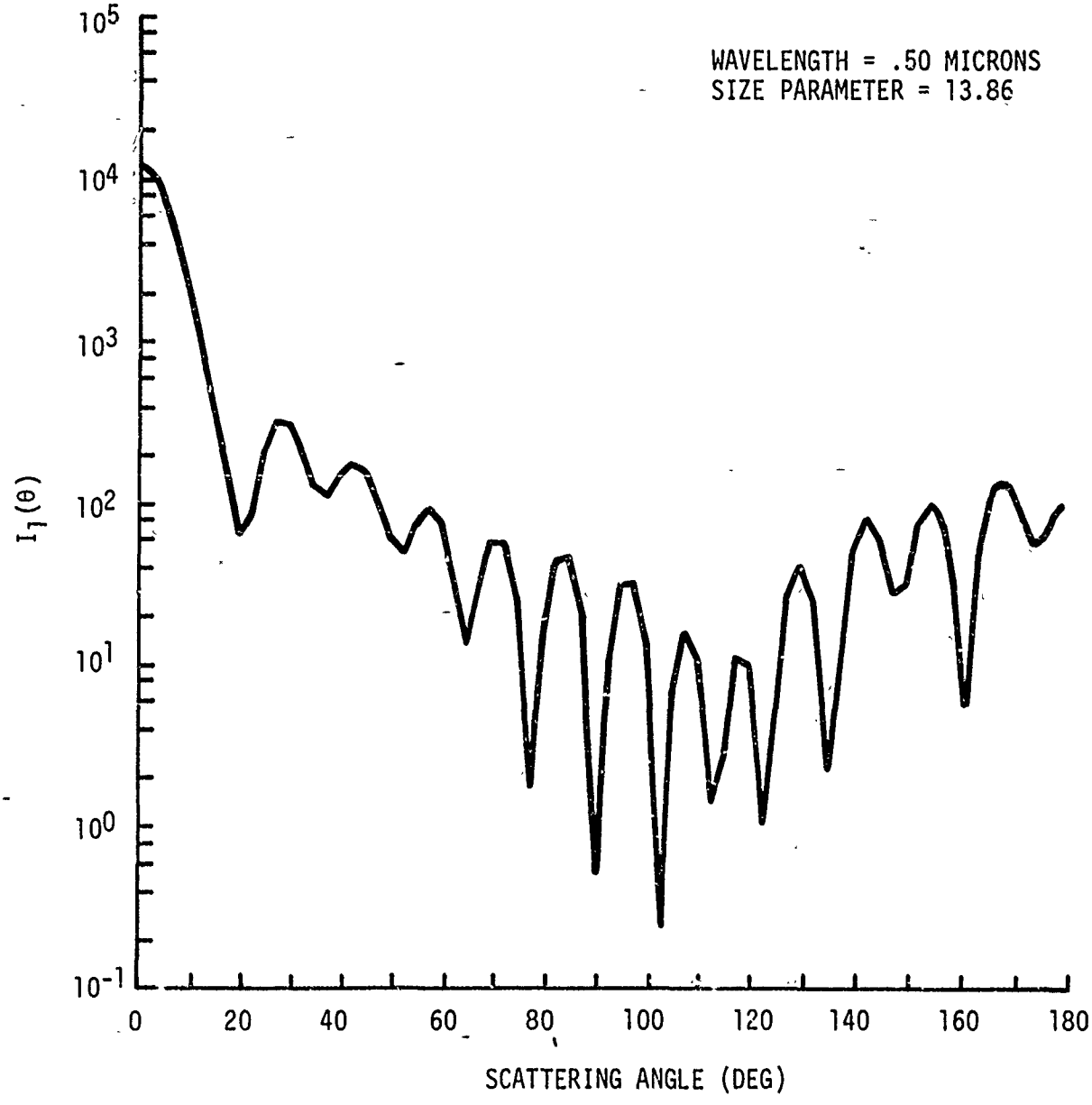

Figure 23. Particle Scattering Function for λ = 0.5μ and X = 13.86, Cumulus Cloud Distribution

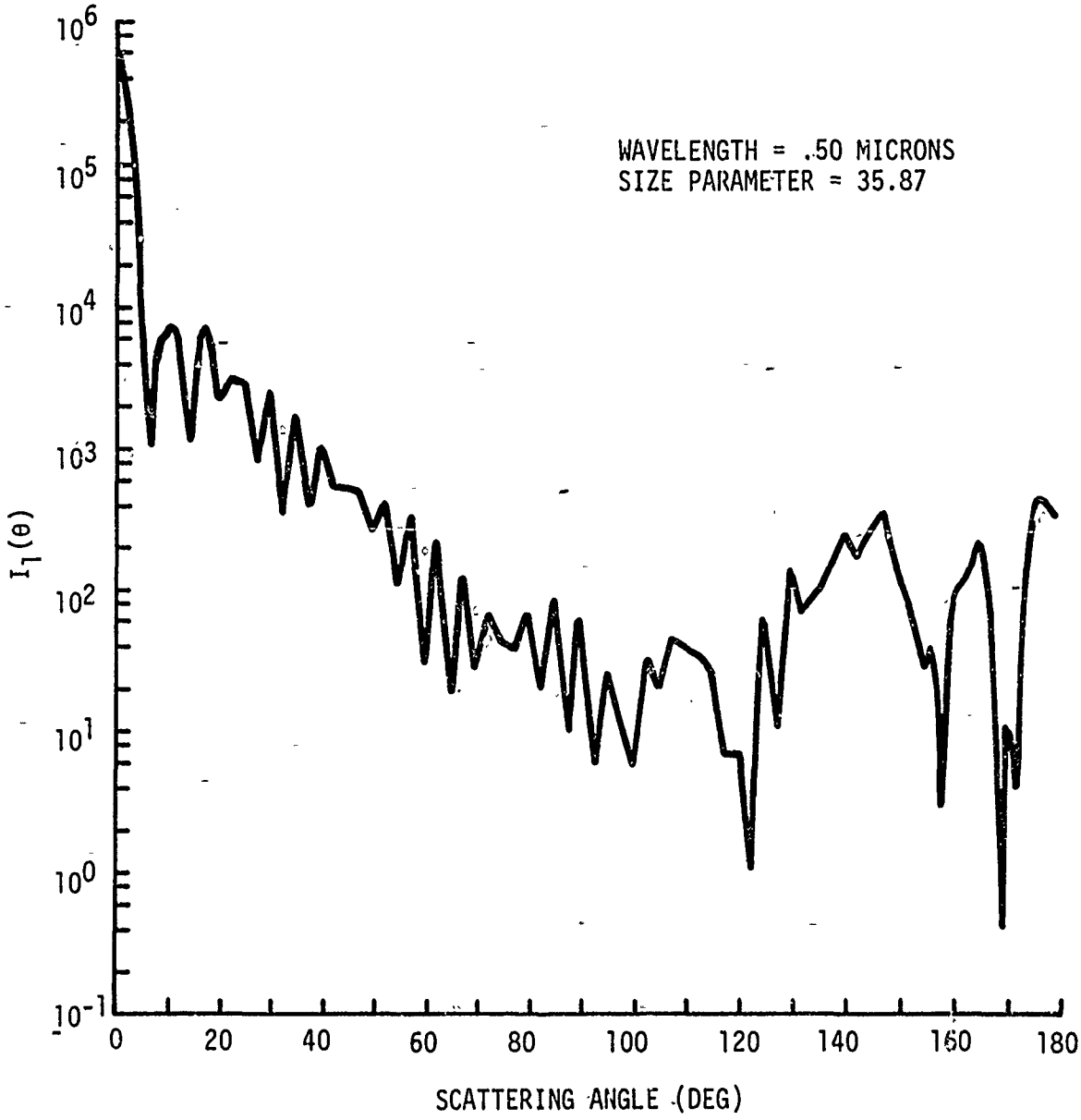

Figure 24. Particle Scattering Function for $\lambda = 0.5\mu$ and $X = 35.87$, Cumulus Cloud Distribution

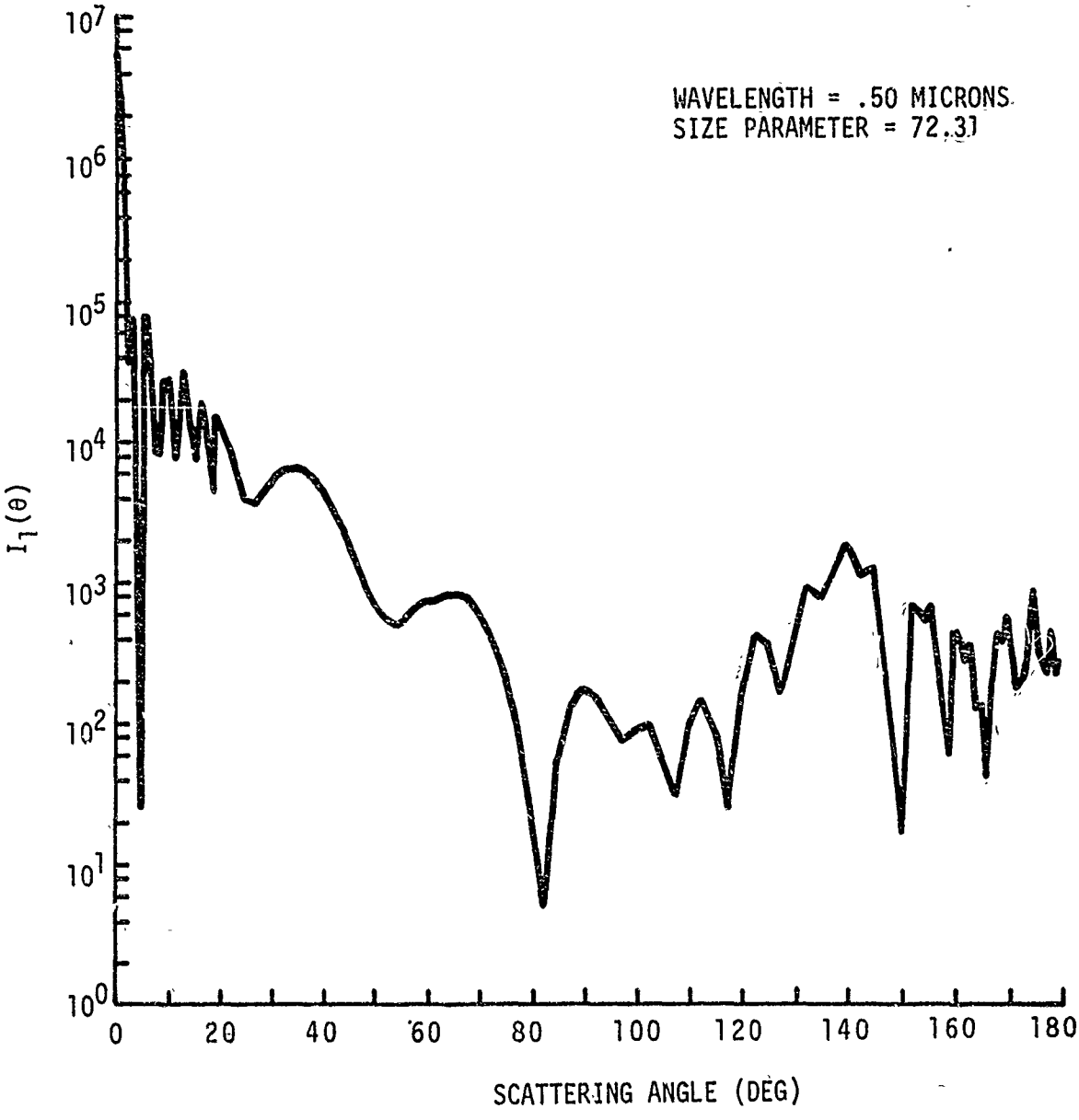

Figure 25. Particle Scattering Function for $\lambda = 0.5\mu$ and $X = 72.31$, Cumulus Cloud Distribution

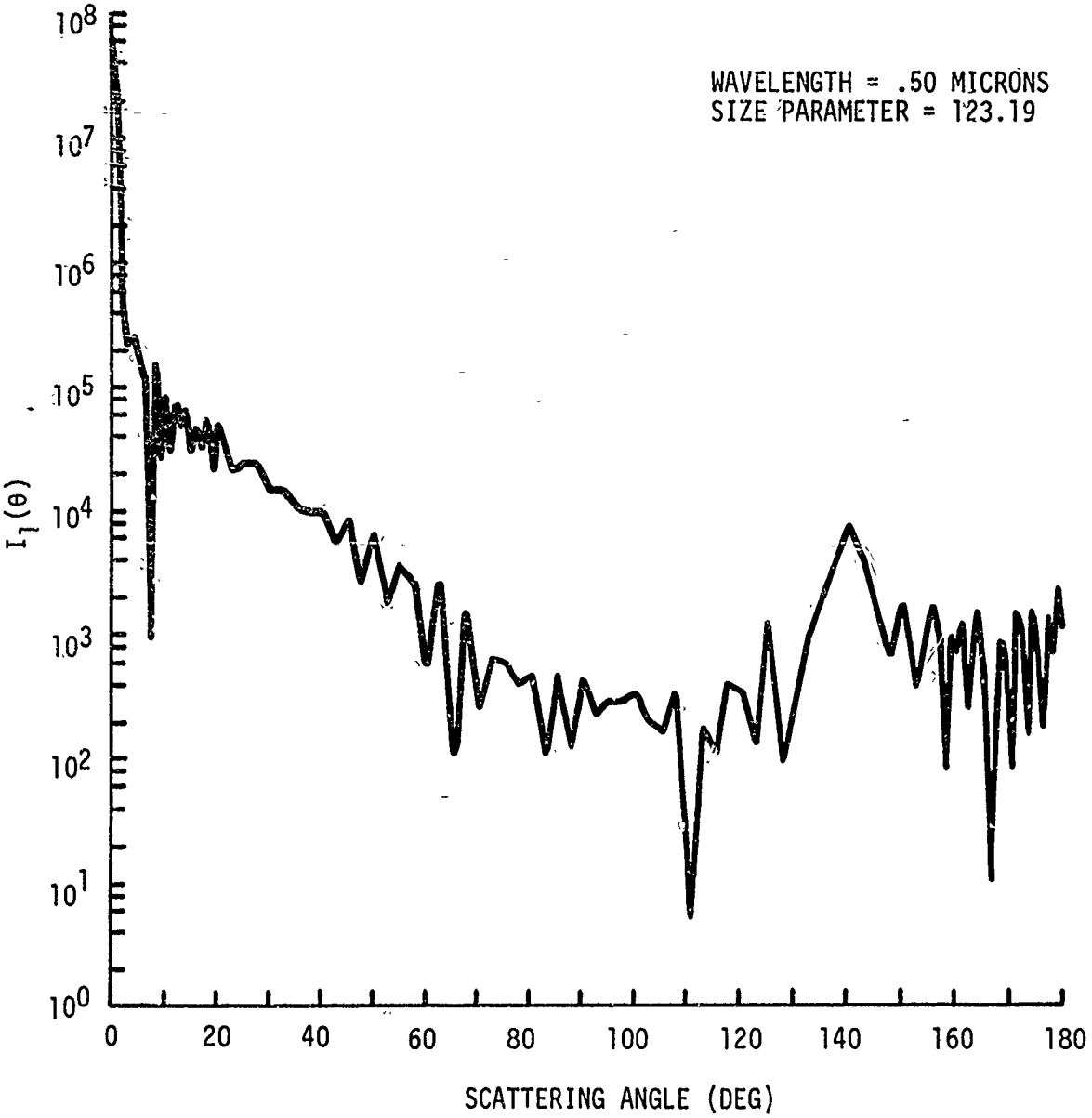

Figure 26. Particle Scattering Function for $\lambda = 0.5\mu$ and $X = 123.19$, Cumulus Cloud Distribution

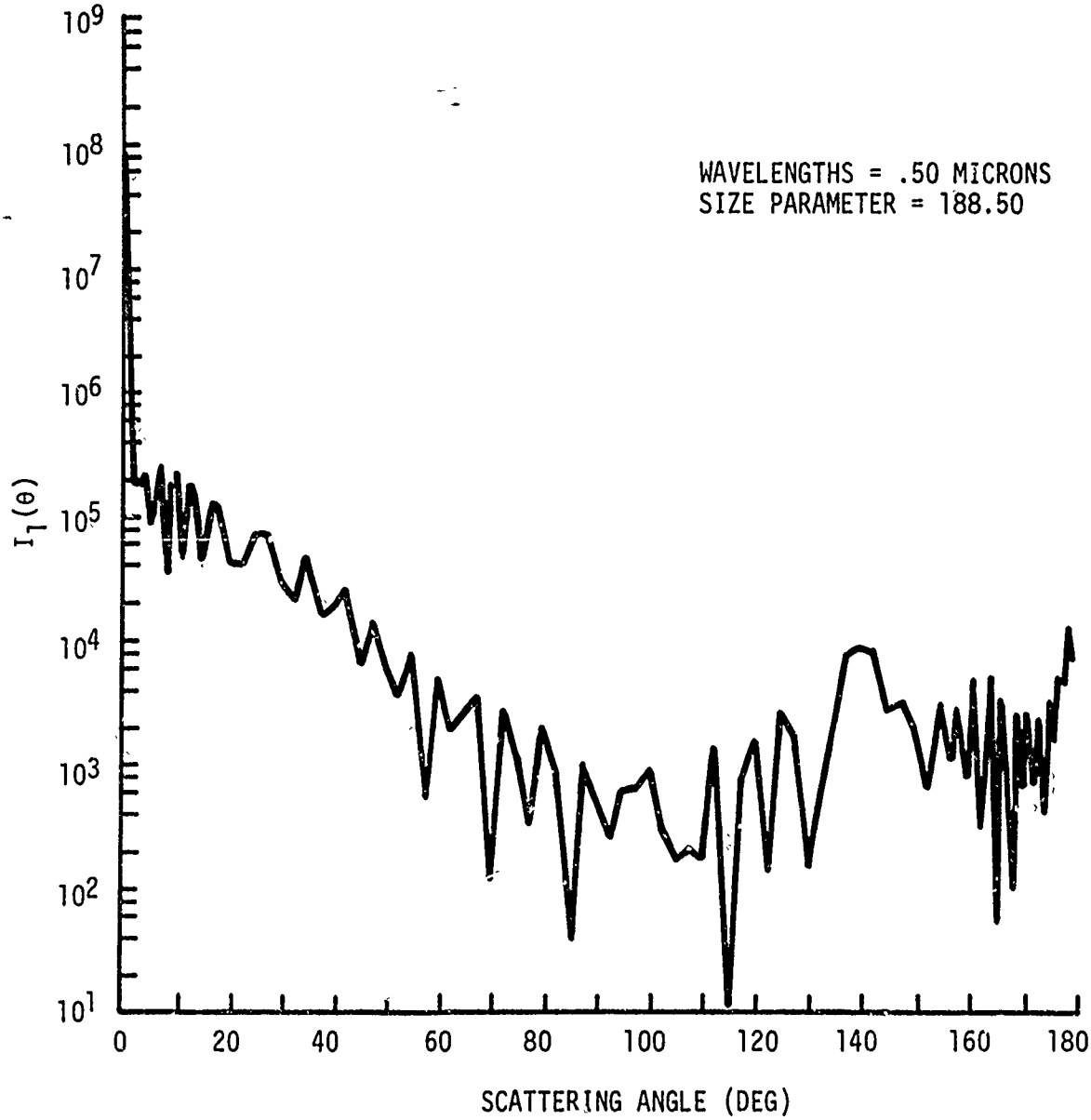

Figure 27. Particle Scattering Function for $\lambda = 0.5\mu$ and $X = 188.50$, Cumulus Cloud Distribution

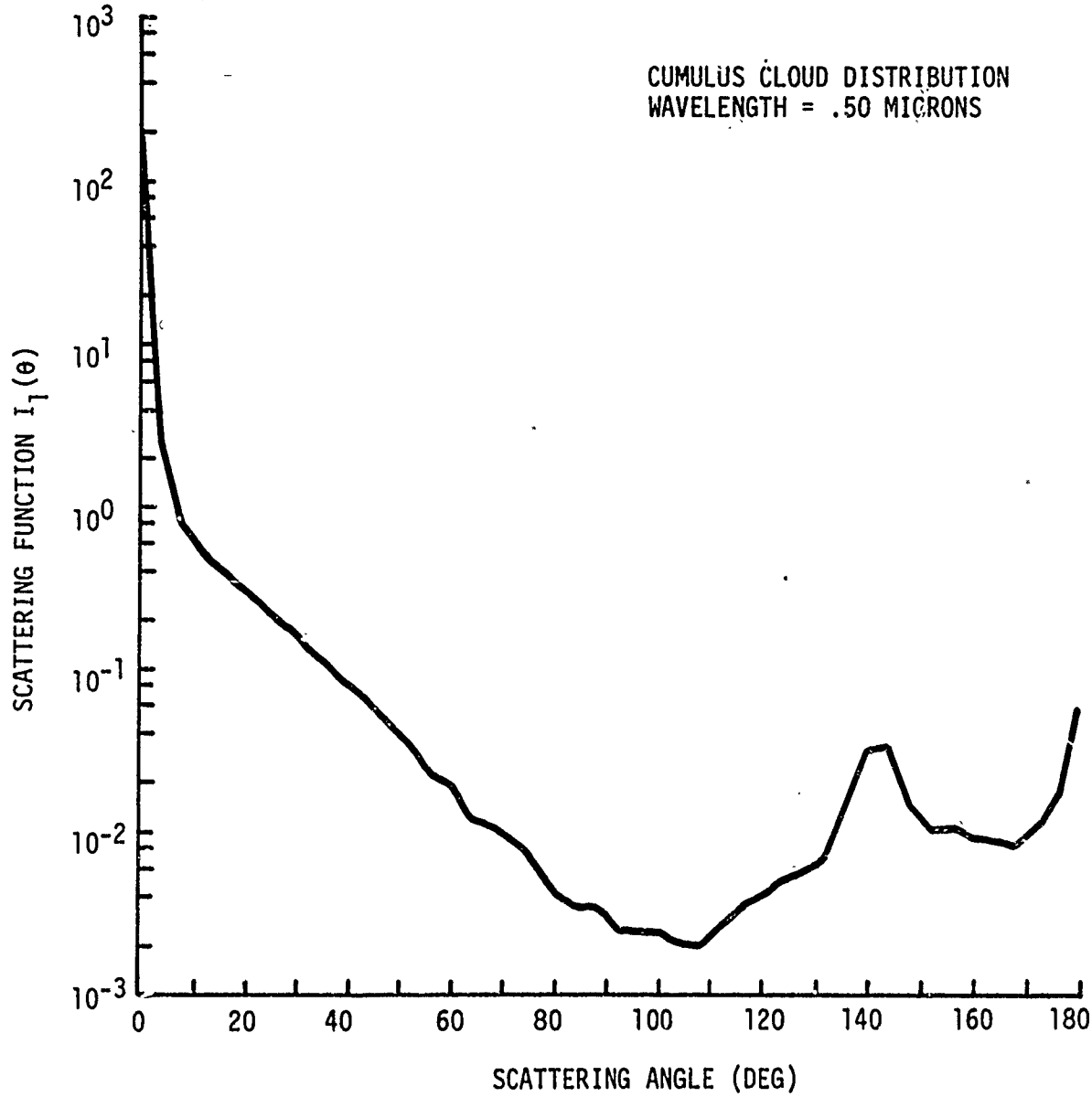

Figure 28. Volume Scattering Function $I_1(\theta)$ for Cumulus Cloud Distribution at $\lambda = 0.5\mu$

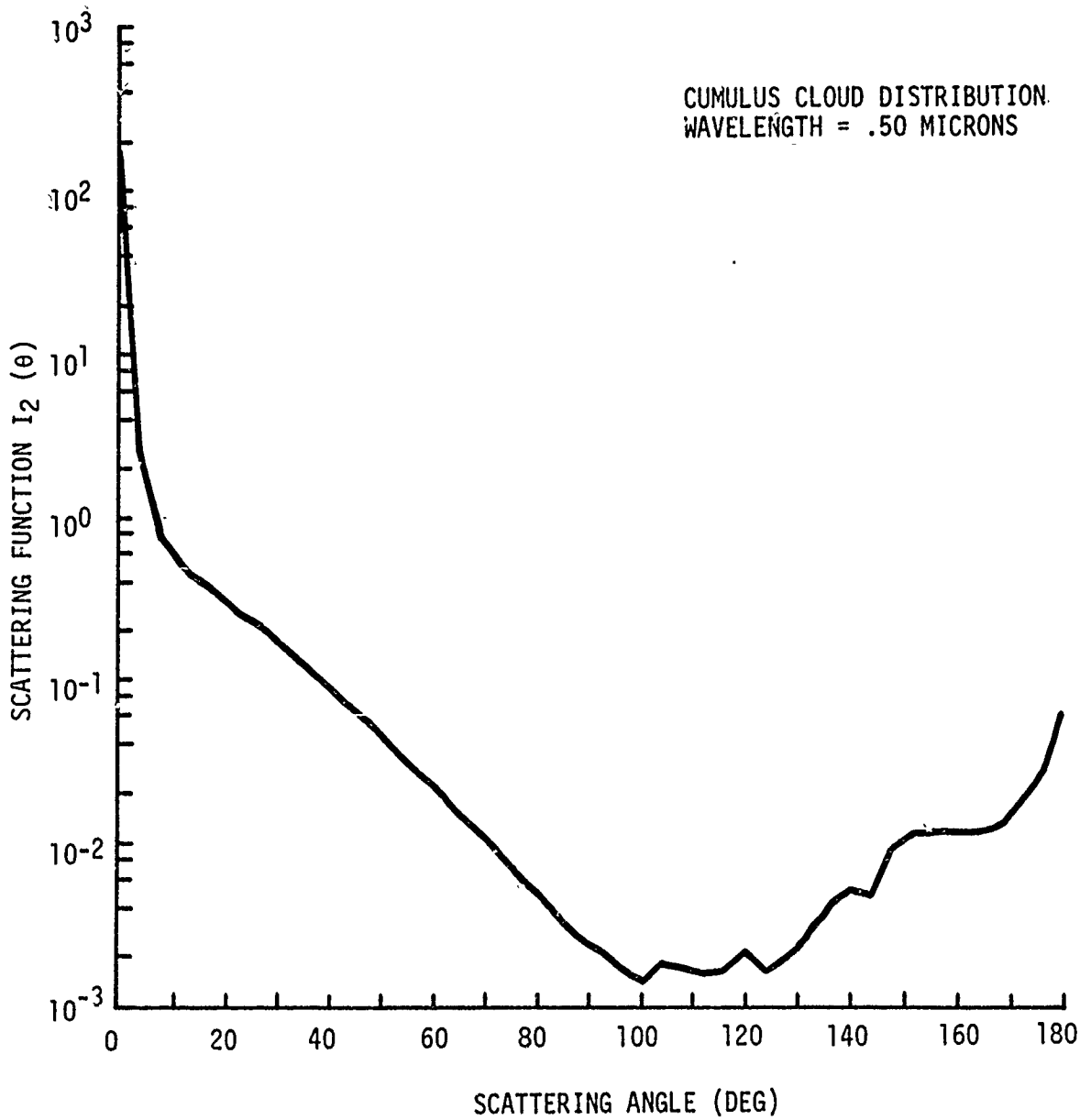

Figure 29. Volume Scattering Function $I_2(\theta)$ for Cumulus Cloud Distribution at $\lambda = 0.5\mu$

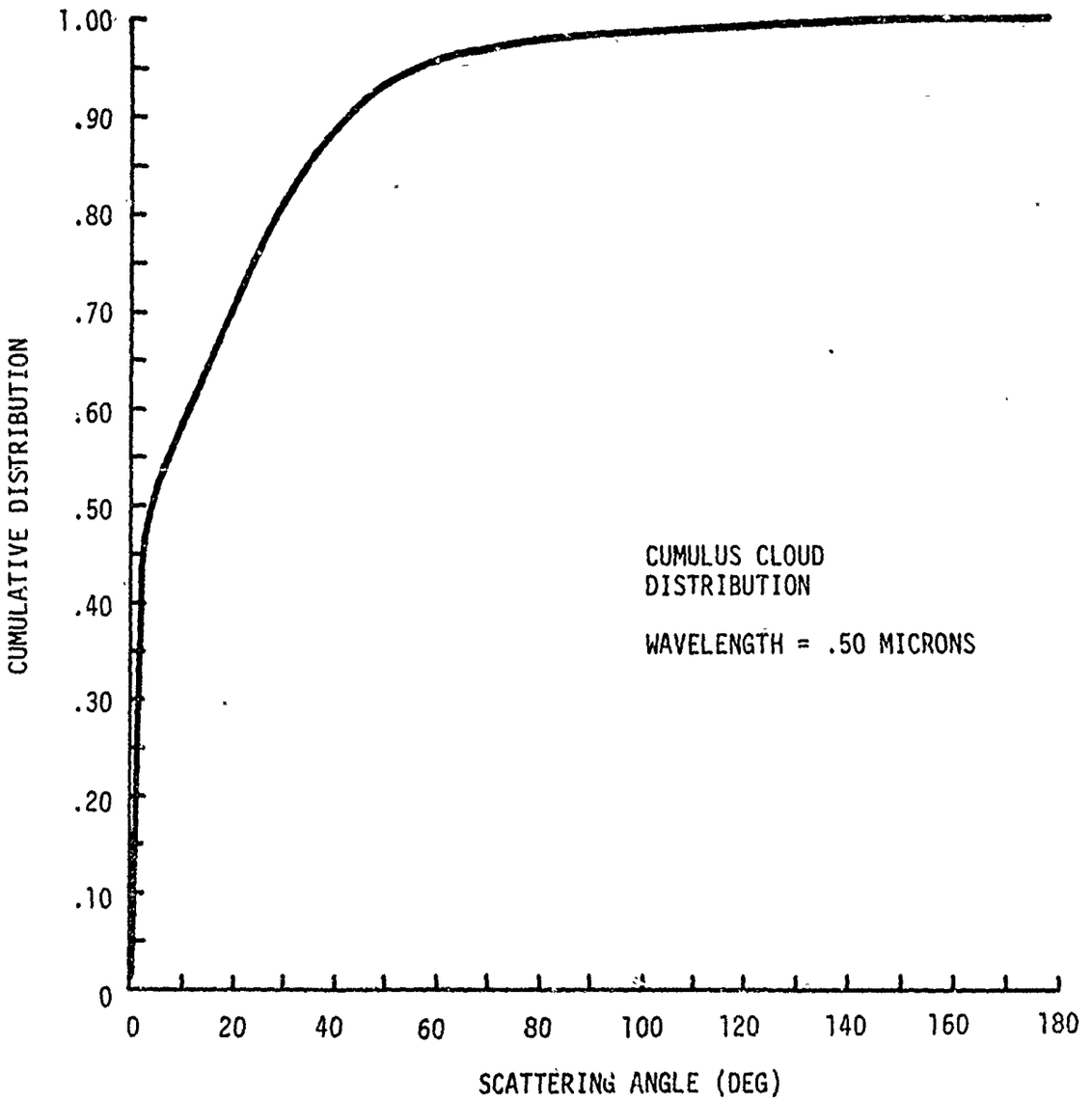

Figure 30. Cumulative Distribution for Cumulus Cloud Distribution at $\lambda = 0.5\mu$

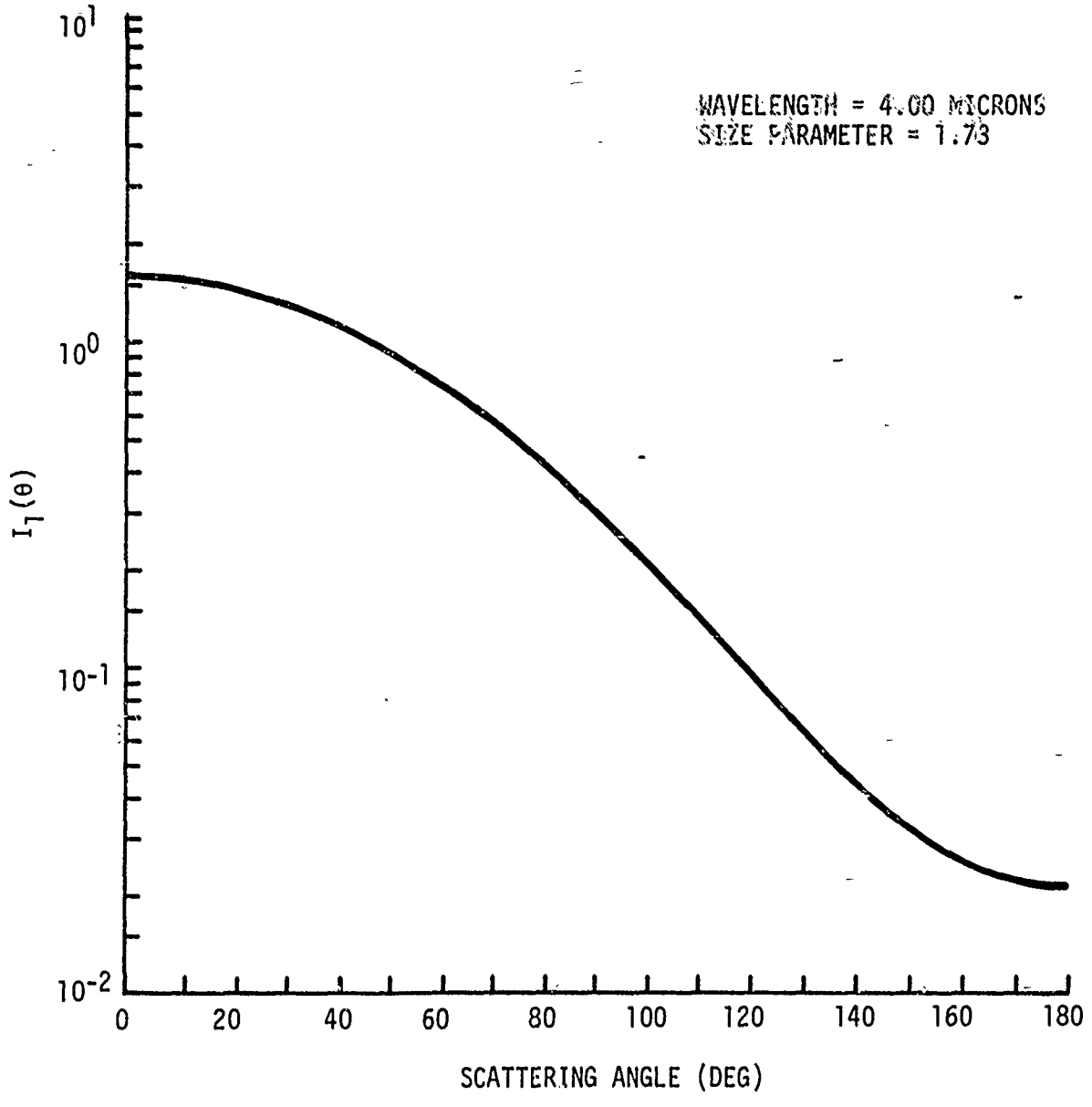

Figure 31. Particle Scattering Function for λ = 4.0μ and X = 1.73, Cumulus Cloud Distribution

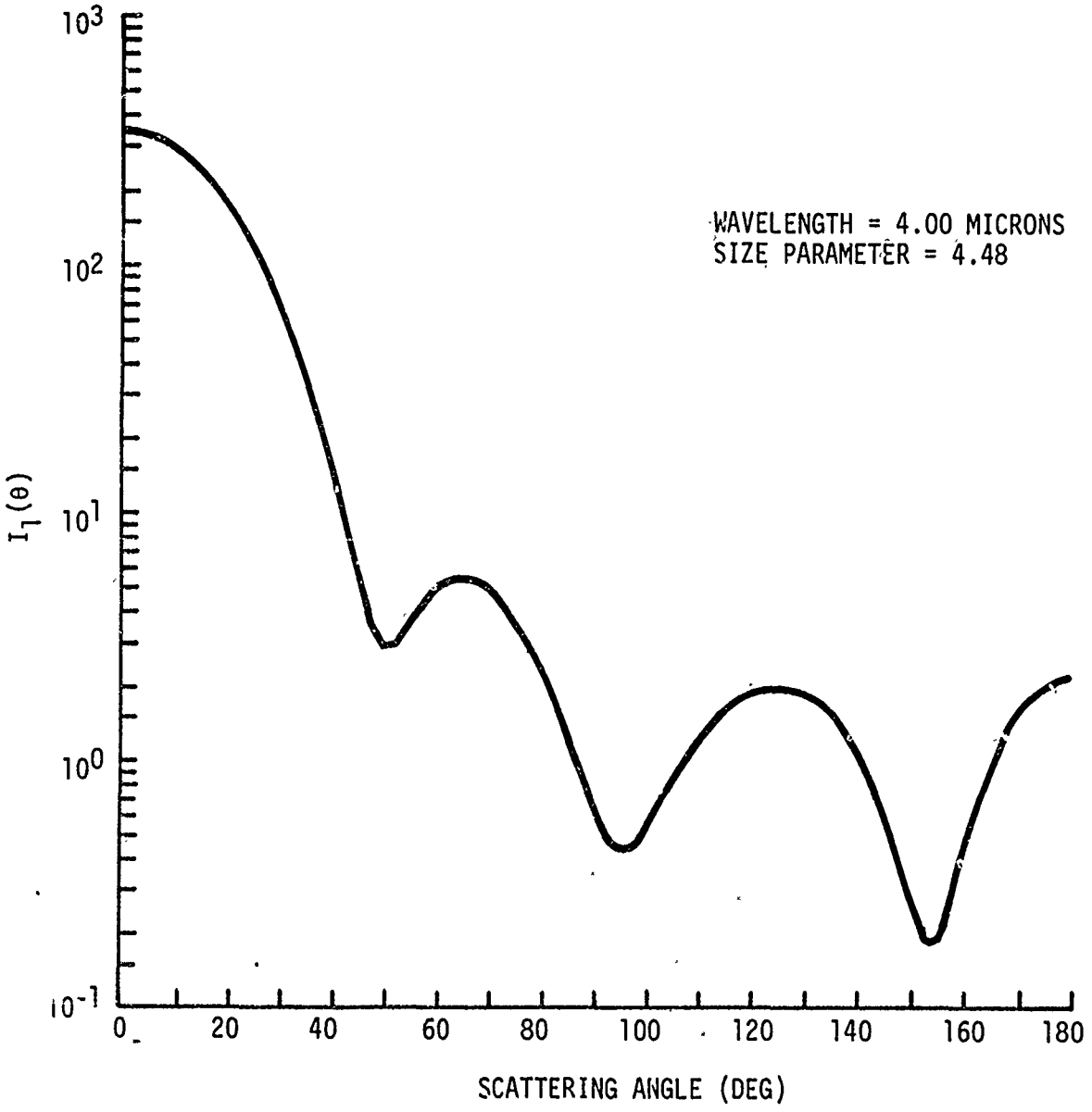

Figure 32. Particle Scattering Function for λ = 4.0μ and X = 4.48, Cumulus Cloud Distribution

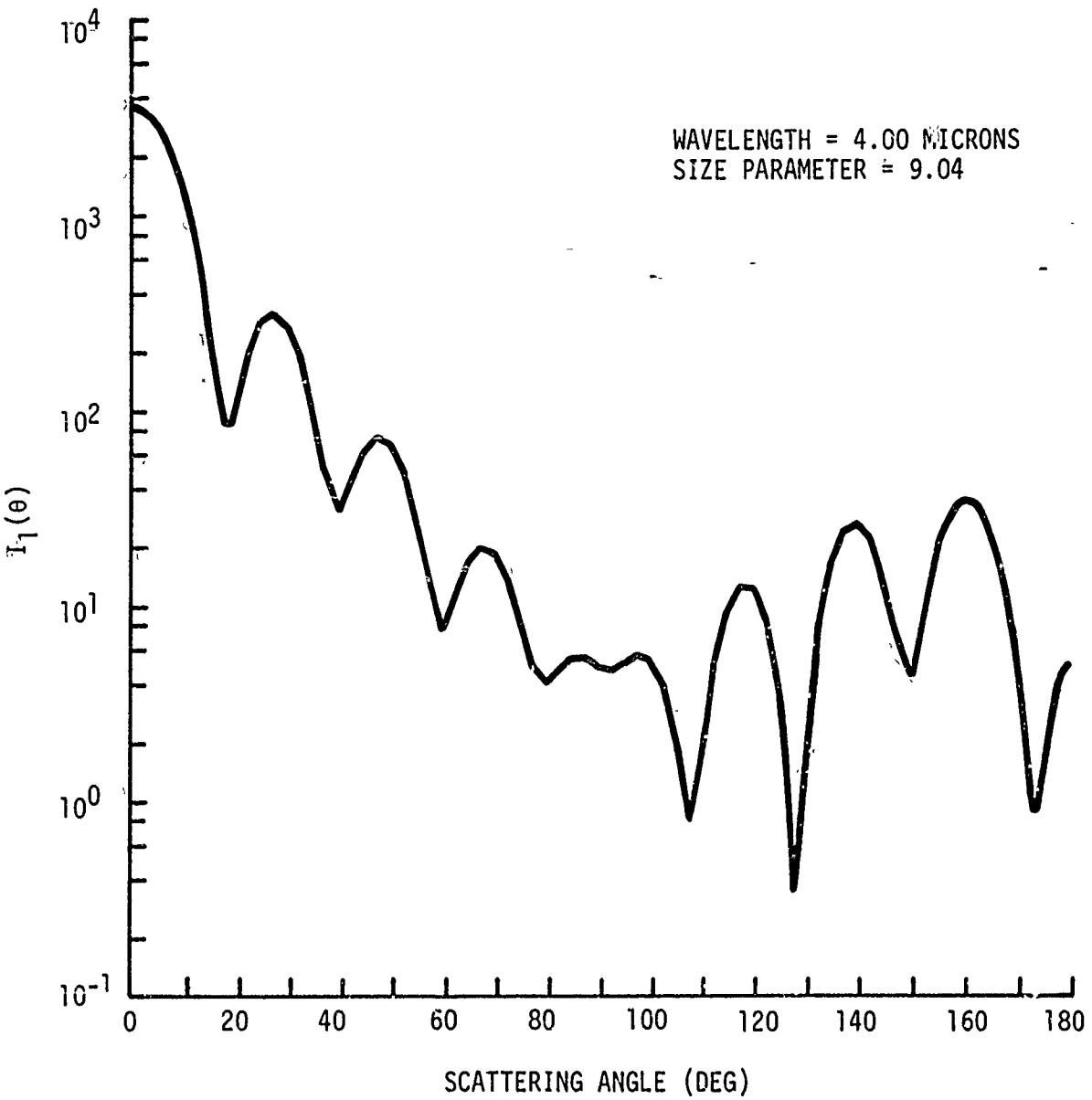

Figure 33. Particle Scattering Function for $\lambda = 4.0\mu$ and $x = 9.04$, Cumulus Cloud Distribution

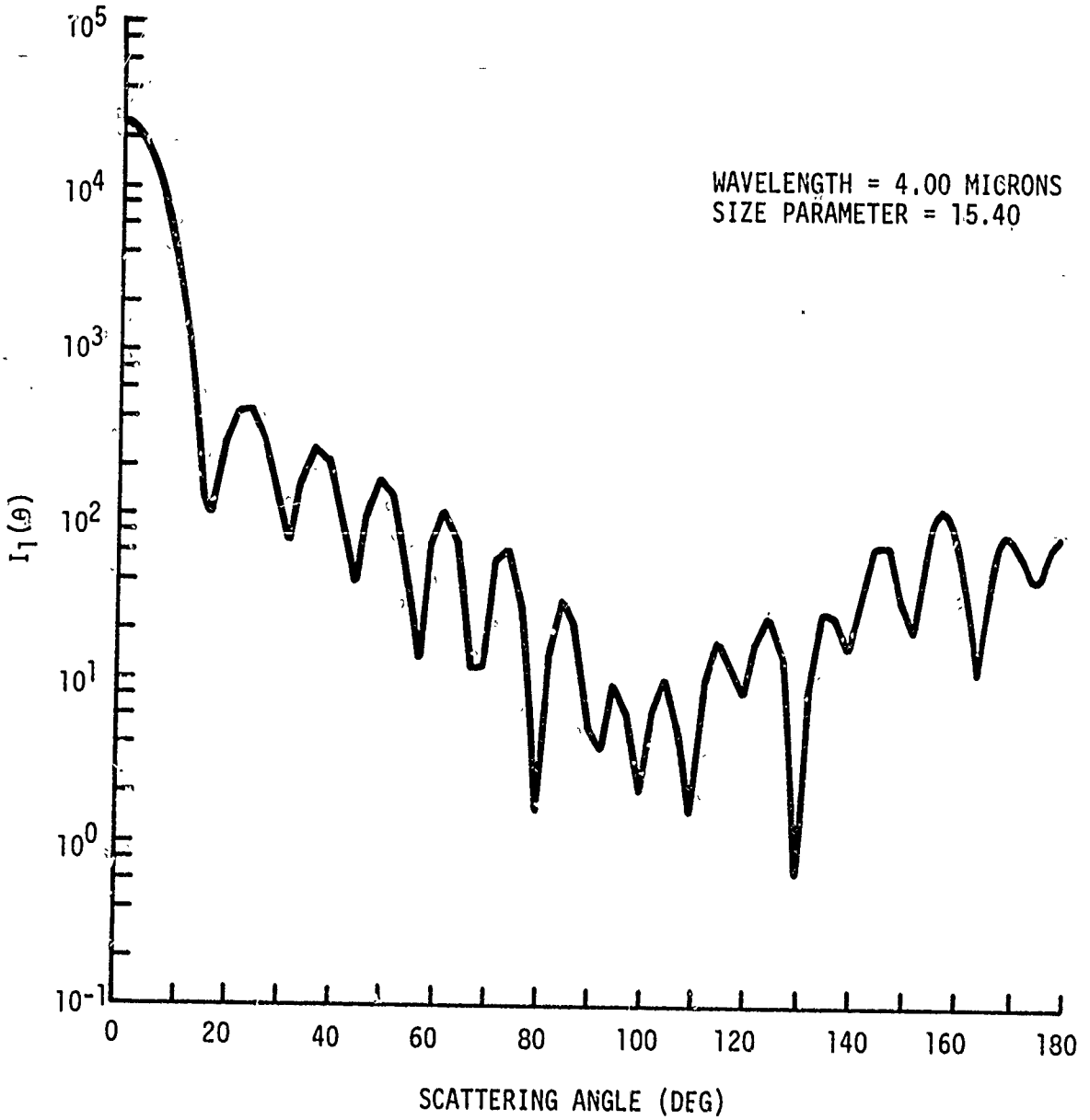

Figure 34. Particle Scattering Function for λ = 4.0μ and X = 15.40, Cumulus Cloud Distribution

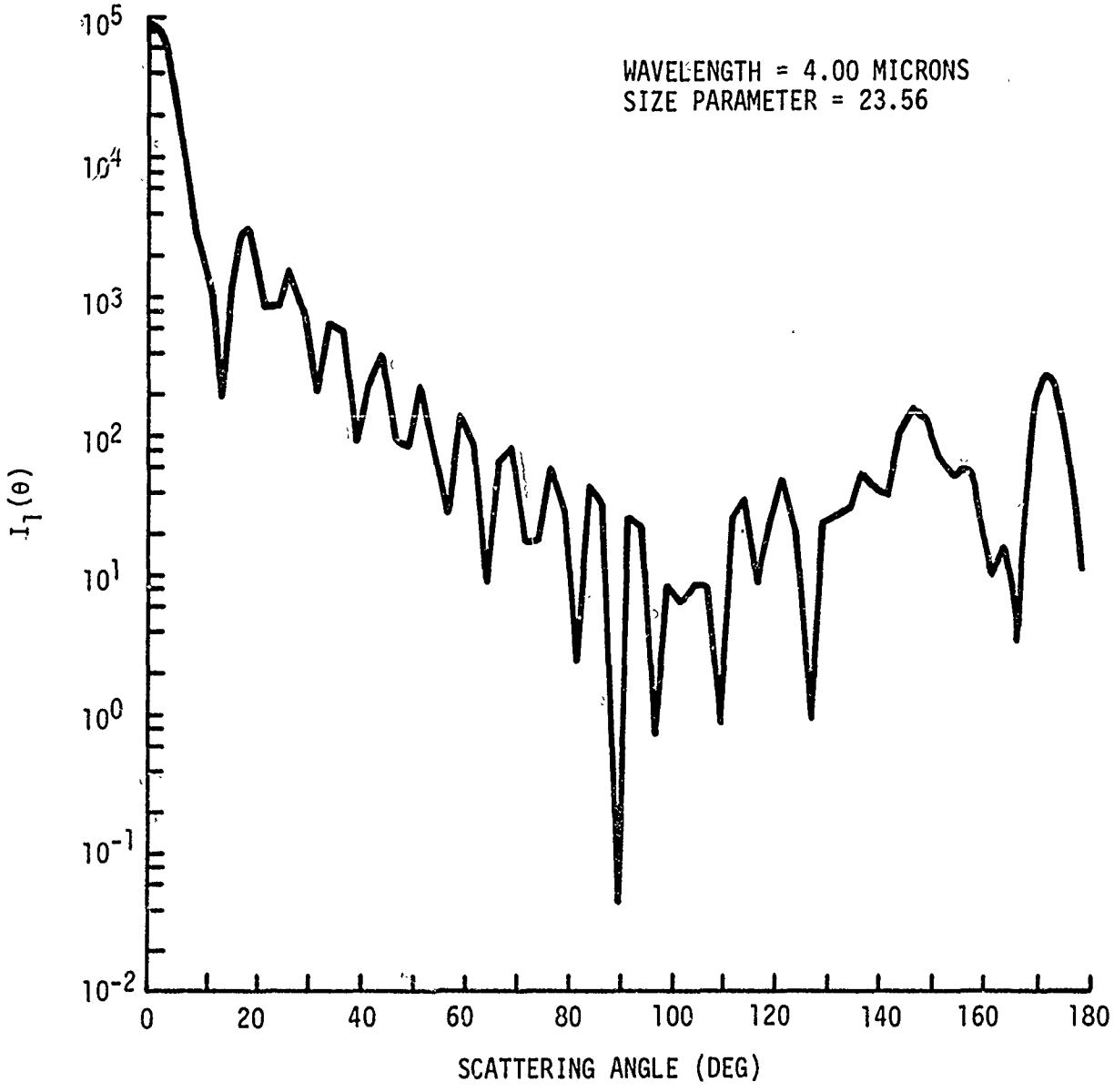

Figure 35. Particle Scattering Function for $\lambda = 4.0\mu$ and $x = 23.56$, Cumulus Cloud Distribution

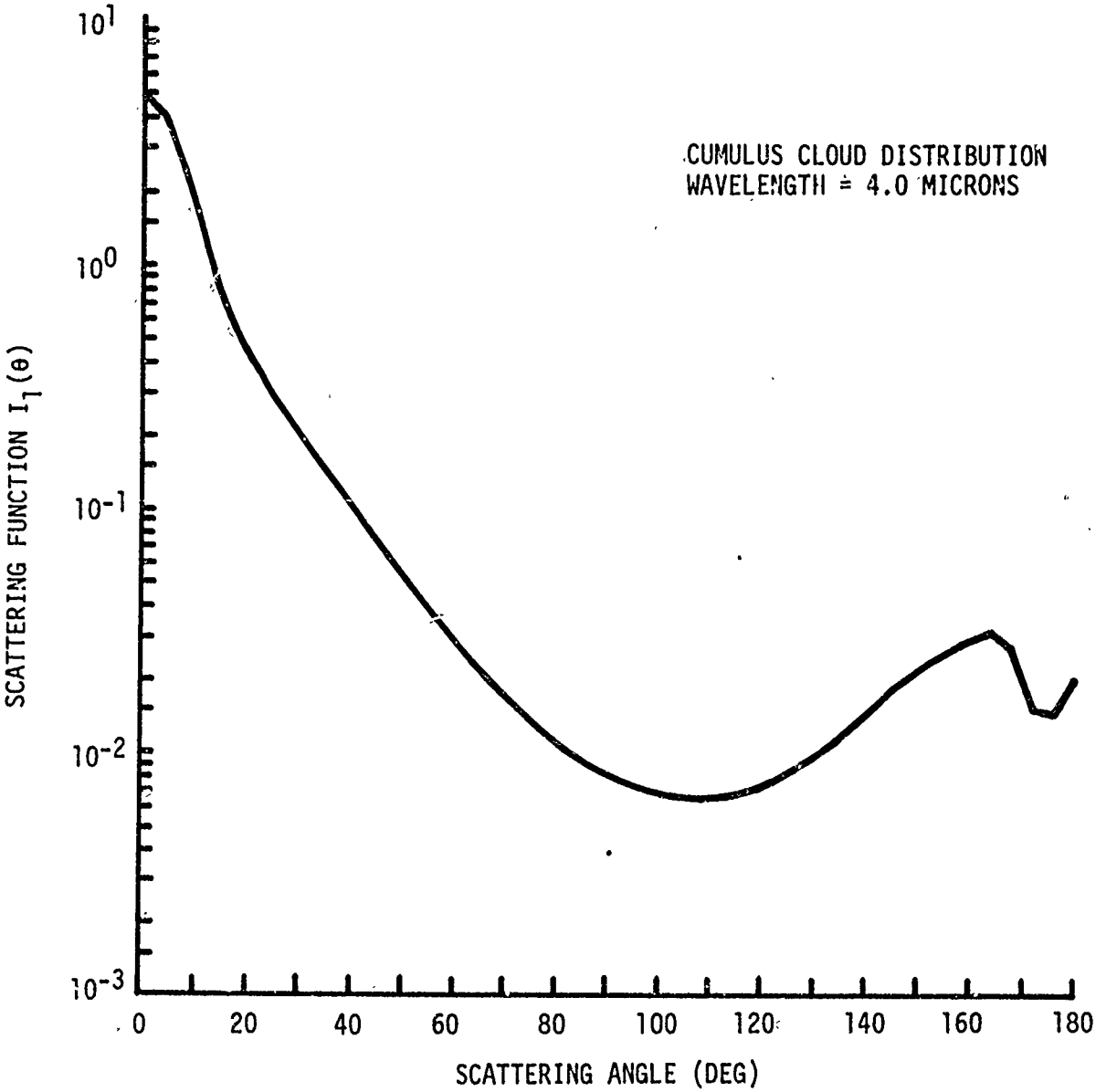

Figure 36. Volume Scattering Function $I_1(\theta)$ for Cumulus Cloud Distribution at $\lambda = 4.0\mu$

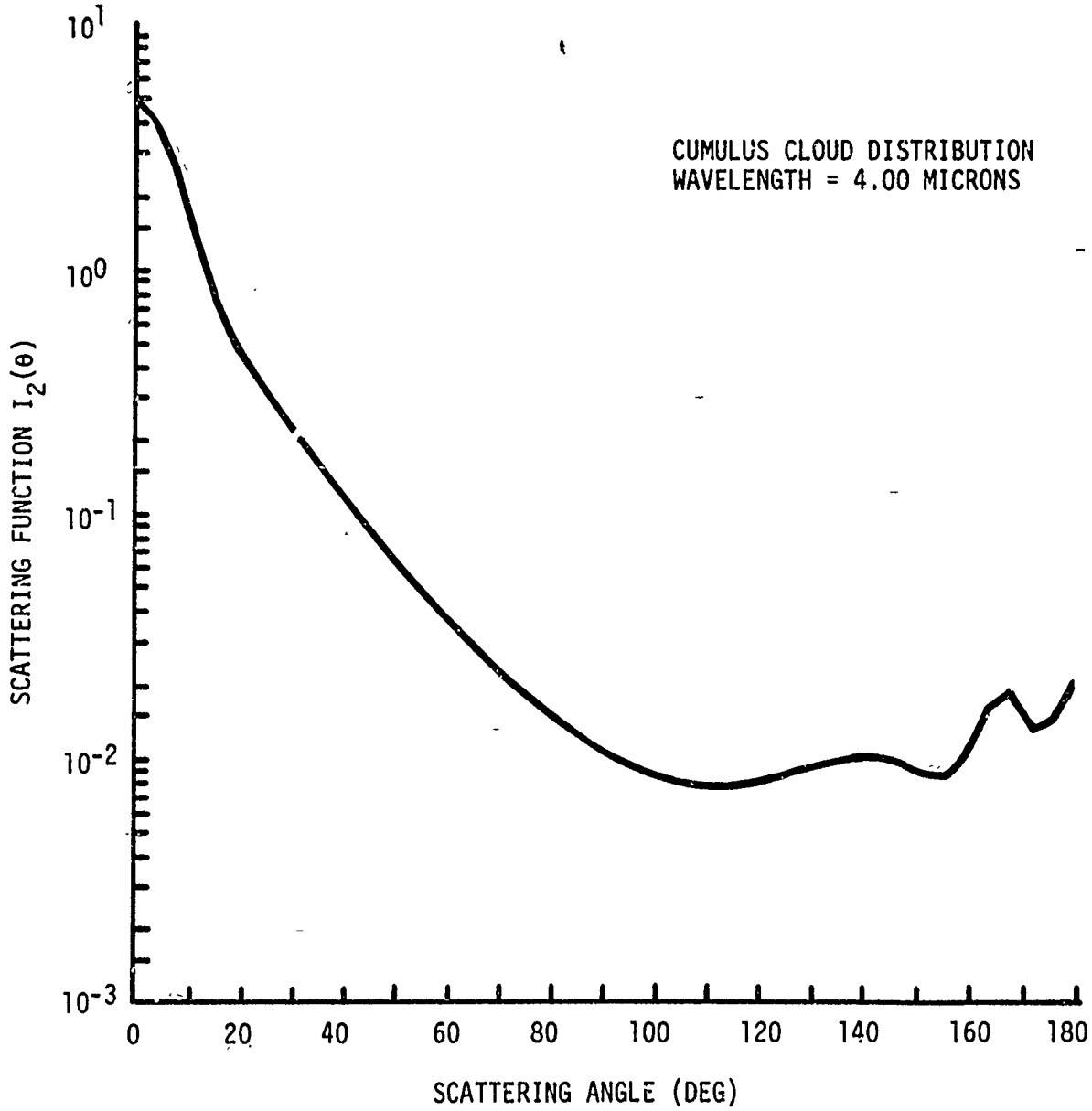

Figure 37. Volume Scattering Function $I_2(\theta)$ for Cumulus Cloud Distribution at $\lambda = 4.0\mu$

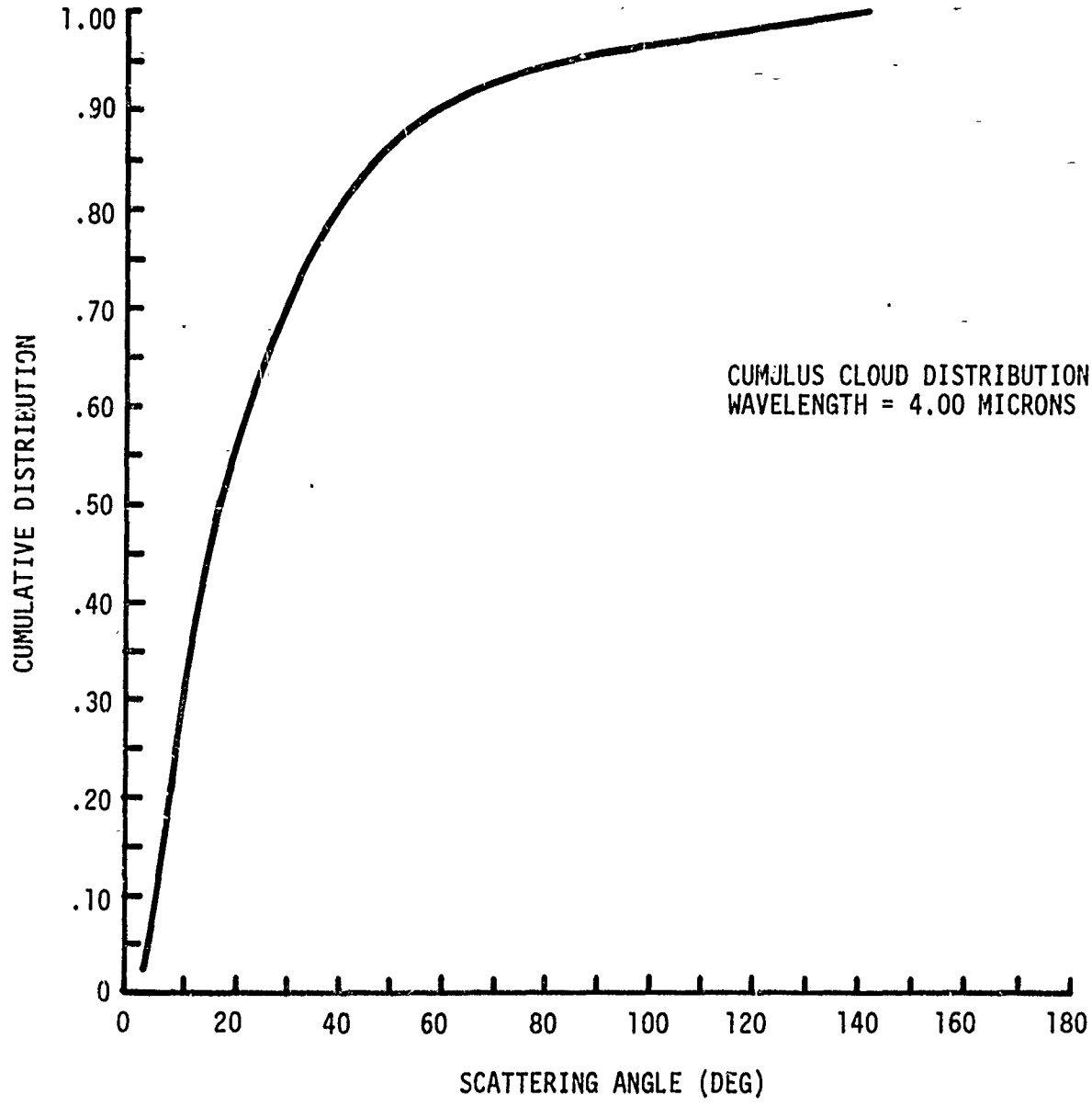

Figure 38. Cumulative Distribution for Cumulus Cloud Distribution at $\lambda = 4.0\mu$

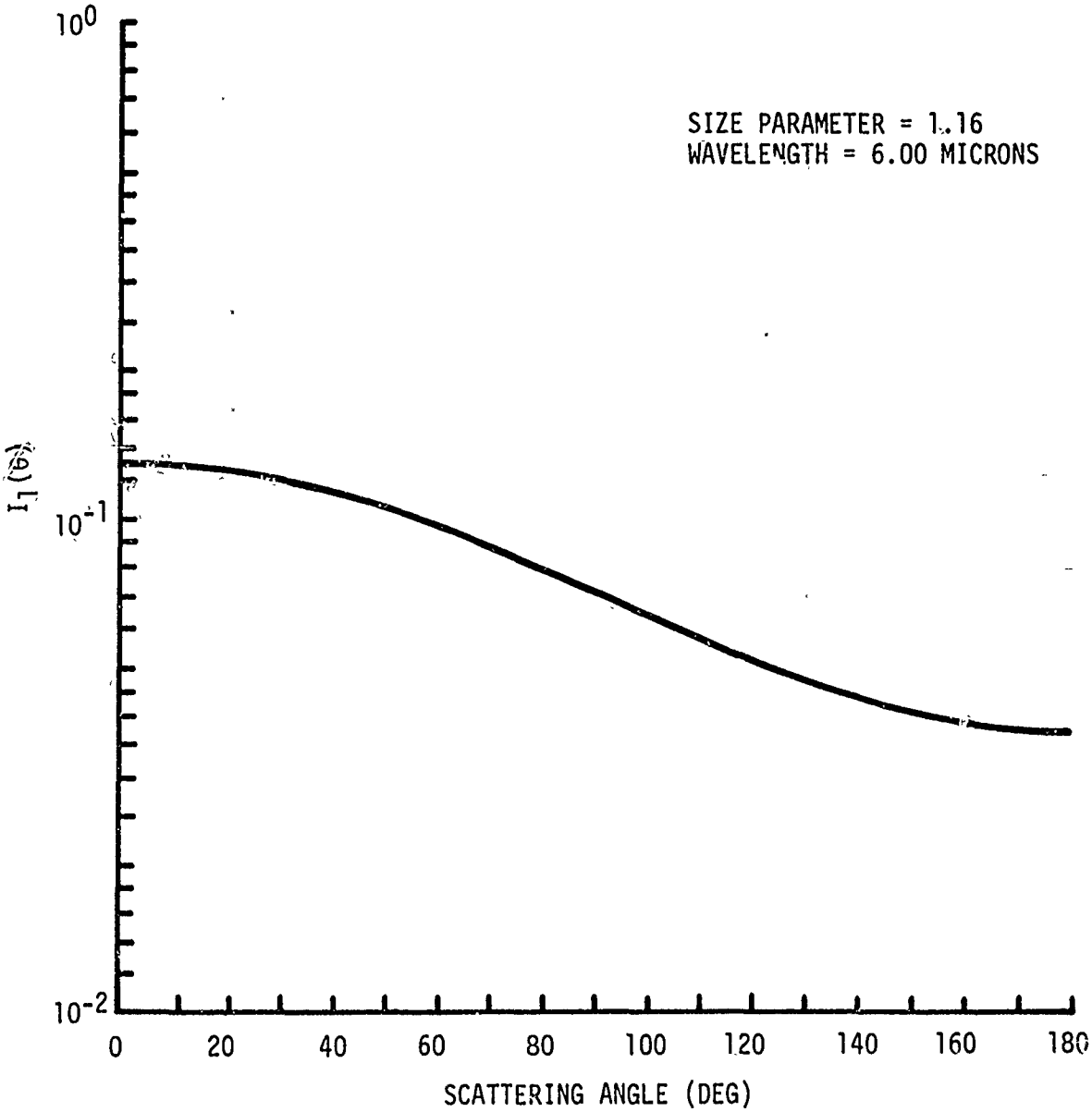

Figure 39. Particle Scattering Function for λ = 6.0μ and X = 1.16, Cumulus Cloud Distribution

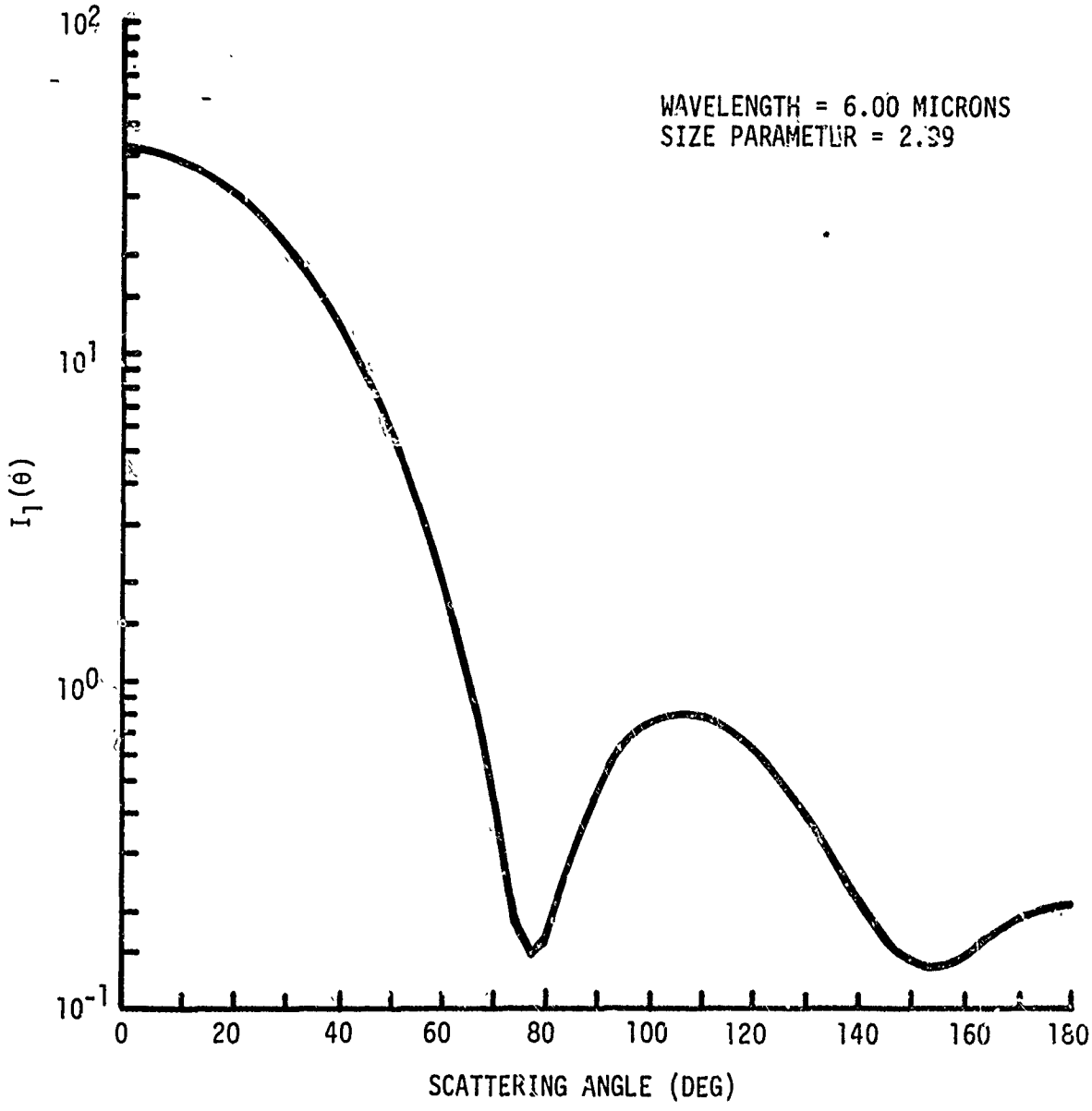

Figure 40. Particle Scattering Function for $\lambda = 6.0\mu$ and $x = 2.99$, Cumulus Cloud Distribution

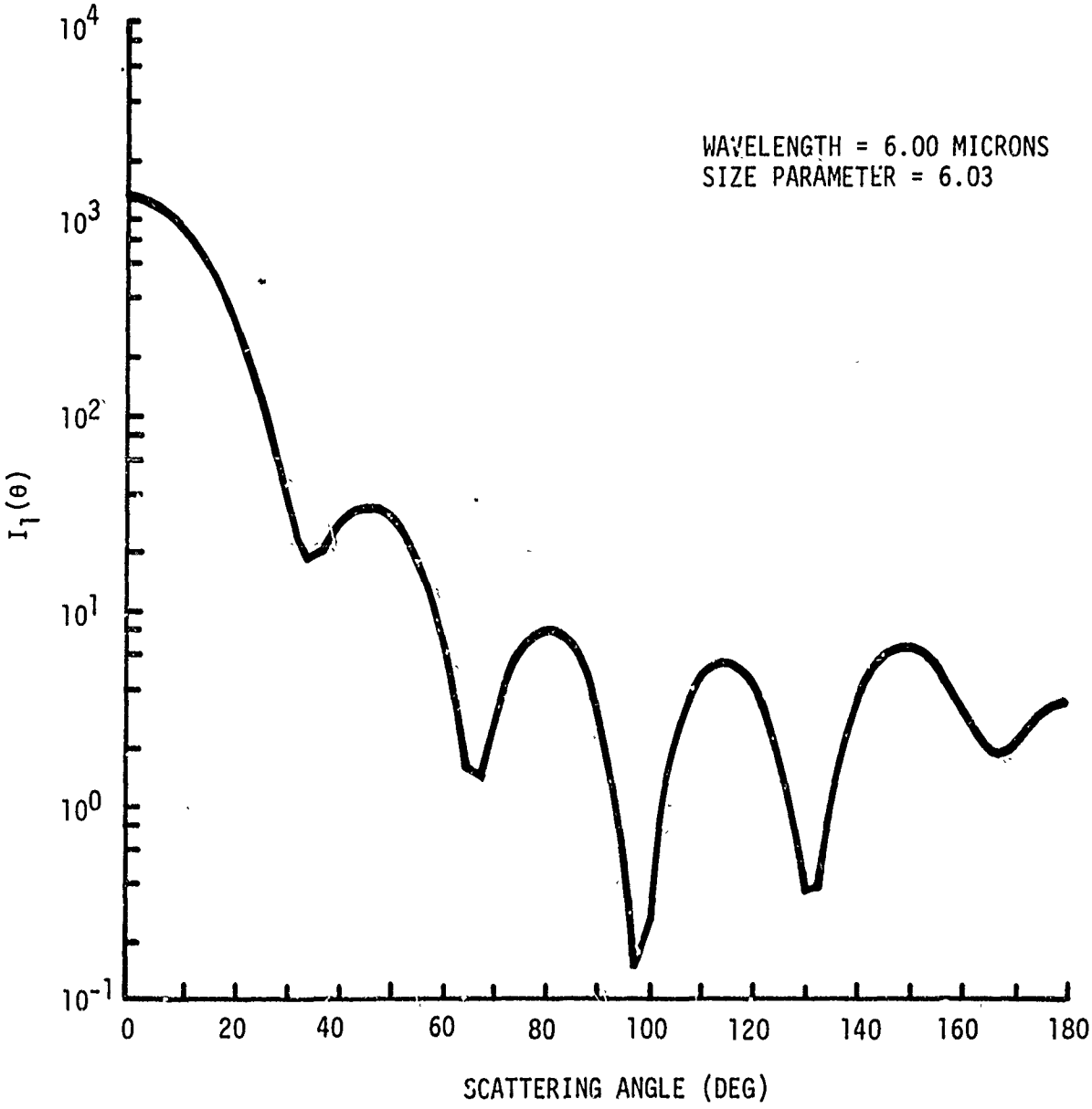

Figure 41. Particle Scattering Function for λ = 6.0μ and x = 6.03, Cumulus Cloud Distribution

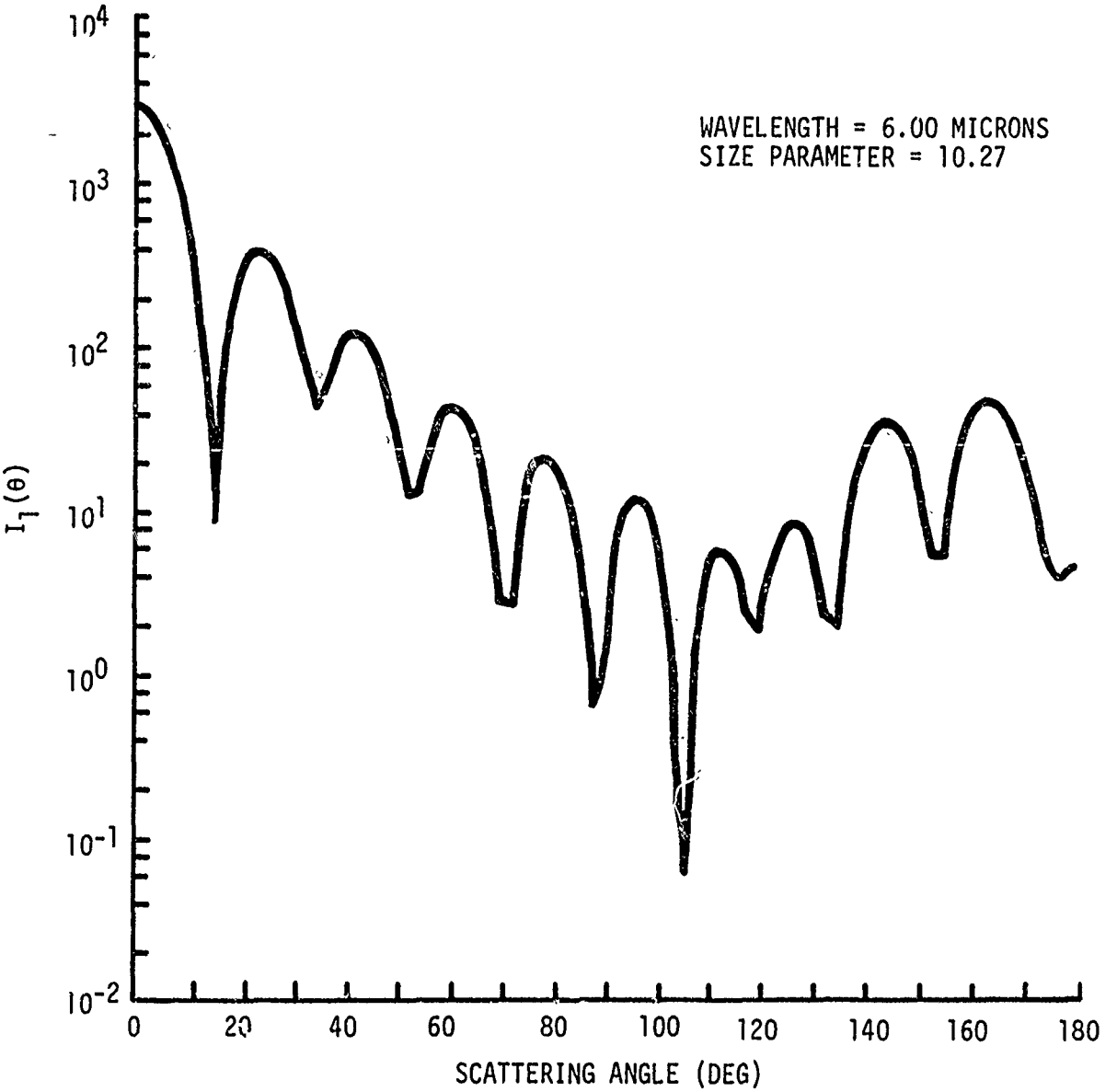

Figure 42. Particle Scattering Function for $\lambda = 6.0\mu$ and $x = 10.27$, Cumulus Cloud Distribution

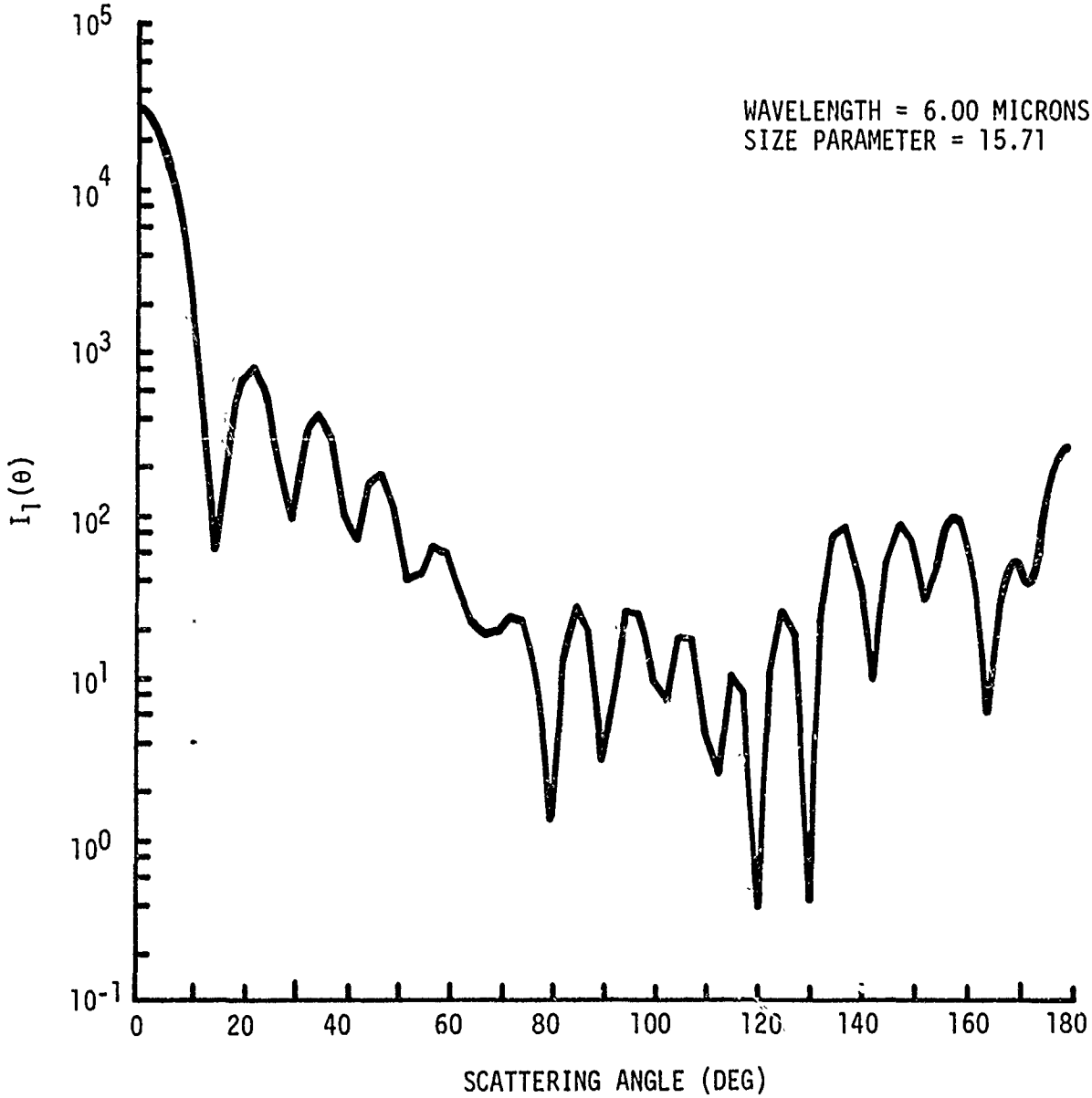

Figure 43. Particle Scattering Function for λ = 6.0μ and x = 15.71, Cumulus Cloud Distribution

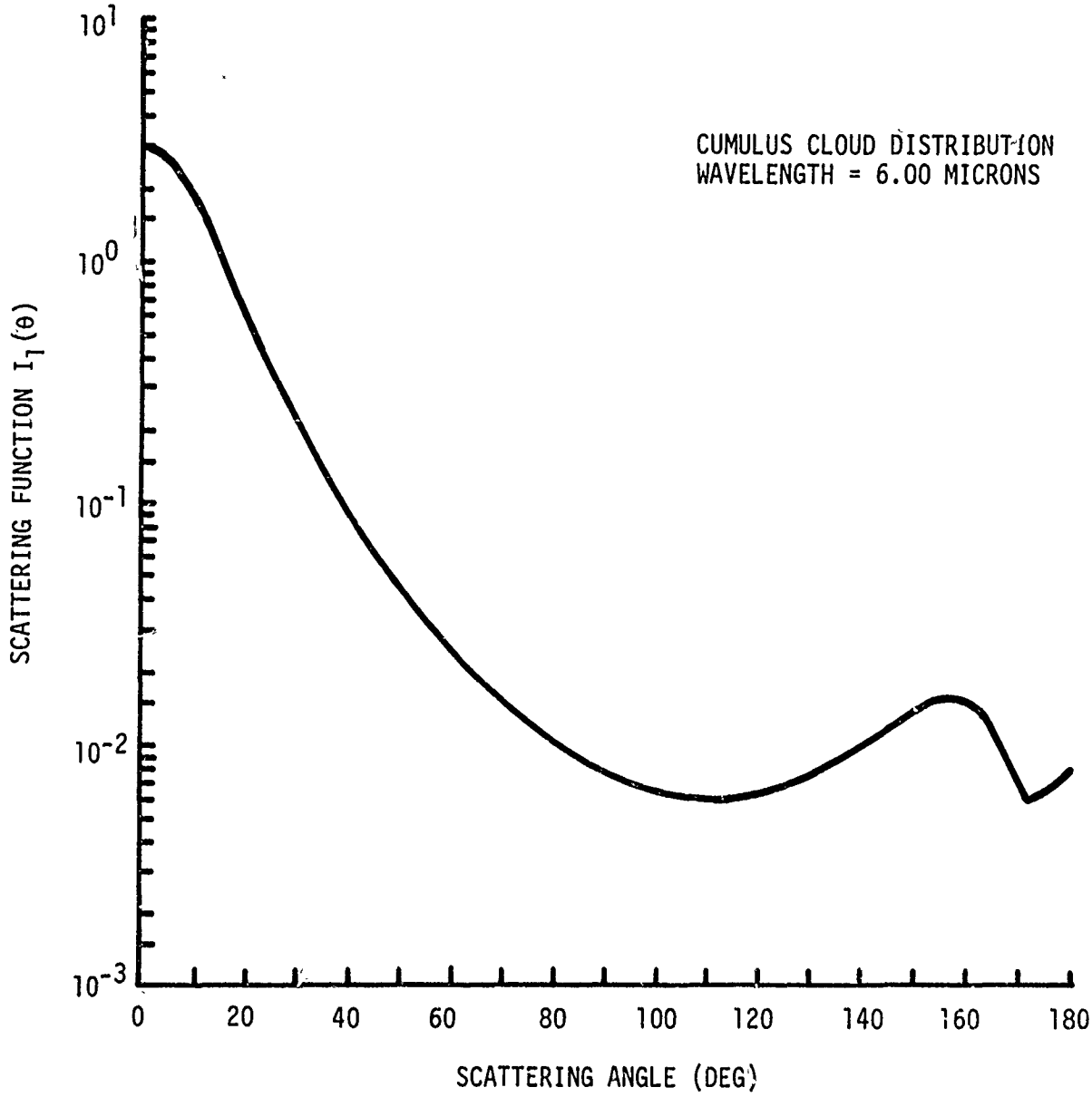

Figure 44. Volume Scattering Function $I_1(\theta)$ for Cumulus Cloud Distribution at $\lambda = 6.0\mu$

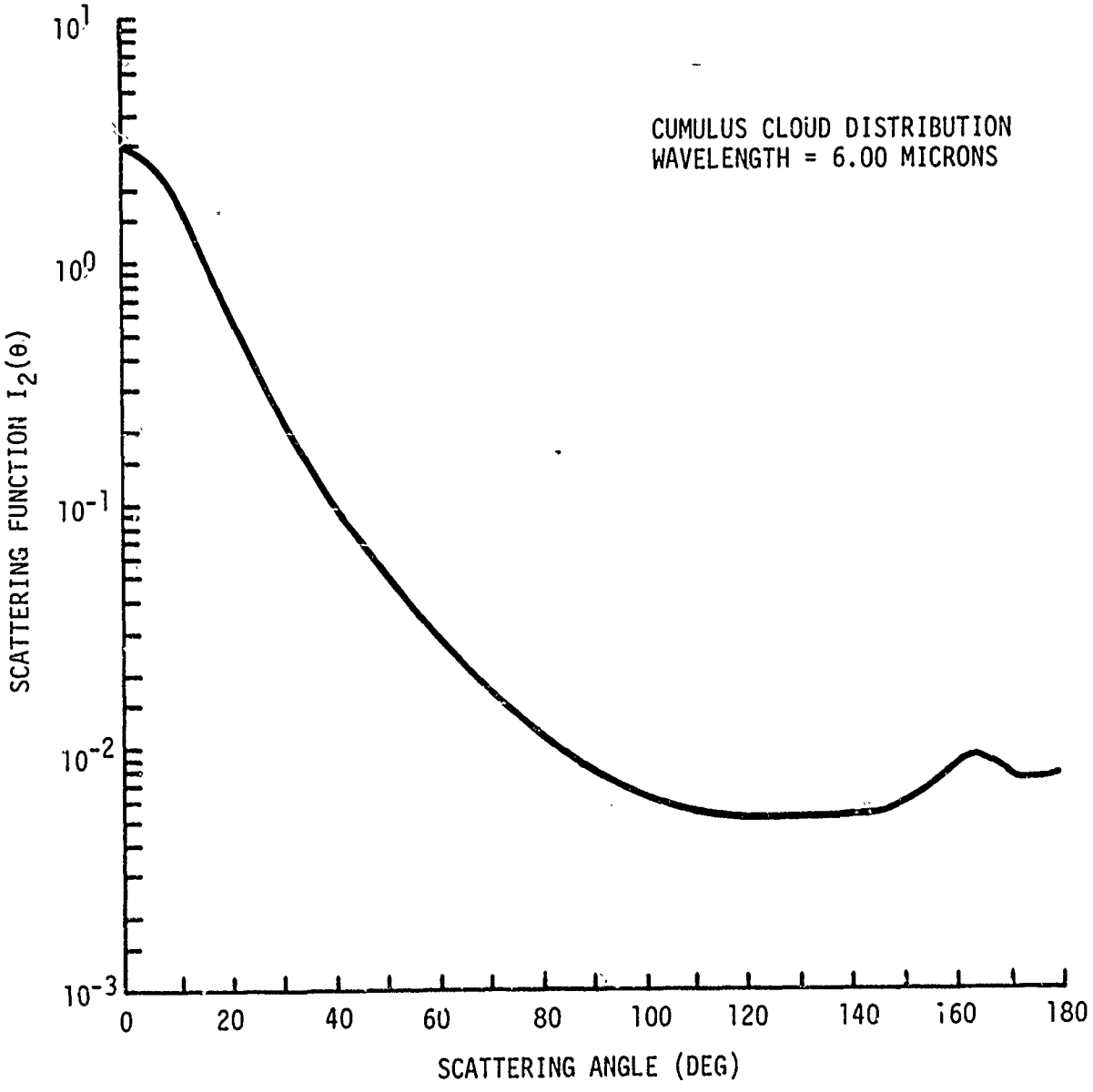

Figure 45. Volume Scattering Function $I_2(\theta)$ for Cumulus Cloud Distribution at $\lambda = 6.0\mu$

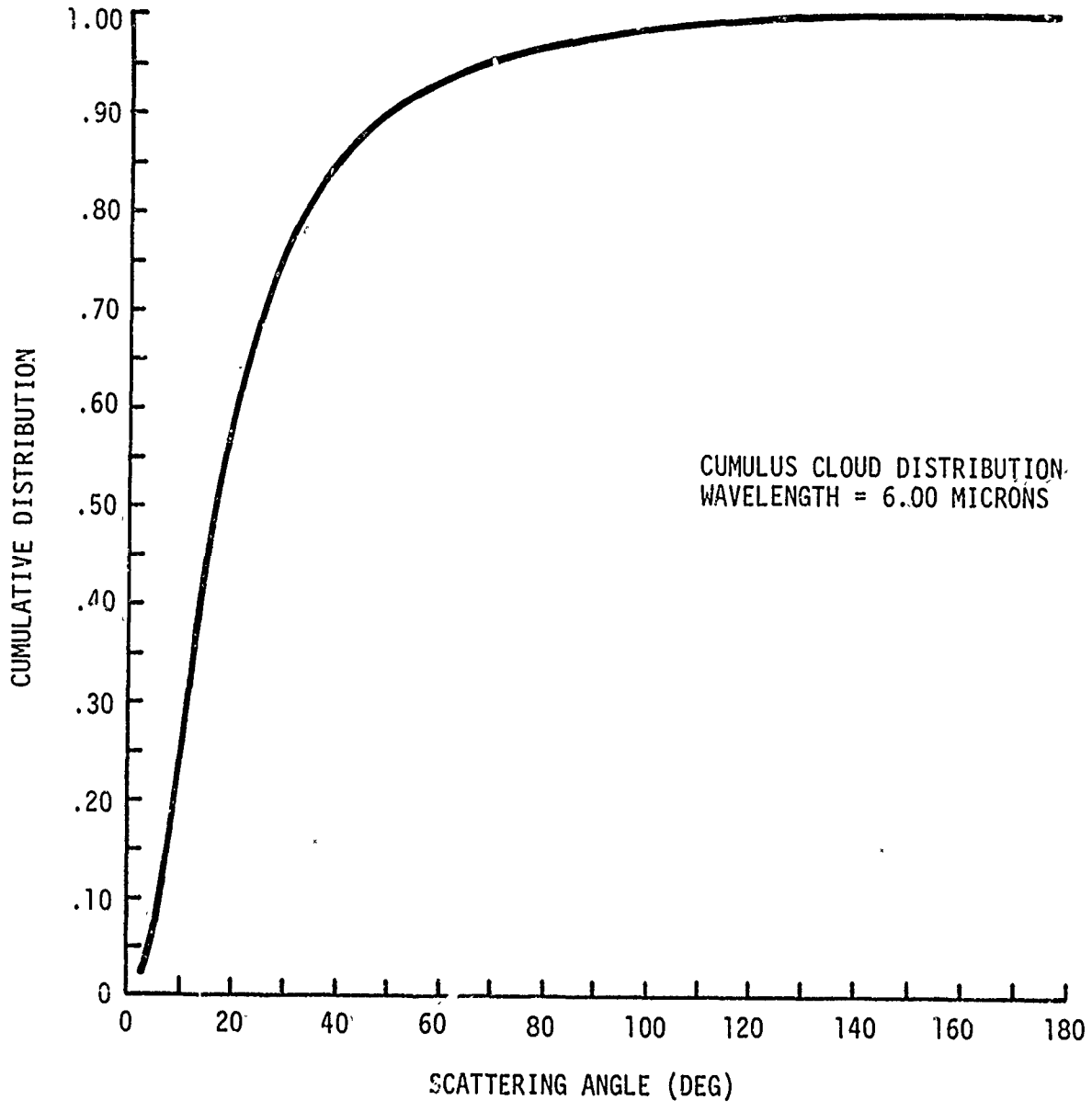

Figure 46. Cumulative Distribution for Cumulus Cloud Distribution at $\lambda = 6.0\mu$

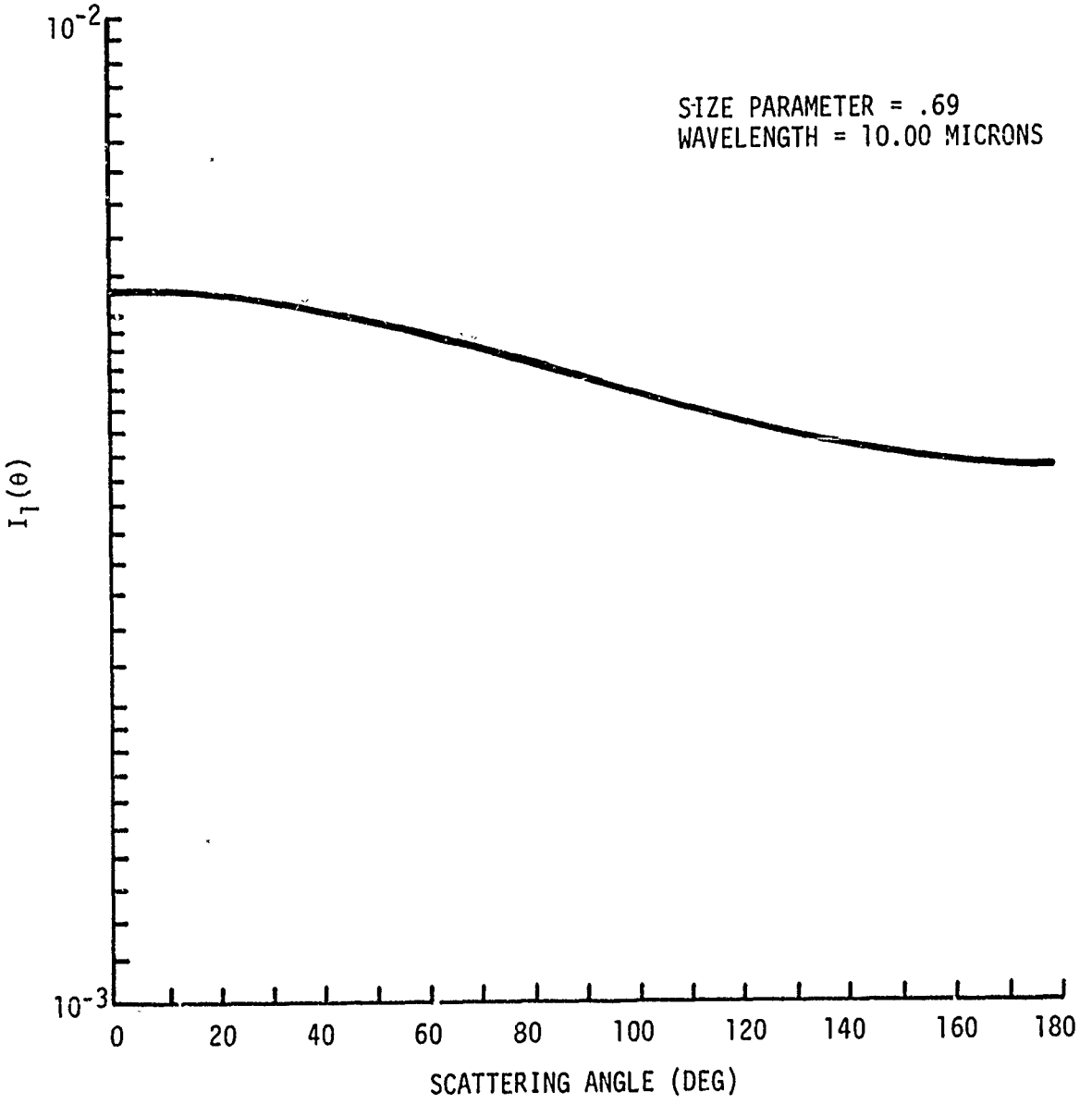

Figure 47. Particle Scattering Function for λ = 10.0μ and x = 0.69, Cumulus Cloud Distribution

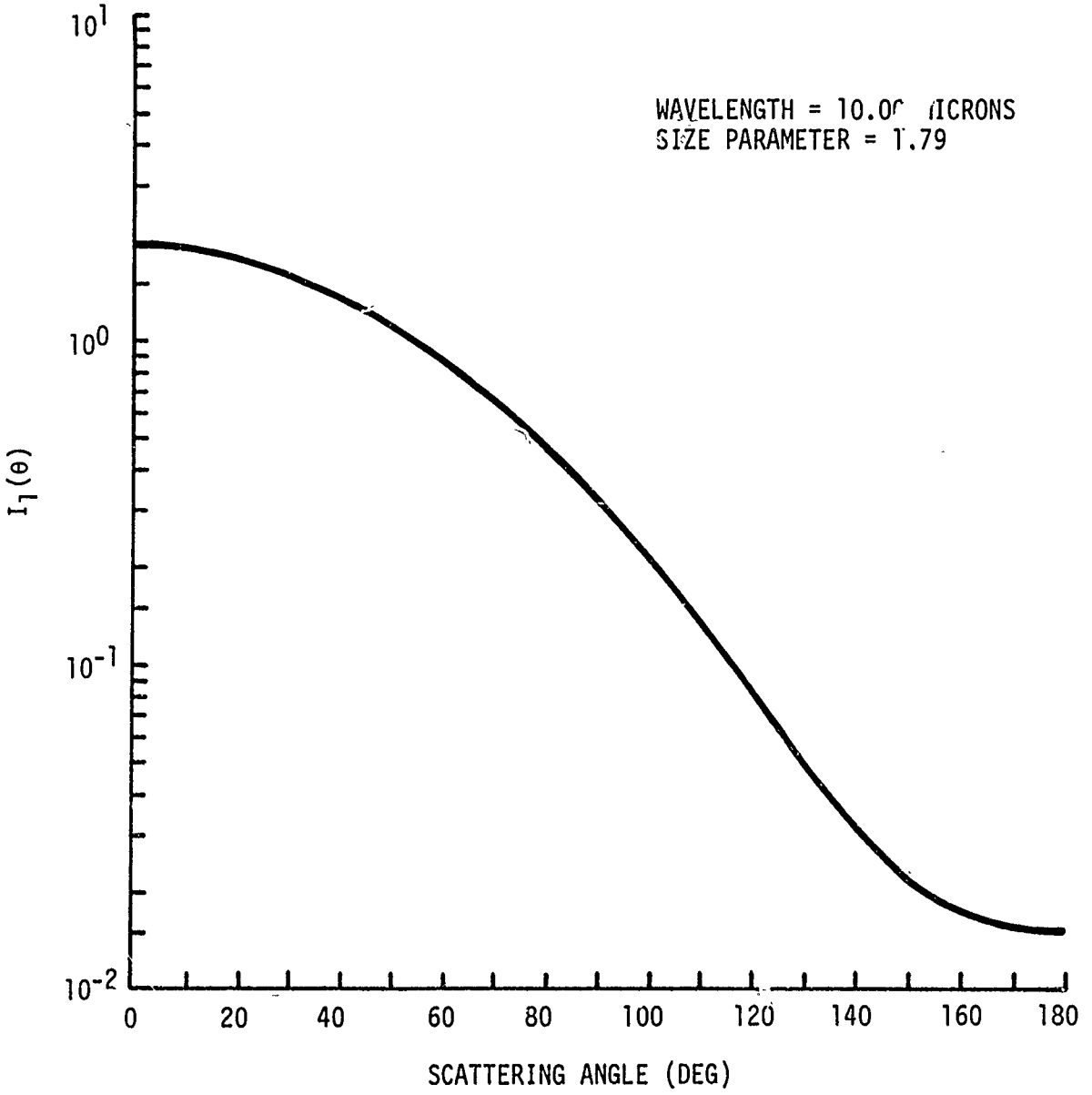

Figure 48. Particle Scattering Function for λ = 10.0μ and X = 1.79, Cumulus Cloud Distribution

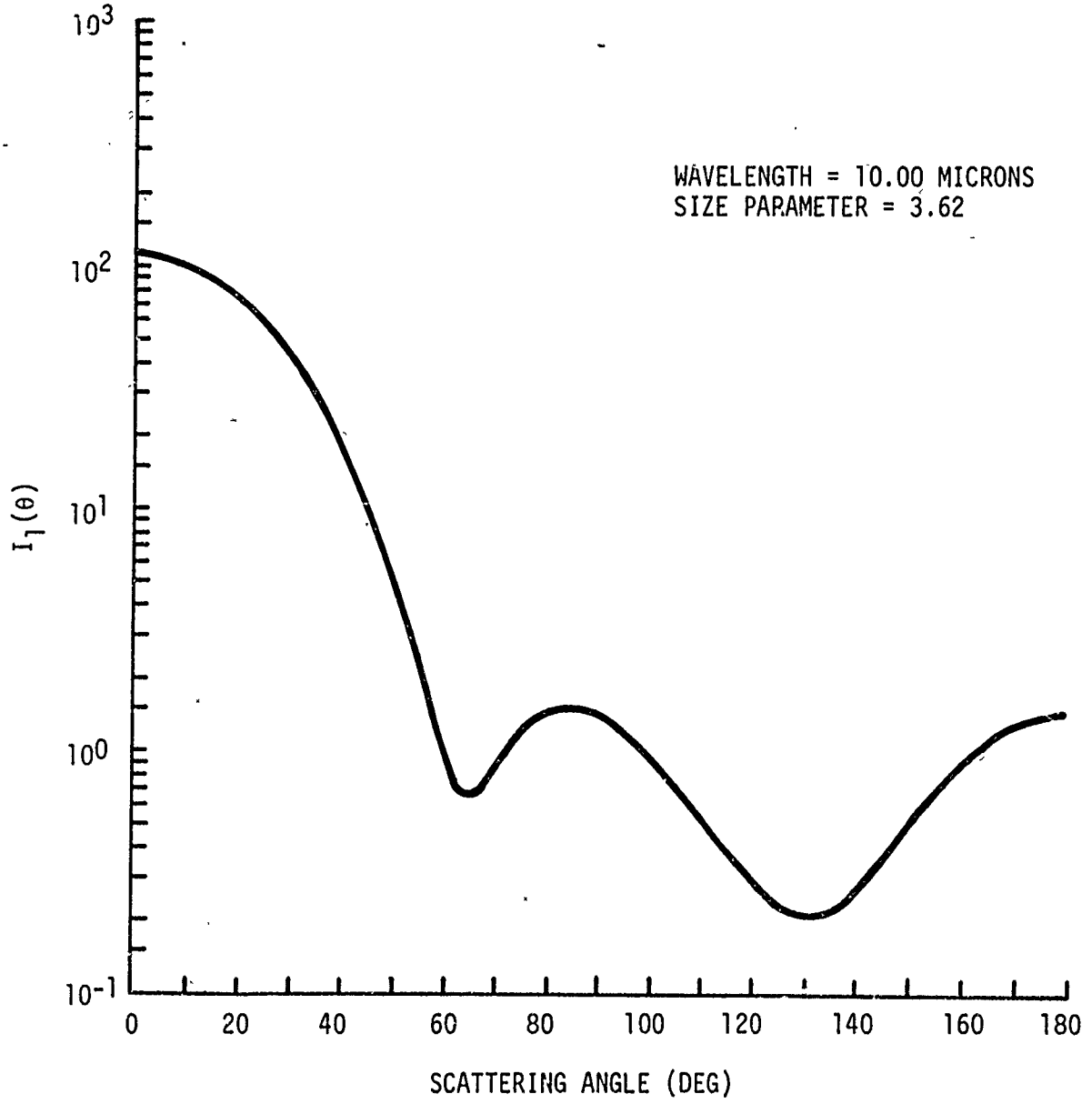

Figure 49. Particle Scattering Function for λ = 10.0μ and X = 3.62, Cumulus Cloud Distribution

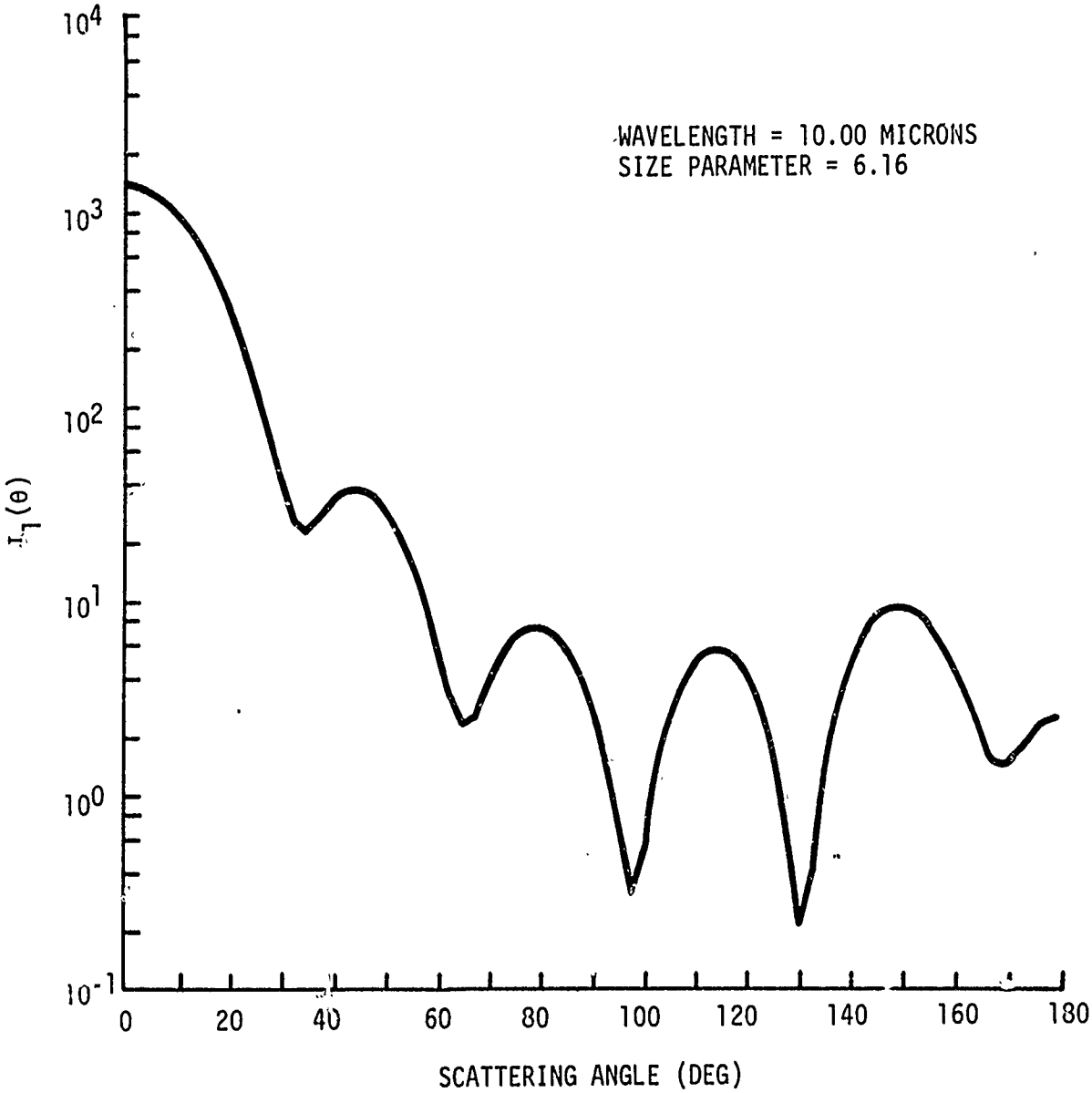

Figure 50. Particle Scattering Function for λ = 10.0μ and X = 6.16, Cumulus Cloud Distribution

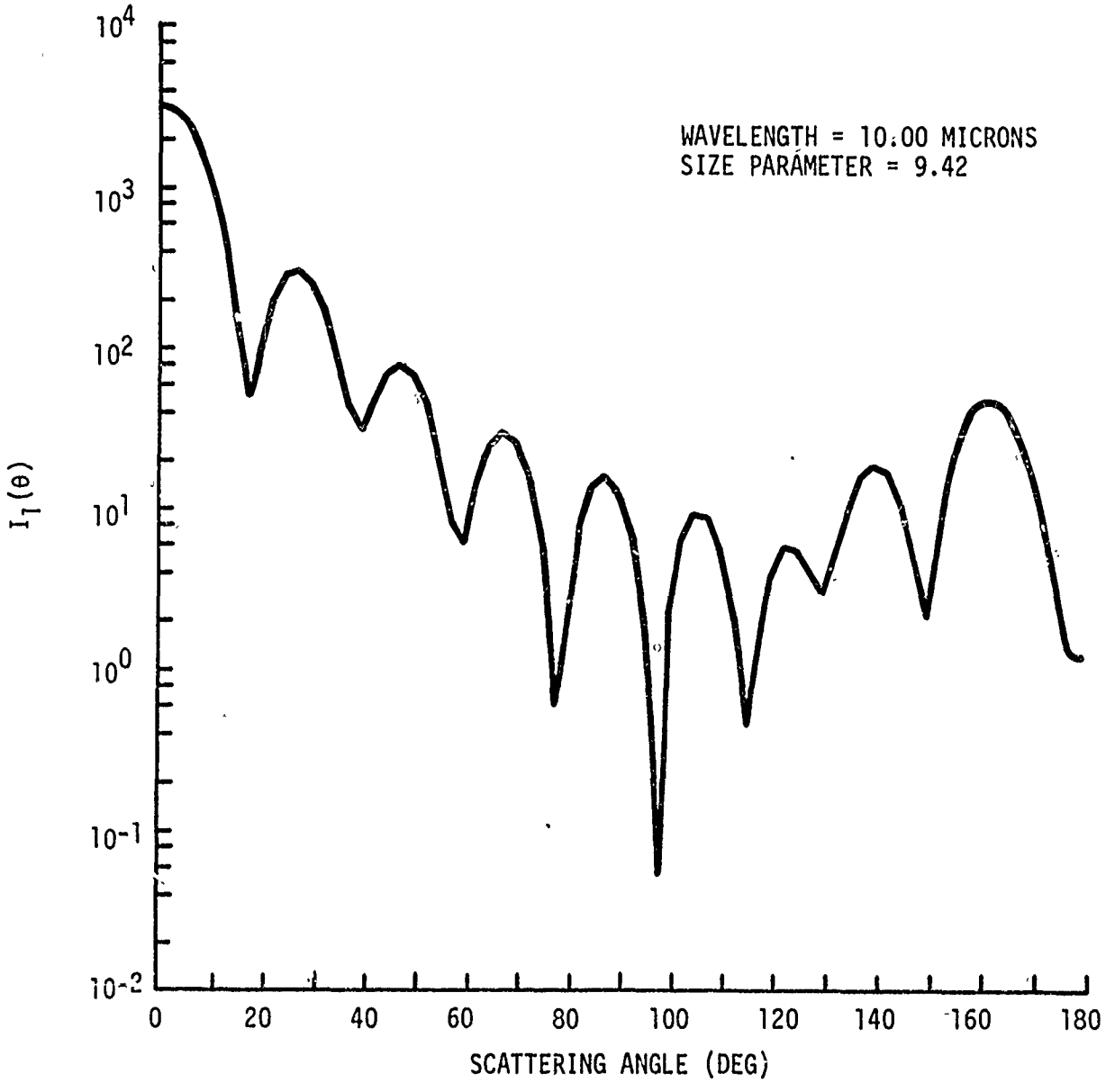

Figure 51. Particle Scattering Function for λ = 10.0μ and x = 9.42, Cumulus Cloud Distribution

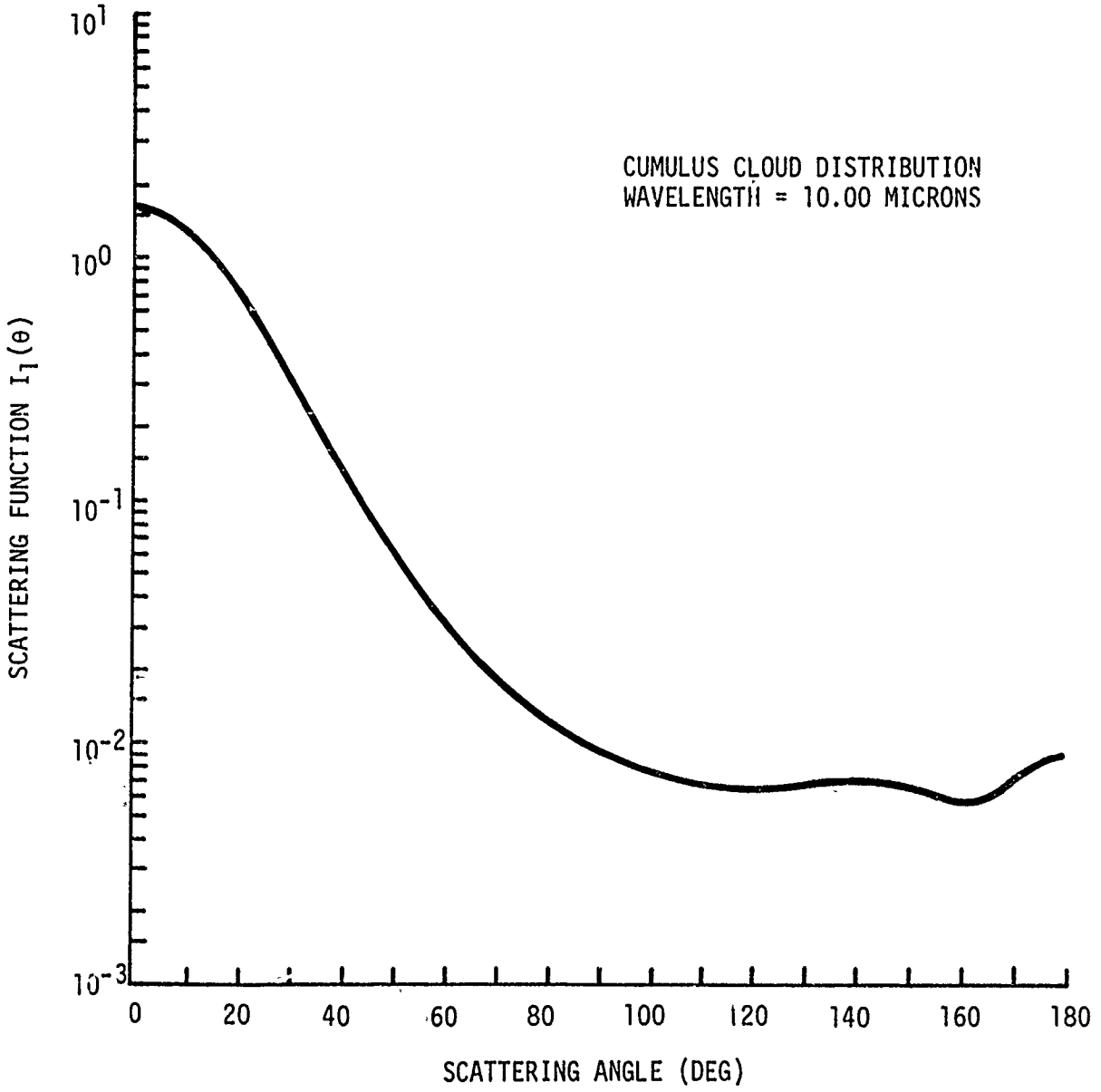

Figure 52. Volume Scattering Function $I_1(\theta)$ for Cumulus Cloud Distribution at $\lambda = 10.0\mu$

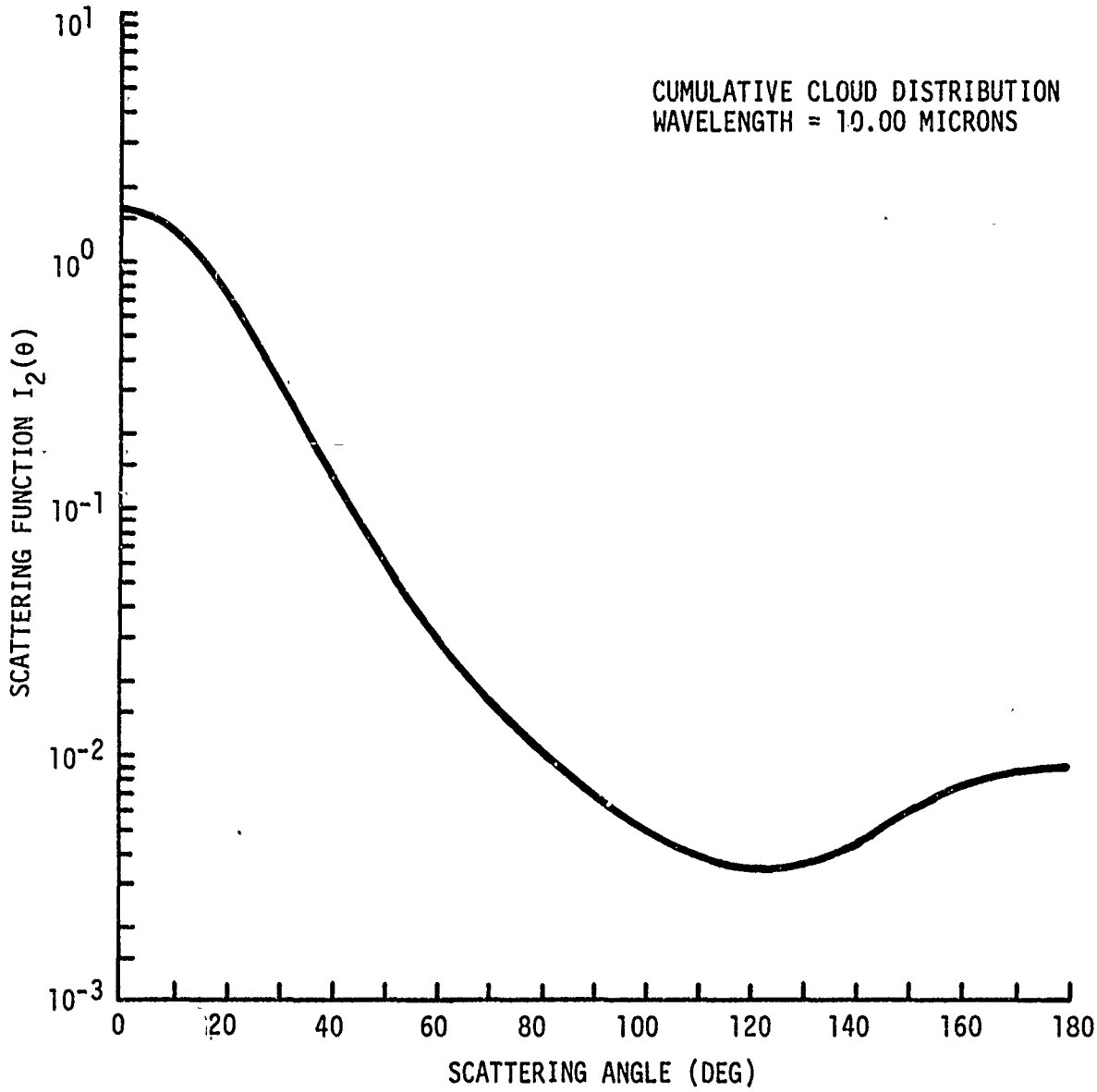

Figure 53. Volume Scattering Function $I_2(\theta)$ for Cumulus Cloud Distribution at $\lambda = 10.0\mu$

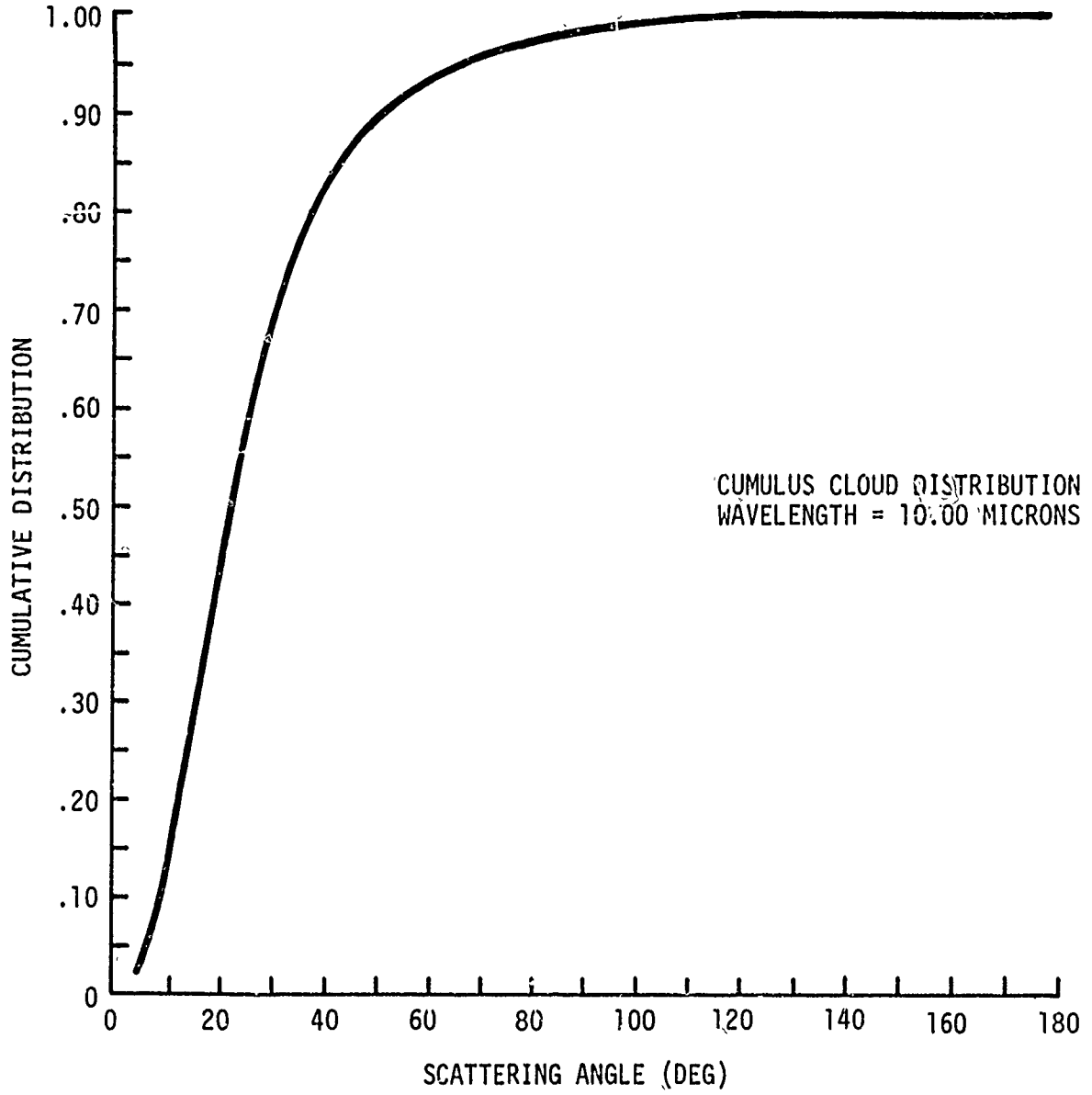

Figure 54. Cumulative Distribution for Cumulus Cloud Discribution at $\lambda = 10.0\mu$

Table 1

EXTINCTION COEFFICIENTS FOR THE CUMULUS CLOUD DISTRIBUTION

$\lambda(\mu)$	Σ_{ext}
0.5	1.657×10^{-4}
1.0	1.712×10^{-4}
2.0	1.812×10^{-4}
4.0	2.179×10^{-4}
6.0	2.537×10^{-4}
8.0	2.303×10^{-4}
10.0	1.865×10^{-4}

where r is the particle radius. Then by integrating over the size distribution [24] we obtain the volume extinction cross section as

$$\Sigma_{ext}(\lambda,m) = \int_{r_1}^{r_2} \pi r^2 Q_{ext}\left(\frac{r}{\lambda},m\right) n(r)\, dr \qquad (324)$$

Since we are not considering complex indexes of refraction in this study the extinction cross section is equal to the scattering cross section. We also notice on comparing the extinction coefficients in table 1 for each wavelength that they are almost constant as a function of wavelength.

3. PARTICLE SCATTERING FUNCTIONS FOR HAZE M DISTRIBUTION

We now consider the particle size distribution (figure 55)

$$n(r) = 5.33 \times 10^4\, r\, e^{-8.944\sqrt{r}} \qquad (325)$$

which is typical of a Maritime Haze [24]. As before we normalize the distribution

$$p(r) = \frac{n(r)}{N} \tag{326}$$

where again $N = 100 \frac{\text{particles}}{\text{cm}^3}$, and

and

$$p(r) = 533\ r\ e^{-8.944\sqrt{r}} \tag{327}$$

The expected value is

$$E[r] = \int_0^\infty 533\ r^2\ e^{-8.944\sqrt{r}}\ dr$$

$$= 533\ (8.944)^{-6}\ \Gamma(6)$$

$$= 0.125\mu \tag{328}$$

The mode radius is

$$r_m = 0.05\mu$$

The variance is

$$\text{Var}[r] = E[r^2] - (E\ [r])^2 \tag{329}$$

with

$$E[r^2] = \int_0^\infty 533\ r^3\ e^{-8.944\sqrt{r}}\ dr$$

$$= 533\ (8.944)^{-8}\ \Gamma(8)$$

$$= 0.07\mu^2 \tag{330}$$

and

$$\text{Var}[r] = 0.07 - (0.125)^2$$

$$= 0.05\mu^2 \tag{331}$$

The standard deviation is then

$$\sigma_H = \sqrt{\text{Var}[r] = 0.22\mu} \tag{332}$$

Comparing the mode radius with the expected value we can see that particles with radii greater than the mode radius will again contribute heavily to the normalized scattering function.

We can compare the ratios of the standard deviation to the expected value for the Cumulus Cloud distribution and for the Haze M distribution. We have for the cumulus distribution

$$\frac{\sigma_C}{E[r]} = \frac{1.78}{4.66} = 0.38 \tag{333}$$

while for the Haze M distribution

$$\frac{\sigma_H}{E[r]} = \frac{0.22}{0.125} = 1.76 \tag{334}$$

from which we can see that the relative spread is larger for the Haze M distribution and we conclude that a wider range of particle sizes will contribute to a greater extent for the Haze M model than for the Cumulus model.

Figures 56 through 60 show the scattering functions for perpendicular polarization and $\lambda = 0.5\mu$ for individual particles of radius 0.09, 0.33, 0.73, 1.29, and 2.00μ with size parameters of 1.06, 4.09, 9.12, 16.13, and 25.13, respectively. Here again we see an increase in forward scattering with increasing size parameter. Figures 61 and 62 are the normalized scattering functions for perpendicular and parallel incident polarizations, respectively. In comparing figures 56 through 60 with figure 61 we can see that the larger particles contribute to the normalized scattering function more than do the smaller particles. The cumulative probability distribution is shown in figure 63.

Comparing figures 30 and 63 we see that the scattering angles are distributed over a slightly wider range for the Haze M model than for the Cumulus model, i.e., the probability of scattering between the angles 0° to 17° is 0.5 for Haze M while for Cumulus for the same probability the interval is between 0° and 4°. Therefore, for a given wavelength and density we would expect more multiple scattering for Haze M than for Cumulus.

As we increase the wavelength to 2.0μ the particle scattering functions increase significantly as shown in figures 64 through 68 which results in a fairly wide normalized scattering function as shown in figures 69 and 70. The cumulative probability function is shown in figure 71.

The particle scattering function continues to widen (figures 72 through 76) for $\lambda = 6.0\mu$, with figure 72 showing an almost isotropic scattering function for $x = 0.09$ and a radius of 0.09μ. The normalized scattering functions in figures 77 and 78 show this increase in width as does the cumulative probability function in figure 79.

At a wavelength of 10.0μ the normalized scattering function for perpendicular incident polarization (figure 85) is almost isotropic and the normalized scattering function for parallel incident polarization is almost equal in the forward and back directions with a null at 90°. This type of scattering function is typical of Rayleigh scattering, i.e., the particles in a Haze M distribution may just as well be considered as Rayleigh scatterers for wavelengths greater than 10μ. It is only for the larger particles, cf. figures 80 through 84, which occur with small probability, that we see any appreciable peakedness in the forward direction. The cumulative probability function also indicates the near isotropy at $\lambda = 10.0\mu$. Here the probability of

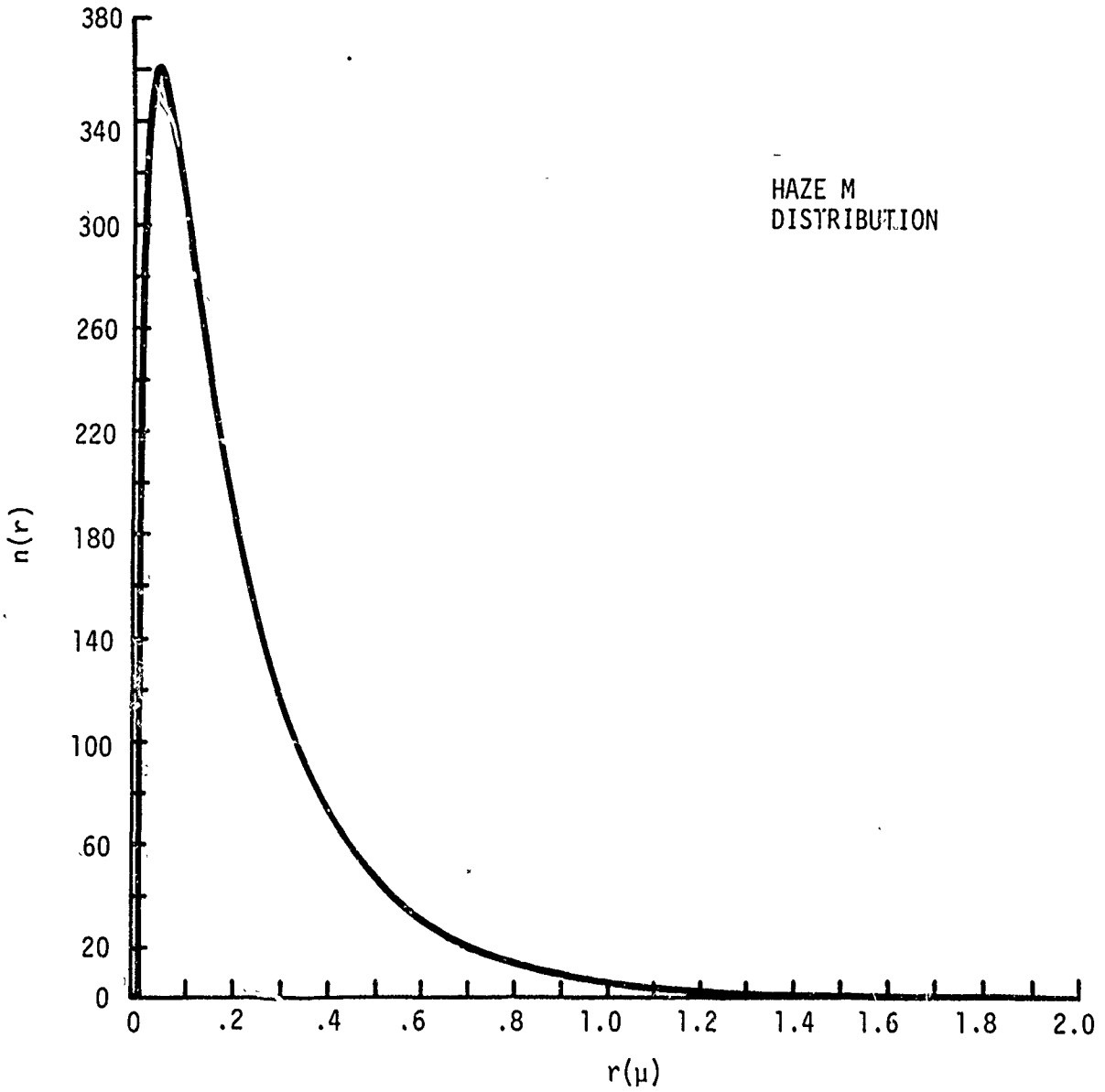

Figure 55. Haze M Distribution

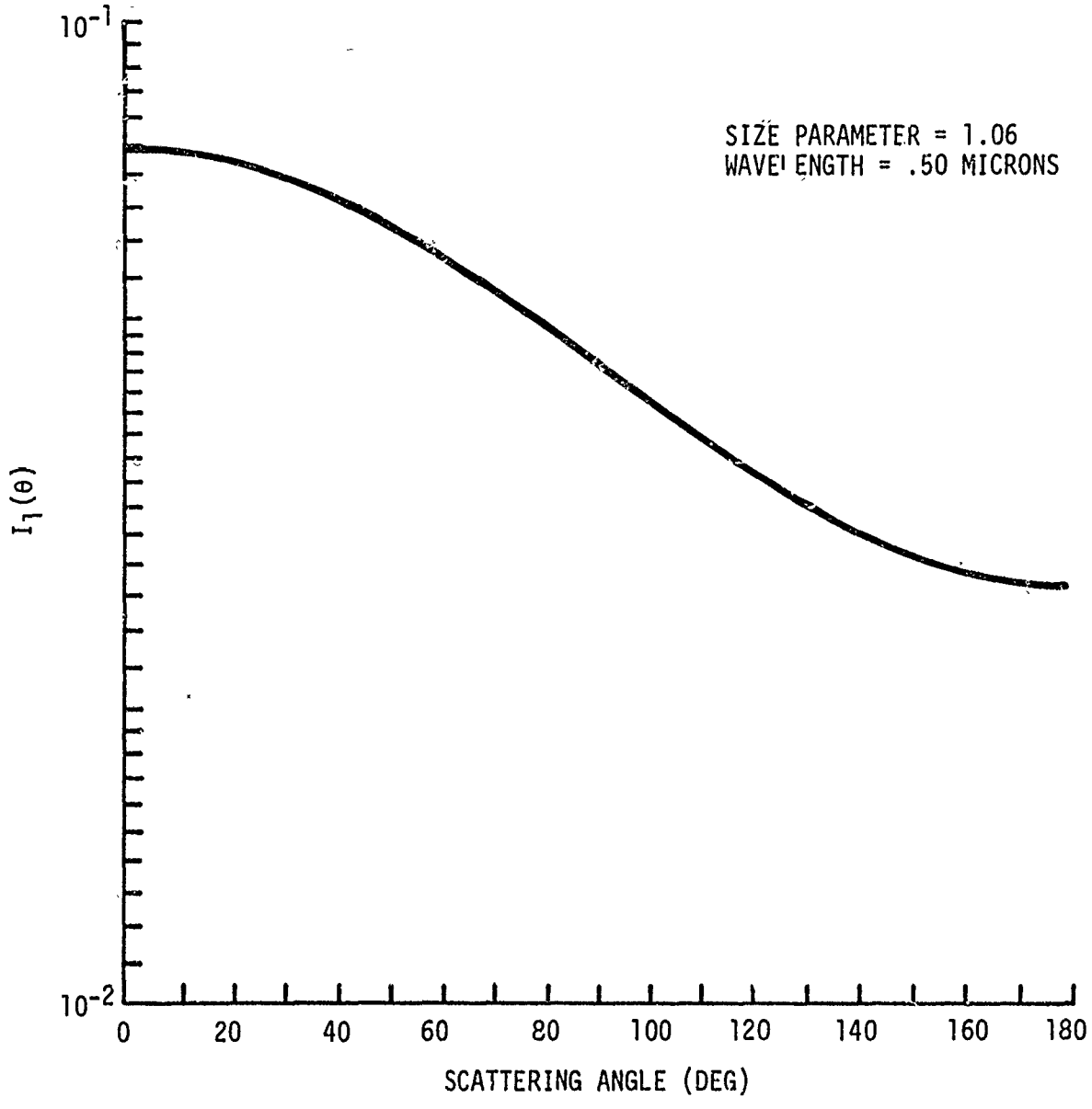

Figure 56. Particle Scattering Function for $\lambda = 0.5\mu$ and $x = 1.06$, Haze M Distribution

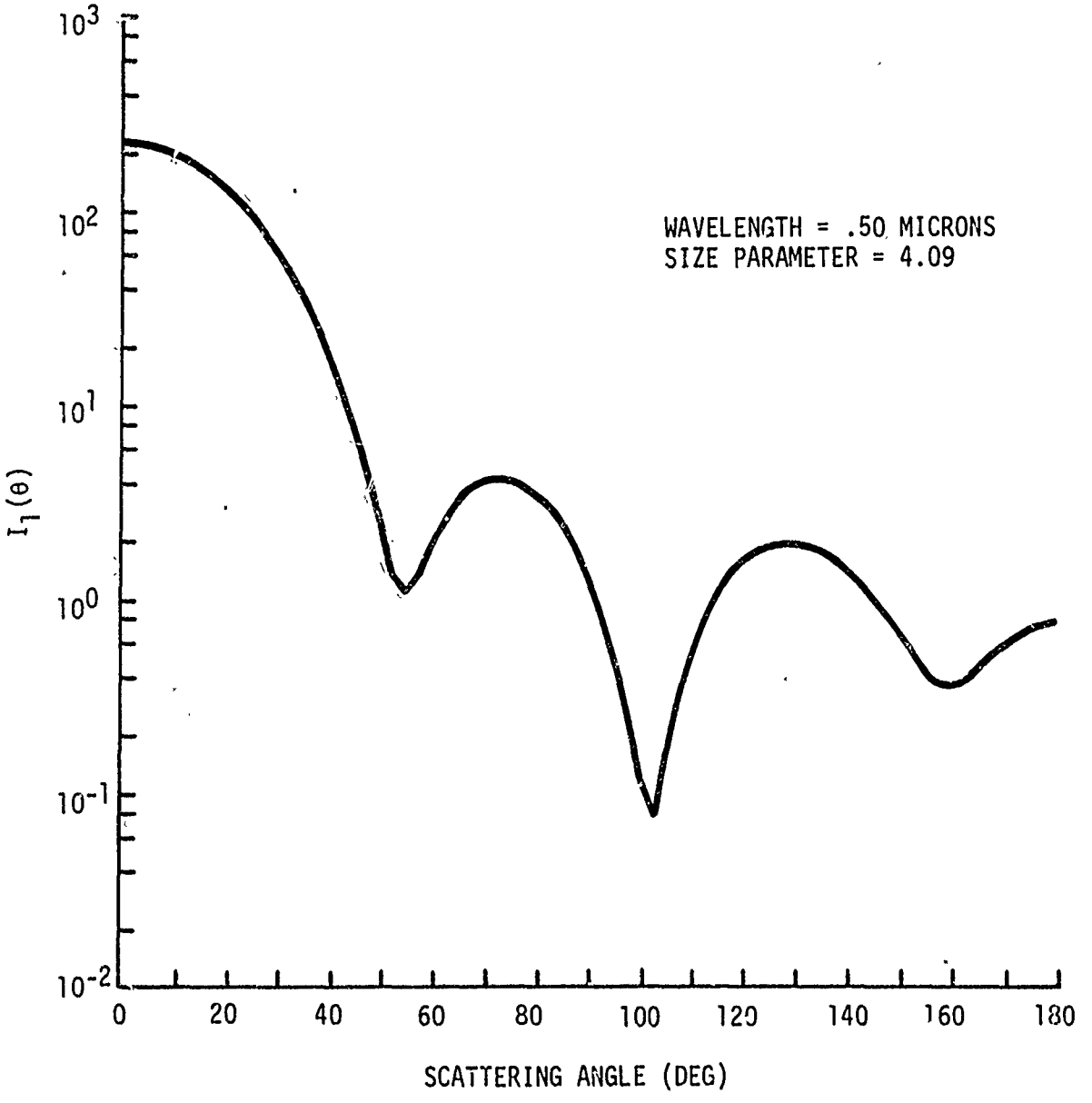

Figure 57. Particle Scattering Function for $\lambda = 0.5\mu$ and $x = 4.09$, Haze M Distribution

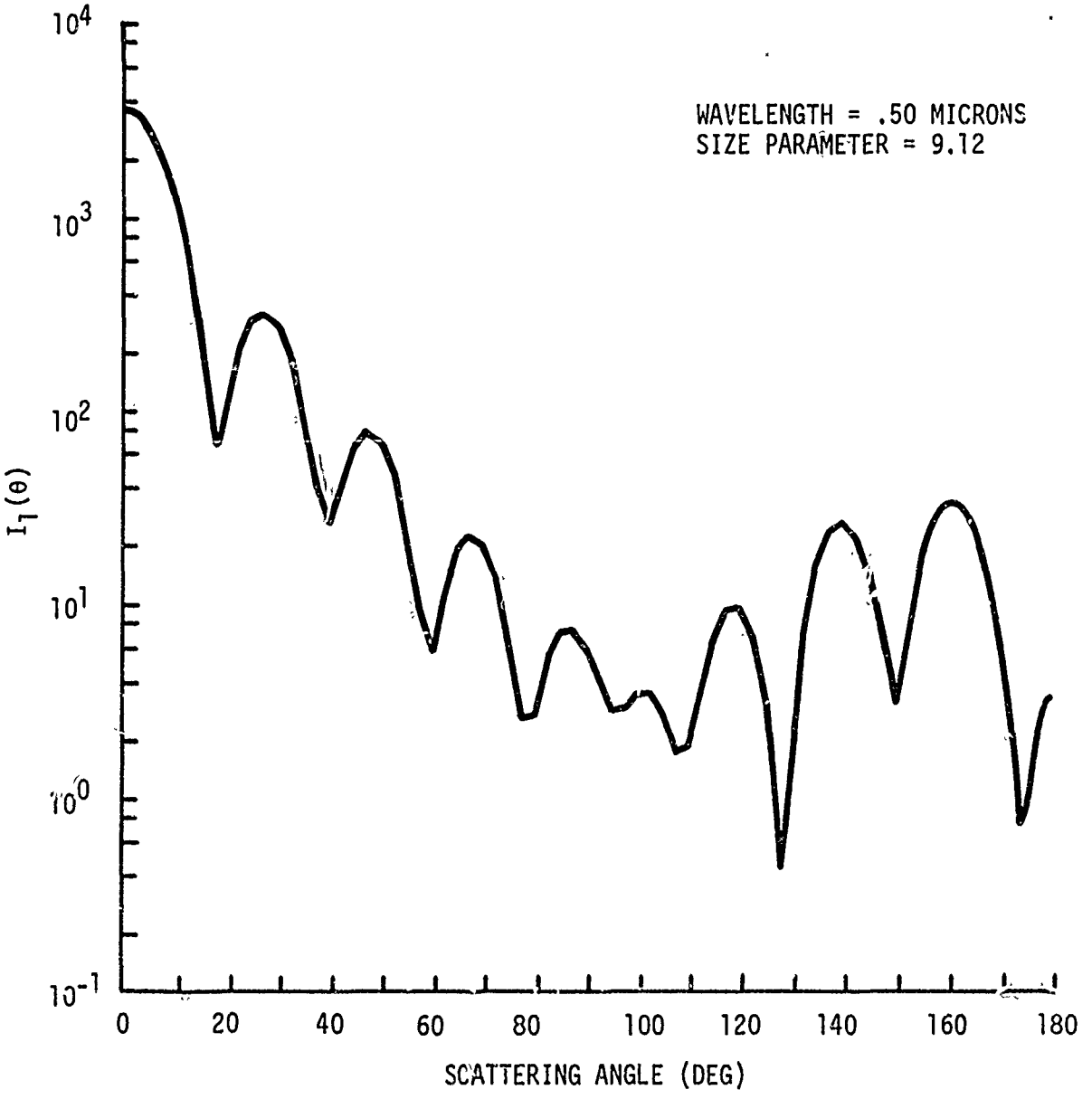

Figure 58. Particle Scattering Function for $\lambda = 0.5\mu$ and $x = 9.12$, Haze M Distribution

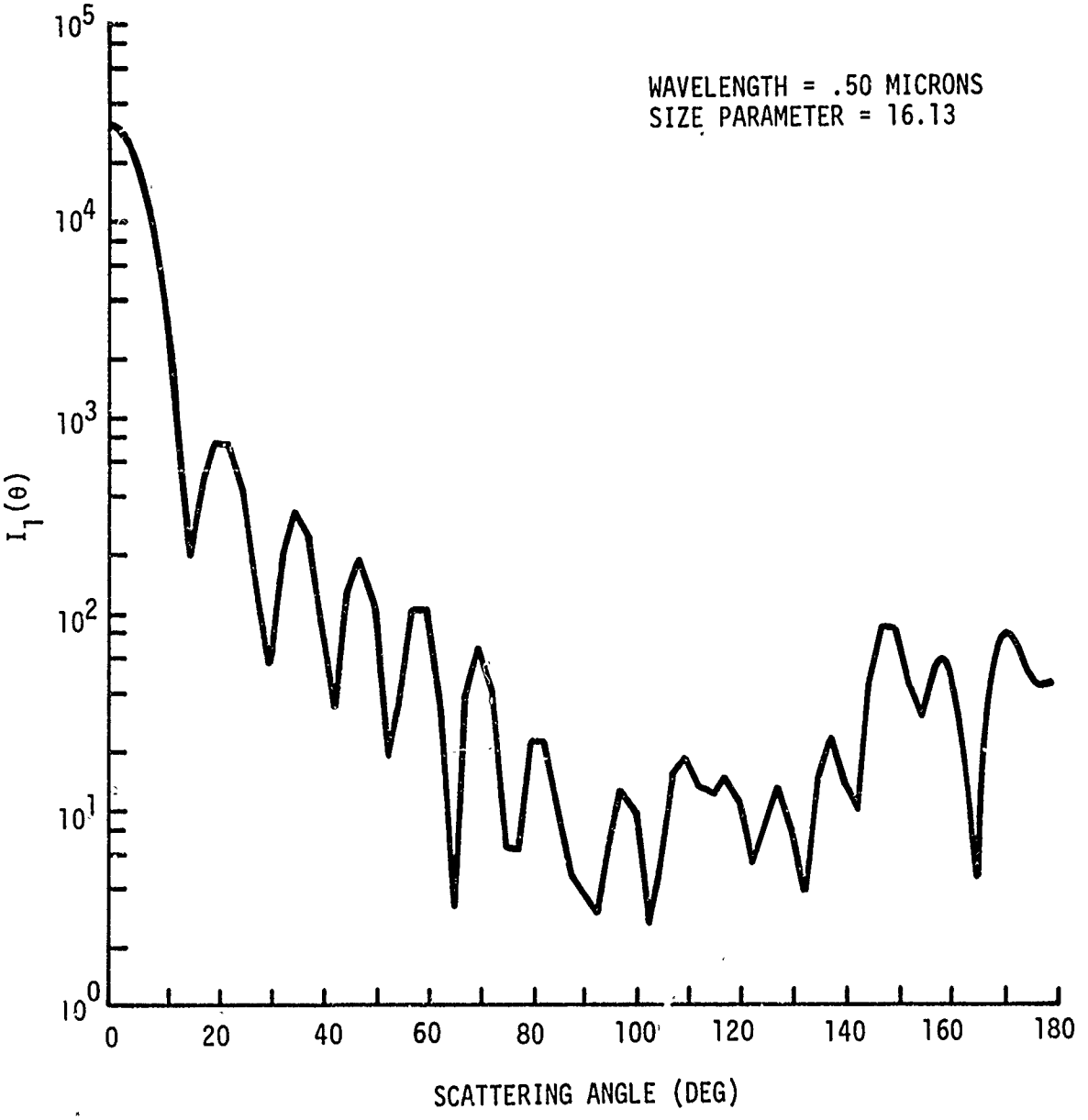

Figure 59. Particle Scattering Function for $\lambda = 0.5\mu$ and $x = 16.13$, Haze M Distribution

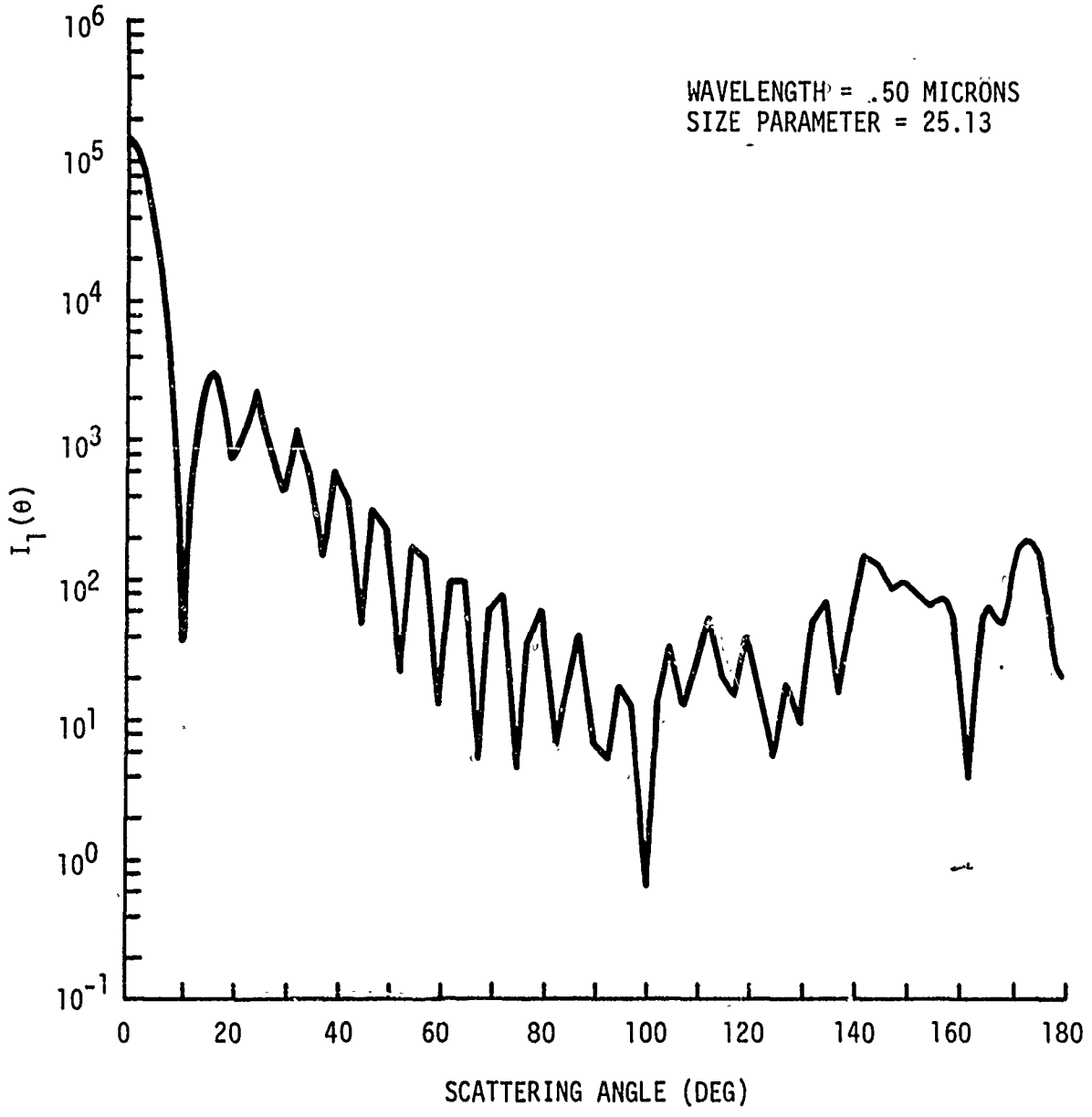

Figure 60. Particle Scattering Function for $\lambda = 0.5\mu$ and $x = 25.13$, Haze M Distribution

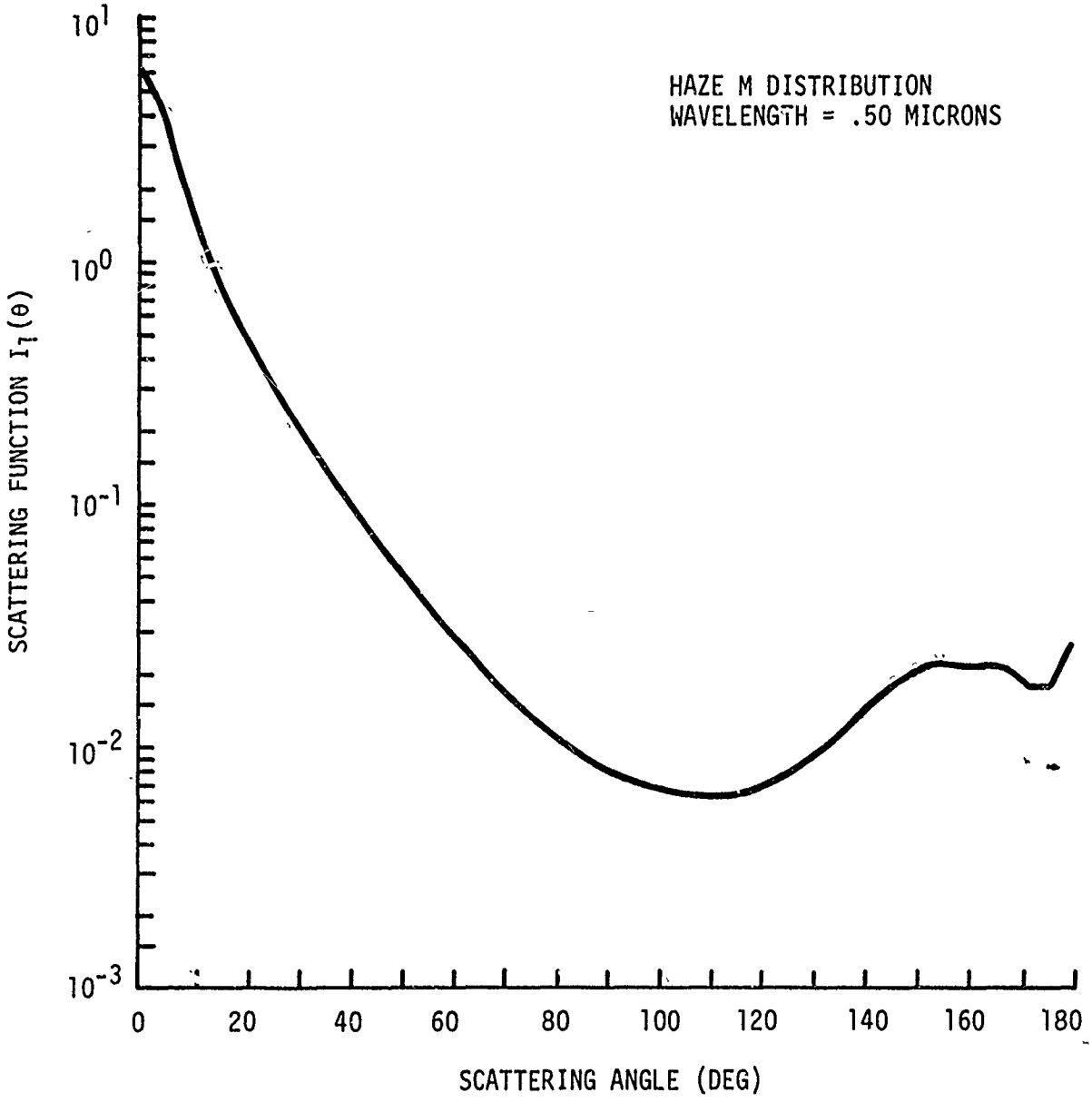

Figure 61. Volume Scattering Function $I_1(\theta)$ for Haze M Distribution at $\lambda = 0.5\mu$

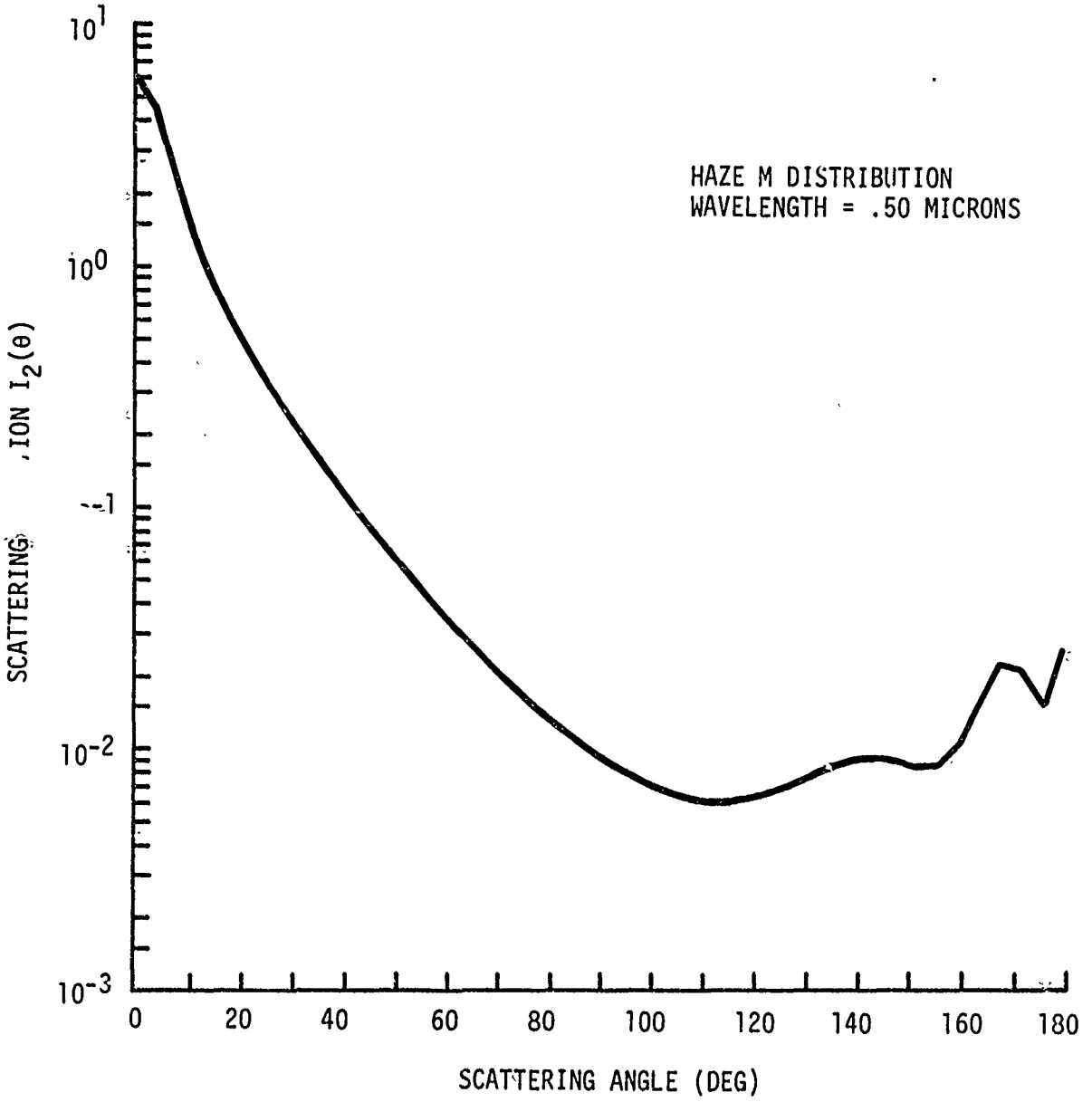

Figure 62. Volume Scattering Function $I_2(\theta)$ for Haze M Distribution at $\lambda = 0.5\mu$

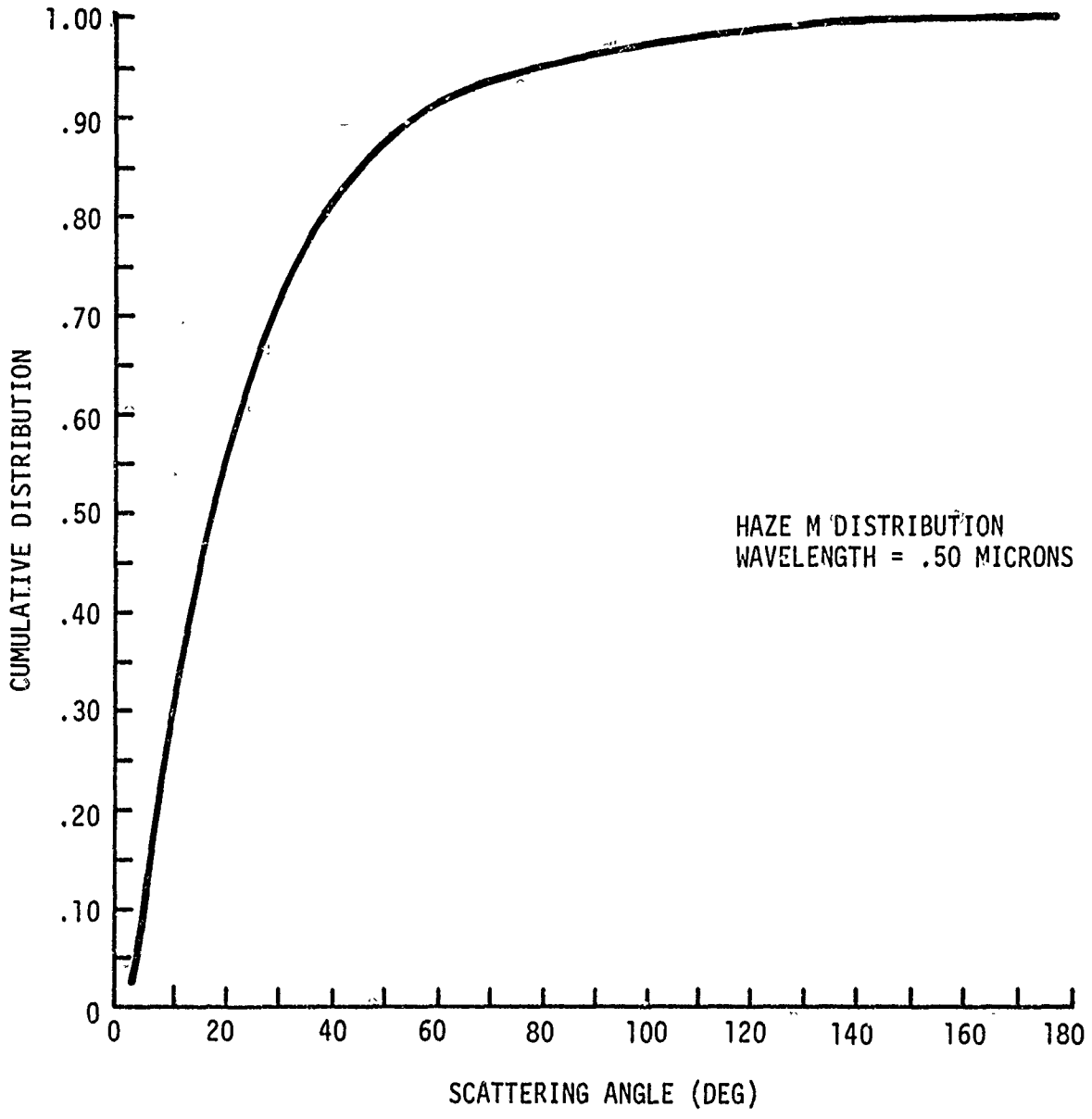

Figure 63. Cumulative Distribution for Haze M Distribution at λ - 0.5μ

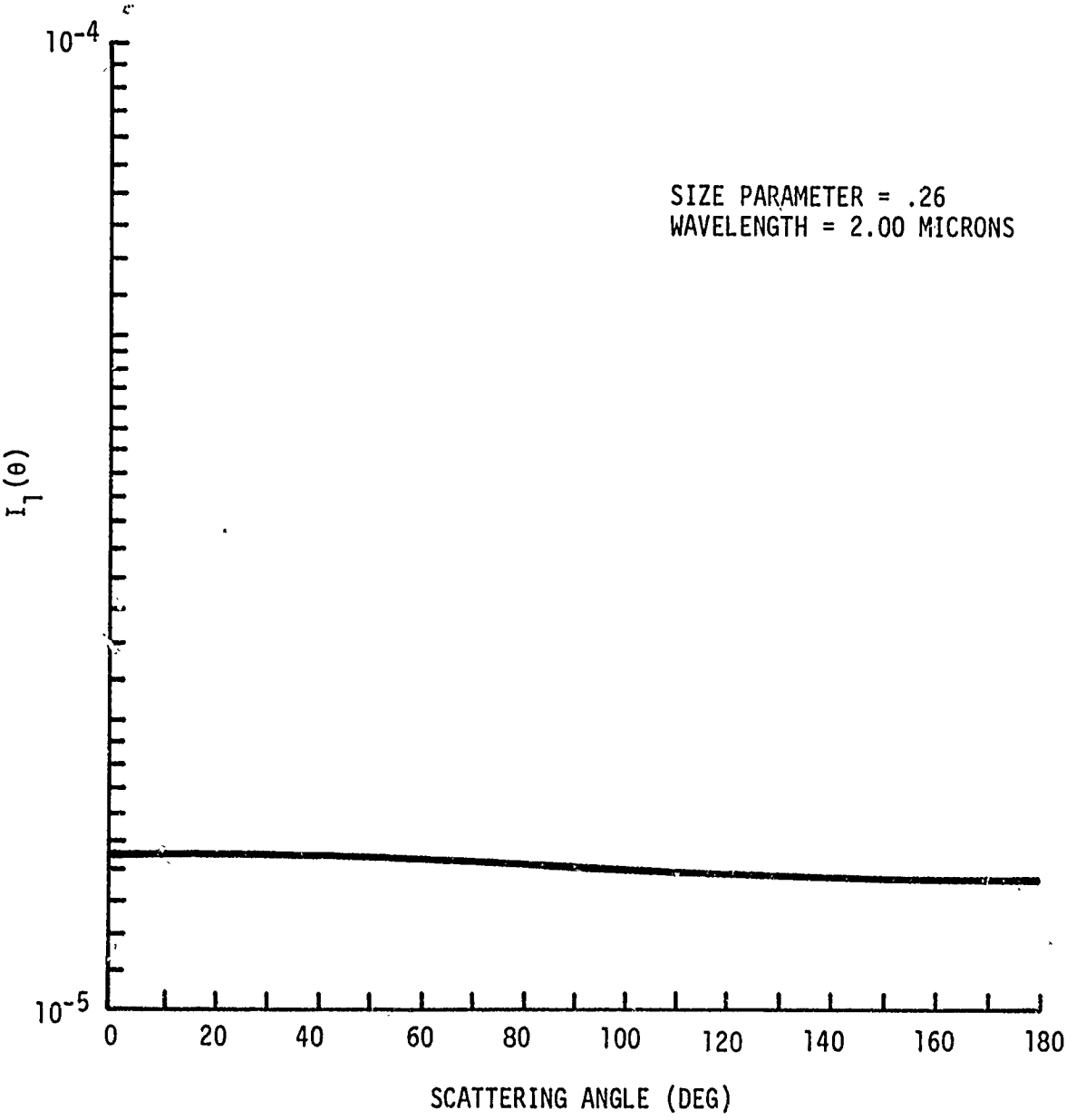

Figure 64. Particle Scattering Function for $\lambda = 2.0\mu$ and $x = 0.26$, Haze M Distribution

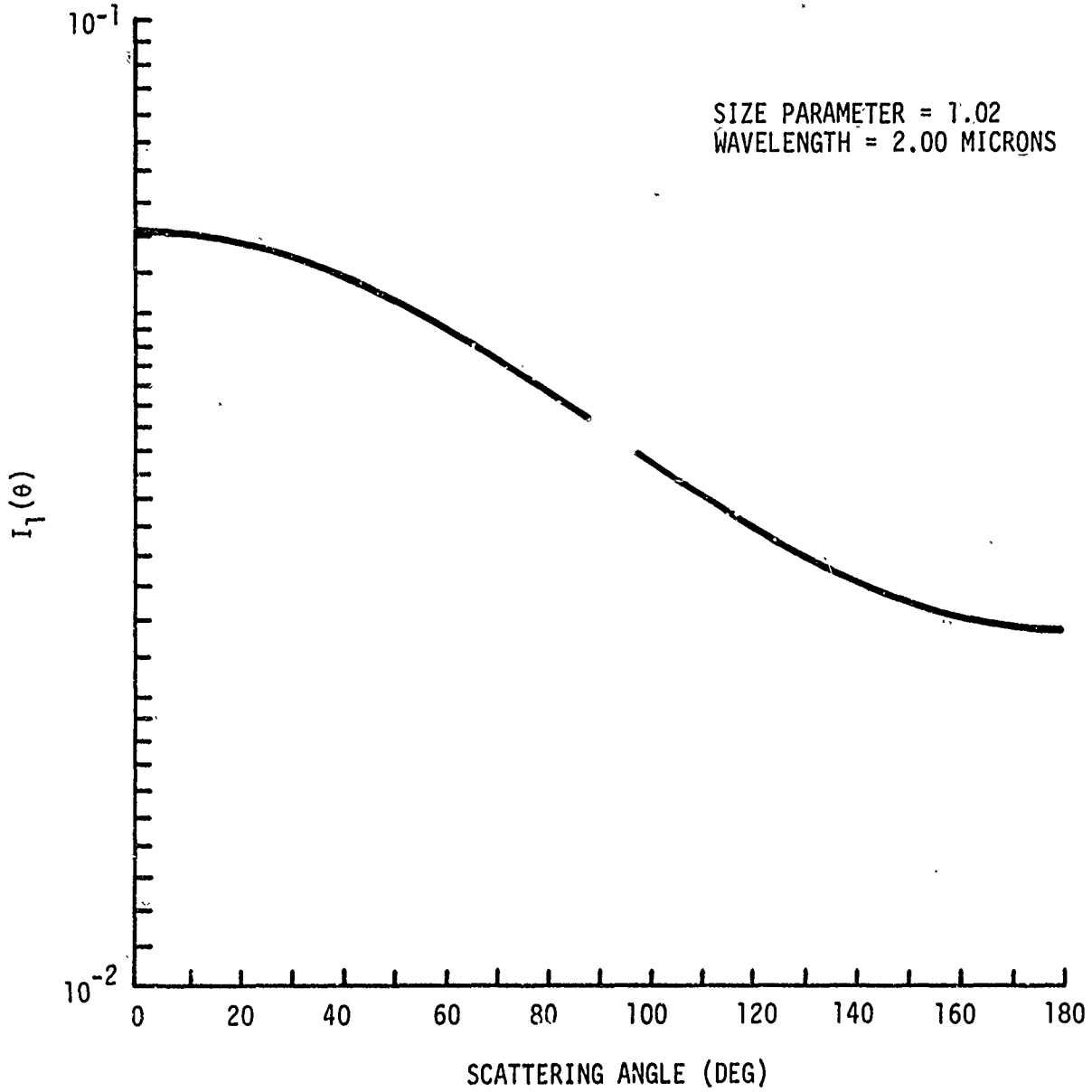

Figure 65. Particle Scattering Function for $\lambda = 2.0\mu$ and $x = 1.02$, Haze M Distribution

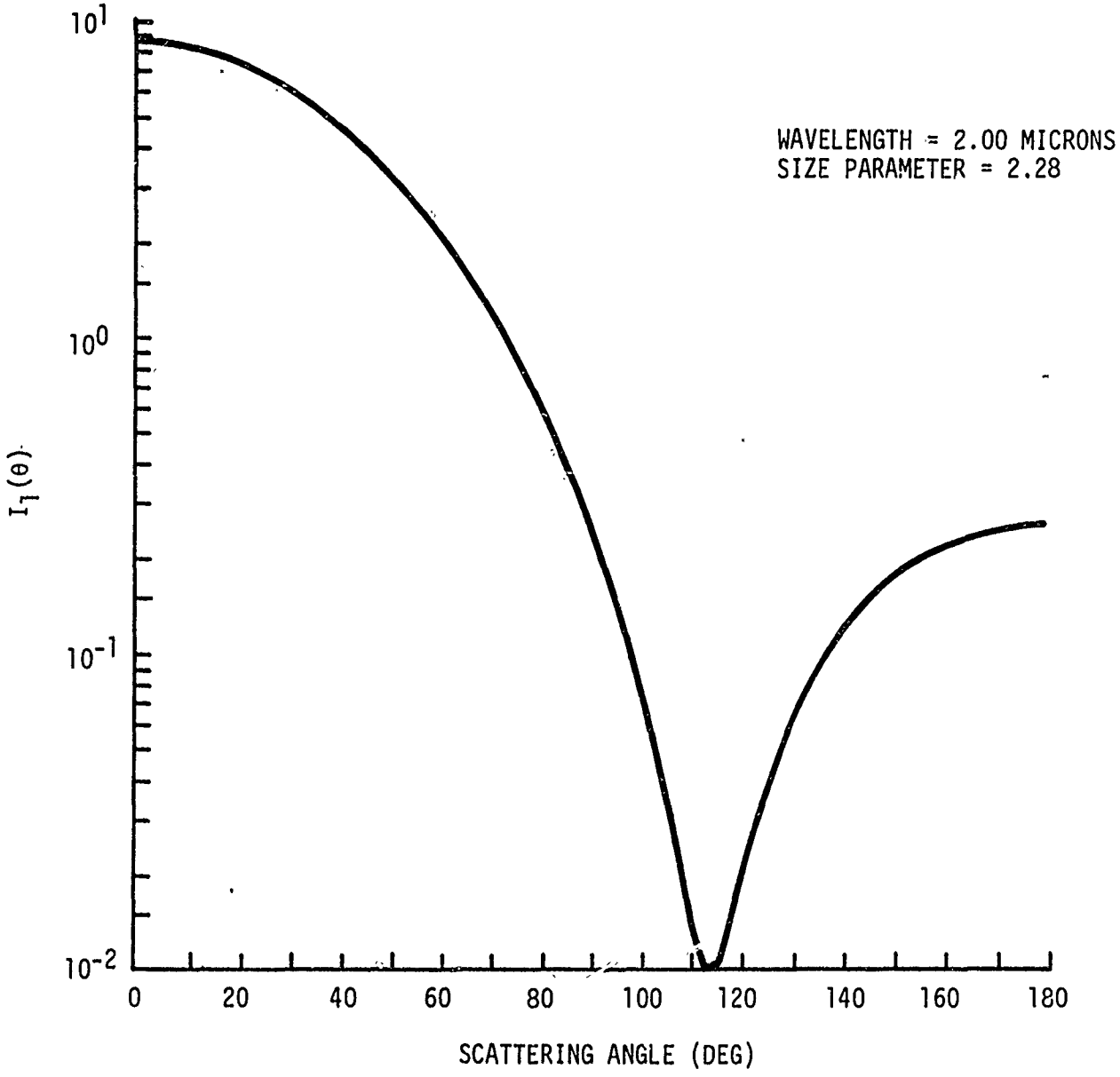

Figure 66. Particle Scattering Function for $\lambda = 2.0\mu$ and $x = 2.28$, Haze M Distribution

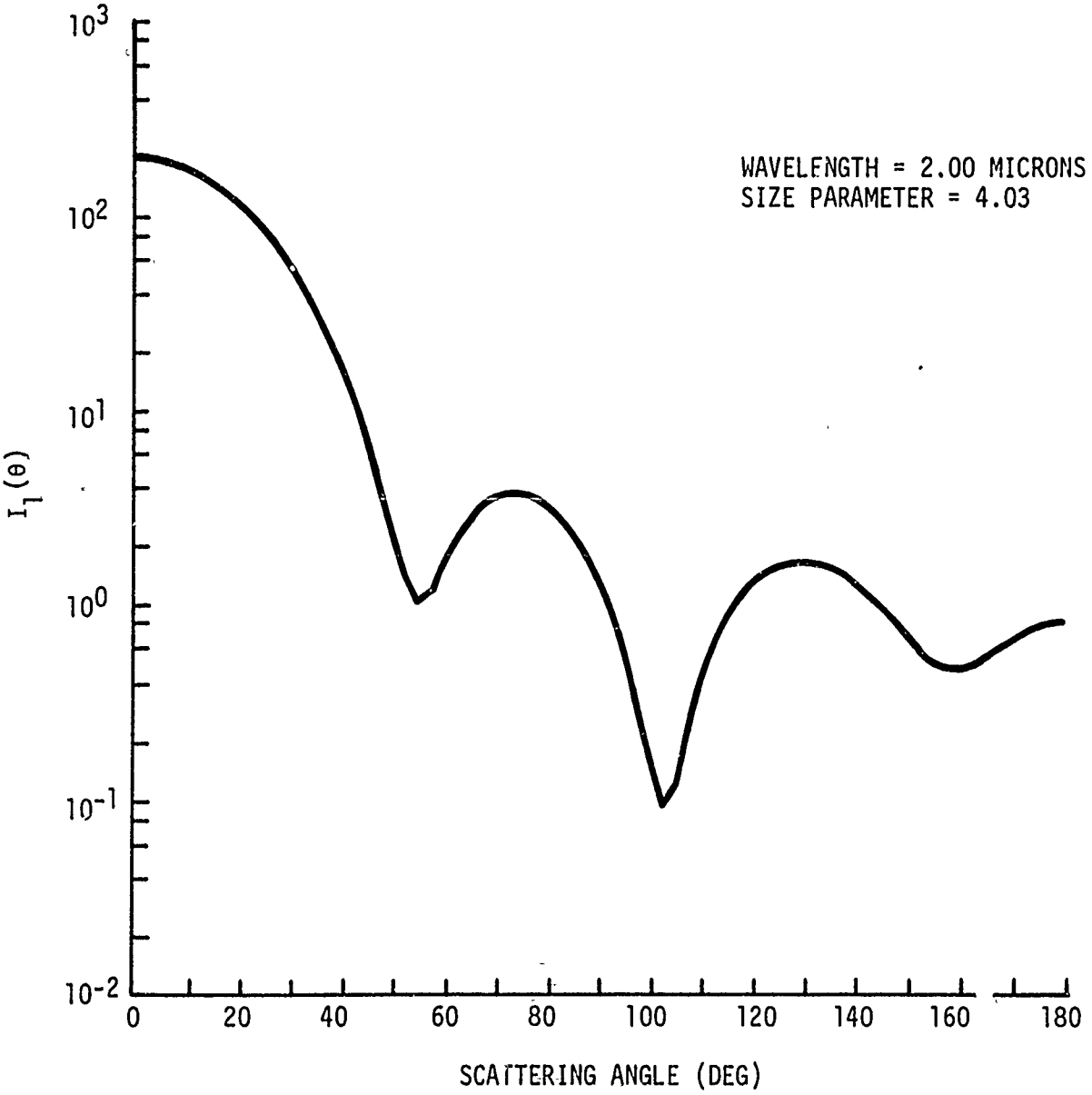

Figure 67. Particle Scattering Function for λ = 2.0μ and x = 4.03, Haze M Distribution

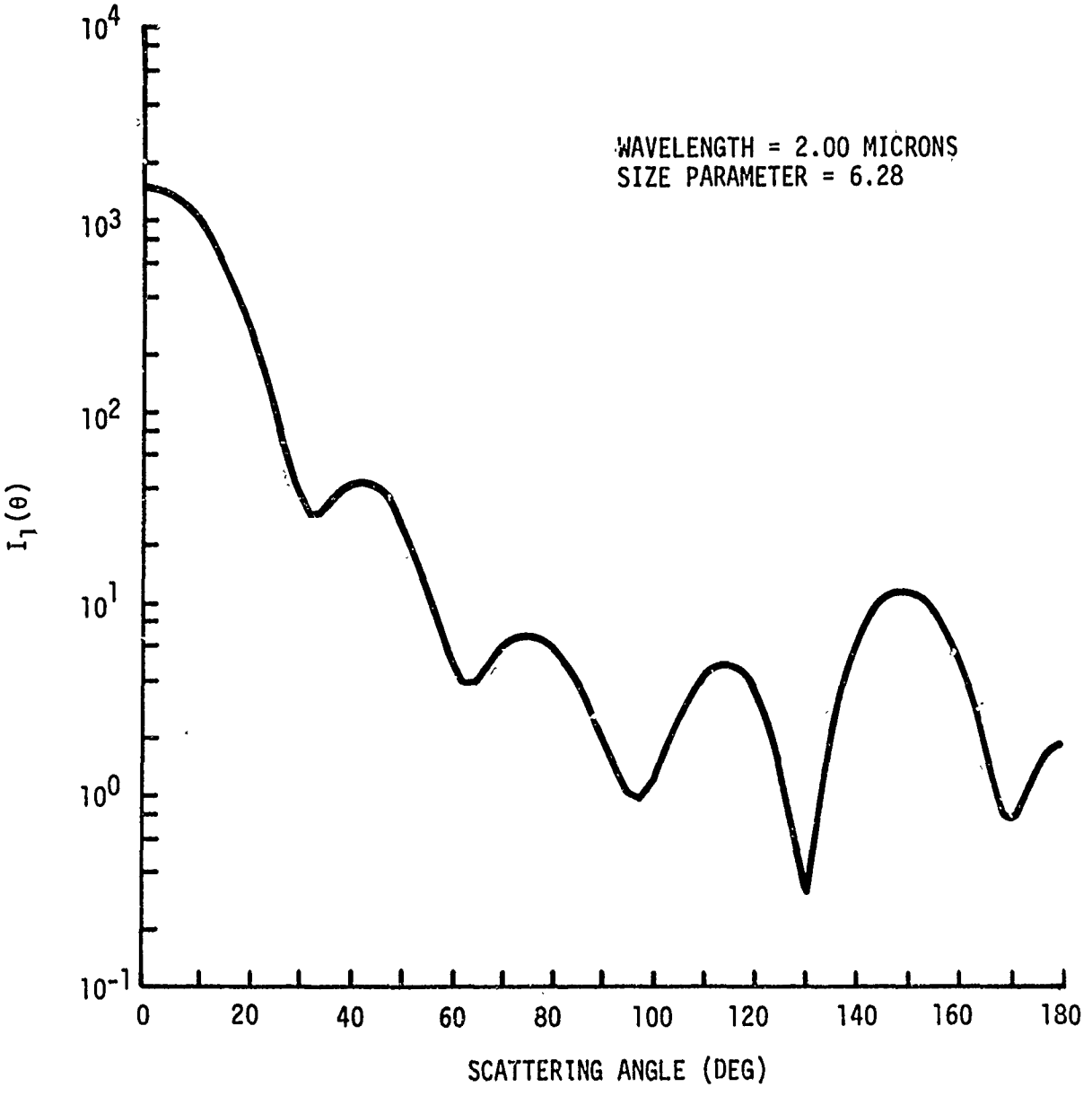

Figure 68. Particle Scattering Function for $\lambda = 2.0\mu$ and $x = 6.28$, Haze M Distribution

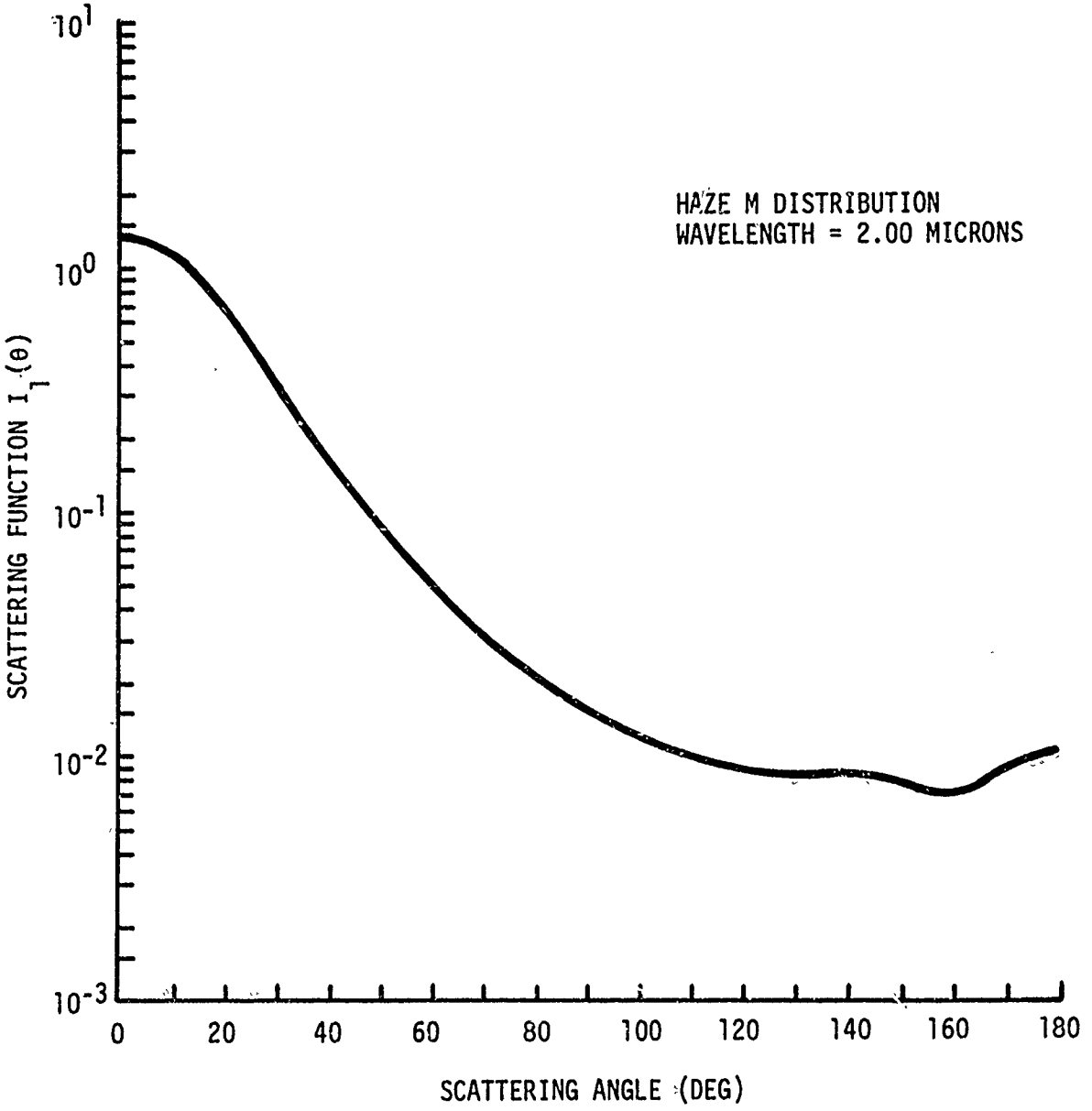

Figure 69. Volume Scattering Function $I_1(\theta)$ for Haze M Distribution at $\lambda = 2.0\mu$

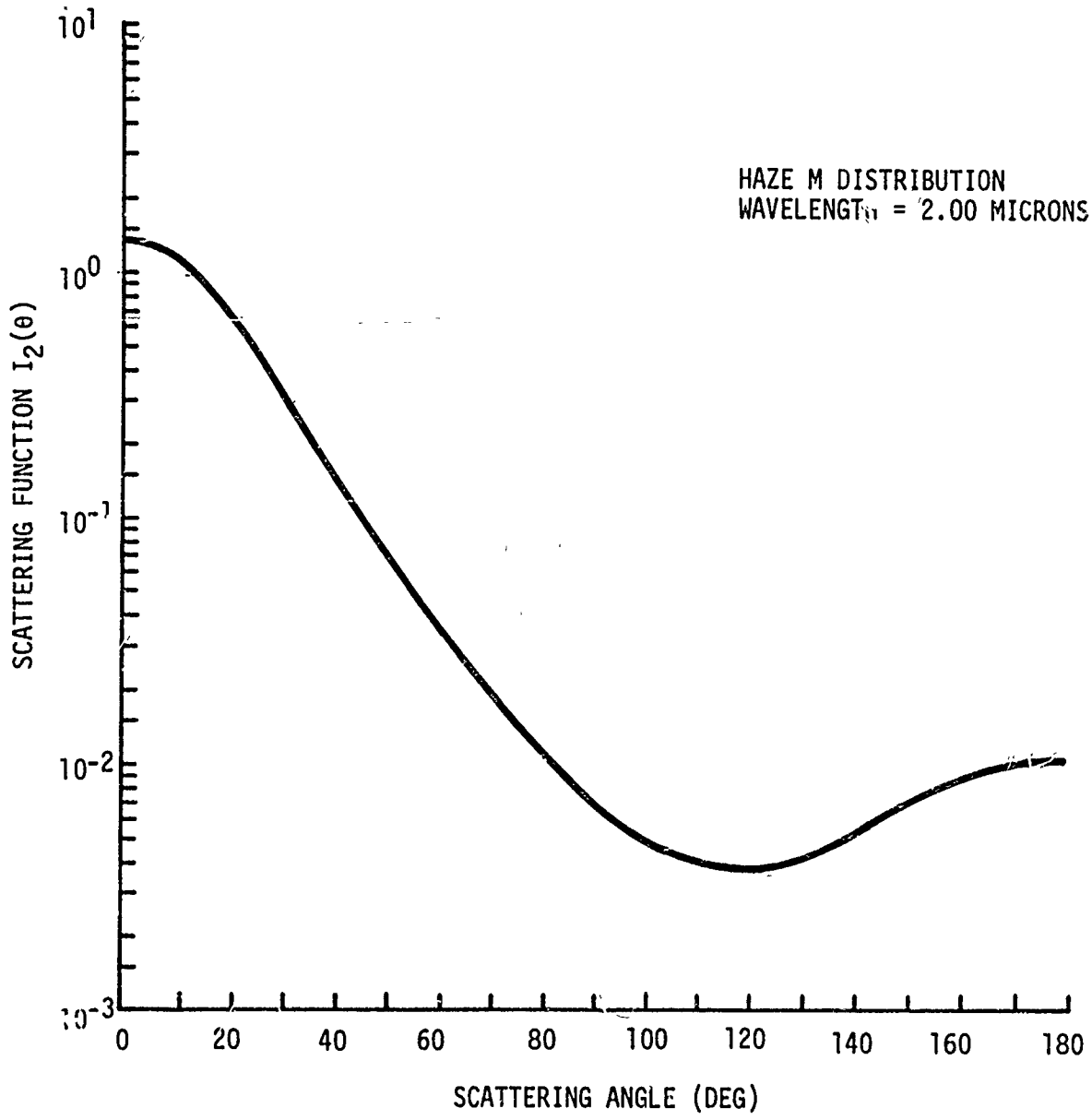

Figure 70. Volume Scattering Function $I_2(\theta)$ for Haze M Distribution at $\lambda = 2.0\mu$

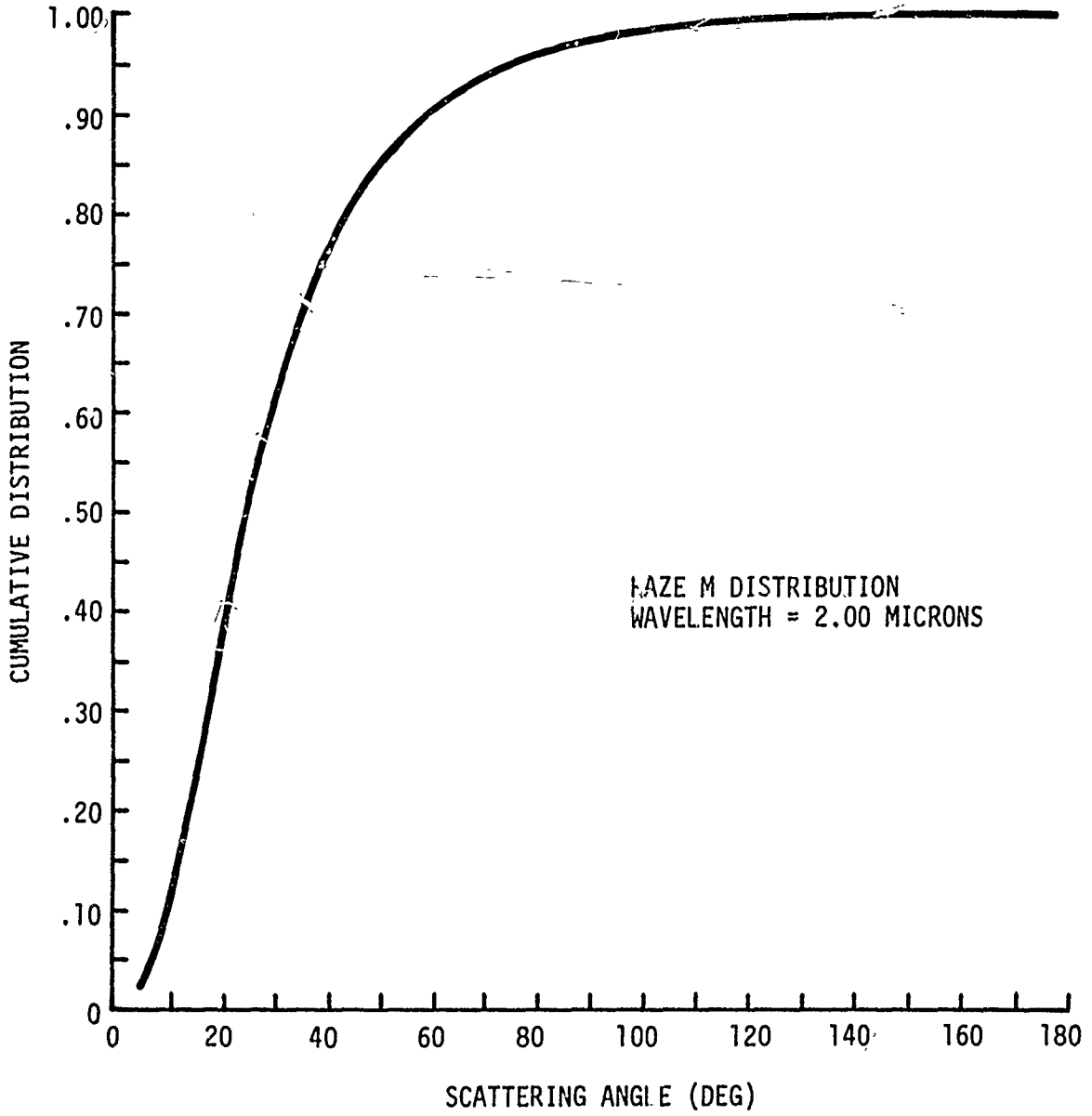

Figure 71. Cumulative Distribution for Haze M Distribution at $\lambda = 2.0\mu$

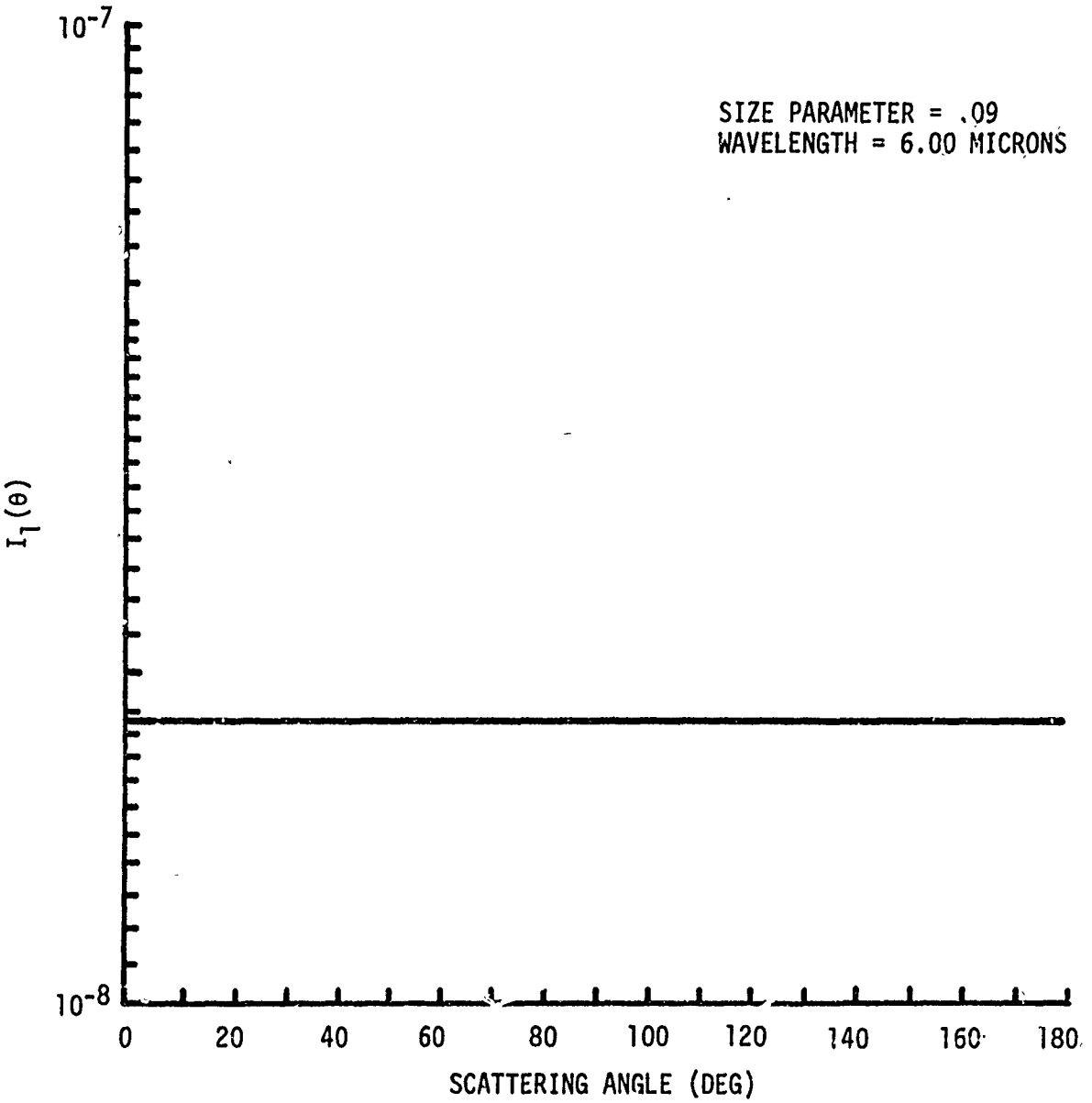

Figure 72. Particle Scattering Function for λ = 6.0μ and x - 0.09, Haze M Distribution

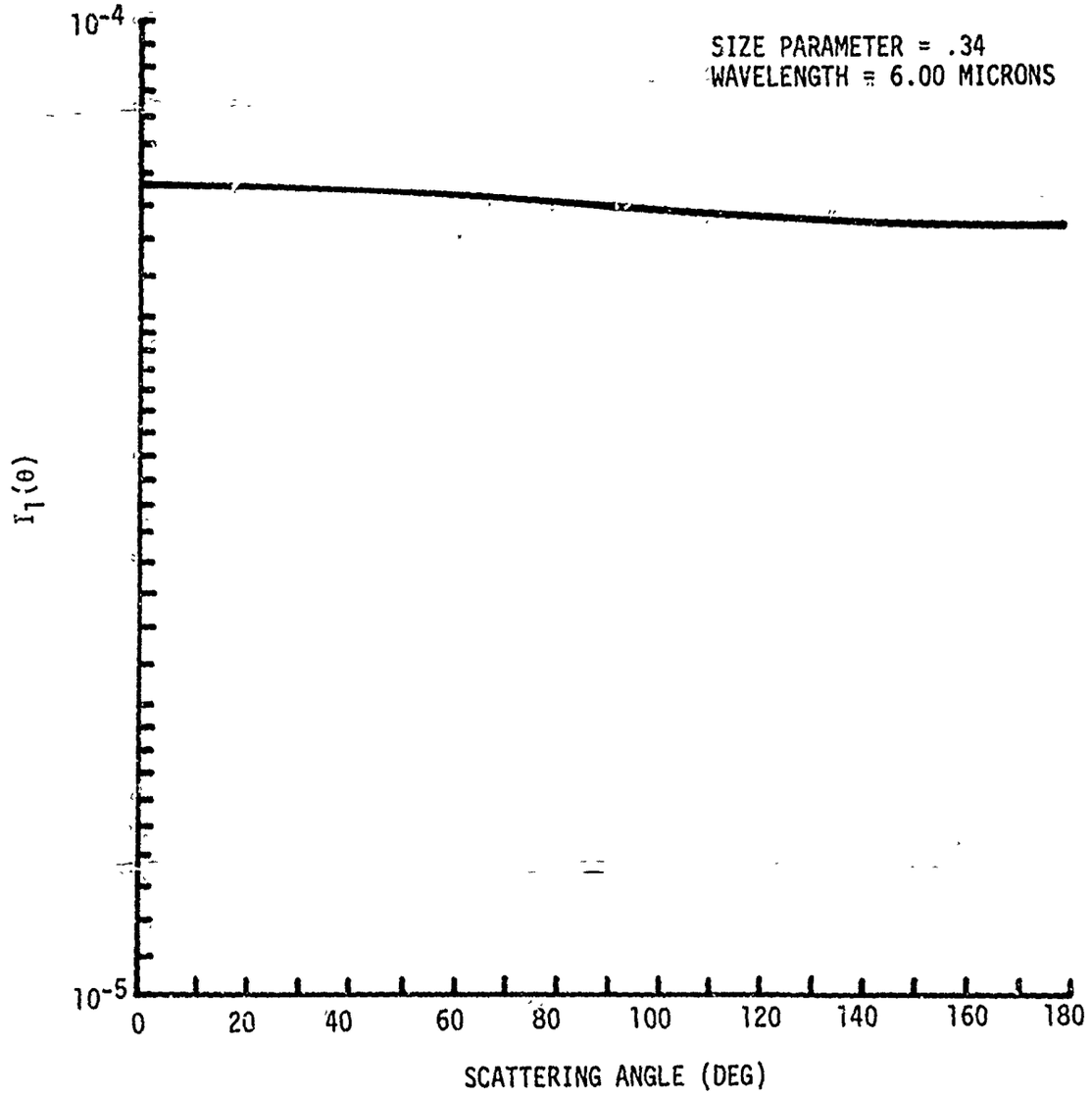

Figure 73. Particle Scattering Function for λ = 6.0μ and κ = 0.34, Haze M Distribution

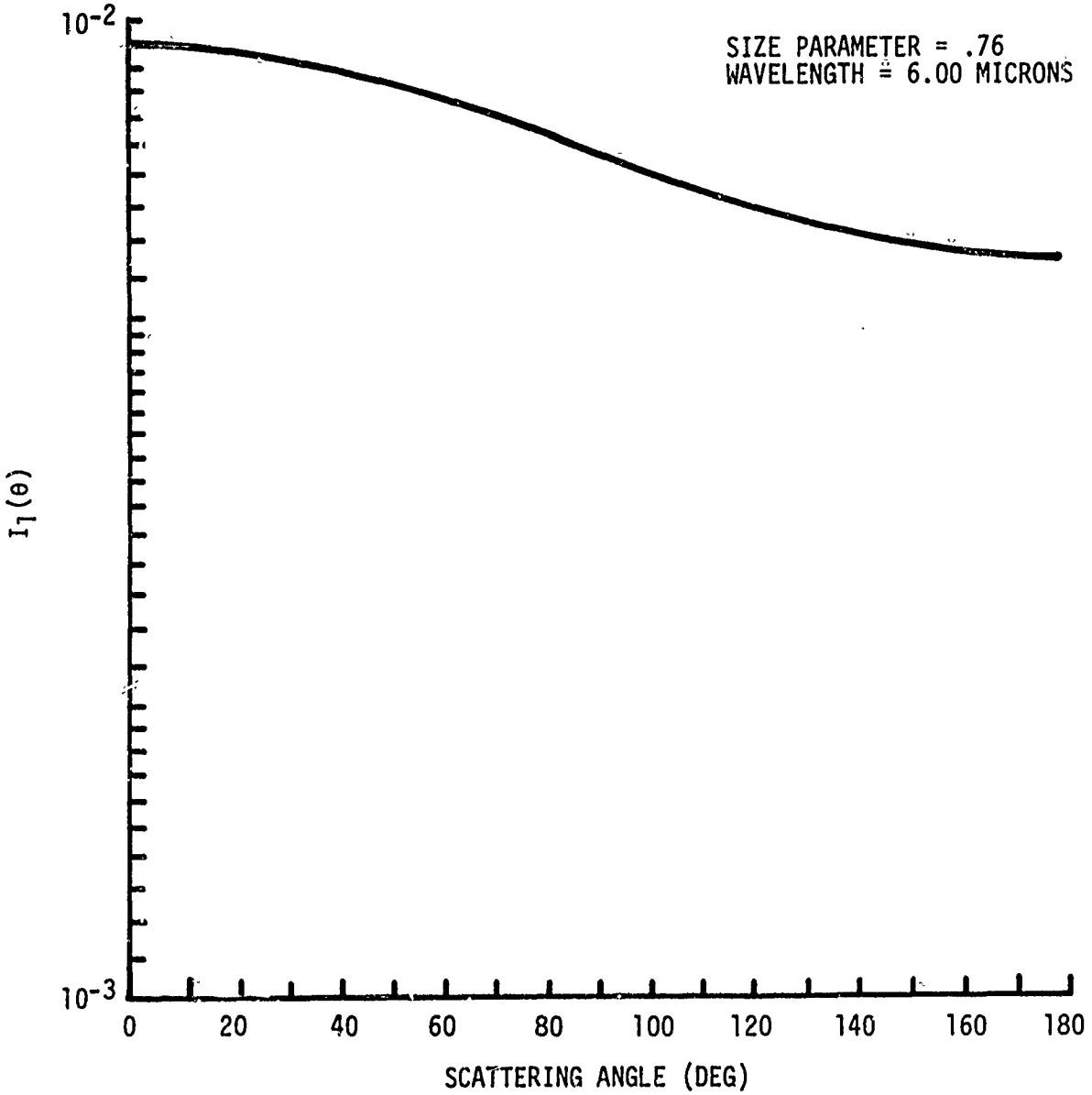

Figure 74. Particle Scattering Function for $\lambda = 6.0\mu$ and $x = 0.76$, Haze M Distribution

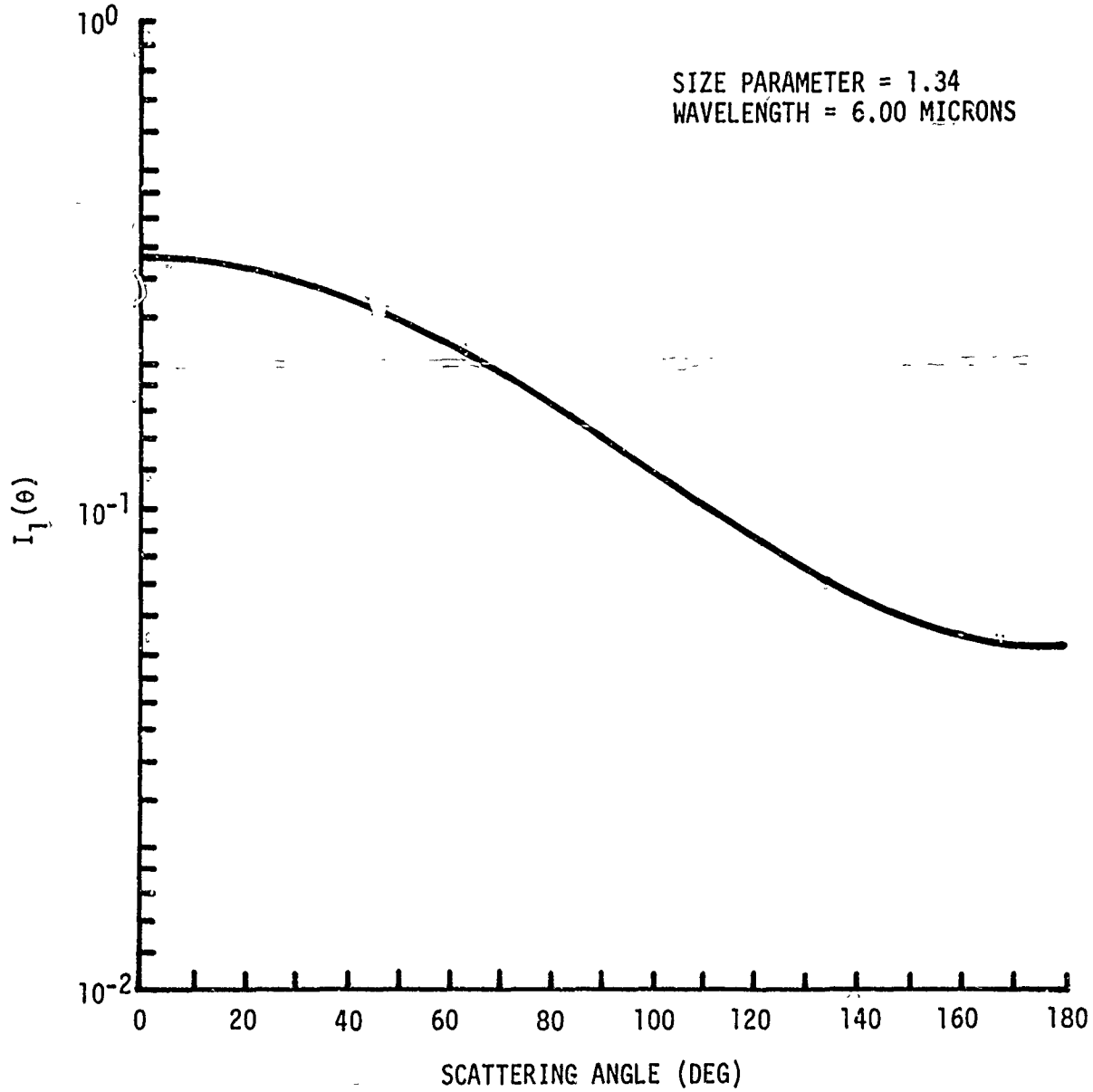

Figure 75. Particle Scattering Function for λ = 6.0μ and x = 1.34, Haze M Distribution

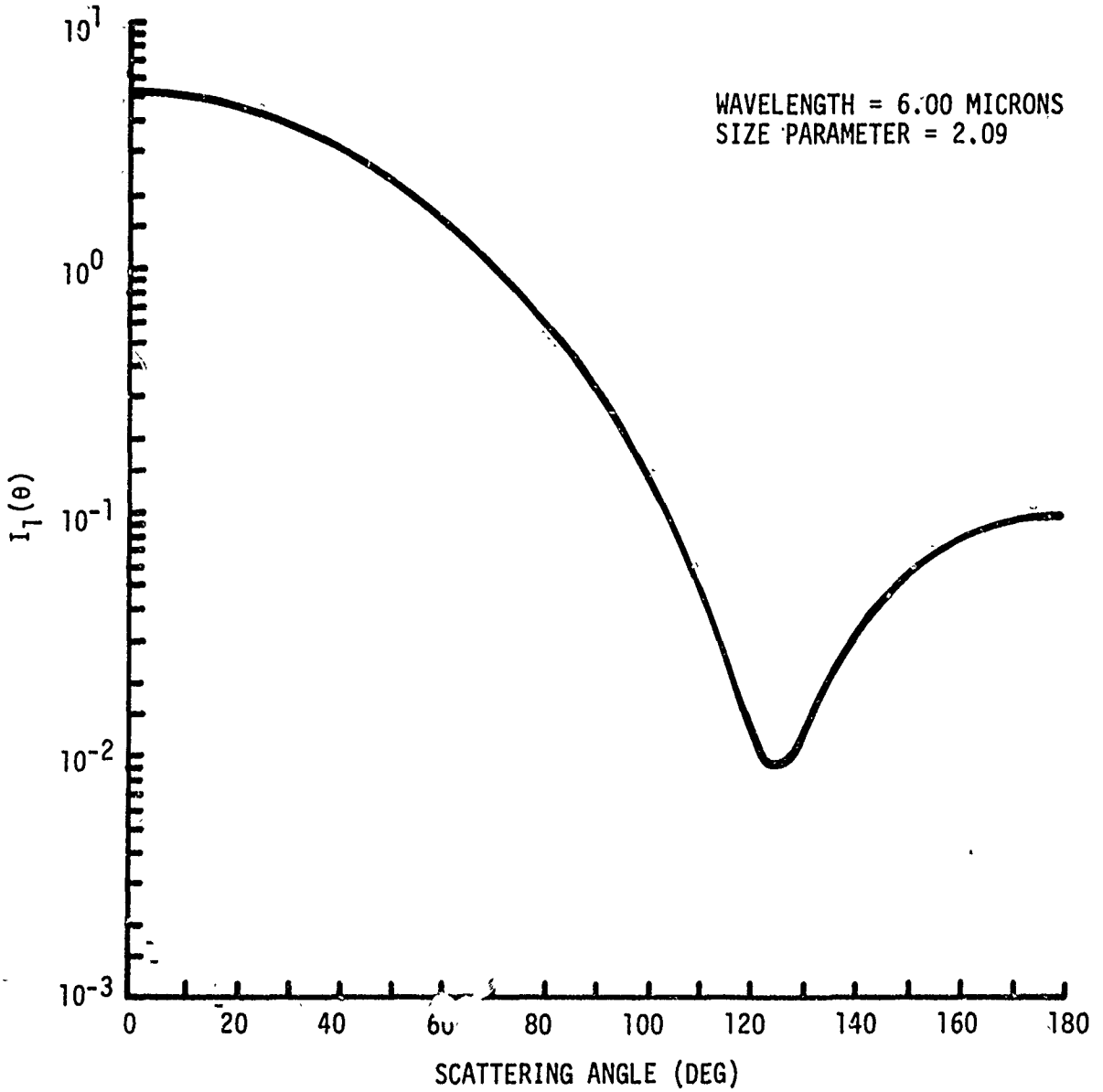

Figure 76. Particle Scattering Function for λ = 6.0μ and x = 2.09, Maze M Distribution

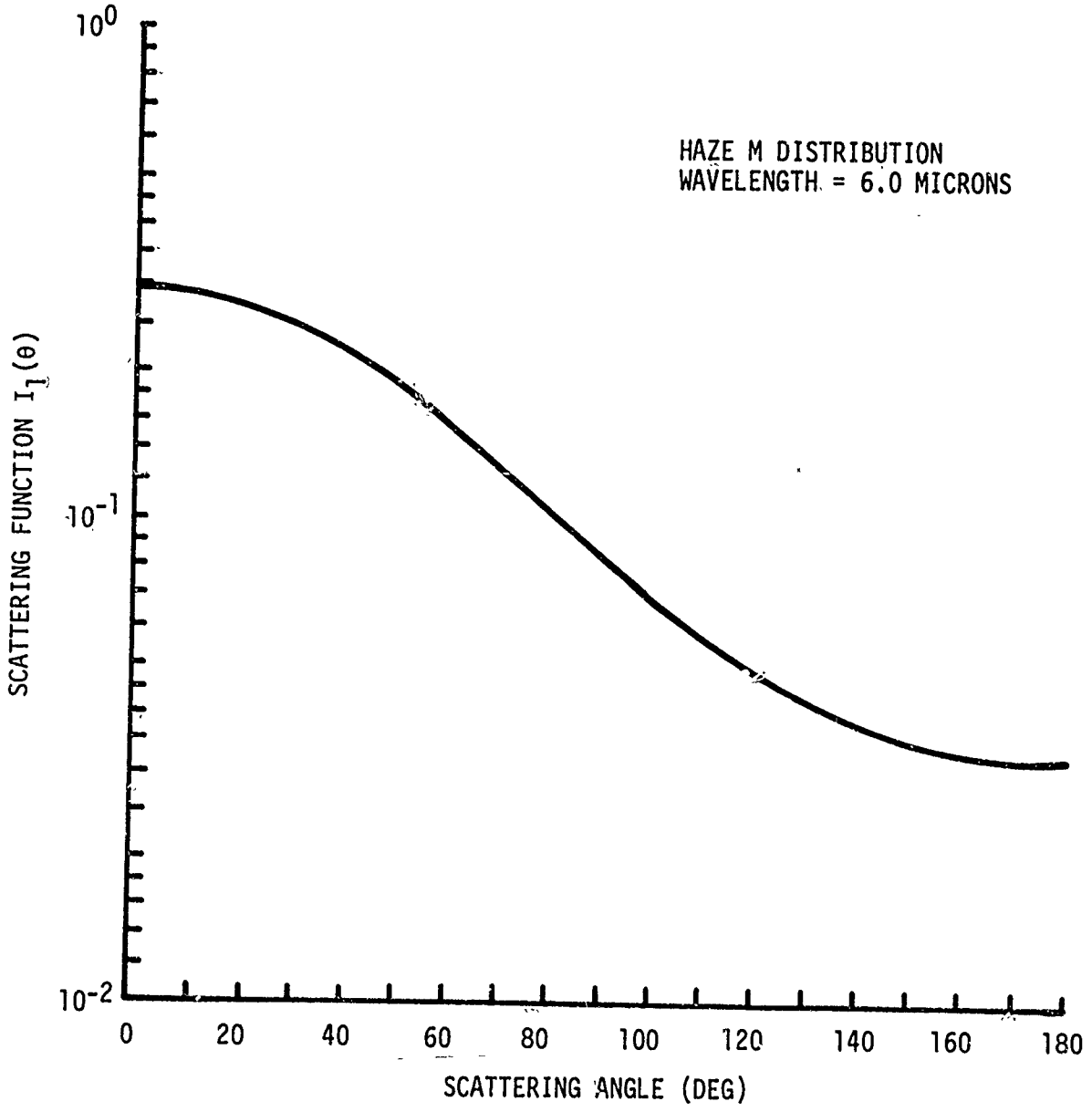

Figure 77. Volume Scattering Function $I_1(\theta)$ for Haze M Distribution at $\lambda = 6.0\mu$

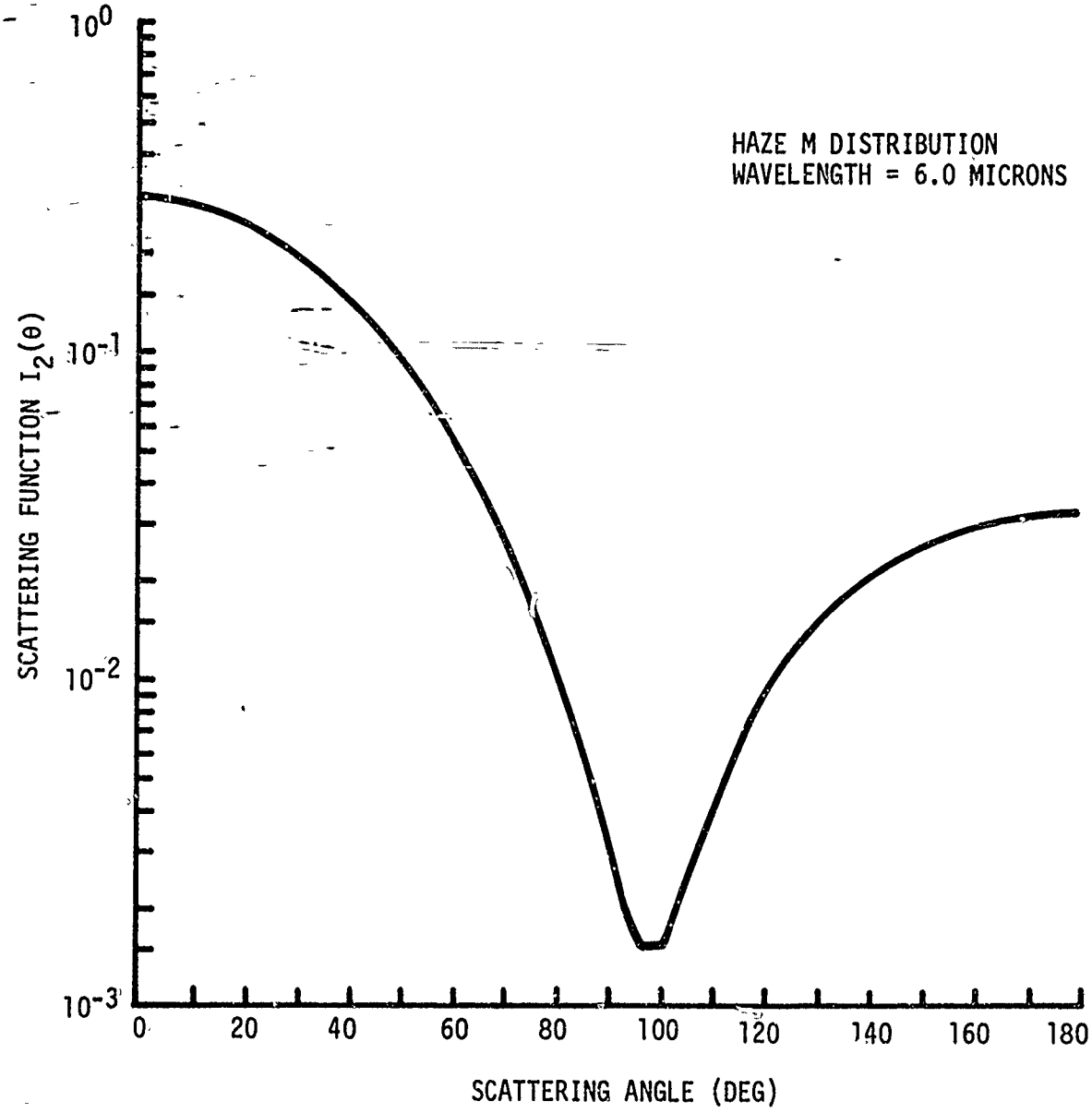

Figure 78. Volume Scattering Function $I_2(\theta)$ for Haze M Distribution at $\lambda = 6.0\mu$

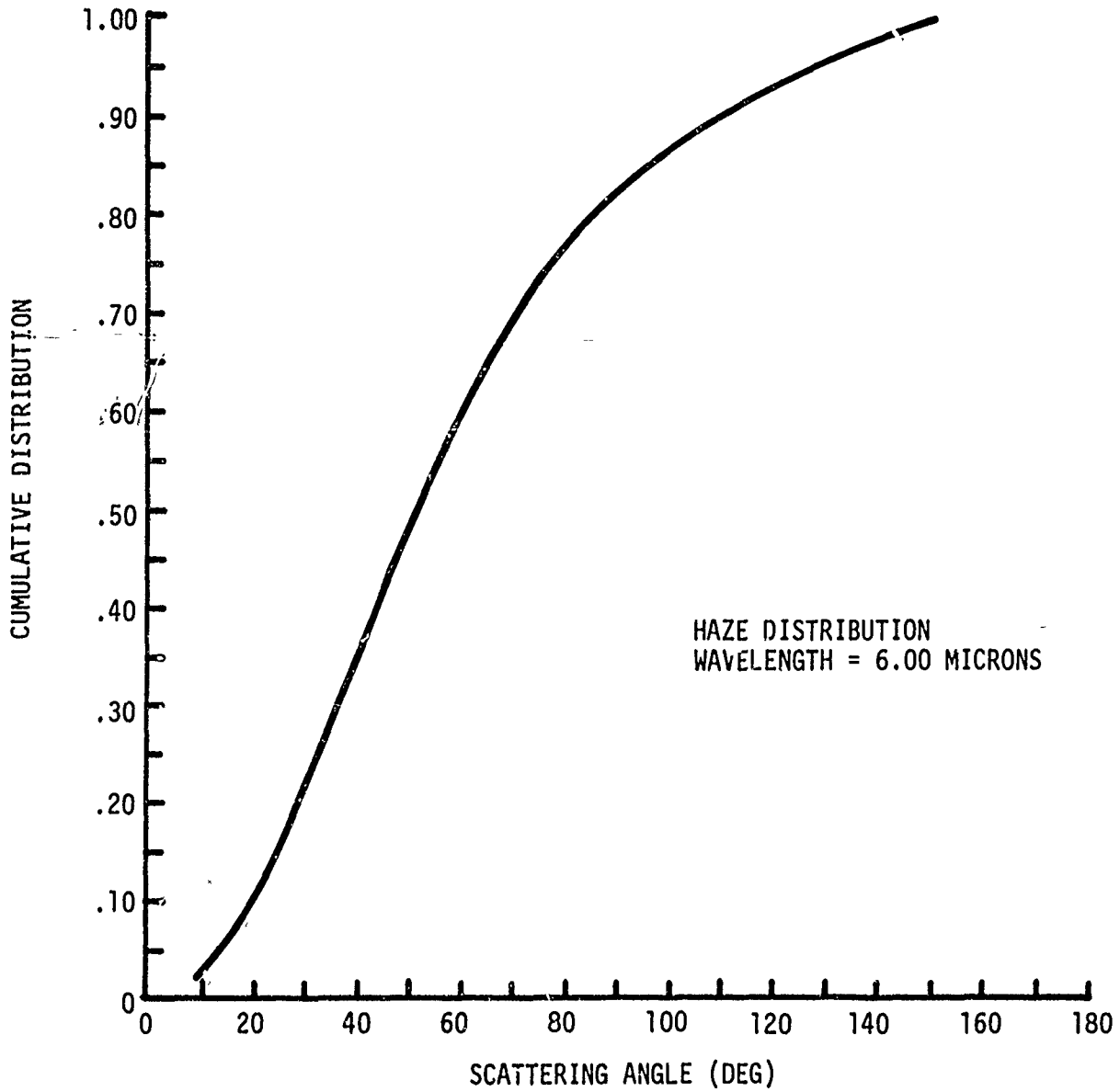

Figure 79. Cumulative Distribution for Haze M Distribution at $\lambda = 6.0\mu$

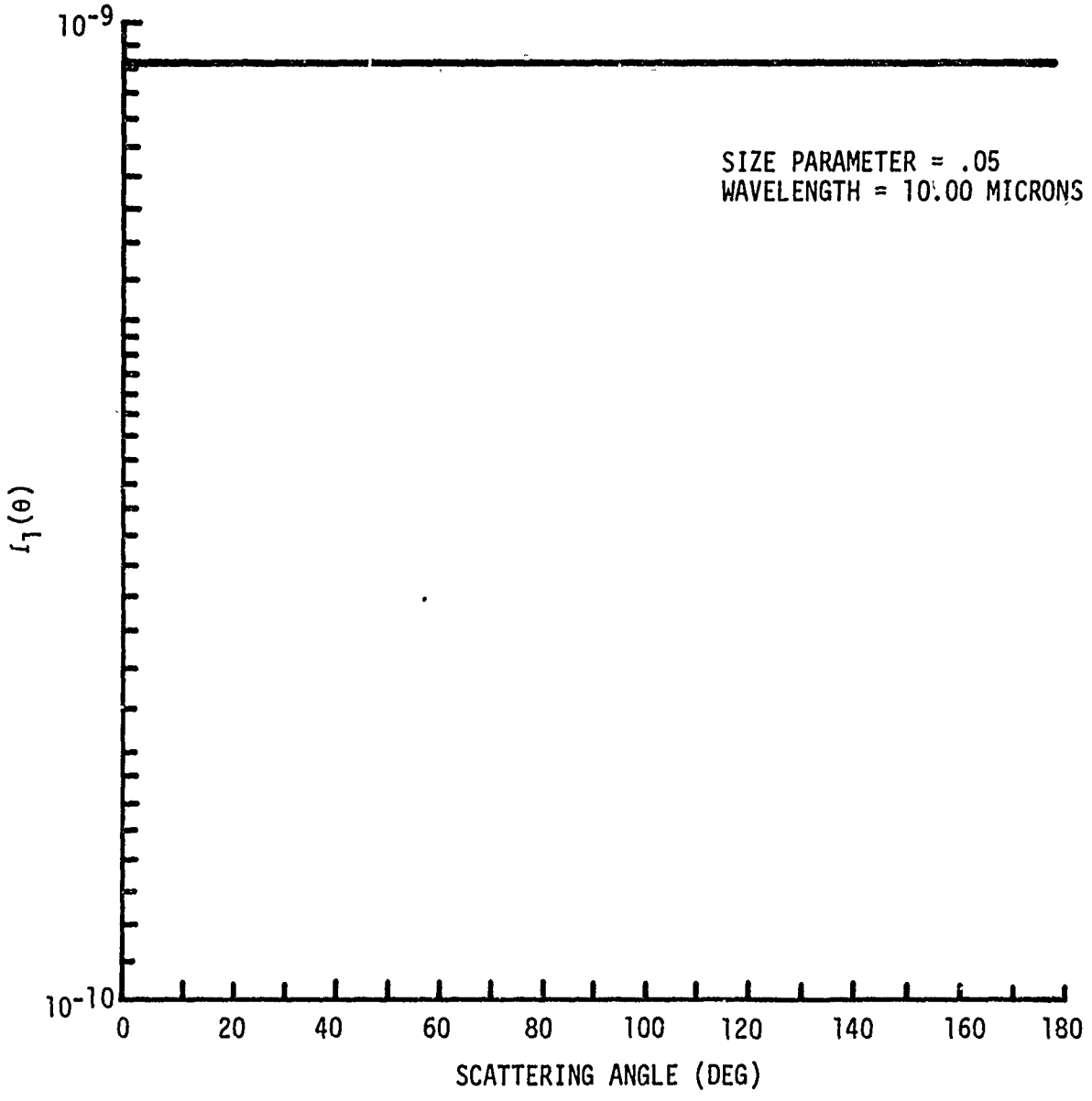

Figure 80. Particle Scattering Function for λ = 10.0μ and x = 0.05, Haze M Distribution

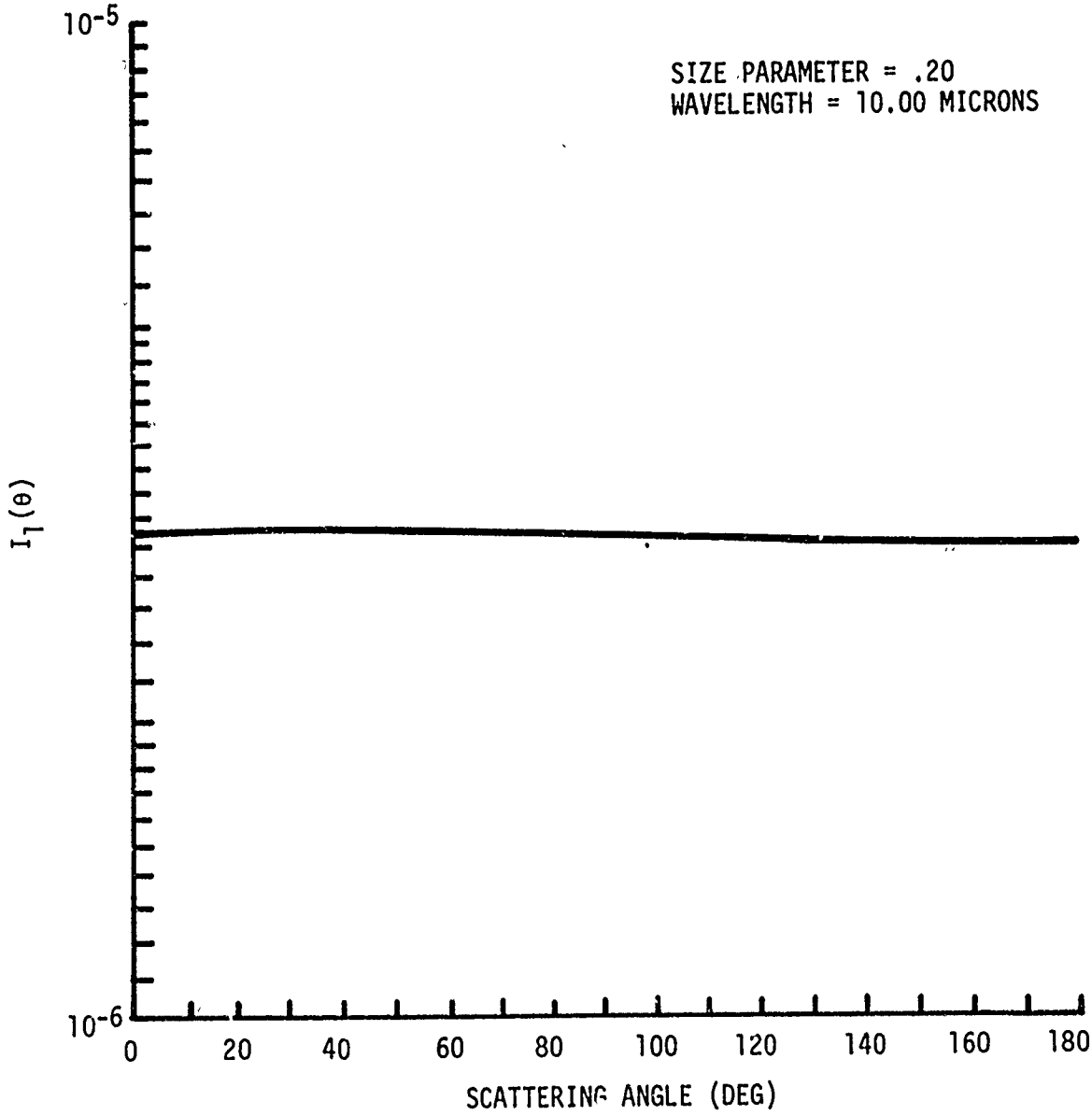

Figure 81. Particle Scattering Function for λ = 10.0μ and x = 0.20, Haze M Distribution

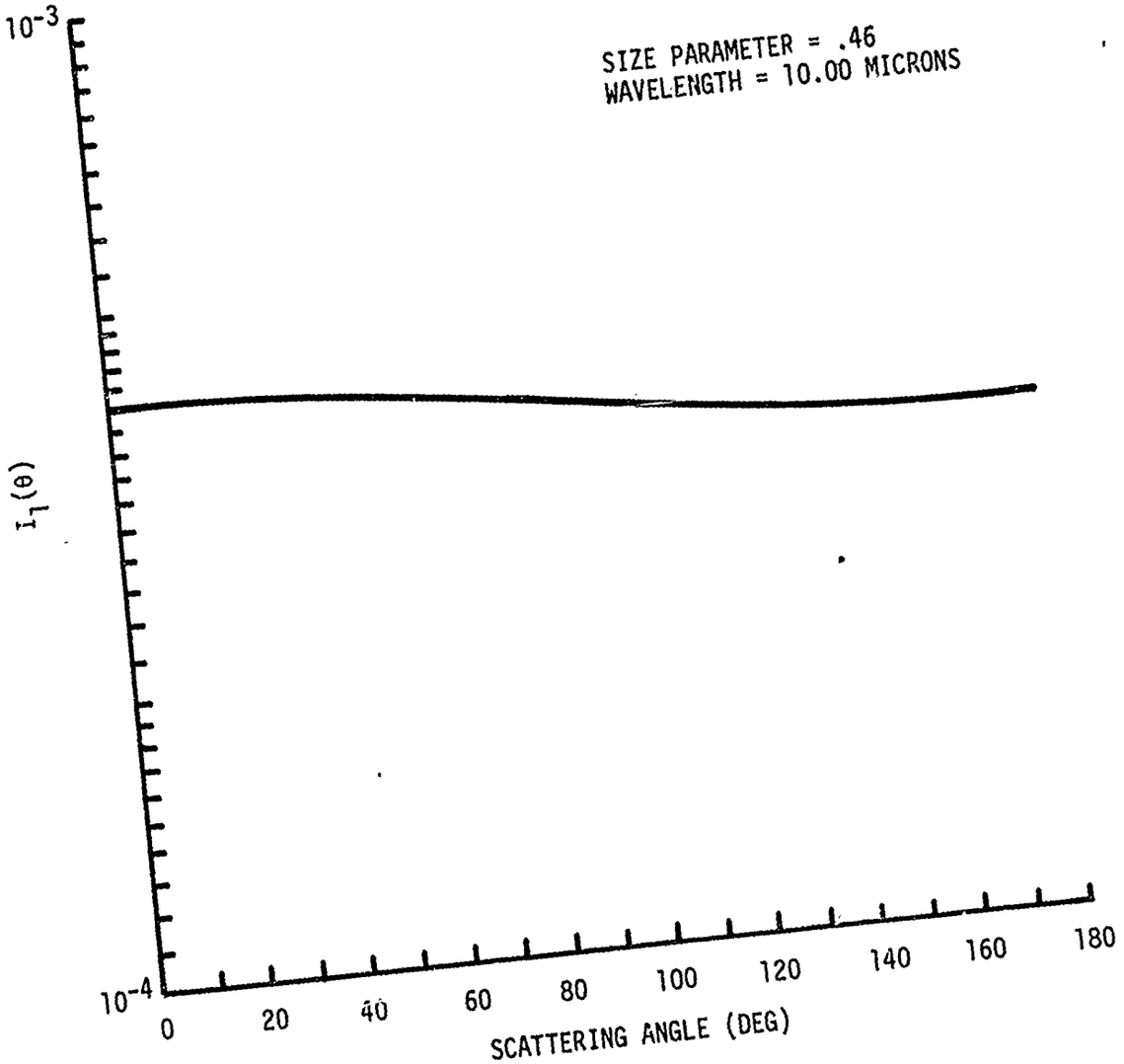

Figure 82. Particle Scattering Function for λ = 10.0μ and x = 0.46, Haze M Distribution

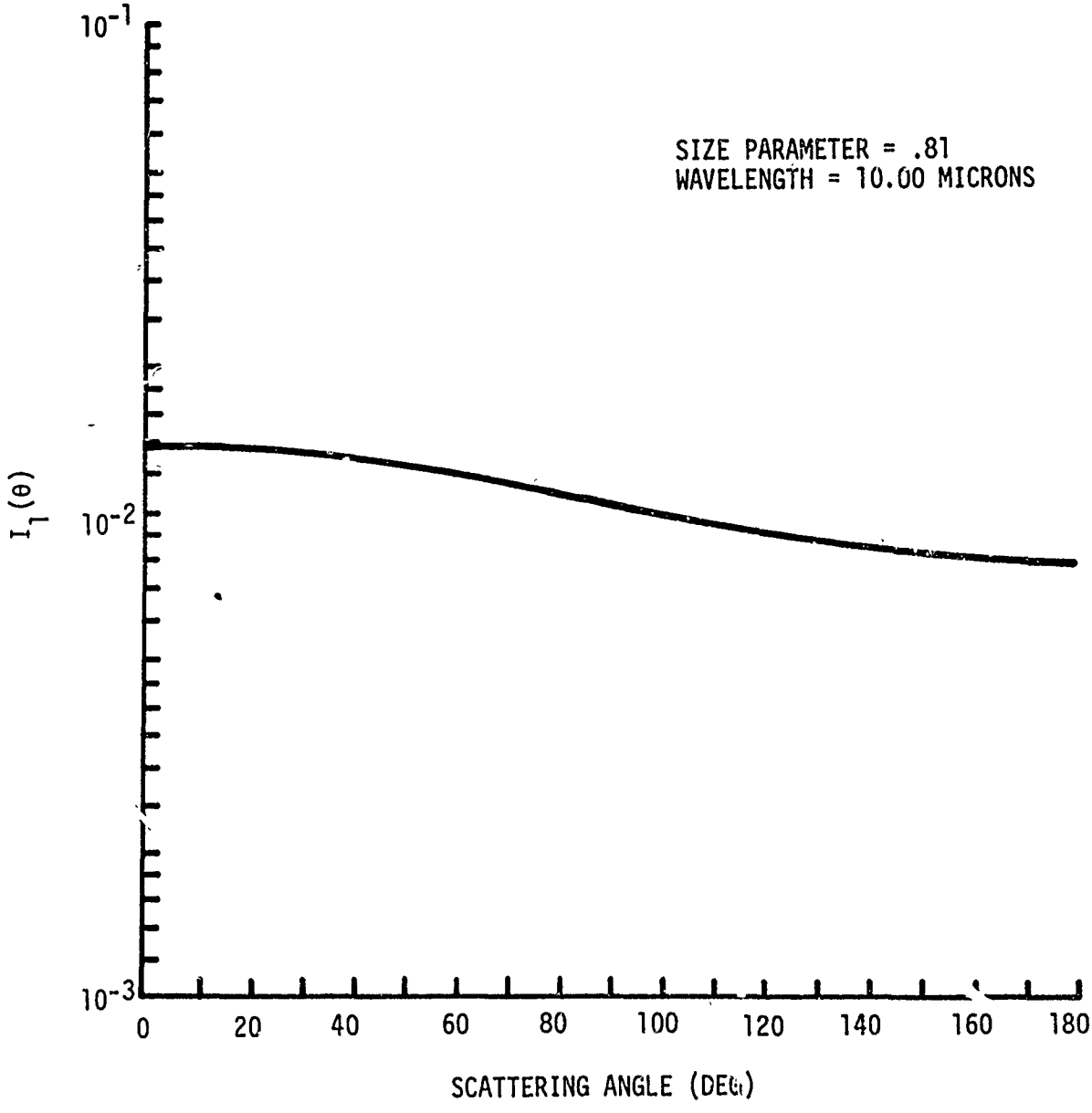

Figure 83. Particle Scattering Function for λ = 10.0μ and x = 0.81, Haze M Distribution

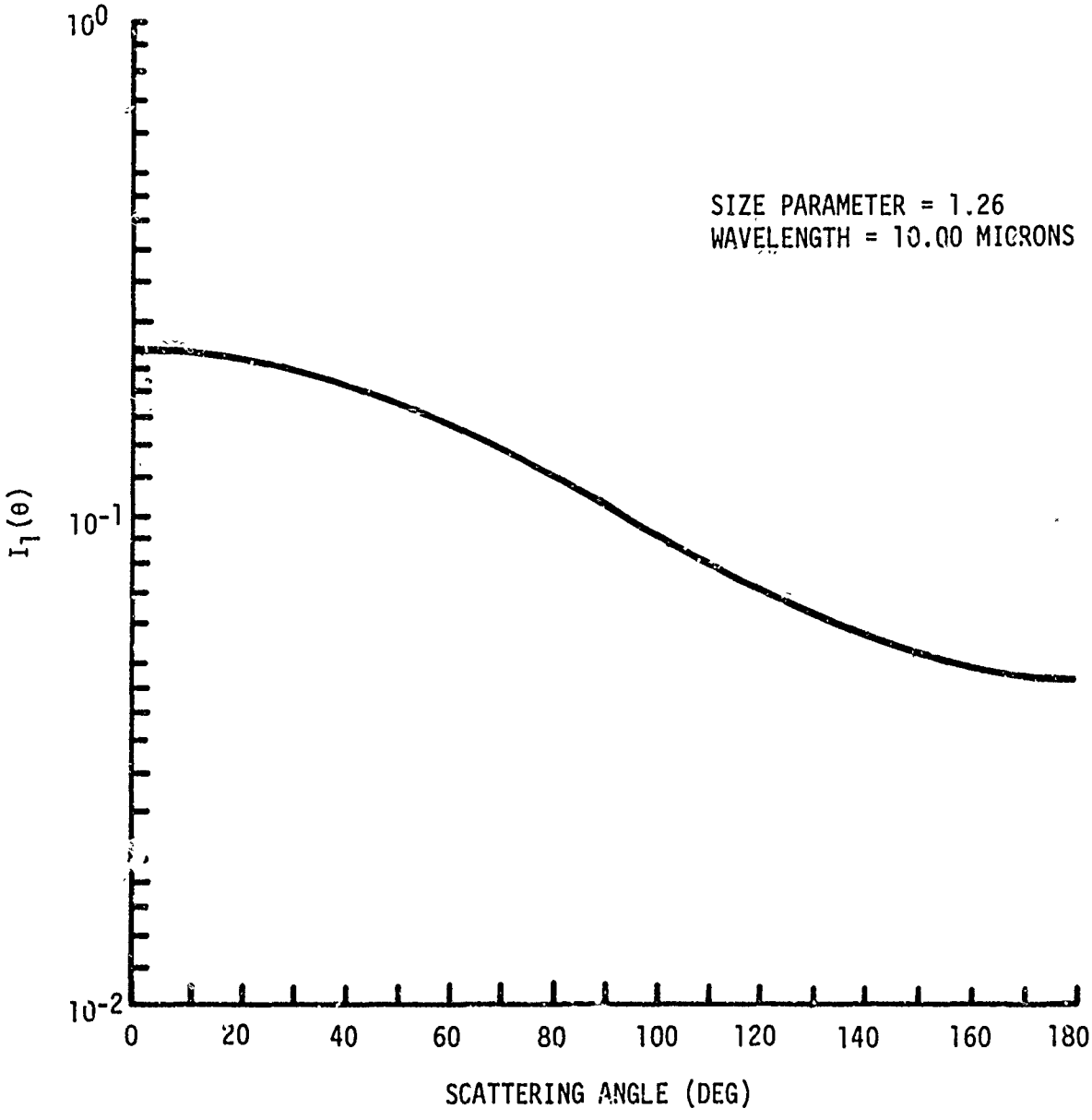

Figure 84. Particle Scattering Function for λ = 10.0μ and x = 1.26, Haze M Distribution

scattering through an angle between 0° and 71° is the same as that for angles between 0° and 21° for the cumulus distribution and $\lambda = 10.0\mu$. One can see from figures 85 and 86 that the normalized scattering function at $\lambda = 10.0\mu$ resemble scattering functions for Rayleigh scattering. Figure 87 shows the almost uniform cumulative probability functions. Table 2 contains the extinction coefficients for the Haze M distribution as defined by equation (324). We note that the extinction coefficient decreases with an increase in wavelength, i.e., red is attenuated less than the shorter wavelengths as was first shown by Rayleigh.

Table 2

EXTINCTION COEFFICIENTS FOR THE HAZE M DISTRIBUTION

$\lambda(\mu)$	Σ_{ext}
0.5	1.001×10^{-6}
1.0	9.083×10^{-7}
2.0	4.297×10^{-7}
4.0	1.222×10^{-7}
6.0	4.040×10^{-8}
8.0	1.677×10^{-8}
10.0	7.931×10^{-9}

4. DEPOLARIZATION BY A CLOUDY ATMOSPHERE AT 0.5, 4.0, and 10.0μ

In this subsection we consider the propagation of an electromagnetic wave through an atmosphere containing cumulus clouds. The photon source will be pointed in the downward direction (see figure 88) from a fixed altitude of 13 km. We assume that the source is linearly parallel polarized and that the source beamwidth is 2° x 2°. The

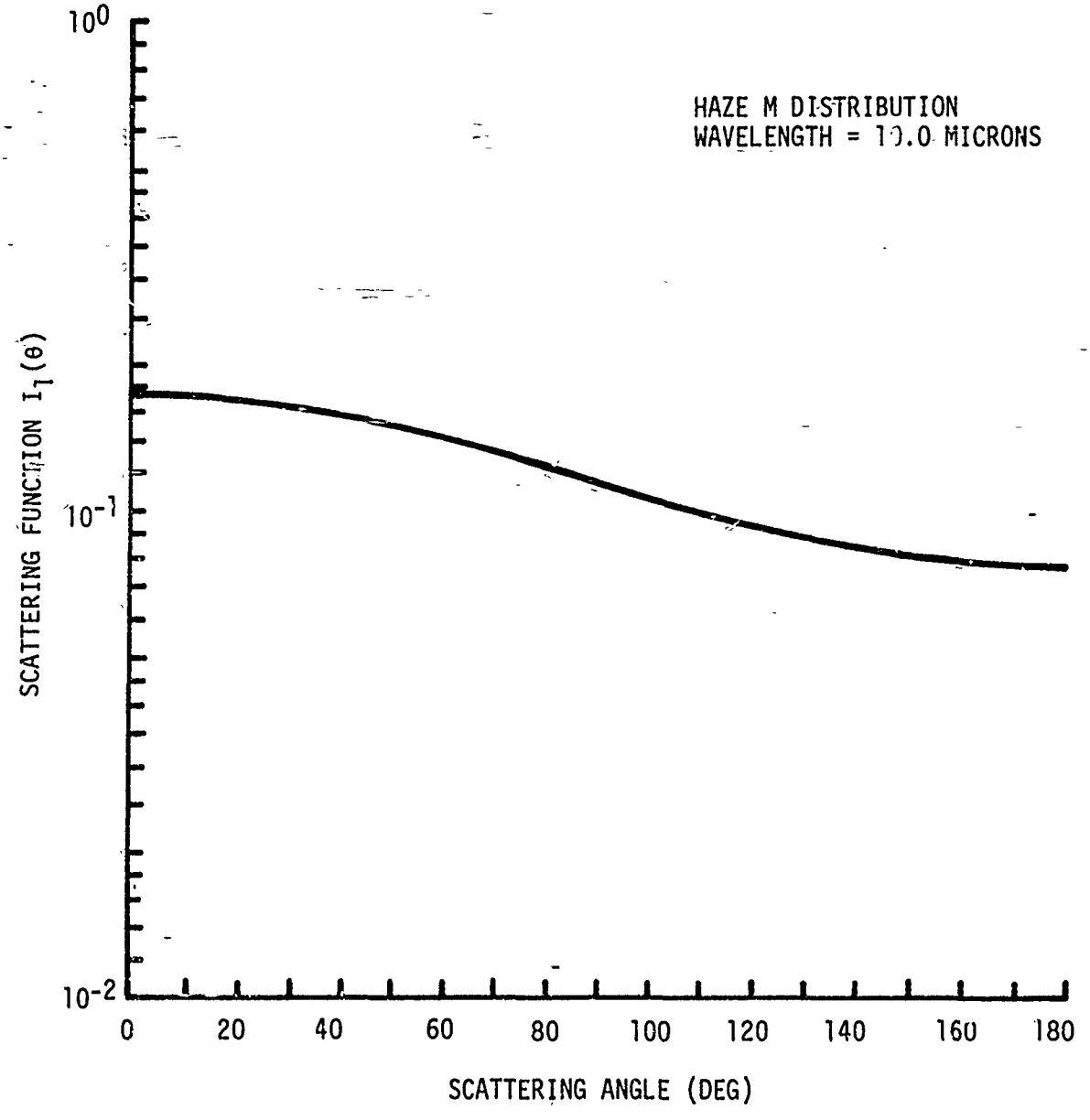

Figure 85. Volume Scattering Function $I_1(\theta)$ for Haze M Distribution at $\lambda = 10.0\mu$

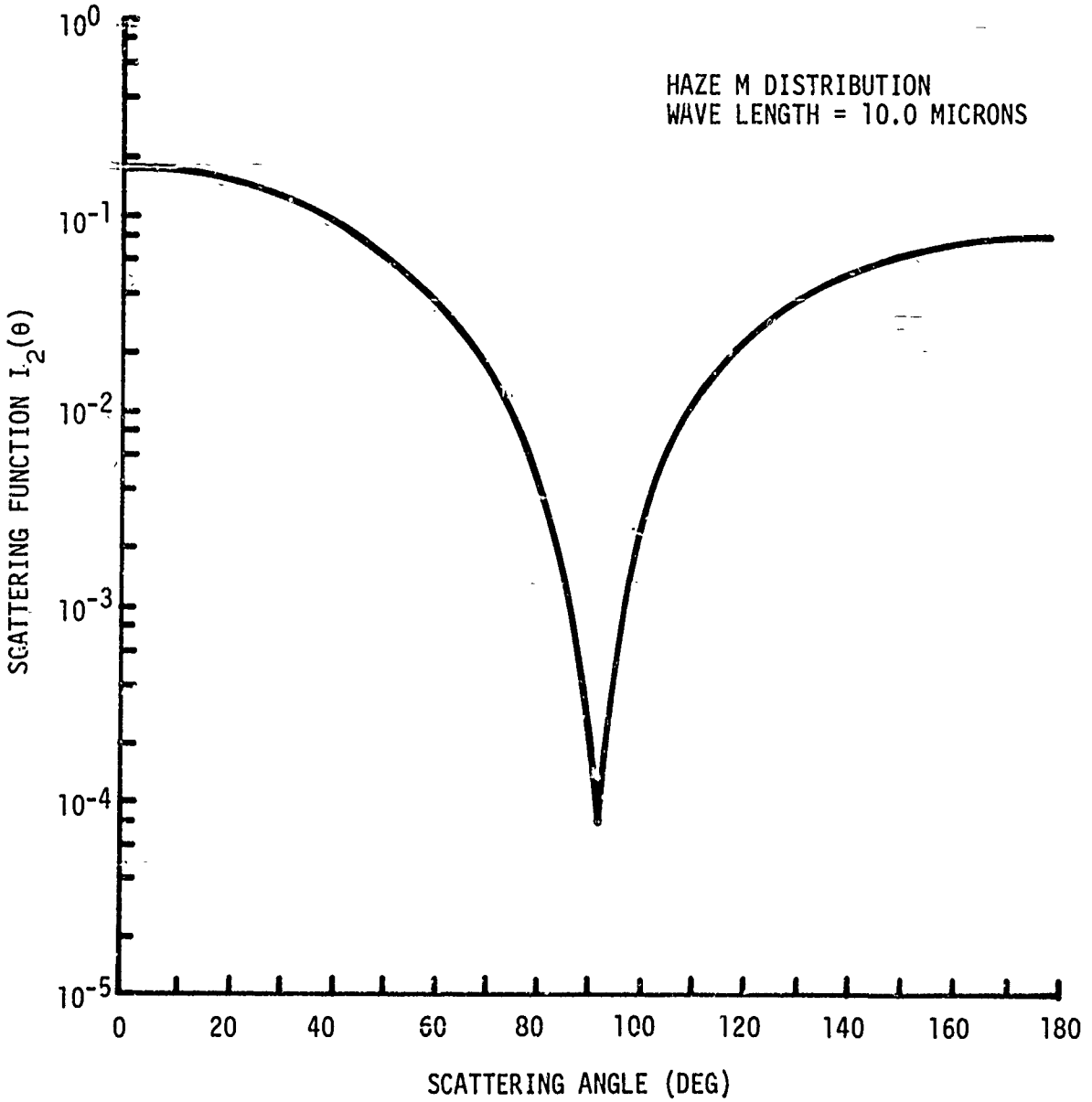

Figure 86. Volume Scattering Function $I_2(\theta)$ for Haze M Distribution at $\lambda = 10.0\mu$

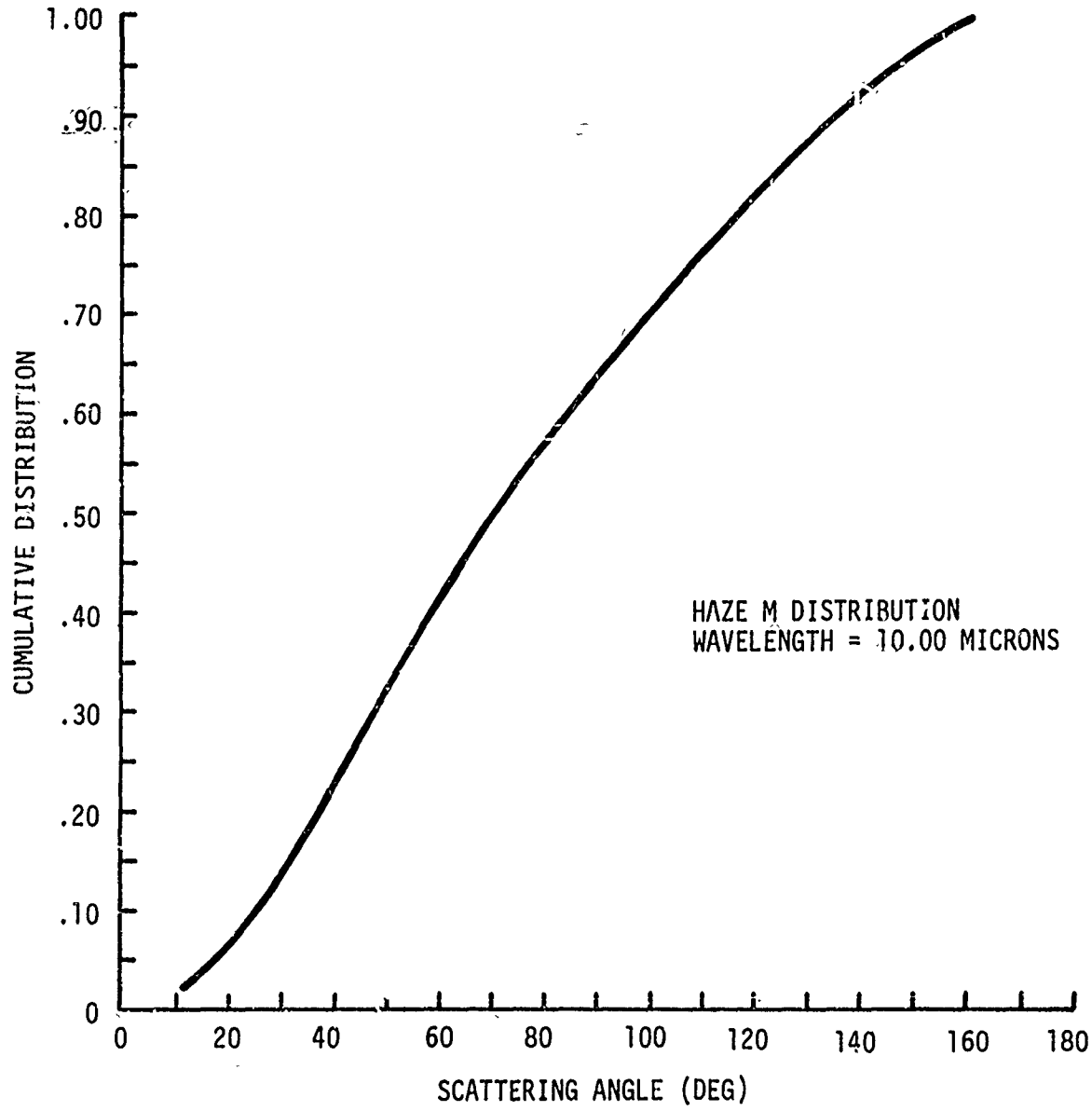

Figure 87. Cumulative Distribution for Haze M Distribution at λ = 10.0μ

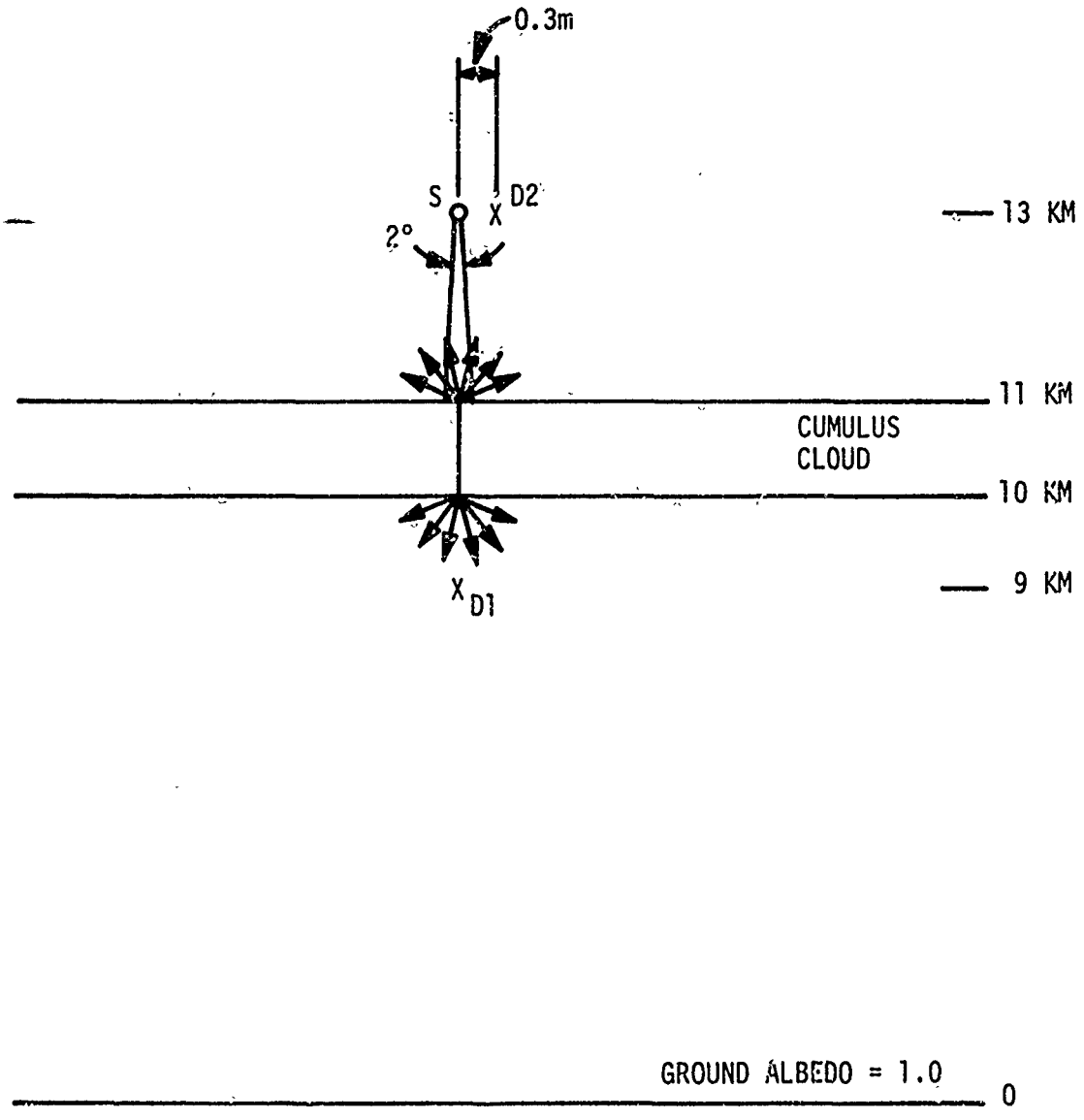

Figure 88. Cumulus Cloud Geometry

altitude of the cloud bottom is 10 km while the altitude of the cloud top is 11 km. We first assume that only Rayleigh scattering exists above and below the cloud, then only Mie scattering, and finally we assume that no scattering occurs outside the cloud. Inside the cloud we consider only Mie scattering. We determine the depolarization of the linearly polarized wave at wavelengths of 0.5, 4.0, and 10.0μ. The ground is assumed to be a diffuse scatterer so that the incident wave is completely depolarized, i.e., equal parallel and perpendicular components are scattered. We initially assume a ground albedo of 1.0, i.e., all incident energy is scattered back into the atmosphere, then we assume that no ground scattering occurs. The source is placed at an altitude of 13 km. Two isotropic detectors are placed at altitudes of 9 km (D1) and 13 km (D2) with D2 displaced horizontally by 0.3m from the source.

In simulating the problem described above using the Monte Carlo technique we use 5,000 and 10,000 histories. Experience gained in running several problems has lead to the selection of 10 collisions (see figure 109). Actually, as we can see from figure 109, at 6 collisions the received intensity has dropped by 3 orders of magnitude and we could probably carry the number of collisions out to only 6 with acceptable results.

Figure 89 shows the assumed stratification for the atmosphere. The optical depth increases linearly with altitude in steps as follows

$$\tau(h) = \begin{cases} 10^{-5}h & 0 \leq h \leq 10 \text{ km} \\ 10^{-3}h - 9.9 & 10 \text{ km} \leq h \leq 11 \text{ km} \\ 6.1 \times 10^{-7}h + 1.1 & 11 \text{ km} \leq h \leq 500 \text{ km} \end{cases} \qquad (335)$$

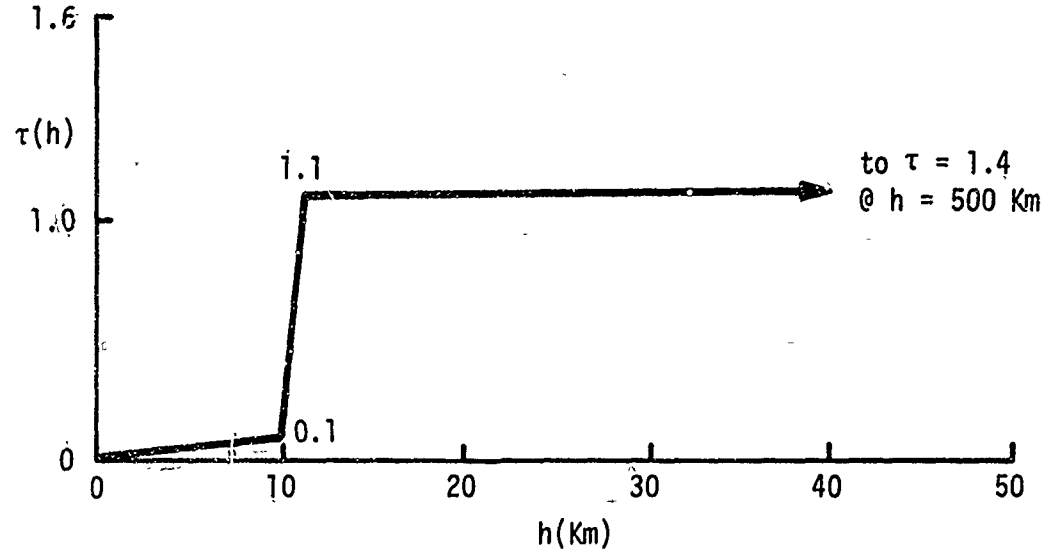

Figure 89. Atmospheric Stratification

The optical depth of the cloud is 1.0 as can be seen from figure 89. Normally the atmosphere is stratified exponentially [15] but for small distances as we have assumed for this problem linear stratification is a good assumption for the type of atmosphere selected. This basic stratification will be scaled up for simulation of greater densities.

As we have stated the polarization assumed for this problem is parallel. This means that the electric field vector, according to the convention adopted in section III, is in the vertical plane through the propagation vector and the vertical axis referred to the source. Figure 90 portrays our polarization convention. The source is located at the origin. In this example a photon is being emitted from the source in the direction (θ,ϕ), the electric field vector $\vec{E}_\ell$ is in a vertical plane containing the propagation vector $\vec{k}$ and the vertical axis.

Figure 91 shows the results of the Monte Carlo simulation for this problem. The ordinate is the polarization factor and is defined as

$$D = \frac{I_r - I_\ell}{I_r + I_\ell} \tag{336}$$

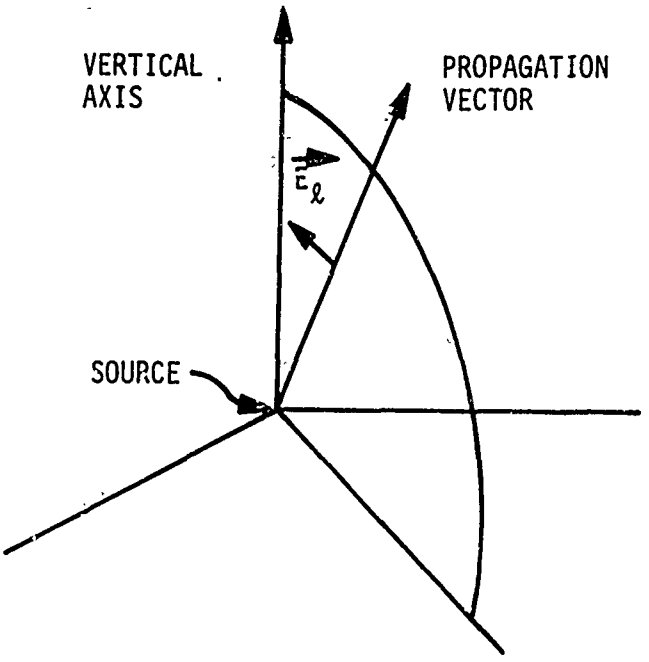

Figure 90. Polarization Reference Plane for Emitted Intensity

where I_r and I_ℓ are the perpendicular and parallel intensity components, respectively. The abscissa is the cosine of the polar angle for each detector. Recall that the polar angle is measured from the line joining the detector and the source with 0° toward the source and 180° away from the source behind the detector. Therefore in figure 91 both detectors are "looking" directly at the source when the polar cosine is euqal to +1.0 and directly away when the polar cosine is -1.0. Detector 2 is only 0.3 meters from the source and the magnitude of the intensity from all directions is such that the variance of the samples is less than two orders of magnitude from the mean. Detector 1 is 4 kilometers from the source and due to the narrowness of the source beam (2° x 2°) the variation of the intensity and therefore also of the polarization factor is large between values of the polar cosine equal to -0.7 and +0.7, i.e., the data are meaningful only for forward scattering angles from 0° to 45° and for back scattering angles from 135° to 180°.

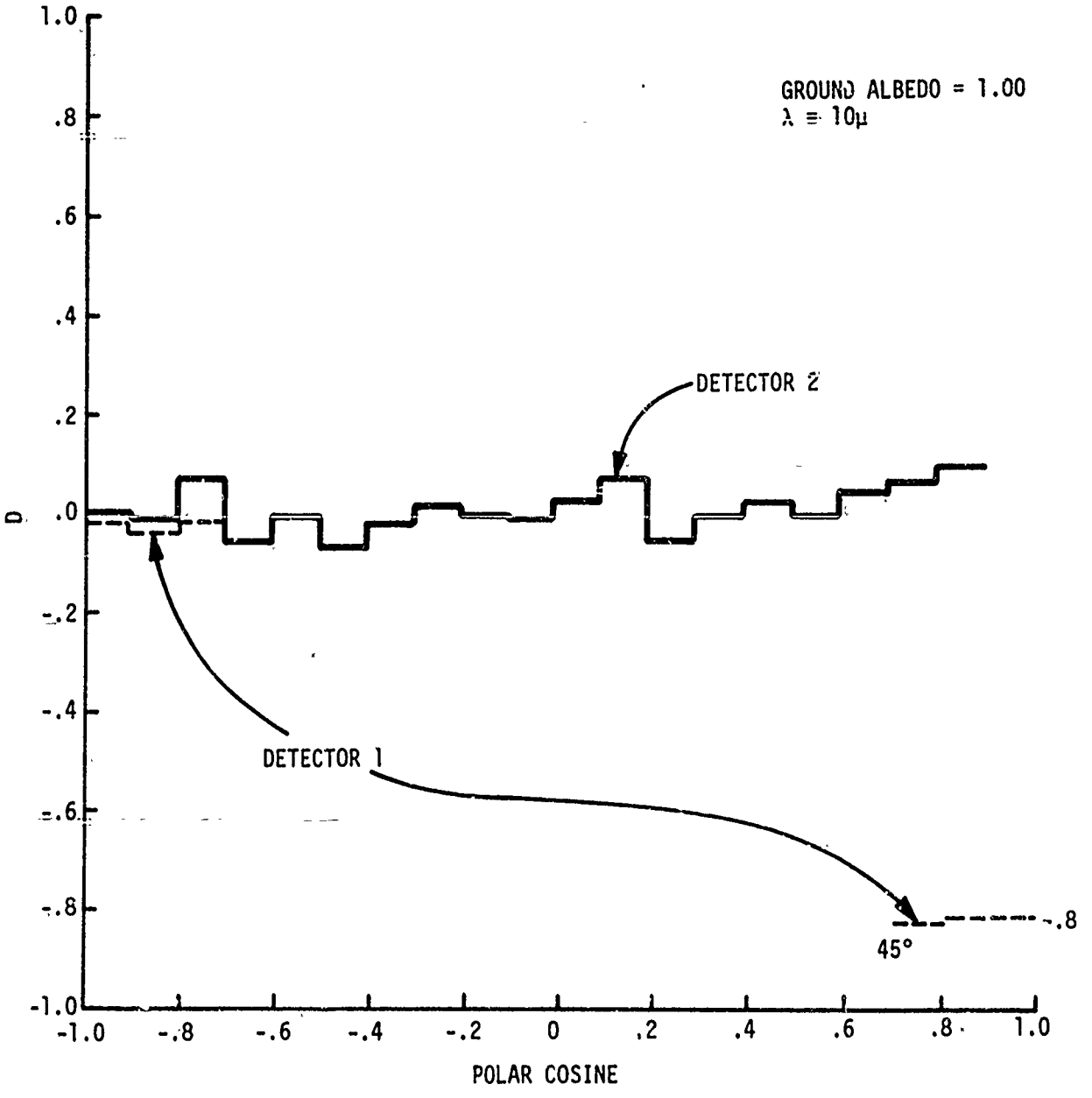

Figure 91. Polarization Factor for Cumulus Cloud at λ = 10.0μ with Ground Scatter

In figure 92 we show the depolarization factor for the same problem except at $\lambda = 0.5\mu$. In comparing figures 91 and 92 we can see that for detector 1 the depolarization is not quite as great as it is for detector 2 at 0.5μ. The intensity scattered directly back from the cloud and the ground to detector 2 remains depolarized at 0.5μ and at 10.0μ.

Figures 93 and 94 show the same data as shown in figure 92 except expanded. Figure 93 gives the polarization factor for detector 1 for polar angles from 0° to 2°, i.e., forward scattering through the cloud and figure 94 gives the polarization factor for polar angles from 89° to 91°, i.e., backscattering from the cloud.

Figure 91 shows that for detector 1 located below the cloud (see figure 68) that the forward scattered energy (polar cosine equal to +1.0) is only partially depolarized and at that point

$$D = 0.8 \tag{337}$$

while for backscattering (polar cosine equal to -1.0) from the ground with an albedo equal to 1.0 the wave is completely depolarized, i.e.,

$$I_r = I_\ell \tag{338}$$

or

$$D = 0 \tag{339}$$

This is as expected since we are assuming that the ground is a diffuse scatterer and completely depolarizes the incident wave.

For detector 2 we can see, if we ignore the small variations, that the received intensity is almost completely depolarized for all directions. The cloud and ground are in the direction where the polar cosine is equal to 0. For figure 91 and subsequent data the received intensity is integrated over all azimuth angles, but the magnitude of the intensity received from angles other than forward and backscatter can be considered to be negligible; for example, for detector 2 the intensity

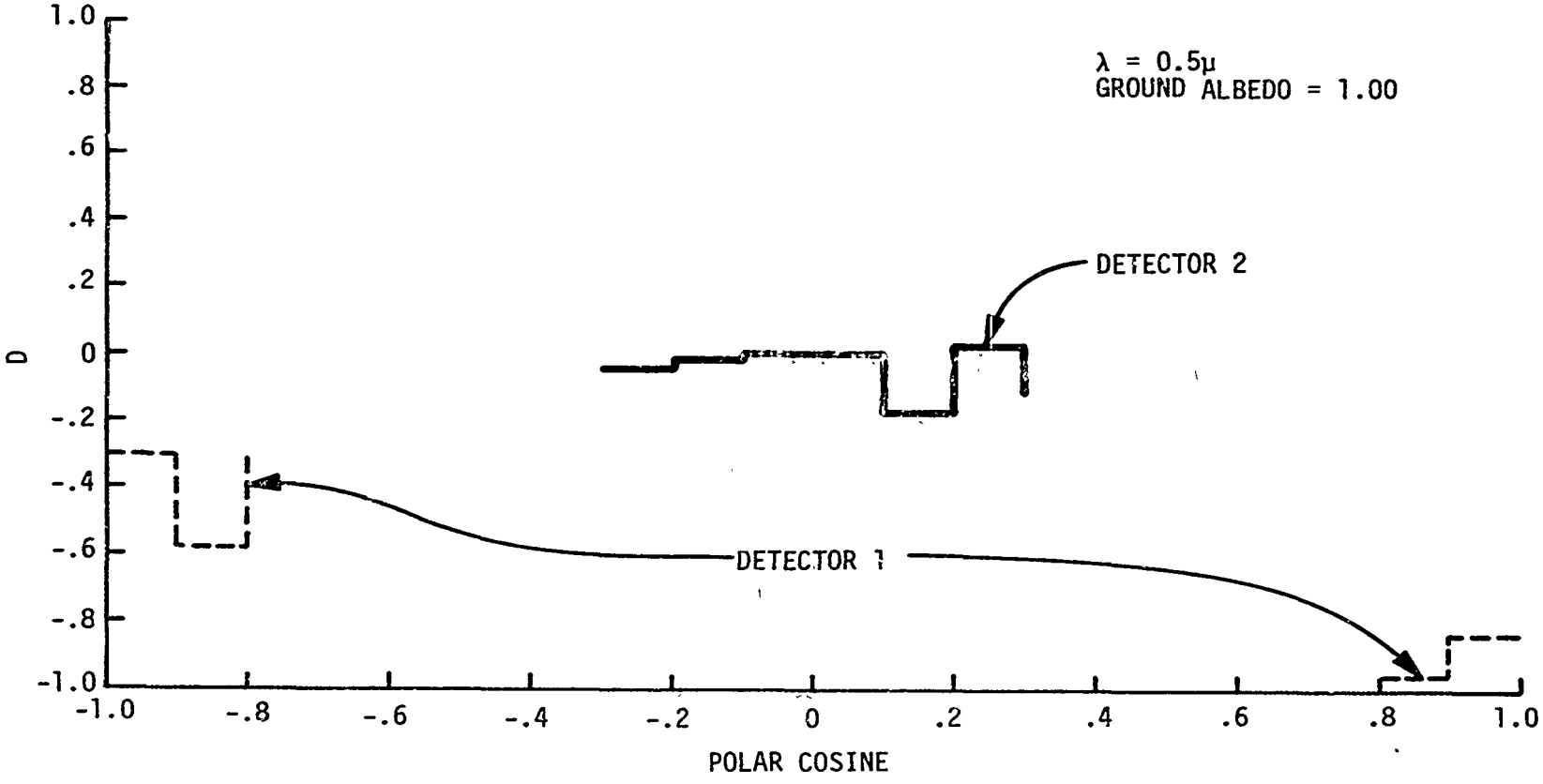

Figure 92. Polarization Factor for Cumulus Cloud at λ = 0.5μ with Ground Scatter

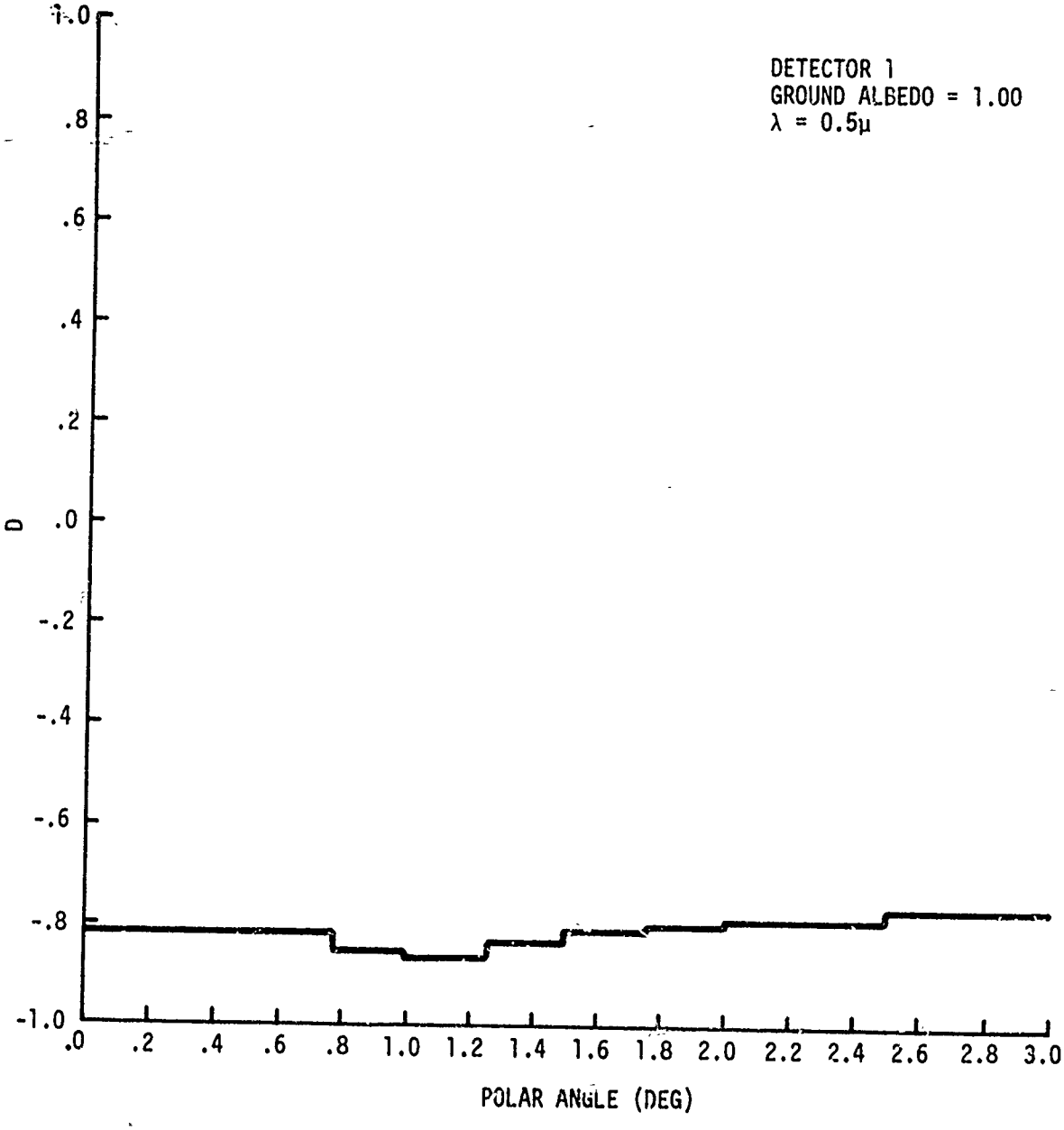

Figure 93. Forward Scatter Polarization Factor for Cumulus Cloud at λ = 0.5μ with Ground Scatter

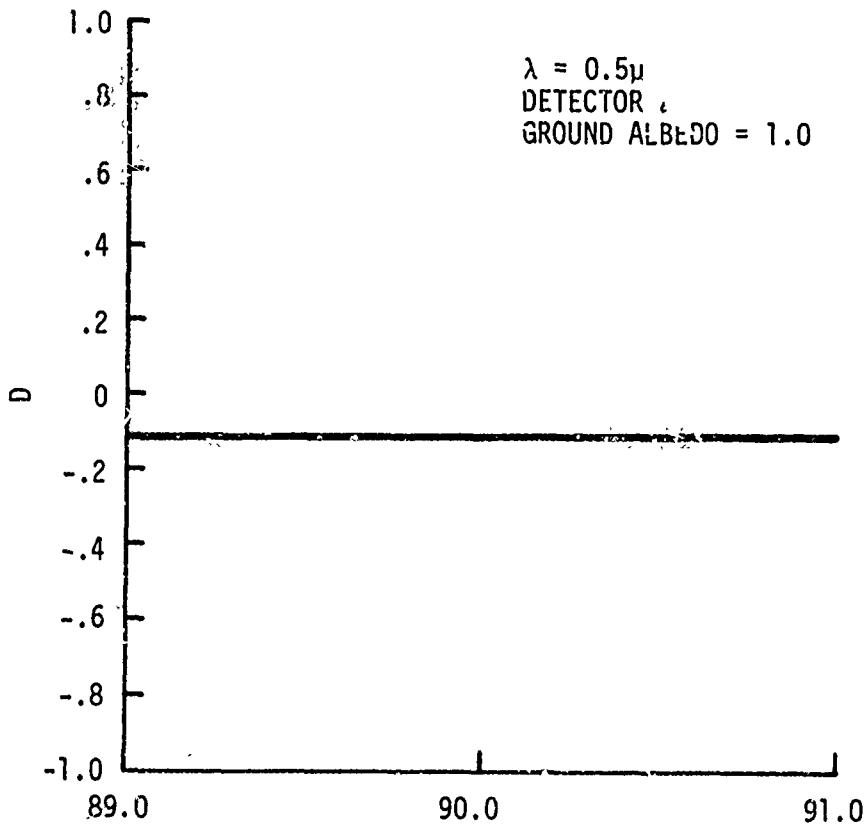

Figure 94. Backscatter Polarization Factor for Cumulus Cloud at $\lambda = 0.5\mu$ with Ground Scatter

received from an azimuthal interval of 45° while pointing directly at the cloud is four orders of magnitude greater than the intensity received from an interval of 45° but pointed 180° from the cloud, i.e., in the positive vertical direction.

The data just presented in figures 91, 92, 93, and 94 include, as pointed out, reflections from the ground as well as from the cloud. In order to determine the effect of the ground on the depolarization of the incident wave the ground was assumed to be highly absorbent and an albedo of 0.001 was selected compared to an albedo of 1.0 for the previous figures. Figures 95 and 96 show the results of this modification for 5,000 histories and $\lambda = 10.0\mu$. In figure 95 we can see that the average depolarization factor for detector 1 is approximately 0.9 compared to 0.8 for forward scatter in figure 91. The approximate average polarization factor for detector 2 for intensity backscattered from the cloud in figure 96 is approximately 0.7 while if ground reflections are included as in figure 91 the backscattered intensity is completely depolarized. One can therefore conclude that at $\lambda = 10.0\mu$, for the problem defined, the diffuse scattering ground will cause a major portion of the depolarization of the incident wave. It should be pointed out that the data obtained for figures 95 and 96 was obtained while allowing up to 10 photon collisions. A separate problem was run using 10,000 histories while allowing only 1 collision; the scattered intensity was not depolarized at all which agrees with theory. Therefore we can see that for a fairly thin cloud with an optical depth of 1.0, depolarization due to multiple scattering is significant.

In pursuing this problem further we determined the degree of depolarization for thicker cumulus clouds at $\lambda = 0.5\mu$ and 4.0μ. The wavelength 4.0μ was selected to coincide with the mode radius for the

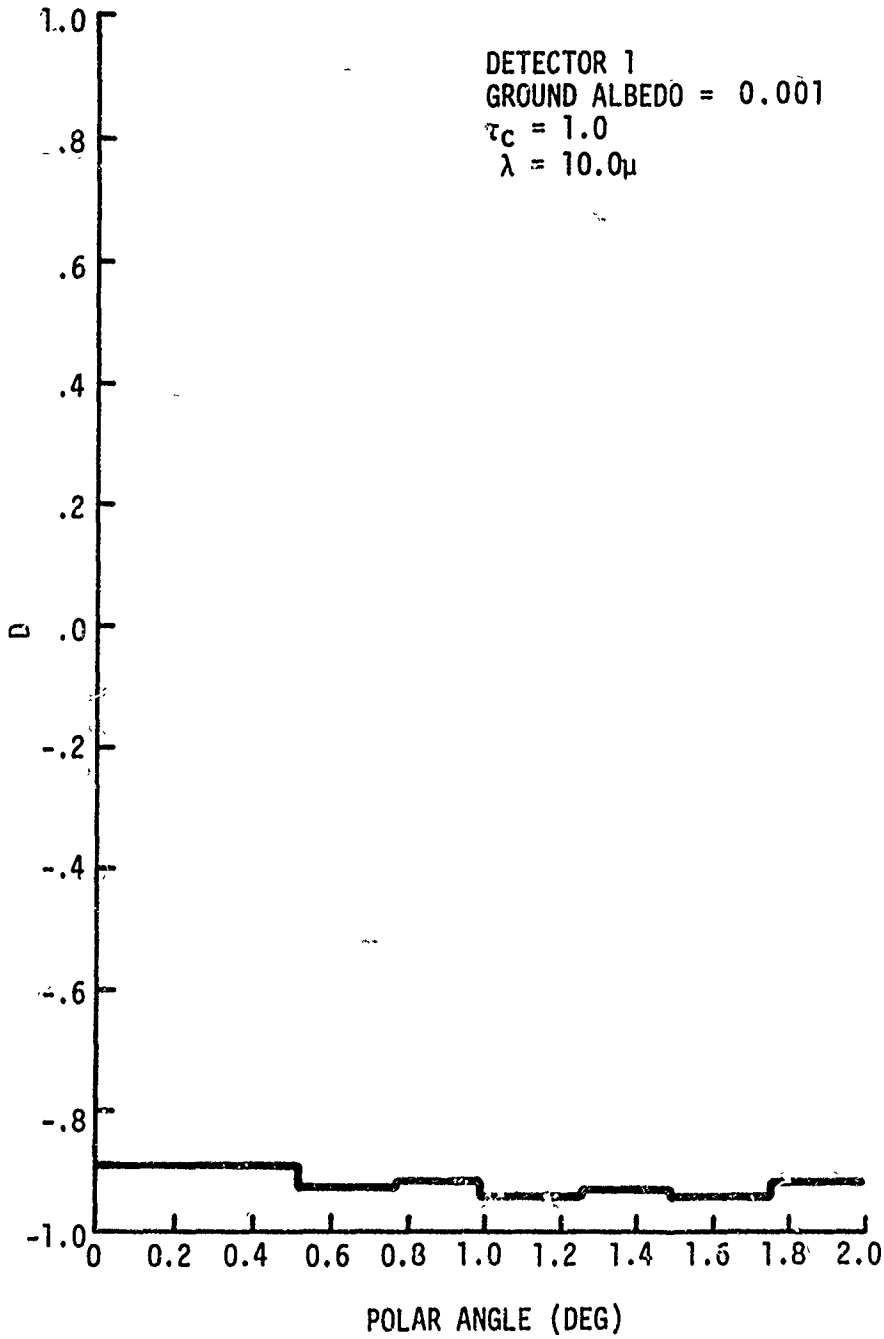

Figure 95. Forward Scatter Polarization Factor for Cumulus Cloud at λ = 10.0μ with No Ground Scatter

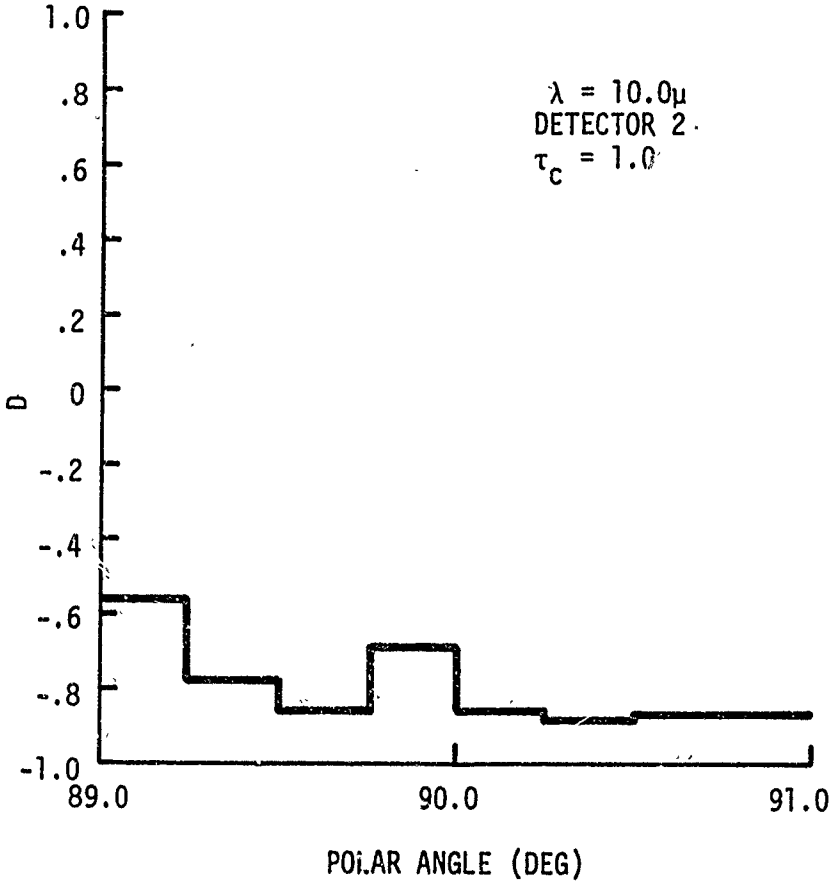

Figure 96. Backscatter Polarization Factor for Cumulus Cloud at λ = 10.0μ with no Ground Scatter

size distribution of the cumulus cloud (figure 22). The optical depth for $\lambda = 0.5\mu$ was selected to be 3.0 while at $\lambda = 4.0\mu$ we selected $\tau = 4.0$. The values of the optical depth at 0.5μ and 4.0μ were scaled according to the ratio of the individual extinction coefficients which are

$$\frac{\sigma_{ext}\ (4.0\mu)}{\sigma_{ext}\ (0.5\mu)} \approx \frac{4}{3} \tag{340}$$

The scaling in the optical depth τ follows from equations (273) and (274) where we see that the volume scattering functions are proportional to λ^2. Any differences in τ due to frequency change for a particular size distribution must therefore be scaled according to the change in extinction coefficient. This scaling allows us to maintain the same physical atmospheric model. Again we assume a highly absorbent ground. Figures 97 and 98 show the backscattered and forward scattered polarization factors at $\lambda = 0.5\mu$, respectively. Figures 99 and 100 show the backscattered and forward scattered polarization factors at $\lambda = 4.0\mu$, respectively. We can see that at $\lambda = 0.5\mu$

$$D \approx -0.65 \tag{341}$$

while at $\lambda = 4.0\mu$

$$D \approx -0.45 \tag{342}$$

We therefore conclude that for the cumulus cloud distribution that a greater amount of depolarization occurs at $\lambda = 4.0\mu$ than at $\lambda = 0.5\mu$. This can be explained by noting that the scattering functions for cumulus cloud distributions are not as highly peaked in the forward and backward directions at larger wavelengths (figures 36 and 37) as they are at the smaller wavelengths (figures 28 and 29). This change

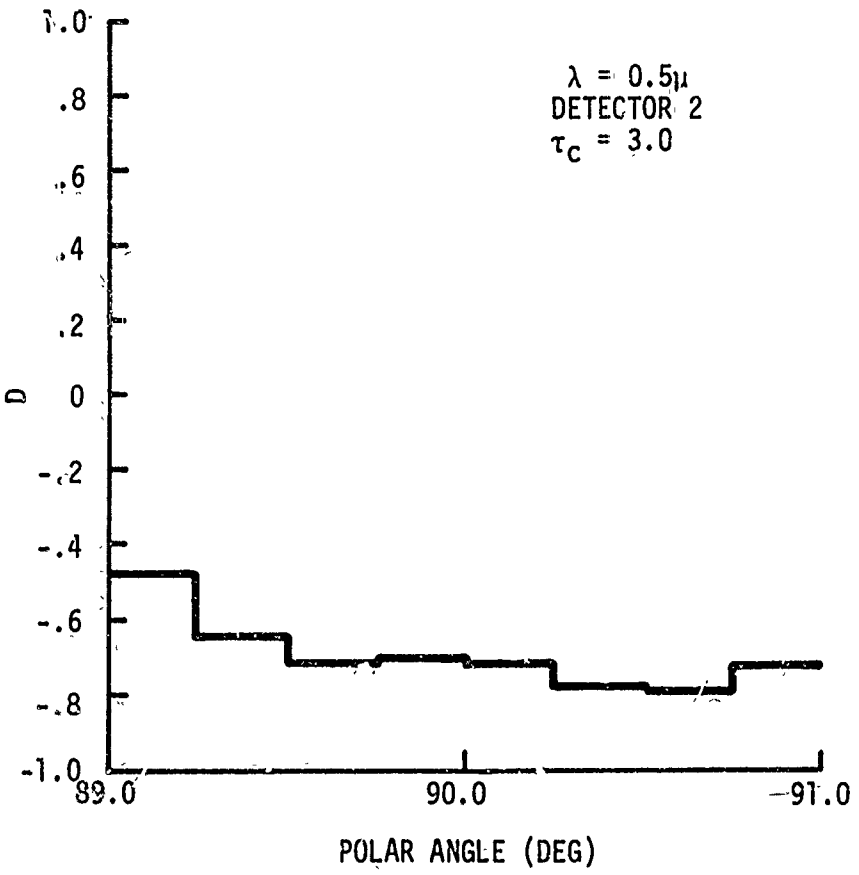

Figure 97. Backscatter Polarization Factor for Cumulus Cloud at λ = 0.5μ with no Ground Scatter

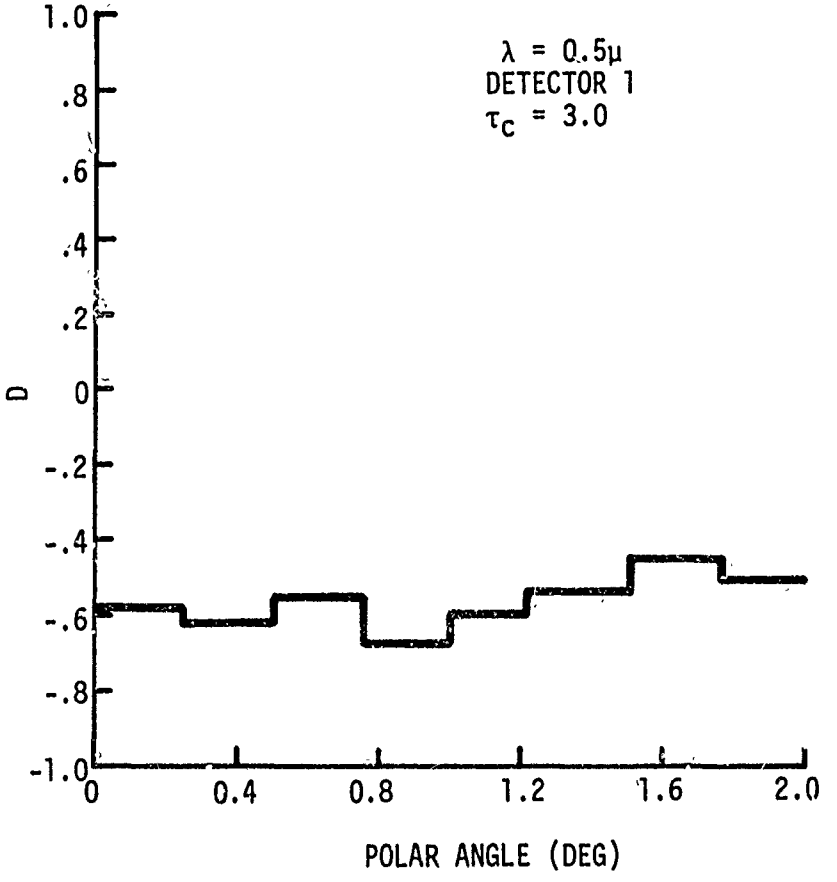

Figure 98. Forward Scatter Polarization Factor for Cumulus Cloud at λ = 0.5μ with no Ground Scatter

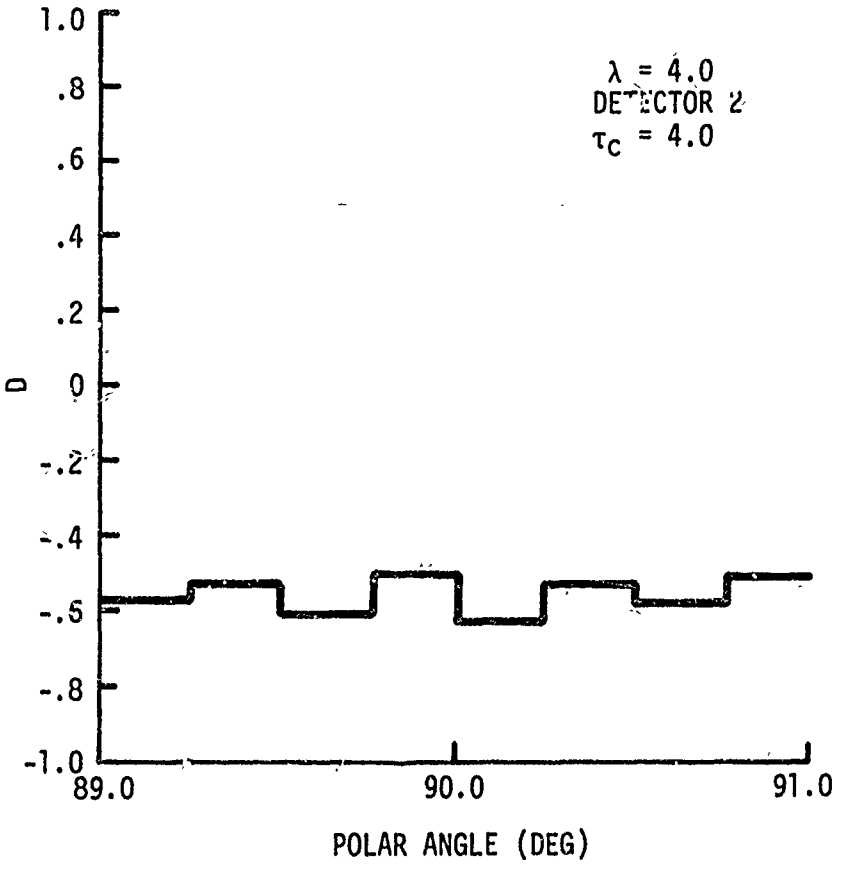

Figure 99. Backscatter Polarization Factor for Cumulus Cloud at $\lambda = 4.0\mu$ with no Ground Scatter

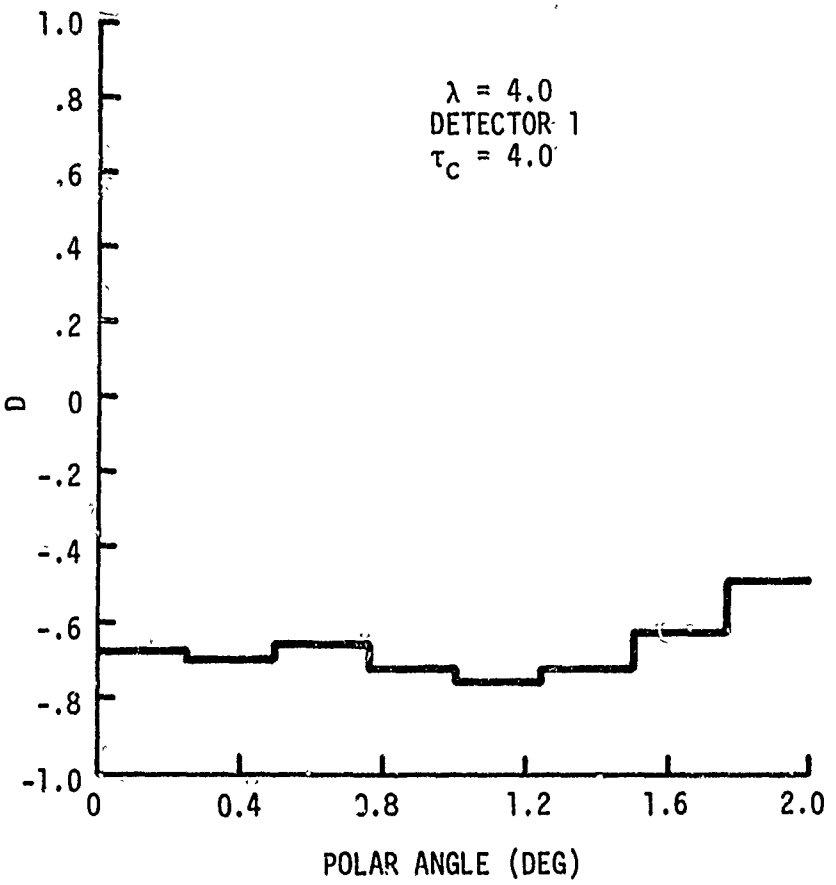

Figure 100. Forward Scatter Polarization Factor for Cumulus Cloud at $\lambda = 4.0\mu$ with no Ground Scatter

in scattering function results in a greater degree of multiple scattering for longer wavelengths and thus causes a smaller polarization factor at that wavelength compared to that of 0.5μ.

The forward-scattered polarization factors at $\lambda = 0.5\mu$ and $\lambda = 4.0\mu$ are shown in figures 98 and 100 and we can see that the average value for both wavelengths is approximately

$$D \approx -0.6 \tag{343}$$

and we therefore conclude that the forward scattered polarization is not as sensitive to frequency as is the backscattered intensity.

We continue to isolate the cause of depolarization by not allowing either ground or Rayleigh scattering at $\lambda = 4.0\mu$. Figure 101 is the polarization factor for backscatter from the cloud; we note that now $D \approx -0.65$ versus $D \approx -0.58$ in figure 99 when we include Rayleigh scattering. Figure 102 shows the polarization factor for forward scatter from the cloud for no ground or Rayleigh scattering. Comparing figure 102 with figure 100 we note that at 0° $D \approx -0.88$ in figure 102 versus $D \approx -0.68$ in figure 100. We now conclude that Rayleigh scattering causes an increase in depolarization. We should note that although we have eliminated Rayleigh scattering, we have replaced it with Mie scattering particles outside the cloud taken from the cumulus distribution.

Now we completely eliminate any form of scattering outside the cloud. Figure 103 shows the backscatter polarization factor from the cloud and figure 104 the forward scatter polarization factor. On comparing figures 101 and 102 with figures 103 and 104 we note that the change is small.

We now compare the polarization factors for no scattering outside the cloud at $\lambda = 0.5\mu$ and $\lambda = 4.0\mu$. Figure 105 shows the backscatter polarization factor at $\lambda = 0.5\mu$ and we note that at 90° $D \approx -0.78$ versus

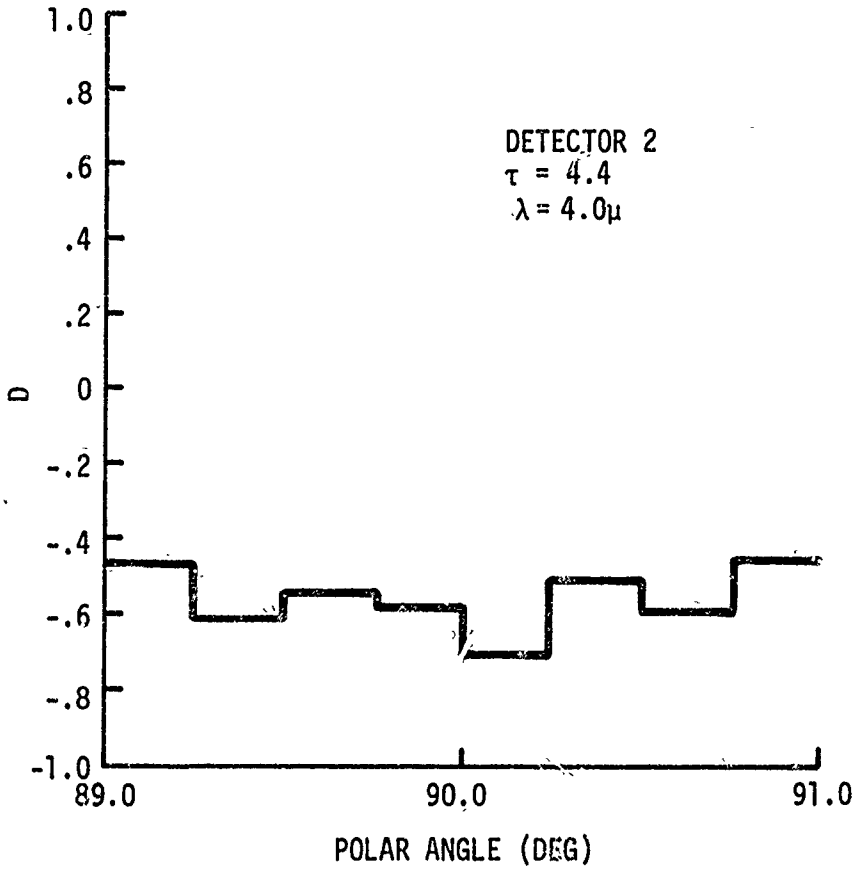

Figure 101. Backscatter Polarization Factor for Cumulus Cloud at $\lambda = 4.0\mu$ with no Ground or Rayleigh Scattering

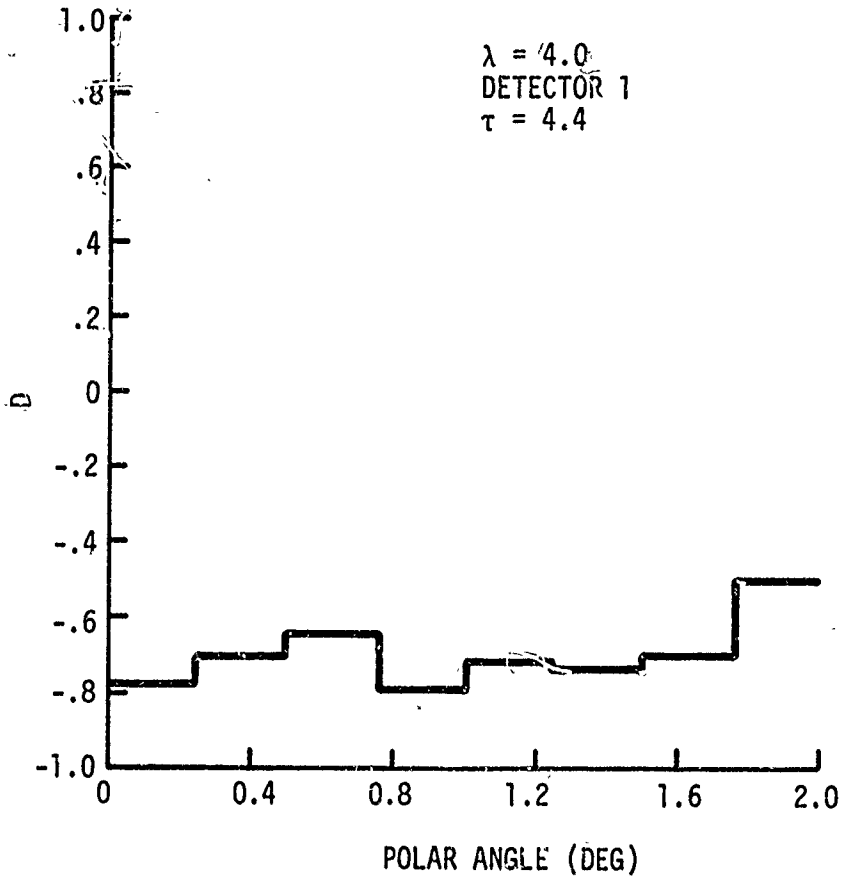

Figure 102. Forward Scatter Polarization Factor for Cumulus Cloud at λ = 4.0μ with no Ground or Rayleigh Scattering

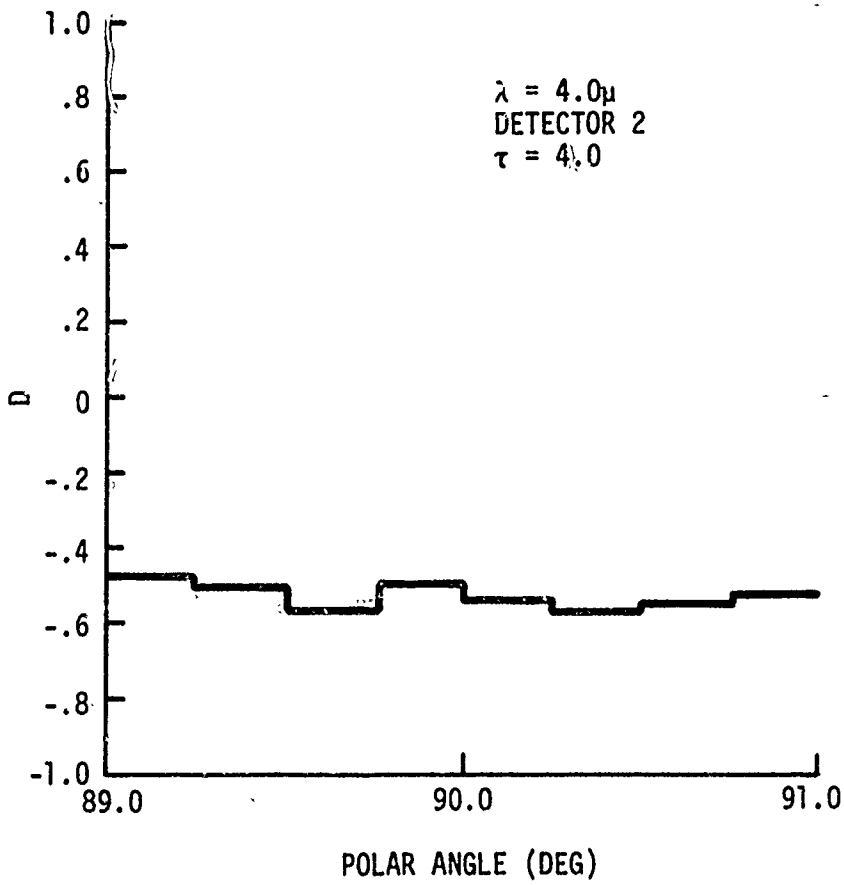

Figure 103. Backscatter Polarization Factor for Cumulus Cloud at $\lambda = 4.0\mu$ with no Scattering Outside Cloud

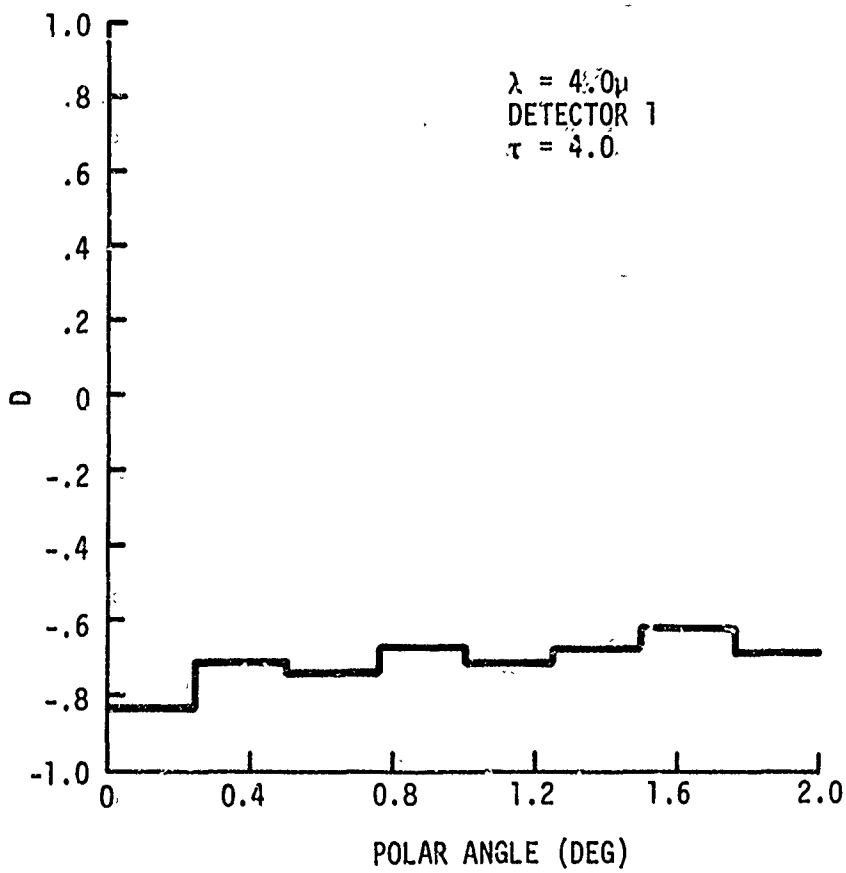

Figure 104. Forward Scatter Polarization Factor for Cumulus Cloud at $\lambda = 4.0\mu$ with no Scattering Outside Cloud

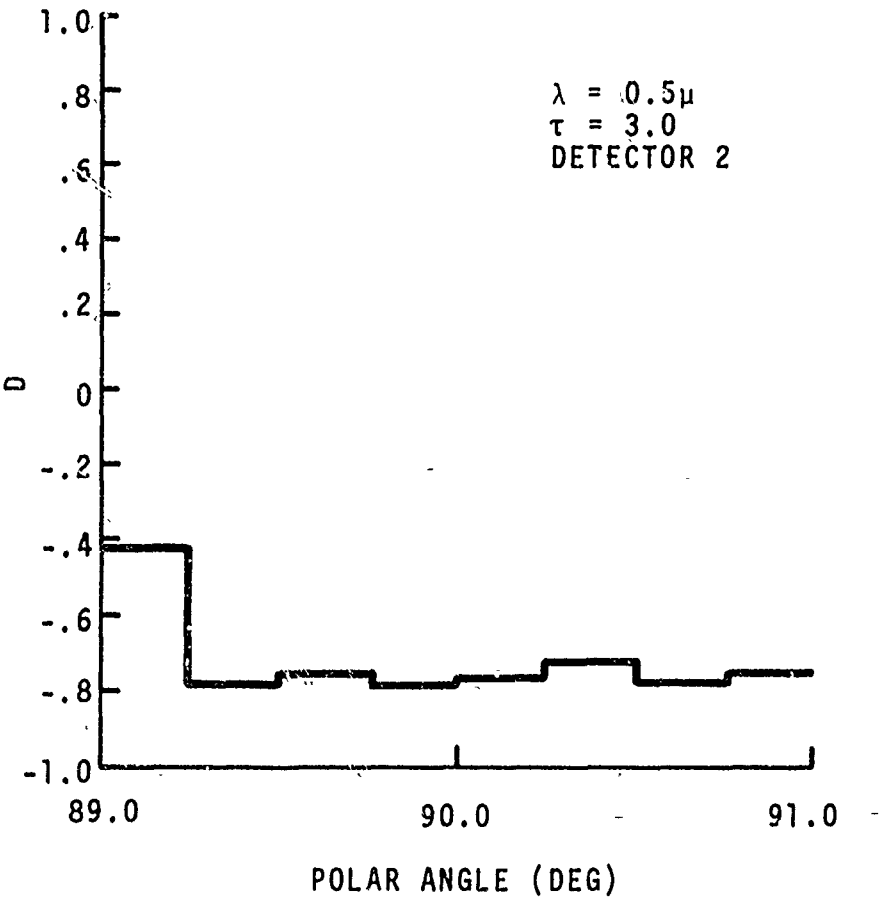

Figure 105. Backscatter Polarization Factor for Cumulus Cloud at $\lambda = 0.5\mu$ with no Scattering Outside Cloud

$D \approx -0.65$ at $\lambda = 4.0\mu$ in figure 101. Figure 106 shows the forward scatter polarization factor at $\lambda = 0.5\mu$ and at 0° $D \approx -0.8$ versus $D \approx -0.78$ at $\lambda = 4.0\mu$ in figure 102. We therefore conclude that the degree of depolarization is greater at $\lambda = 4.0\mu$ than at $\lambda = 0.5\mu$ for a Cumulus Cloud distribution. Ther percentage change in polarization factor from $\lambda = 0.5\mu$ to $\lambda = 4.0\mu$ is approximately 9 percent for a cloud of medium thickness ($\tau = 4.0$).

5. DEPOLARIZATION BY A HAZY-CLOUDY ATMOSPHERE AT 0.866μ

Consider now the geometry shown in figure 107. Again as in the last problem we have a source and two detectors. Here detector 1 is located just 10 meters off the ground. The source and detector 2 are located at an altitude of 5 km with detector 2 located 0.5 meter horizontally from the source. The source beamwidth is 2° x 2° and emits photons at $\lambda = 0.866\mu$. The atmosphere is composed of Haze M with a cumulus cloud between 1 km and 3 km from the ground. For this problem the ground albedo is assumed to be 0.8.

Here we assumed that the atmosphere is exponentially stratified and the optical depth is given by (see section V) [24]

$$\tau(h) = \sigma_0 H\left(1 - e^{-h/H}\right) \qquad (344)$$

where

$\sigma_{OM} = 1.02 \times 10^{-6}$ for Haze M

$\sigma_{OC} = 1.70 \times 10^{-4}$ for cumulus clouds

$H_M = 0.98$ km for Haze M, and

$H_C = 2.00$ km for cumulus clouds

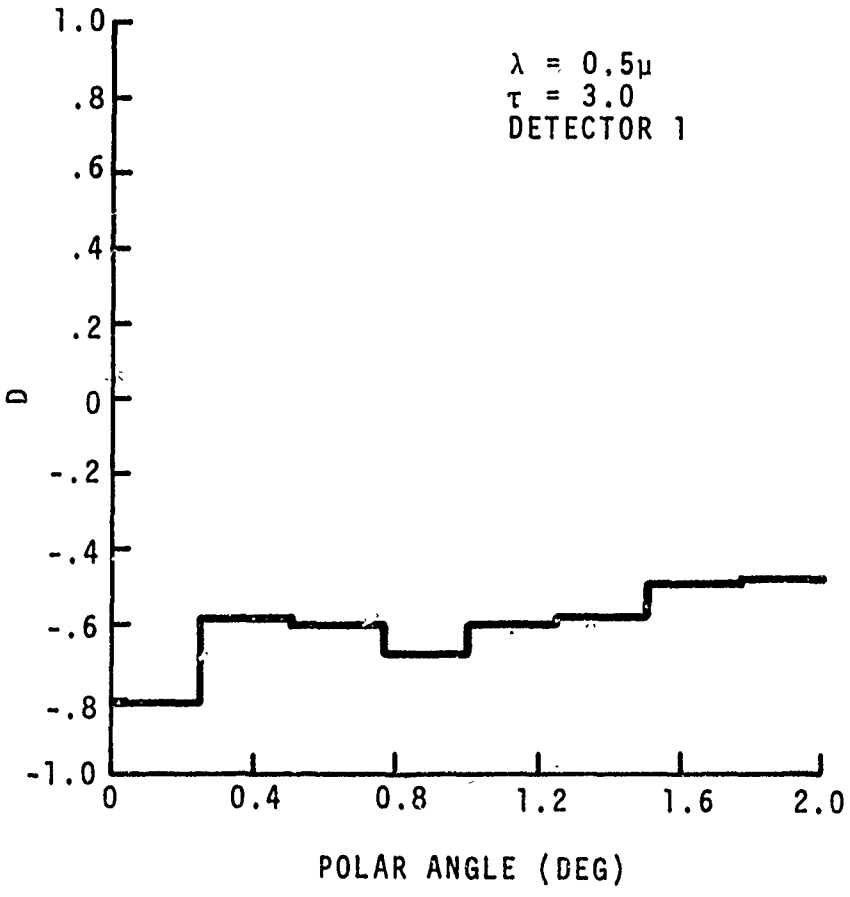

Figure 106. Forward Scatter Polarization Factor for Cumulus Cloud at $\lambda = 0.5\mu$ with no Scattering Outside Cloud

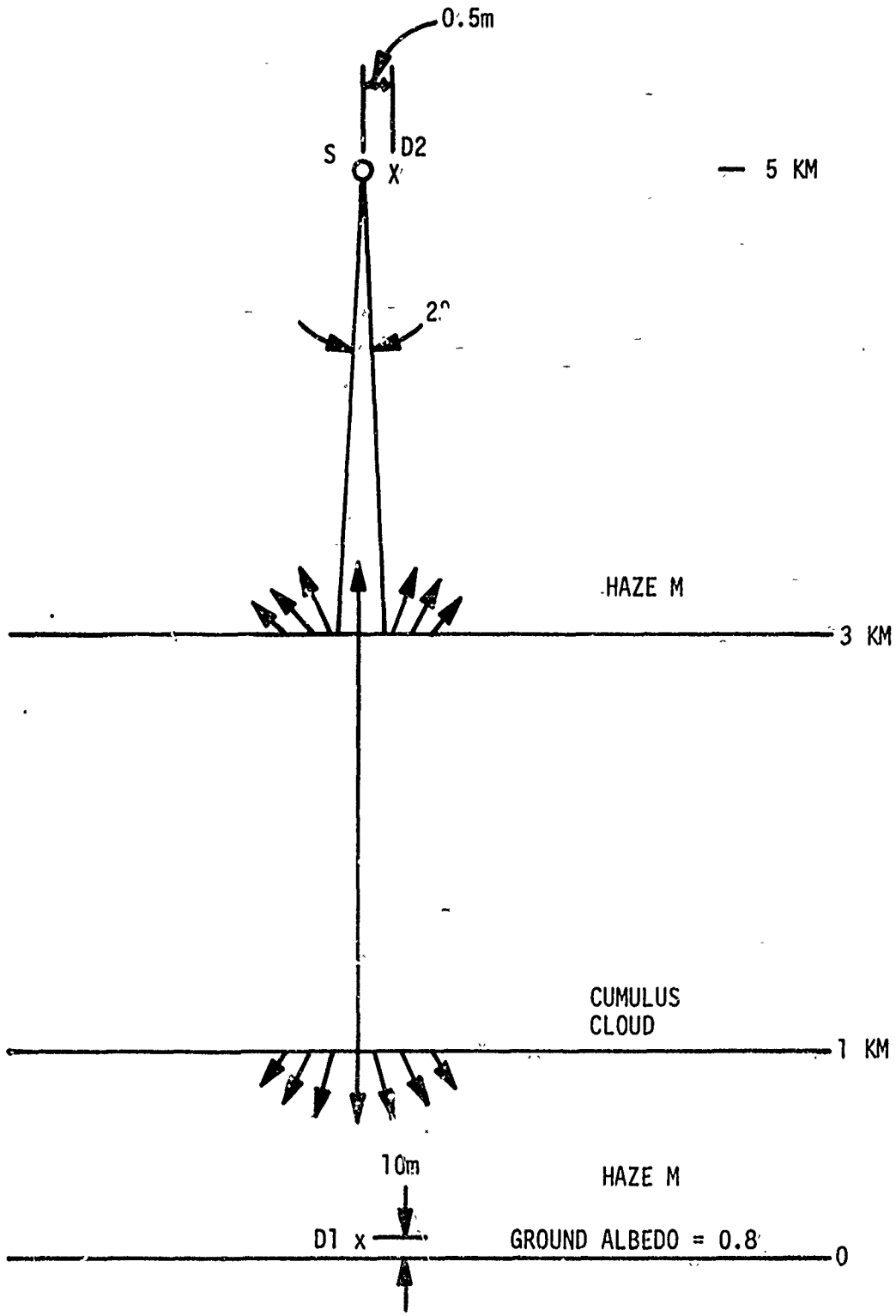

Figure 107. Cumulus Cloud/Haze M Geometry

The value H_c = 2.00 km was assumed while σ_{OM}, σ_{OC}, and H_M are measured values [15]. Figure 108 is a plot of equation (344) for the geometry shown in figure 107. For this model the optical depth of the atmosphere is 1.7. The size particle distributions for Cumulus Clouds and Haze M are given by equations (311) and (325), respectively. We assume that Rayleigh scattering is negligible everywhere so that only Mie scattering occurs. Up to three reflections from the ground were allowed.

In figure 109 we have shown the relative intensity at detector 1 as a function of the number of collisions during a single history for 10,000 histories. In the simulation we consider up to 10 collisions and we can see that the intensity becomes negligible for collisions greater than, say, 5 collisions.

Figures 110 and 111 represent the depolarization factor as a function of the polar cosine where the polar angle is defined as in subsection 4. From figure 110 we can see that for detector 1 which is located directly below the source and 10 meters above the ground (see figure 107) the received intensity is only slightly depolarized when "looking" directly at the source, i.e.,

$$D = -0.8 \tag{345}$$

for polar cosine equal to +1.0. On the other hand the intensity is completely depolarized for scattering from the ground at a polar cosine of -1.0. Depolarization increases gradually reaching a value of zero at approximately 90° or polar cosine equal to 0.

For detector 2 which is located next to the source the received intensity is almost completely depolarized, i.e., $D \approx 0$. The problem was then rerun with no ground reflections to influence the polarization

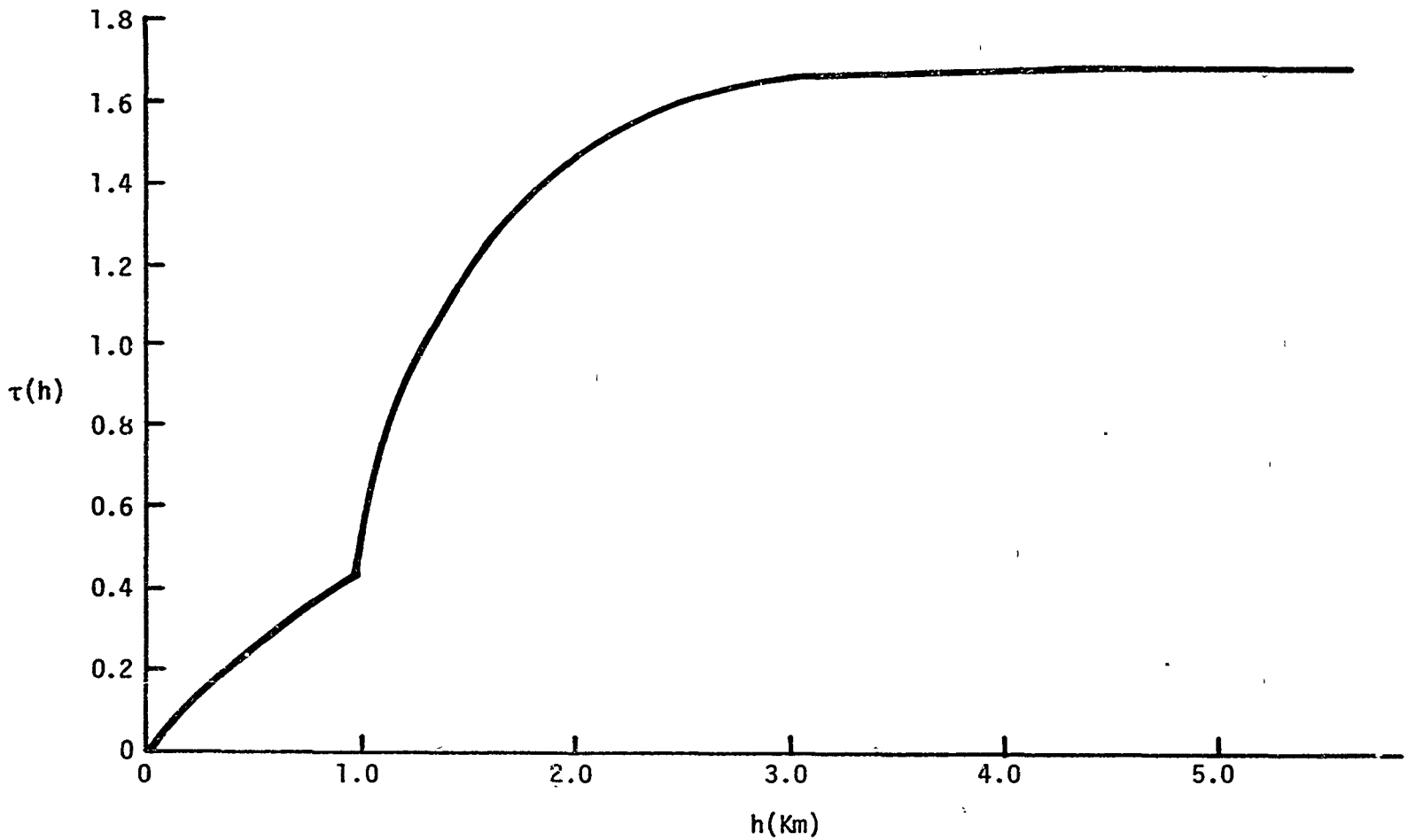

Figure 108. Exponential Stratification

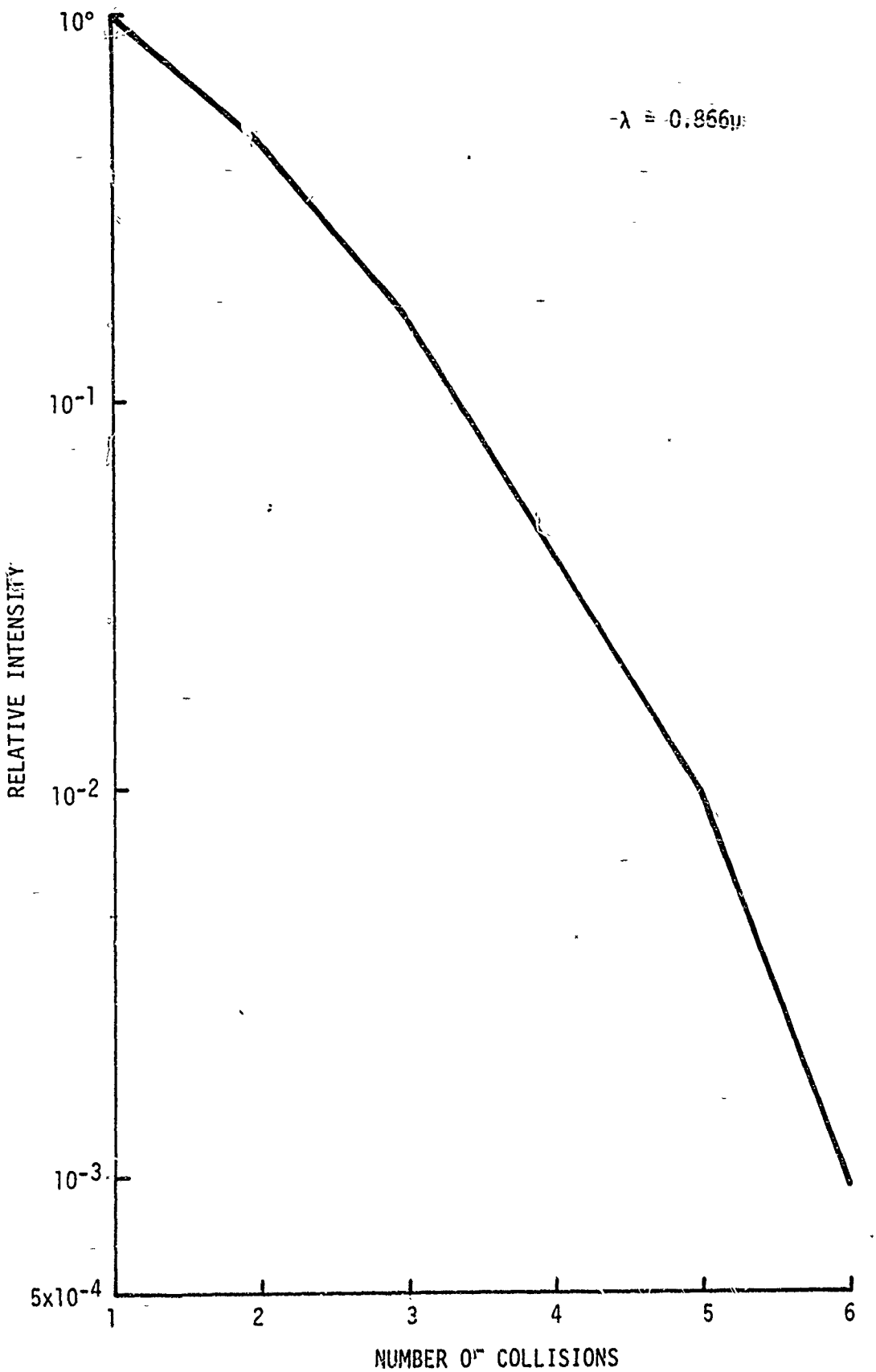

Figure 109. Relative Intensity versus Number of Collisions

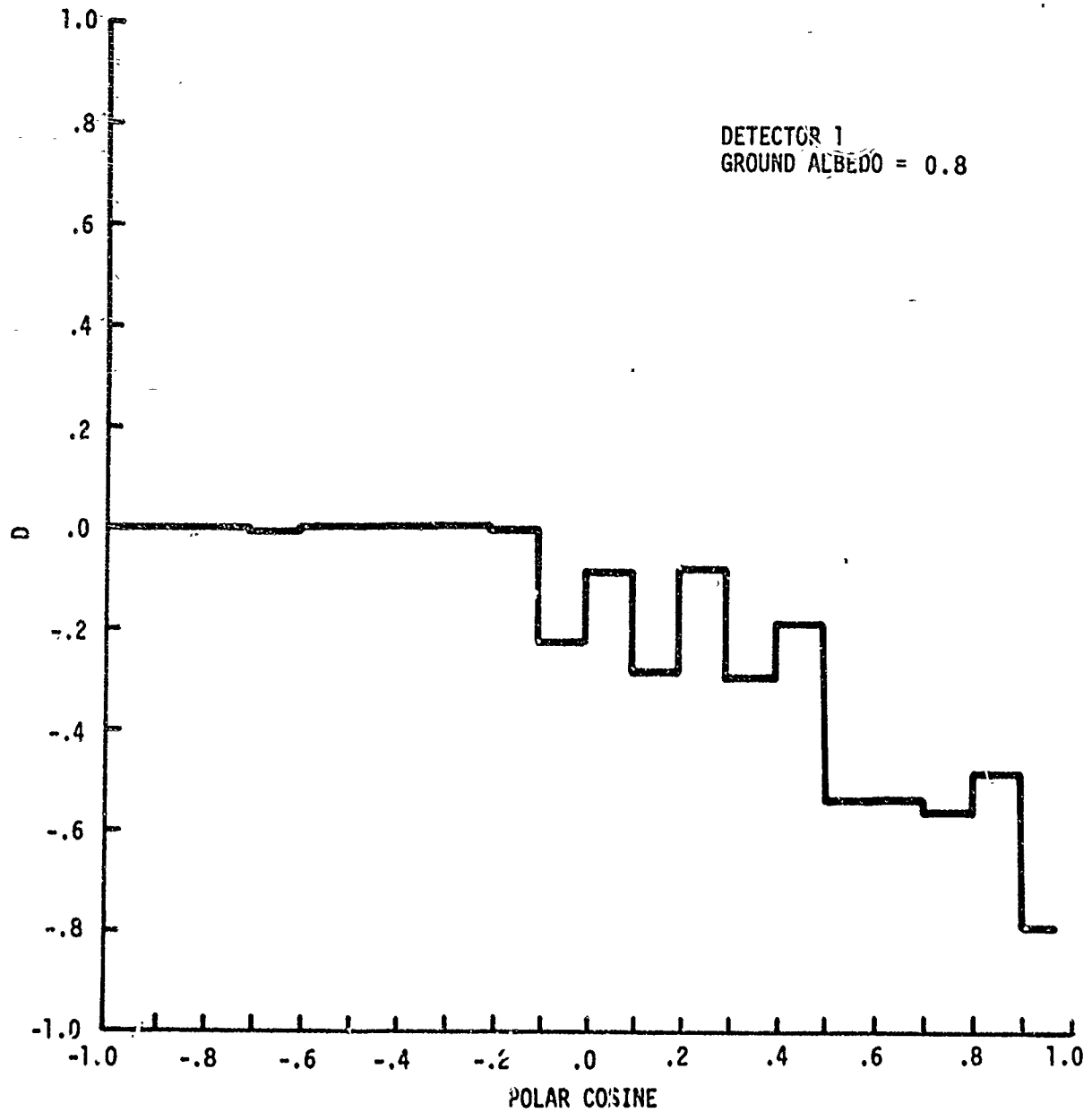

Figure 110. Polarization Factor for Cumulus/Haze M for D1

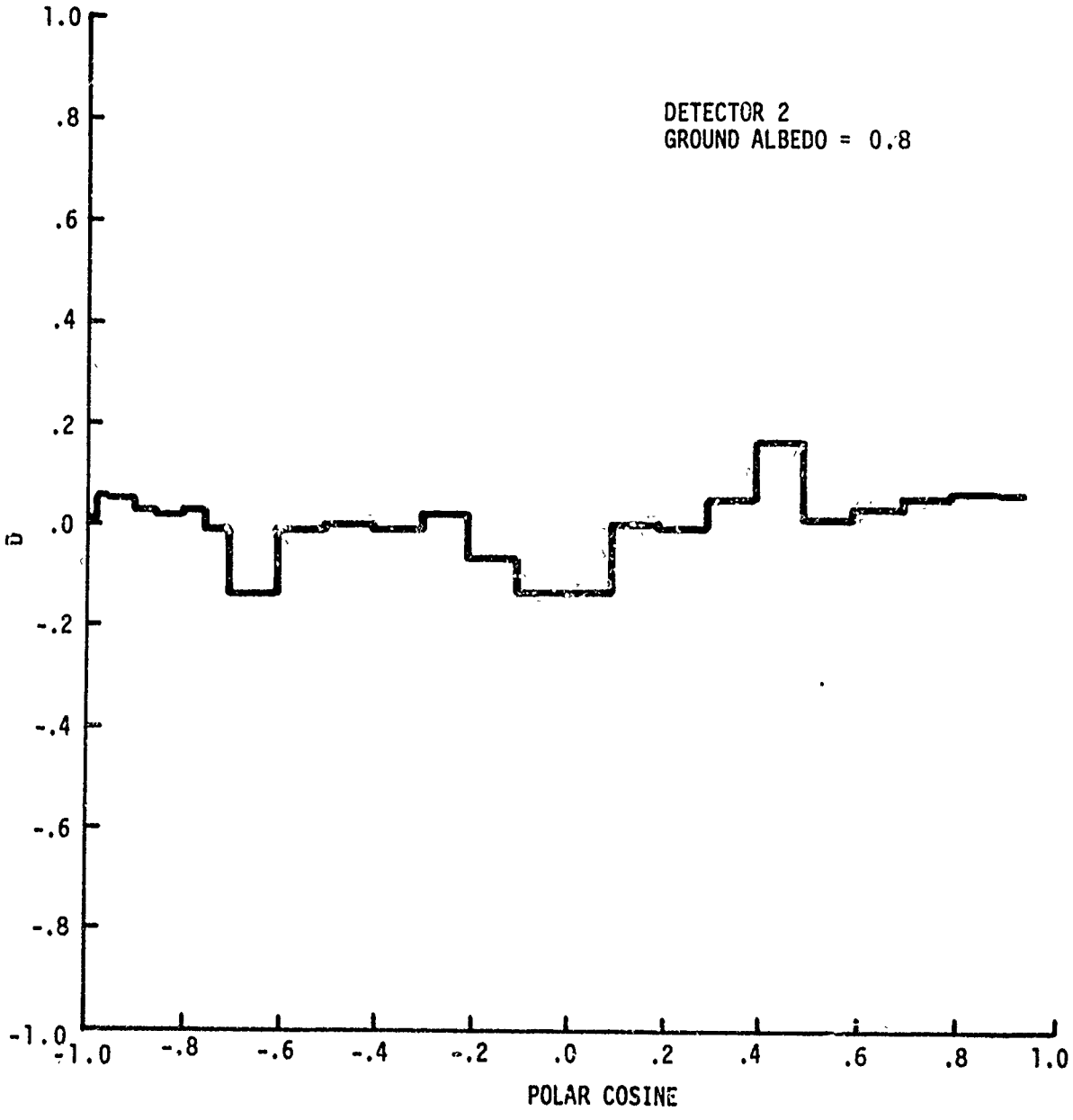

Figure 111. Polarization Factor for Cumulus/Haze M for D2

factor. For this case the backscattered intensity from the cloud at D2 was found to remain parallel polarized, i.e.,

$$D = -1 \tag{346}$$

6. DEPOLARIZATION WITHIN A CUMULUS CLOUD AT 0.5 and 10.0μ

Let us now investigate the problem of depolarization of a parallel polarized wave when both the source and detectors are within a cumulus cloud (figure 112). The cumulus cloud size distribution as given by equation (311). Here again we will assume that the source emits photons in a 2° x 2° beam which is pointed horizontally in line with two isotropic detectors. The source and detectors are located at an altitude of 10 km. The cloud extends from the ground up to an altitude of 20 km above which no scatterers exist. The ground albedo was selected to be small (0.1) in order to simulate a highly absorbent ground. We again allowed up to three reflections from the ground. Detector D1 is 0.3 meters from the source while detector D2 is 1 km from the source. With D1 we will measure the backscattered perpendicular and parallel polarization components while with D2 we will measure the perpendicular and parallel forward scattered components. The optical thickness of the cloud is assumed to be uniformly increasing with altitude as shown in figure 113. This variation of optical depth with altitude can be represented by equation

$$\tau(h) = 5 \times 10^{-4} h \tag{347}$$

Figure 114 shows the result at 10.0μ; we can see that the backscattered intensity at detector D1 is slightly more than half depolarized and we have

$$D = -0.4 \tag{348}$$

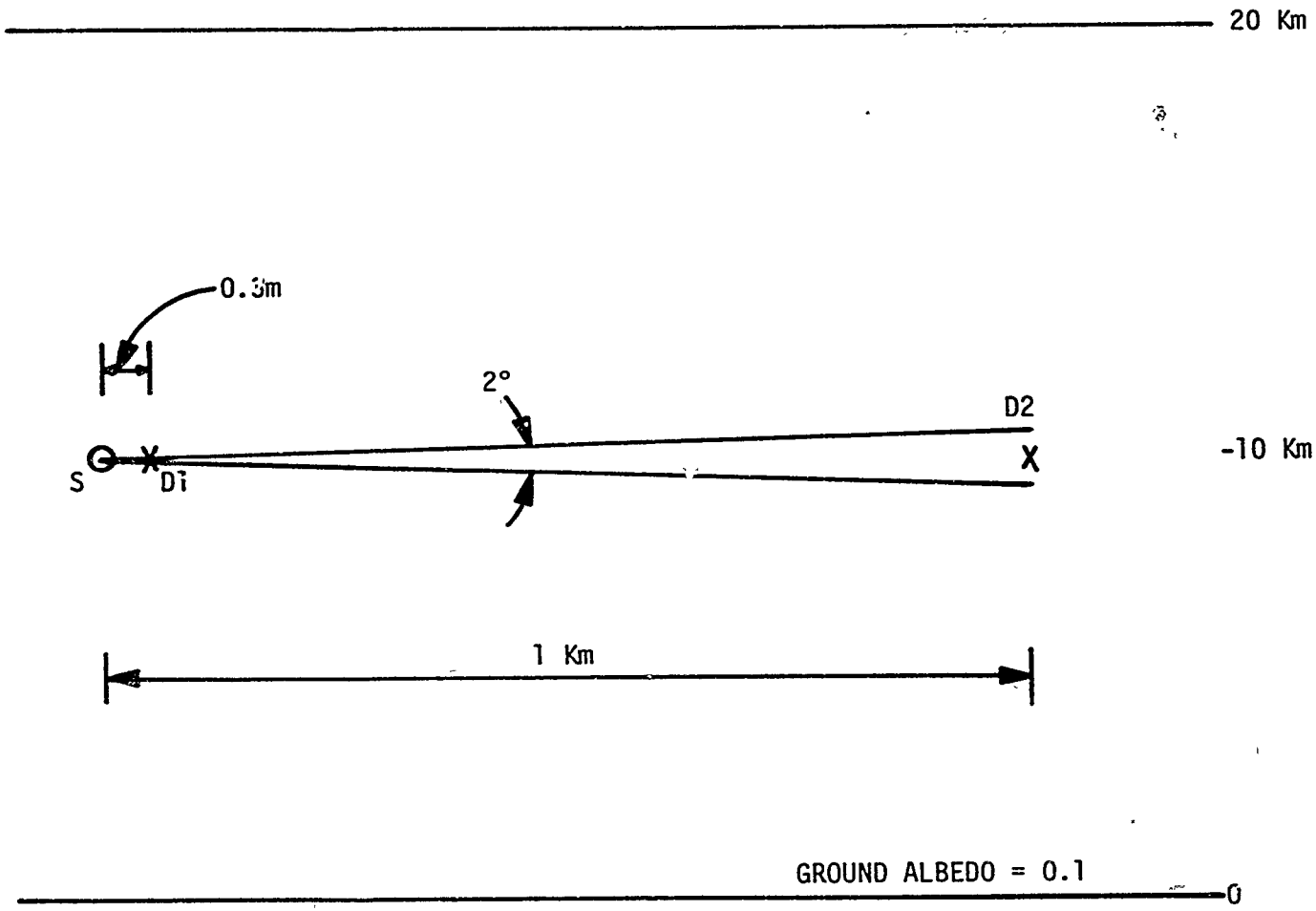

Figure 112. Geometry for Transmit-Receive System within a Cumulus Cloud

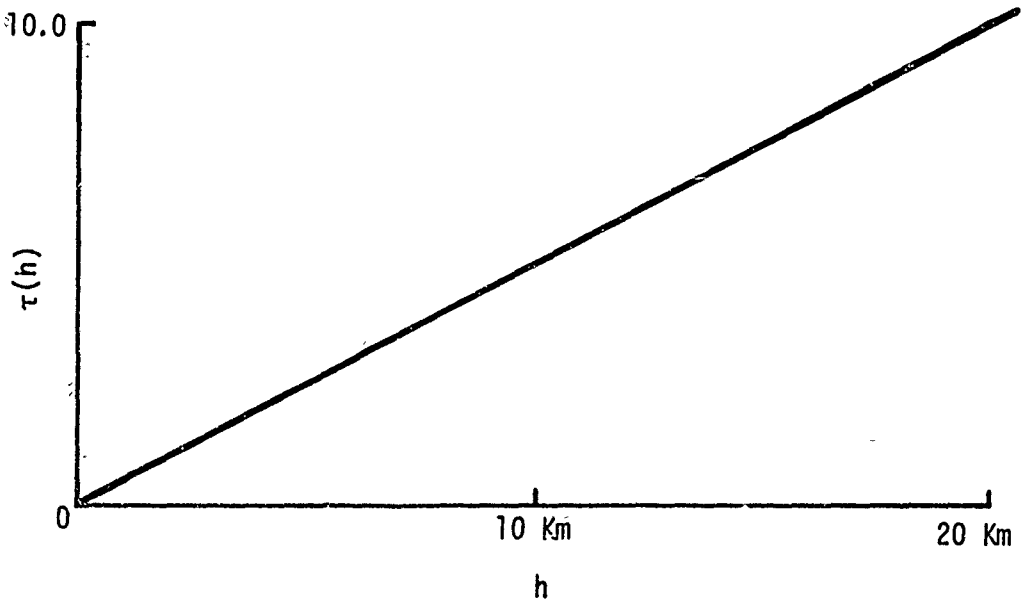

Figure 113. Uniform Stratification

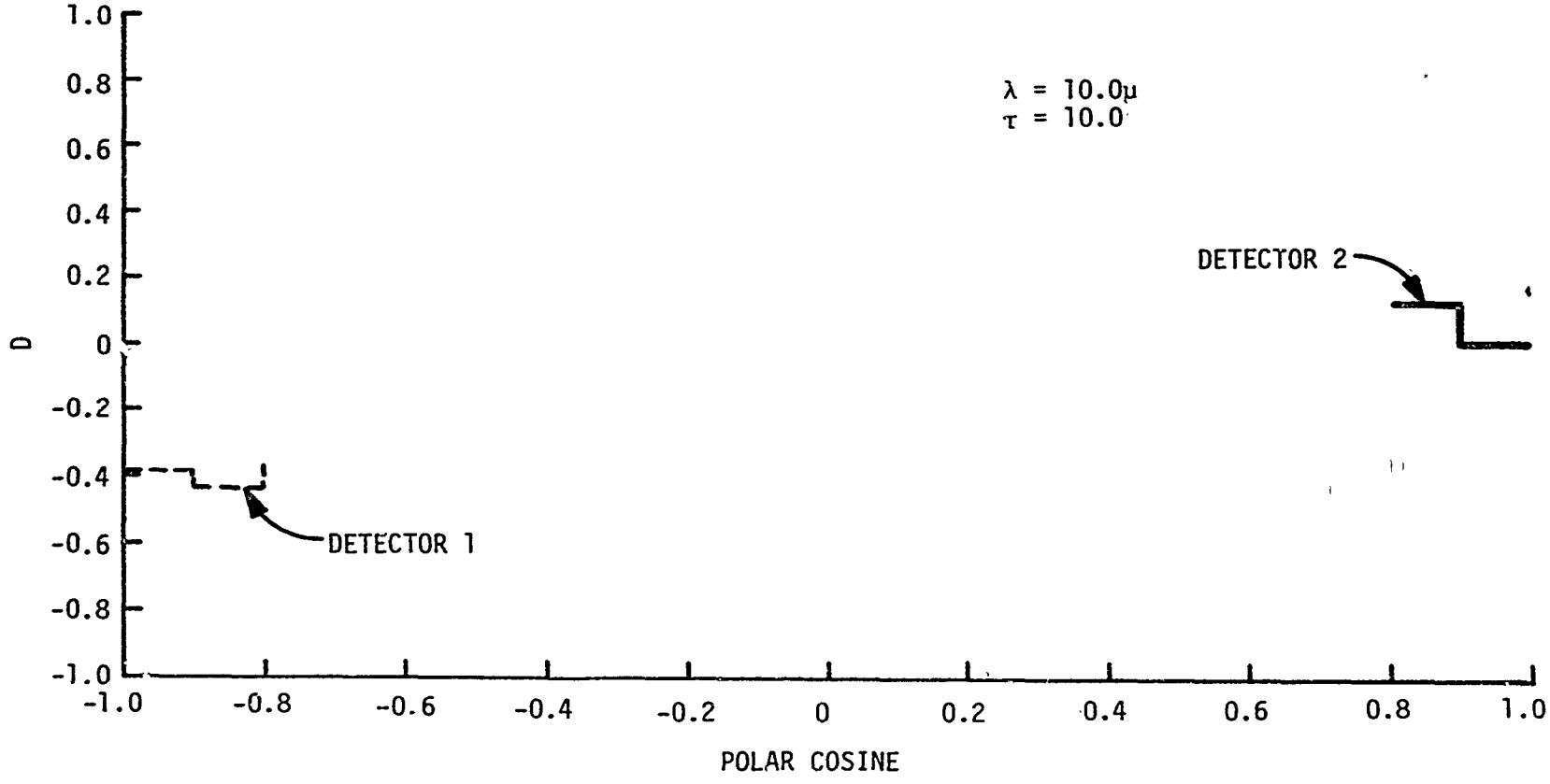

Figure 114. Polarization Factor for Cumulus Cloud at $\lambda = 10.0\mu$ and $\tau = 10.0$

At detector D2 the received intensity is completely depolarized. The complete depolarization at D2 was later found to be caused by ground scatter. We can see that for D2 the polarization factor begins to vary considerably for polar cosines less than 0.9 (≈26°). Here, again, we have allowed 10 collisions per history and the photon intensity is attenuated quite rapidly as it propagates toward D2 from the source. Rayleigh scattering was not allowed for this problem.

Figure 115 shows the polarization factor for detector 1 for the backscattered intensity at 10.0μ. Notice that the polar angle covers the interval from 177° to 180°, therefore for direct and quasi-direct backscatter the intensity is not completely depolarized and agrees with the larger angle interval shown in figure 114.

Figure 116 is an expanded version of figure 114 for detector 2 in the interval from 0° to 2°; here one can see, if one neglects the small statistical fluctuations, that the wave is completely depolarized.

To determine the degree of depolarization caused by ground reflections and scattering within the cloud, we eliminated all ground reflections and found that for $\tau = 10.0$ the received intensity was, for all practical purposes, still parallel polarized, i.e., D = -1 for parallel polarization. We thus conclude that, for this specific problem, the depolarization is caused by ground scatter.

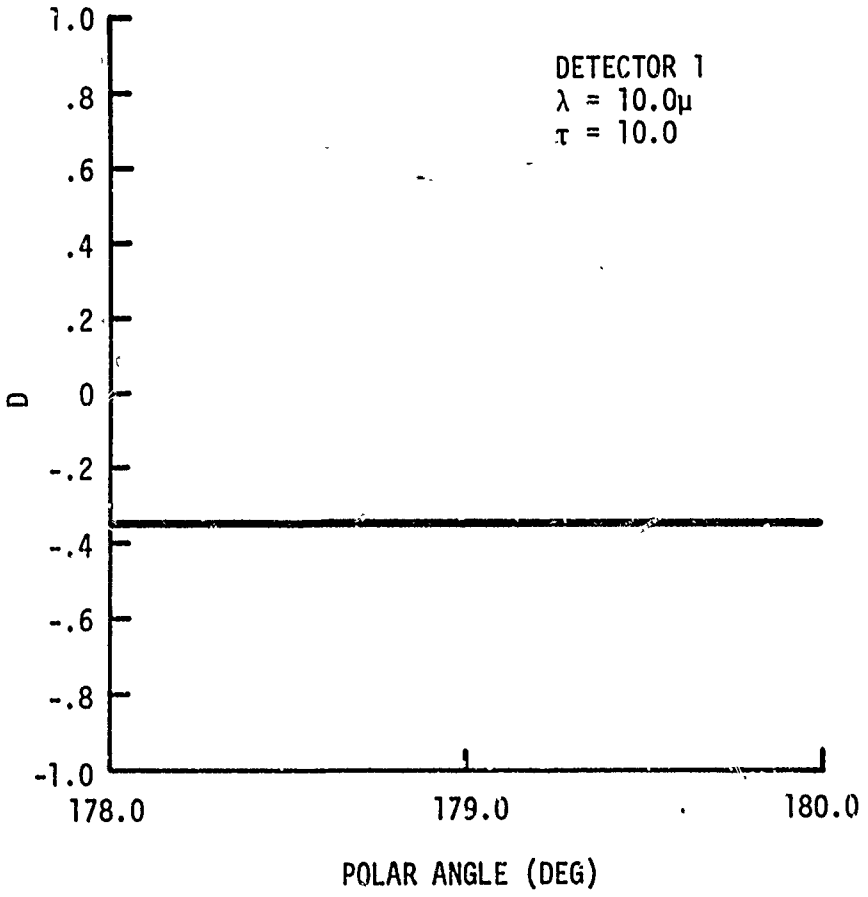

Figure 115. Backscatter Polarization Factor for Cumulus Cloud at $\lambda = 10.0\mu$ and $\tau = 10.0$

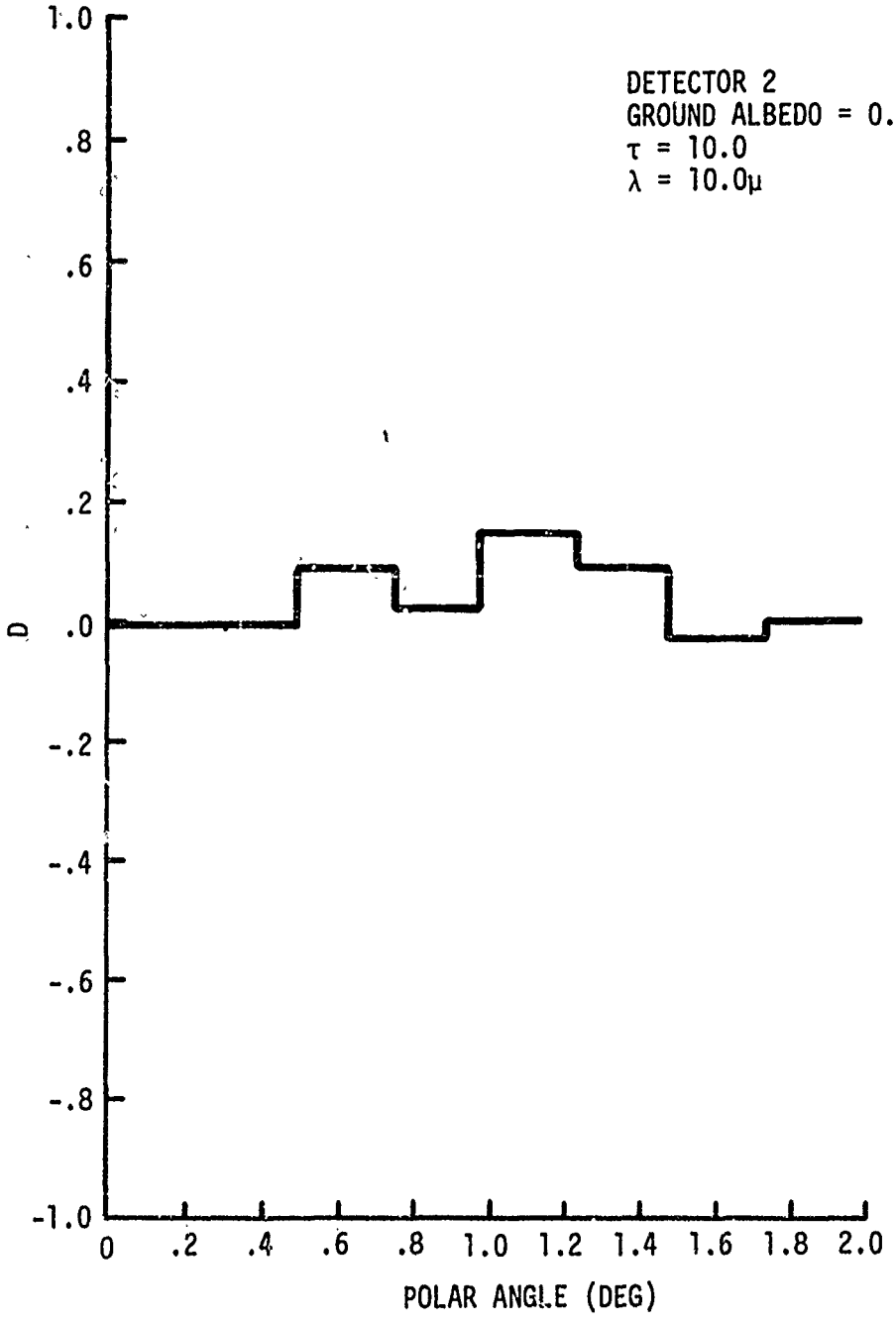

Figure 116. Forward Scatter Polarization Factor for Cumulus Cloud at $\lambda = 10.0\mu$ and $\tau = 10.0$

SECTION VI

DISCUSSION AND CONCLUSIONS

In this study we have set out to determine the effect of scattering on waves propagating through the atmosphere. We have centered our attention in the infrared part of the spectrum although we have compared our results to $\lambda = 0.5\mu$ which is in the visible portion of the spectrum.

In section I, we presented a brief discussion of the various mechanisms which may cause the depolarization of electromagnetic waves including nonlinear effects. We stated that although polarization has been used in extracting information concerning scattering tragets, problems in controlling the polarization state of an electromagnetic wave are usually encountered especially at the microwave frequencies. We also pointed out that in separating the intensity scattered back from multiple targets the effects of multiple scattering must be taken into account for dense media.

In sections II and III we derived the transfer equation for polarized waves and showed how one might treat a polarized wave of arbitrary polarization. In section II we gave an indication on how we would approach the modeling of scattering of polarized waves in the atmosphere. In section III we derived the scattering matrixes for Mie and Rayleigh scattering which we subsequently used in modeling the scattering process in the atmosphere. All scattering particles in the atmosphere were assumed to be either Rayleigh or Mie particles, Rayleigh particles being those less than a wavelength in size while Mie particles being spheres of arbitrary size.

In section IV we presented the simulation model. We derived the probability functions which characterize the path of a photon in the atmosphere. We showed that through the Monte Carlo simulation of a large number of photon histories we could obtain approximate numerical results to the scattering of electromagnetic waves in the atmosphere including the effects of multiple scattering.

In section V we obtained some results for specific problems. We used the Cumulus Cloud and Haze M size distributions to obtain the volume scattering functions for incident perpendicular and parallel polarization. Using the volume scattering functions we modeled cloudy and hazy atmospheres for different optical depths and wavelengths. In subsection 4 of section V we saw that under the assumption of a diffuse scattering ground which caused complete depolarization, i.e., equal parallel and perpendicular components, the backscattered intensity was completely depolarized while the forward scattered intensity was only slightly depolarized. We showed this to be true at wavelengths of 0.5, 4.0, and 10.0μ. We then saw that if we considered only the intensity scattered from the cloud that there was no depolarization for single scattering and a significant amount of depolarization for multiple scattering. By comparing the backscattered polarization factor at wavelengths of 0.5 and 4.0μ for the same physical cloud, we saw that the depolarization was greater at 4.0μ than at 0.5μ. A comparison of the volume scattering functions at these two frequencies (figures 38 and 44) reveals that this result is to be expected since the function width increases with wavelength.

In subsection 5 of section V we modeled a low lying cumulus cloud in a hazy atmosphere. The depolarization for this model is comparable to that discussed above. In addition we showed how the relative

scattered intensity varies as a function of collision number. The results shown in figure 109 compare favorably to those obtained by Bruning and Lo [29] for multiple scattering of electromagnetic waves by spheres.

Thus, based on the results of this study we are lead to the conclusion that the degree of depolarization of electromagnetic waves by scattering in the atmosphere can be obtained through a Monte Carlo simulation similar to the one used in this study. We have shown that the polarization state of an electromagnetic wave could be used to discriminate between a diffuse scattering ground and a cloud or haze if the cloud or haze is not "too dense." By "too dense" we mean optical distances of approximately 3.0 per km or greater, i.e., it appears that these 3 collisions per kilometer are sufficient to cause significant depolarization of the incident wave for the wavelengths considered here.

Much work remains to be accomplished in order to fully characterize the scattering phenomena in the atmosphere. Measurements of polarization factors at various frequencies under controlled conditions must be made to verify the results presented in this paper. The value of a computer simulation lies in the ability in obtaining accurate results under prescribed conditions. Once a simulation model provides accurate results the economic benefits through the reduction of the required experimental measurements are obvious.

APPENDIX

DERIVATION OF THE TRANSFORMATION MATRIX

The purpose of this appendix is to derive the transformation matrixes of $\mathbf{F}$ and $\tilde{\mathbf{F}}$. Here, we will use the same notation used by Van De Hulst in his excellent book [14].

Let the transformation matrix $\mathbf{F}$ be defined by

$$\begin{pmatrix} I \\ Q \\ U \\ V \end{pmatrix} = \mathbf{F} \begin{pmatrix} I_0 \\ Q_0 \\ U_0 \\ V_0 \end{pmatrix} \tag{1}$$

Where (I, Q, U, V) are the scattered Stokes parameters, and (I_0, Q_0, U_0, V_0) are the incident Stokes parameters.

In general the scattered electric field components are given by

$$\begin{pmatrix} E_\ell^s \\ E_r^s \end{pmatrix} = \begin{pmatrix} A_2 & A_3 \\ A_4 & A_1 \end{pmatrix} \begin{pmatrix} E_\ell^i \\ E_r^i \end{pmatrix} \tag{2}$$

where the A_i constitute a transformation matrix of (E_ℓ^i, E_r^i) into (E_ℓ^s, E_r^s).

The Stokes parameters are defined by

$$\left.\begin{aligned} I &= E_\ell E_\ell^* + E_r E_r^* \\ Q &= E_\ell E_\ell^* - E_r E_r^* \\ U &= E_\ell E_r^* + E_\ell^* E_r \\ V &= i\left(E_\ell E_r^* - E_\ell^* E_r^*\right) \end{aligned}\right\} \tag{3}$$

Using (2) we can find each term of (3) as follows:

$$
\begin{aligned}
I &= \left(A_2\, E_\ell^i + A_3\, E_r^i\right)\left(A_2^*\, E_\ell^i + A_3^*\, E_r^i\right) \\
&+ \left(A_4\, E_\ell^i + A_1\, A_r^i\right)\left(A_4^*\, E_\ell^i + A_1^*\, E_r^i\right) \\
&= \left(|A_2|^2 + |A_4|^2\right) E_\ell^i\, E_\ell^{i*} \\
&+ \left(|A_3|^2 + |A_1|^2\right) E_r^i\, E_r^{i*} \\
&+ \left(A_3\, A_2^* + A_1\, A_4^*\right) E_\ell^{i*}\, E_r^i \\
&+ \left(A_2\, A_3^* + A_1^*\, A_4\right) E_\ell^i\, E_r^{i*} \\
&= \left[\frac{|A_2|^2 + |A_4|^2}{2} - \frac{|A_2|^2 + |A_4|^2}{2} + \frac{|A_1|^2 + |A_3|^2}{2}\right. \\
&\left. - \frac{|A_1|^2 + |A_3|^2}{2}\right] E_\ell^i\, E_\ell^{i*} \\
&+ \left[\frac{|A_1|^2 + |A_3|^2}{2} + \frac{|A_1|^2 + |A_3|^2}{2} + \frac{|A_2|^2 + |A_4|^2}{2}\right. \\
&\left. - \frac{|A_2|^2 + |A_4|^2}{2}\right] E_r^i\, E_r^{i*} \\
&+ \left[\frac{A_3\, A_2^* + A_1\, A_4^*}{2} + \frac{A_3\, A_2^* + A_1\, A_4^*}{2}\right. \\
&\left. + \frac{A_2\, A_3^* + A_1^*\, A_4}{2} - \frac{A_2\, A_3^* + A_1^*\, A_4}{2}\right] E_\ell^{i*}\, E_r^i \\
&+ \left[\frac{A_2\, A_3^* + A_1^*\, A_4}{2} + \frac{A_2\, A_3^* + A_1^*\, A_4}{2}\right. \\
&\left. + \frac{A_3\, A_2^* + A_1\, A_4^*}{2} - \frac{A_3\, A_2^* + A_1\, A_4^*}{2}\right] E_\ell^i\, E_r^{i*}
\end{aligned}
$$

where the last two terms within each bracket were added and subtracted. We can now write

$$I = 1/2 \left[|A_1|^2 + |A_2|^2 + |A_3|^2 + |A_4|^2\right] \left[E_\ell^i E_\ell^{i*} + E_r^i E_r^{i*}\right]$$

$$+ 1/2 \left[- |A_1|^2 + |A_2|^2 - |A_3|^2 + |A_4|^2\right] \left[E_\ell^i E_\ell^{i*} - E_r^i E_r^{i*}\right]$$

$$+ 1/2 \left[A_1 A_4^* + A_1^* A_4 + A_2 A_3^* + A_2^* A_3\right] \left[E_\ell^i E_r^{i*} + E_\ell^{i*} E_r^i\right]$$

$$+ 1/2 \left[- A_1 A_4^* + A_1^* A_4 + A_2 A_3^* - A_2^* A_3\right] \left[E_\ell^i E_r^{i*} - E_\ell^{i*} E_r^i\right]$$

or (cf. 3)

$$\left.\begin{aligned} I = {} & 1/2 \left[|A_1|^2 + |A_2|^2 + |A_3|^2 + |A_4|^2\right] I_0 \\ & + 1/2 \left[- |A_1|^2 + |A_2|^2 - |A_3|^2 + |A_4|^2\right] Q_0 \\ & + 1/2 \left[A_1 A_4^* + A_1^* A_4 + A_2 A_3^* + A_2^* A_3\right] U_0 \\ & - 1/2 \left[- A_1 A_4^* + A_1^* A_4 + A_2 A_3^* - A_2^* A_3\right] V_0 \end{aligned}\right\} \quad (4)$$

Using the same procedure for Q, U, and V, we obtain

$$\left.\begin{aligned} Q = {} & 1/2 \left[- |A_1|^2 + |A_2|^2 + |A_3|^2 - |A_4|^2\right] I_0 \\ & + 1/2 \left[|A_1|^2 + |A_2|^2 - |A_3|^2 - |A_4|^2\right] Q_0 \\ & + 1/2 \left[- A_1 A_4^* - A_1^* A_4 + A_2 A_3^* + A_2^* A_3\right] U_0 \\ & - 1/2 \left[A_1 A_4^* - A_1^* A_4 + A_2 A_3^* - A_2^* A_3\right] V_0 \end{aligned}\right\} \quad (5)$$

$$
\left.
\begin{aligned}
U = {} & 1/2 \left[A_1 A_3^* + A_1^* A_3 + A_2 A_4^* + A_2^* A_4 \right] I_0 \\
& + 1/2 \left[- A_1 A_3^* - A_1^* A_3 + A_2 A_4^* + A_2^* A_4 \right] Q_0 \\
& + 1/2 \left[A_1 A_2^* + A_1^* A_2 + A_3 A_4^* + A_3^* A_4 \right] U_0 \\
& - 1/2 \left[- A_1 A_2^* + A_1^* A_2 - A_3 A_4^* + A_3^* A_4 \right] V_0
\end{aligned}
\right\} \qquad (6)
$$

$$
\left.
\begin{aligned}
V = {} & 1/2 \left[- A_1 A_3^* + A_1^* A_3 + A_2 A_4^* - A_2^* A_4 \right] I_0 \\
& + 1/2 \left[A_1 A_3^* - A_1^* A_3 + A_2 A_4^* - A_2^* A_4 \right] Q_0 \\
& + 1/2 \left[- A_1 A_2^* + A_1^* A_2 + A_3 A_4^* - A_3^* A_4 \right] U_0 \\
& + 1/2 \left[A_1 A_2^* + A_1^* A_2 - A_3 A_4^* - A_3^* A_4 \right] V_0
\end{aligned}
\right\} \qquad (7)
$$

We now make the following definitions

$$
\left.
\begin{aligned}
M_k &= |A_k|^2 \\
S_{jk} &= S_{kj} = 1/2 \left(A_j A_k^* + A_j^* A_k \right) \\
D_{jk} &= -D_{kj} = 1/2 \left(A_j A_k^* - A_j^* A_k \right)
\end{aligned}
\right\} \qquad (8)
$$

for j = 1, 2, 3, 4 and k = 1, 2, 3, 4. Substituting (8) into (4) through (7) results in

$$F = \begin{pmatrix} 1/2\left(M_1 + M_2 + M_3 + M_4\right) & 1/2\left(-M_1 + M_2 - M_3 + M_4\right) & S_{23} + S_{41} & -D_{23} - D_{41} \\ 1/2\left(-M_1 + M_2 + M_3 - M_4\right) & 1/2\left(M_1 + M_2 - M_3 - M_4\right) & S_{23} - S_{41} & -D_{23} + D_{41} \\ S_{24} + S_{31} & S_{24} - S_{31} & S_{21} + S_{34} & -D_{21} + D_{34} \\ D_{24} + D_{31} & D_{24} - D_{31} & D_{21} + D_{34} & S_{21} - S_{34} \end{pmatrix} \quad (9)$$

while

$$\tilde{F} = \begin{pmatrix} M_2 , & M_3 , & S_{23}, & - D_{23} \\ M_4 , & M_1 , & S_{41}, & - D_{41} \\ 2S_{24}, & 2S_{31}, & S_{21} + S_{34}, & - D_{21} + D_{34} \\ 2D_{24}, & 2D_{31}, & D_{21} + D_{34}, & S_{21} - S_{34} \end{pmatrix} \tag{10}$$

Equations (9) and (10) are the most general transformations. For spherical particles $A_3 = A_4 = 0$; then (9) and (10) simplify to

$$F = \begin{pmatrix} 1/2 \left(M_1 + M_2 \right), & 1/2 \left(- M_1 + M_2 \right), & 0 , & 0 \\ 1/2 \left(- M_1 + M_2 \right), & 1/2 \left(M_1 + M_2 \right), & 0 , & 0 \\ 0 , & 0 , & S_{21}, & - D_{21} \\ 0 , & 0 , & D_{21}, & S_{21} \end{pmatrix} \tag{11}$$

and

$$\tilde{F} = \begin{pmatrix} M_2, & 0 , & 0 , & 0 \\ 0 , & M_1, & 0 , & 0 \\ 0 , & 0 , & S_{21}, & - D_{21} \\ 0 , & 0 , & D_{21}, & S_{21} \end{pmatrix} \tag{12}$$

Equations (11) and (12) are the desired transformation matrixes.

REFERENCES

1. Manz, J. E., A Ladar Cloud/Target Polarizaticn Discrimination Technique, Dissertation, University of New Mexico, 1970.

2. Mie, G., "Beitrage zur optik trüber Medien, Speziell Kolloidaler Metallösungen," Ann. der. Phys. 25, pp. 377-445, 1908.

3. Hoffman, W. C., "Scattering of Electromagnetic Waves from a Rough Surface," Quart. Appl. Math., Vol 13, No. 3, pp. 291-304, 1955.

4. Fung, A. K., Scattering Theories and Radar Return, University of Kansas Center for Research Report No. CRES 48-3, 1965.

5. Erteza, A. and Lenhert, D. H., "Field Theory of Depolarization of Radar Back Scatter with Applications to a Distant Slightly Rough Surface," Radio Science, Vol 2, p. 979, 1967.

6. Beckmann, P., The Depolarization of Electromagnetic Waves, The Golem Press, Boulder, Colorado, 1968.

7. Born, M. and Wolf, E., Principles of Optics, 4th Ed., Pergamon Press, 1970.

8. Kraus, J. D., Antennas, McGraw-Hill Book Company, Inc., New York, 1950.

9. Chandrasekhar, S., Radiative Transfer, Dover Publications Inc., New York, 1960.

10. Kourgano V., Basic Methods in Transfer Problems, Oxford University Press, London, 1952.

11. Evans, L. B., et al., "The Effect of Anisotropic Scattering on Radiant Transport," J. of Heat Transfer, Vol 87, No. 3, pp. 381-387, 1965.

12. Hammersley, J. M. and Handscomb, D. C., Monte Carlo Methods, John Wiley and Sons Inc., New York, 1964.

13. Shreider, V. A. (Ed.), The Monte Carlo Method, Pergamon Press, New York, 1966.

14. Van De Hulst, H. C., Light Scattering by Small Particles, John Wiley and Sons, Inc., New York, 1957.

15. Deirmendjian, D., "The Role of Water Particles in the Atmospheric Transmission of Infra-red Radiation," Q. Jour. of the Met. Soc., Vol 85, No. 366, pp. 404-411, 1959.

16. Kattawar, G. W. and Plass, N. P., "Monte Carlo Calculations of Light Scattering from Clouds, App. Opt., Vol 7, No. 3, pp. 415-419, 1968.

17. Collins, D. G. and Wells, M. B., Computer Procedure for Calculating Time Dependent Light Scattering in Plane Parallel Atmospheres, Radiation Research Associates, Inc., Fort Worth, Texas, RRA-T 7016, 1971.

18. Perrin, F., "Polarization of Light Scattered by Isotropic Opalescent Media," J. Chem. Phys., Vol 10, pp. 415-427, 1942.

19. Weidner, R. T. and Sells, R. L., Elementary Modern Physics, (2nd Ed), Allyn and Bacon, Inc., Boston, 1970.

20. Collins, D. G., et al., Monte Carlo Codes for Study of Light Transport in the Atmosphere, Radiation Research Associates, Inc., Fort Worth, Texas, Vols I and II.

21. Shurcliff, W. A. and Ballard, S. S., Polarized Light, Van Nostrand Momentum Book #7, D. Van Nostrand Company, Inc., Princeton, New Jersey, 1964.

22. Stokes, G. C., Trans. Cambr. Phil. Soc., Vol 9, p. 399, 1852.

23. Stratton, J. A., Electromagnetic Theory, McGraw-Hill Book Company, New York, 1941.

24. Deirmendjian, D., "Scattering and Polarization Properties of Water Clouds and Hazes in the Visible and Infra-red," Appl. Opt., Vol 3, No. 2, pp. 187-196, 1964.

25. Khrgian, A. K. and Mazin, I. P., Tr. Tsentr. Aerolog. Observ., Vol 7, p. 56, 1952.

26. Durbin, W. G., "Droplet Sampling in Cumulus Clouds," Tellus, Vol 11, p. 202, 1959.

27. Singleton, F. and Smith, D. J., "Some Observations of Drop-Size Distributions in Low Layer Clouds," Quart. J. R. Met. Soc., Vol 86, p. 454, 1960.

28. Fenn, R. W., et al., Optical Properties of the Atmosphere (Rev.), Air Force Cambridge Research Laboratories, AFCRL-71-0279, 1971.

29. Bruning, J. H. and Lo, Y. T., "Multiple Scattering of EM Waves by Spheres Part I - Multipole Expansion and Ray - Optical Solutions," IEEE Trans. on Antennas and Propagation, Vol AP-19, No. 3, pp. 378-390, 1971.

BIBLIOGRAPHY

Angelakos, D. J. and Kumagai, N., "High-Frequency Scattering by Multiple Spheres," IEEE Trans. on Antennas and Propagation, Vol AP-12, No. 1, pp. 105-109, 1964.

Case, K. M. and Zweifel, P. F., Linear Transport Theory, Addison-Wesley Publishing Company, Reading, Massachusetts, 1967.

Foldy, L. L., "The Multiple Scattering of Waves," Phys. Rev., Vol 67, Nos. 3 and 4, pp. 107-119, 1945.

Goody, R. M., Atmospheric Radiation I, Oxford University Press, 1964.

Irvine, W. M., "The Shadowing Effect in Diffuse Radiation," J. Geo. Res., Vol 71, No. 12, pp. 2931-2937, 1966.

Kerker, M. (Ed), Electromagnetic Scattering, The MacMillan Company, New York, 1963.

Penndorf, R., "The Vertical Distribution of Mie Particles in the Atmosphere," J. Met., Vol 11, pp. 245-247, 1954.

Penndorf, R., "Tables of the Refractive Index of Standard Air and the Rayleigh Scattering Coefficients for the Spectral Region Between 0.2 and 20.0 μ and Their Application to Atmospheric Optics," J. Opt. Soc. Am., Vol 47, No. 2, pp 176-182, 1957.